# Bound Pairs Scattering off a Floquet Driven Impurity

Friedrich Hübner

Masterarbeit in Physik
angefertigt im Physikalischen Institut

vorgelegt der
Mathematisch-Naturwissenschaftlichen Fakultät
der
Rheinischen Friedrich-Wilhelms-Universität
Bonn

August 2021

I hereby declare that this thesis was formulated by myself and that no sources or tools other than those cited were used.

Bonn, ..... .....
Date Signature

1. Gutachterin: Prof. Dr. Corinna Kollath
2. Gutachter: Prof. Dr. Matteo Rizzi

# Acknowledgements

I would like to thank Prof. Dr. Corinna Kollath and Dr. Ameneh Sheikhan for the support and the interesting discussions. I have learned a lot throughout the last year: I dove into new topics and revisited those I already thought I knew, but I also learned how to work and communicate with other people. Both would not have been possible without their help, their questioning of my work and their incredible patience.

I would also like to thank the other members of the group for being friendly and helpful. I always enjoyed our virtual Coffee breaks during lockdown. It is a shame that we were hardly able to meet in person.

Furthermore great thanks to my friends Axel, Dominik, Eugen, Fiona, Kilian, Luka, Sven and Thekla for checking my calculations and proofreading my thesis.

# Contents


**1 Introduction** **1**

**2 Description of the model and techniques** **3**
2.1 The Fermi-Hubbard chain . . . . . 4
2.1.1 One particle . . . . . 4
2.1.2 Two particles of opposite spin . . . . . 4
2.1.3 What about more particles? . . . . . 6
2.1.4 The limit $U/J \to -\infty$ . . . . . 6
2.1.5 Interpretation of the Schrieffer-Wolff transformation . . . . . 8
2.2 Floquet theory . . . . . 9
2.3 Description of the numerical methods . . . . . 12

**3 Scattering in the non-resonant case** **19**
3.1 Model description . . . . . 19
3.2 Analytical results in the limit $J/\omega \to 0$ . . . . . 23
3.2.1 Single particle case . . . . . 23
3.2.2 Particle pair . . . . . 23
3.2.3 Calculating the transmission in the effective models . . . . . 24
3.3 Discussion of the pair transmission . . . . . 27
3.3.1 Discussion of the effective model . . . . . 27
3.3.2 Discussion of the parameters for $|u| > 1$ . . . . . 29
3.3.3 Discussion for $|u| < 1$ . . . . . 36
3.3.4 Discussion for $|u|$ close to an integer . . . . . 38
3.4 Numerical results . . . . . 42
3.4.1 Numerical results in the limit $J/\omega \to 0$ . . . . . 43
3.4.2 Numerical results for finite $J/\omega$ . . . . . 45

**4 Applications** **47**
4.1 Average transmission . . . . . 47
4.2 Pair filter . . . . . 49
4.3 Single particle filter . . . . . 50
4.4 Blocking transmission for both pairs and single particles . . . . . 51
4.5 Parameter proposal for a tunable impurity . . . . . 52
4.6 Pair momentum filter . . . . . 54

**5 Scattering in the resonant case** **57**
5.1 Description of the situation . . . 57
5.2 Analytical results in the limit $J/\omega \to 0$ . . . 57
5.2.1 Expected behaviour . . . 58
5.2.2 Discussion of the different timescales . . . 58
5.2.3 A quick overview about scattering theory . . . 59
5.2.4 Intermezzo: A simple toy model . . . 60
5.2.5 The Lippmann-Schwinger equation for the pairs . . . 62
5.2.6 Applying the theorem . . . 64
5.3 Numerical results . . . 73

**6 Conclusion** **77**

**Bibliography** **79**

**A Perturbative expansions in Floquet theory** **83**
A.1 The high-frequency expansion . . . 83
A.2 The Schrieffer-Wolff transformation . . . 84
A.3 The Floquet-Schrieffer-Wolff transformation . . . 85
A.4 Application to the Fermi-Hubbard model . . . 86

**B A general theorem about scattering from slow to fast modes** **91**
B.1 General considerations . . . 91
B.2 Theorem for only one slow subspace . . . 93
B.3 Theorem for a slow and a fast subspace . . . 97
B.4 Discussion of the technical assumptions . . . 103

**C Useful properties of the Bessel functions** **105**
C.1 Qualitative description . . . 105
C.2 Definition and basic properties . . . 106
C.3 Asymptotic formulas . . . 106
C.4 Distribution of the first maximum of the Bessel functions . . . 107
C.5 Neumann's addition theorem . . . 107
C.6 Taylor expansion of $v_1$ . . . 108

**D Various calculations** **109**
D.1 Gauge transformation . . . 109
D.2 Calculation of transmission amplitude . . . 110
D.3 Transmission in the resonant case . . . 112

**E Error discussion of the numerical method** **117**

CHAPTER 1

# Introduction

Floquet systems became increasingly popular during the last decade. They describe all systems with an external time-periodic drive, a situation which is often encountered in experiments. Especially by applying external time-periodic fields to cold atom systems one is able to induce a variety of interesting effects in them (see [1] for a good introduction) like dynamical localization [2], artificial magnetic fields [3] and even phase transitions [4, 5]. In most situations one tries to apply the external drive homogeneously to the entire system to manipulate the system as a whole. But of course there is also the other option, namely to apply the driving only to small parts. This results in driven impurities which can have interesting properties.

In 2016 Thuberg et al. [6] considered a non-interacting chain with a single driven site 0 at which the local chemical potential oscillates as $\mu_0 = \mu \cos \omega t$. For the transmission through the impurity, depending on the parameters, there exists a wide range of scattering situations. In particular they found that the system possesses a Fano resonance [7], an unusual resonance which is based on bound states inside the continuum. This system can be extended [8] with a spin dependent coupling (i.e. a driven magnetic field) and one can find parameters for which one spin species is fully blocked while the other is fully transmitted. Such a spin filter device could be used in cold atom experiments to manipulate the atoms depending on their spin.

While a non-interacting chain already describes fermionic cold atom systems quite well it still misses an important effect: the on-site Hubbard interaction $U$ between particles [1]. This interaction allows for a completely new physical situation: Bound pairs of particles with opposite spin. In recent years there has been growing interest in observing and studying these bound pairs experimentally [9, 10, 11, 12]. In this thesis we would like to study how these bound pairs scatter at a driven impurity, thereby extending the work of Thuberg et al. [6] to the more general Fermi-Hubbard chain.

The general description of Floquet systems is relatively complicated, especially in scattering situations. Due to the external driving particles can absorb (or deposit) energy quanta corresponding to the driving frequency $\omega$. Already in the non-interacting chain [6] this can lead to many possible final states of the scattering, especially if $\omega$ is small. Luckily once $\omega$ exceeds the band width, the absorption of energy quanta $\omega$ is no longer energetically allowed (i.e. only possible for short times during the scattering). One can use this to derive effective static Hamiltonians for the driven system in the large frequency limit $\omega \to \infty$. For pairs, if $U$ is close to an integer multiple of $\omega$, there is also the possibility of a pair breaking into two single particles by multiple absorption of energy quanta $\omega$. This is not desirable when trying to work with pairs and we will therefore first focus on parameter

ranges where pair breaking is not possible. We will derive an effective Hamiltonian in this regime and use it to calculate the transmission. We will compare the result to the single particles and find that it behaves quite differently. This is great as it opens the possibility to manipulate pairs independent from the single particles, for example to build a pair filter, which blocks single particles but lets pairs pass.

In the second chapter we give a short introduction into all necessary theoretical prerequisites. We introduce the Fermi-Hubbard model, its exact eigenstates for one and two particles and how one can derive an effective Hamiltonian for the pairs. We give a quick overview over Floquet theory with a specific emphasis on how to think about Floquet systems in the scattering scenario. Also we introduce the numerical method we will later use to validate the results of our effective model.

The third chapter then treats the scattering at the driven impurity in the non-resonant case. We derive an effective Hamiltonian for both single particles and pairs in the limit of $J/\omega \to 0$ and discuss their resulting transmission amplitudes. We compare the pair transmission to numerical results and find that they are in good agreement even for finite $J/\omega$ as long as the driving is still non-resonant.

In the fourth chapter we compare the transmission of single particles and pairs and discuss possible applications. By tuning the parameters one can achieve impurities which transmit pairs but block single particles and vice versa.

In the last chapter we complete the discussion of the impurity by also considering the resonant case, i.e. where pair breaking can occur. Although this case is probably not experimentally relevant it is still theoretically interesting. In particular we will find that in the limit of small $J/\omega$ pair breaking is actually suppressed. This is an unintuitive finding as we would have expected exactly the opposite, namely that pair breaking is the dominant process. In addition to the rather complex calculations for the pairs we also discuss this behaviour and its implications in a simpler toy model.

CHAPTER 2

# Description of the model and techniques

The model we will consider in this thesis is given by a Fermi-Hubbard chain (for a comprehensive introduction see [13]) with an additional impurity given by a shaken chemical potential at site 0. The Fermi-Hubbard model describes spin $\frac{1}{2}$ fermions on an infinite chain of lattice sites[1]. The Hamiltonian consists of three parts

$$\mathbf{H} = -J\mathbf{H}_{\mathrm{H}} + U\mathbf{H}_{\mathrm{U}} + \lambda\omega\mathbf{V}\cos(\omega t). \tag{2.1}$$

The first part is the hopping Hamiltonian with hopping parameter $J$. The second one describes the on-site Hubbard interaction with interaction parameter $U$. Their formal definitions are

$$\mathbf{H}_{\mathrm{H}} = \sum_{n=-\infty}^{\infty} \sum_{\sigma\in\{\uparrow,\downarrow\}} \mathbf{c}^{\dagger}_{n\sigma}\mathbf{c}_{n+1\sigma} + \mathbf{c}^{\dagger}_{n+1\sigma}\mathbf{c}_{n\sigma} \tag{2.2}$$

$$\mathbf{H}_{\mathrm{U}} = \sum_{n=-\infty}^{\infty} \mathbf{n}_{n\uparrow}\mathbf{n}_{n\downarrow}. \tag{2.3}$$

Here $\mathbf{c}_{n\sigma}$ is the (fermionic) annihilation operator and $\mathbf{n}_{n\sigma} = \mathbf{c}^{\dagger}_{n\sigma}\mathbf{c}_{n\sigma}$ is the number operator at site $n$ with spin $\sigma$. The third part adds the impurity. Here $\lambda$ is the driving strength (in units of $\omega$), $\omega$ is the driving frequency and $\mathbf{V}$ describes the impurity:

$$\mathbf{V} = \mathbf{n}_{0\uparrow} + \mathbf{n}_{0\downarrow}. \tag{2.4}$$

We give a sketch of the model in figure 2.1. Our aim is to study scattering at this impurity which we will do in chapter 3. Before we can do that we first need to understand the plain Fermi-Hubbard chain without the impurity, as it is going to be the reference model for the scattering process.

[1] Note that we will set $\hbar = 1$ throughout the thesis. Also the lattice spacing is 1.

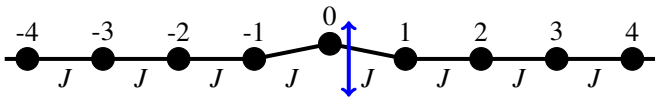


Figure 2.1: Sketch of the model: It is a Fermi-Hubbard chain with hopping parameter $J$ and on-site Hubbard interaction $U$ (not shown). The impurity consists of a single site which local chemical potential is periodically shaken (blue).

## 2.1 The Fermi-Hubbard chain

In this section we will consider the plain Fermi-Hubbard chain:

$$\mathbf{H}_{\mathrm{FH}} = -J\mathbf{H}_{\mathrm{H}} + U\mathbf{H}_{\mathrm{U}}. \tag{2.5}$$

The Fermi-Hubbard chain conserves the particle numbers for each spin separately. We will mostly consider either one or two particles of opposite spin.

### 2.1.1 One particle

For one particle the Hubbard interaction vanishes and the model reduces to the standard tight-binding model. This case together with a driven impurity was already analyzed in [6]. We are going to drop the spin index[2]. The Hamiltonian can be diagonalized by a Fourier transform and has a continuous spectrum. The eigenstates are given by plane waves

$$\left|\psi_k\right\rangle \sim \sum_n e^{ikn} \left|n\right\rangle \tag{2.6}$$

where the momentum $k$ is a real number between $-\pi$ and $\pi$. Here we denote $\left|n\right\rangle = \mathbf{c}_n^\dagger \left|\Omega\right\rangle$ which describes a particle at site $n$ ($\left|\Omega\right\rangle$ is the vacuum state). The eigenenergy of the eigenstate is $E = -2J\cos k$.

### 2.1.2 Two particles of opposite spin

For two particles of opposite spin the analysis of the Hamiltonian is more complicated. We will denote a state with the first particle at $n$ and the second one at $m$ as $\left|n,m\right\rangle = \mathbf{c}_{n\uparrow}^\dagger \mathbf{c}_{m\downarrow}^\dagger \left|\Omega\right\rangle$. Instead of thinking about the system as a 1D system with two particles on it, it is actually more intuitive to think of the system as a single particle on an infinite 2D lattice. The position along the x-axis (y-axis) corresponds to the position of the first (second) particle. We will make frequent use of this picture and call the 2D system a layer. The Hamiltonian on this layer is given by an usual 2D hopping Hamiltonian with an extra potential $U$ acting on the diagonal $n = m$ (see figure 2.2(a)).

From this picture it is clear that the system will factorize into the degrees of freedom along the diagonal (center-of-mass coordinate) and perpendicular to it (relative coordinate). Along the diagonal an eigenstate will be given by a plane wave. Perpendicular to the diagonal we can either have a symmetric or antisymmetric wavefunction. In the antisymmetric case the wavefunction vanishes at the diagonal and therefore describes two non-interacting particles. Thus this case is not interesting for us.

[2] Since both types of spin are treated equally by the Fermi-Hubbard model the spin of the particle is irrelevant.

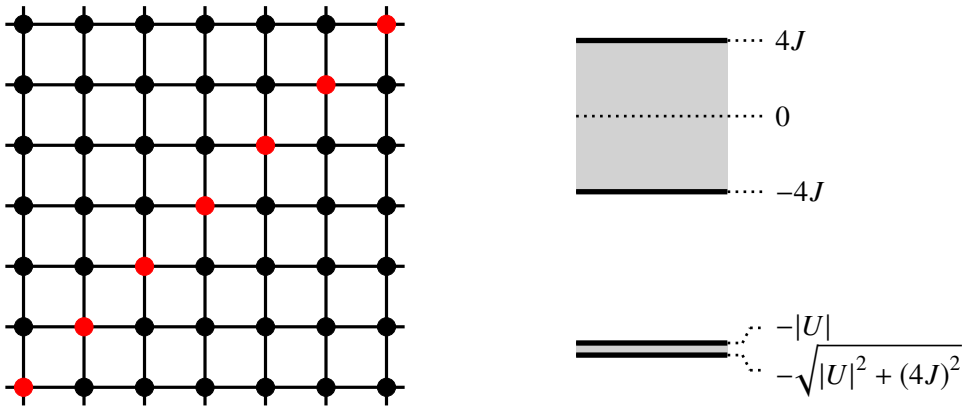


(a) (b)

Figure 2.2: Fermi-Hubbard chain (2.5) for two particles: a) View from top onto the layer for two particles. The x and y components are the position of the first and second particle respectively. The sites are linked by hopping parameter $J$ (solid lines). The Hubbard interaction $U$ acts on the sites marked in red. b) Sketch of the energy bands of the two particle Fermi-Hubbbard chain. There are two bands: A free particle band (upper band) with energies between $-4J$ and $4J$ and a bound pair band (lower band) with energies between $-\sqrt{|U|^2+(4J)^2}$ and $-|U|$. For $|U| < 4J$ both bands merge.

For the symmetric case an ansatz for the wavefunction is given by

$$\left|\psi_{K,\gamma}\right\rangle \sim \sum_{n,m} e^{iK(n+m)} e^{-\gamma|n-m|} \left|n,m\right\rangle . \tag{2.7}$$

Here $K$ (half of the center-of-mass momentum) is between $-\pi/2$ and $\pi/2$ and $\gamma$ (the relative momentum[3]) can either be a real positive or a purely imaginary number[4]. The later case describes an incoming plane wave scattering at the diagonal and escaping to infinity (this corresponds to the scattering of two particles). The energy of such a state is

$$E = -4J \cos K \cos|\gamma|. \tag{2.8}$$

This is a continuum of states with energies ranging from $-4J$ up to $4J$. We will call this band the free particle band because (away from the diagonal $n = m$) it is a superposition of two free particle states. Note that this also means that scattering at an impurity at site 0 is not different from the single particle case (unless the improbable case, that both particles are simultaneously at site 0). Therefore we are also not interested in the free particle band.

The case which adds a new phenomenon is when $\gamma$ is actually a positive real number. The state then corresponds to a bound pair of the two fermions with center-of-mass momentum $2K$. The energy of the bound pair is given by

$$E = -4J \cos K \cosh\gamma. \tag{2.9}$$

[3] If $\gamma$ is imaginary it describes the relative momentum. Otherwise it describes the size of a bound pair.

[4] In fact in this case the wavefunction is a superposition of two waves with $\gamma$ and $-\gamma$

Furthermore as described in [14] by solving the Schroedinger equation at the diagonal $n = m$ one obtains (see [14] (17a)):

$$E = -\sqrt{U^2 + (4J\cos K)^2} \tag{2.10}$$

for attractive $U < 0$[5]. For simplicity and because it is much more intuitive we will only consider the attractive case $U < 0$. The repulsive case $U > 0$ can be mapped onto the attractive case by setting $\gamma \to \gamma + i\pi$.

To summarize in the attractive case $U < 0$ the spectrum of the Hamiltonian for two particles with opposite spin consists of two (possibly overlapping) bands. A band for free single particles with energies between $-4J$ and $4J$ and a second band for bound pairs with energies between $-\sqrt{U^2 + 16J^2}$ and $-|U|$ (see figure 2.2(b)).

### 2.1.3 What about more particles?

For more particles the Fermi-Hubbard model becomes more complicated. In principle one can still solve it exactly using the Bethe ansatz [13]. The full solution will include many particles and pairs all scattering from each other. However we are not interested in studying the Fermi-Hubbard model, but want to study scattering at the impurity. To study this one single particle or one pair is enough. For more particles or pairs the overall scattering will be given by a complicated interference between scattering at the impurity as well as scattering between the particles away from the impurity. However as long as long as no two particles are simultaneously at the impurity the scattering factorizes and therefore reduces to the single particle or pair case. The scattering is only influenced if two particles are simultaneously at the impurity. As long as the particle density is not too high this happens only rarely. Therefore it is enough to restrict our attention to single particles or pairs.

### 2.1.4 The limit $U/J \to -\infty$

In order to get a better understanding of the bound pair states it is instructive to look at the limit $U/J \to -\infty$. As we will see this limit is the 'natural' limit to realize and study pairs. We are first going to discuss how the energy and wavefunctions of the Fermi-Hubbard model behave in this limit. After that we will show we can arrive at the same results using perturbation theory. The perturbative treatment is instructive for later calculations where the impurity will also be included. In that case we do not know the full solution to the Schrödinger equation and so we will have to rely on perturbation theory.

#### Wavefunctions and energies

Before we start let us note that the single particle case is not affected by this limit because the Hubbard interaction $U$ is irrelevant here. For two particles we get well separated energy bands, one for free particles and one for pairs. The energies for pairs $E \sim -|U|$ are much lower than the energies for free particles $E \sim J$. Due to the huge energy difference between both bands they fully decouple in the

[5] Note that [14] considers a pair of bosons. However the result is the same because we consider a symmetric wavefunction.

limit. What happens to the wavefunction of the pair? The size of the pair is given by

$$\frac{1}{\gamma} = \frac{1}{\operatorname{arcsinh}\left(\frac{|U|}{4J\cos K}\right)}. \tag{2.11}$$

Note that the size depends on the momentum of the pair. We observe that the size of the pair will go to zero as $U/J \to -\infty$. Already for $|U|/J > 4\sinh(1) \approx 4.7$ the size of pair is below one lattice spacing $1/\gamma < 1$ and therefore the overall majority of the wavefunction will concentrate on the diagonal, that is where both particles are at the same position.

The limit $U/J \to -\infty$ is therefore given by nicely bound and localized paired states. Note that the concentration of paired states onto the diagonal also implies that for the free states the probability of having both particles at the same site vanishes. This is another manifestation of the decoupling of paired and free states.

#### Derivation via Perturbation theory

In the last subsection we made use of the full solution for general $J$ and $U$ and analyzed the limit. Now we would like to go a different way starting from the original model and deriving the limit without knowing the general solution.

Before we start let us adopt a different mindset for solving this problem. Since perturbation theory works with small quantities instead of $|U|/J \to \infty$ we will consider the limit $J/|U| \to 0$. To avoid confusion we note that this limit should not be understood as making the hopping parameter small, but rather as increasing $|U|$ to infinity.

Let us define $\alpha = J/|U|$. We want to study the limit $\alpha \to 0$ of the Hamiltonian given by:

$$\mathbf{H}_\alpha = |U|\big(-\alpha\mathbf{H}_\mathrm{H} - \mathbf{H}_\mathrm{U}\big). \tag{2.12}$$

Perturbation theory will allow us to consider not only one or two particles, but an arbitrary number of them. For simplicity we will restrict ourselves to the case where we have an arbitrary but equal number of particles for each spin $N_\uparrow = N_\downarrow = N/2$.

In the ultimate limit $\alpha = 0$ the Hamiltonian is given by only $-|U|\mathbf{H}_\mathrm{U}$. The ground state is given by states where all particles are paired. The energy of these states is $E_0 = -|U|N_\uparrow$. This ground state is highly (in fact infinitely) degenerate and therefore we will need to employ degenerate perturbation theory. A particular famous and useful method here is the Schrieffer-Wolff transformation. It was originally developed to relate the Anderson model to the Kondo model [15] but can be applied to basically any model. We give a short introduction and a quick derivation of the Schrieffer-Wolff transformation for our purposes in the appendix A.2. A good and more mathematical treatment can be found in [16].

Define the projectors $\mathbf{P}$, which projects on all completely paired states, and $\mathbf{Q} = 1 - \mathbf{P}$. The idea behind the Schrieffer-Wolff transformation is to find a unitary transformation $\mathbf{W}_\alpha$ which block diagonalizes the Hamiltonian into the $\mathbf{P}$ and $\mathbf{Q}$ subspaces[6], i.e. we want $\mathbf{P}\mathbf{H}_\alpha^\mathrm{eff}\mathbf{Q} = \mathbf{Q}\mathbf{H}_\alpha^\mathrm{eff}\mathbf{P} = 0$ where $\mathbf{H}_\alpha^\mathrm{eff} = \mathbf{W}_\alpha^\dagger\mathbf{H}_\alpha\mathbf{W}_\alpha$.

[6] Note that we use a different notation than usual. Usually instead of the unitary $\mathbf{W}_\alpha$ one introduces the anti-hermitian $\mathbf{S}_\alpha$, s.t. $\mathbf{W}_\alpha = e^{-\mathbf{S}_\alpha}$.

By expanding $\mathbf{W}_\alpha = 1 + \alpha\mathbf{W}_1 + \alpha^2\mathbf{W}_2 + \ldots$ one can recursively solve for $\mathbf{W}_\alpha$ up to arbitrary order (Note that $\mathbf{W}_1$ denotes the first Taylor coefficient[7] $\frac{\mathrm{d}}{\mathrm{d}\alpha}\mathbf{W}_\alpha\big|_{\alpha=0}$ and not $\mathbf{W}_\alpha$ evaluated at $\alpha = 1$). In particular we derive in appendix A.2 the first order $\mathbf{QW}_1\mathbf{P}$ (see equation (A.10)) which is given for the Hubbard model by:

$$\mathbf{QW}_1\mathbf{P} = \frac{1}{|U|}\mathbf{QH}_\mathrm{H}\mathbf{P}. \tag{2.13}$$

Using this result and further simplifying the formulas we find that the new Hamiltonian (A.14) in the $\mathbf{P}$ sector is given by

$$\begin{aligned}\mathbf{PH}_\alpha^{\mathrm{eff}}\mathbf{P} &= E_0 - \frac{J^2}{|U|}\mathbf{PH}_\mathrm{H}\mathbf{QH}_\mathrm{H}\mathbf{P} + O\left(\alpha^3\right) \\ &= -|U|N_\uparrow - \frac{4J^2}{|U|}\sum_n\left[\frac{1}{2}\left(\eta_n^+\eta_{n+1}^- + \eta_{n+1}^+\eta_n^-\right) - \mathbf{n}_{n\uparrow}\mathbf{n}_{n+1\uparrow} - \mathbf{n}_{n\uparrow}\right] + O\left(\alpha^3\right).\end{aligned} \tag{2.14}$$

In the second step we used the general formula derived for the Floquet setting (A.33) with $g_{na} = \delta_{a,0}$. The limiting effective Hamiltonian for pairs is therefore

$$\mathbf{H}^{\mathrm{pair}} = -|U|N_\uparrow - 4\frac{J^2}{|U|}\sum_n\left[\frac{1}{2}\left(\eta_n^+\eta_{n+1}^- + \eta_{n+1}^+\eta_n^-\right) - \mathbf{n}_{n\uparrow}\mathbf{n}_{n+1\uparrow} - \mathbf{n}_{n\uparrow}\right]. \tag{2.15}$$

Here we defined the 'creation' and 'annihilation' operators of a pair as

$$\eta_n^+ = \mathbf{c}_{n\uparrow}^\dagger\mathbf{c}_{n\downarrow}^\dagger \tag{2.16}$$

$$\eta_n^- = \mathbf{c}_{n\downarrow}\mathbf{c}_{n\uparrow}. \tag{2.17}$$

These operators do not satisfy the commutation relations for creation and annihilation operators but rather form a spin $\frac{1}{2}$ algebra with a suitable $\eta_n^z = (\mathbf{n}_{n\uparrow} + \mathbf{n}_{n\downarrow} - 1)/2$ operator[8].

We will regard the new Hamiltonian in (2.15) as an effective Hamiltonian for bound pairs in the limit $\alpha \to 0$. The first and the last term are proportional to the total particle number and therefore just numerical constants which can be ignored. The second term describes a pair hopping term with effective pair hopping parameter $2\frac{J^2}{|U|}$ (in original units). The third term is a (repulsive) nearest neighbour pair interaction term. Note that instead of $\mathbf{n}_{n\uparrow}$ we could have equivalently used $\mathbf{n}_{n\downarrow}$ (both are necessary equal in the $\mathbf{P}$ sector and either 0 or 1). Since we are later on going to restrict ourselves to two particles , i.e. one bound pair, the pair interaction term will not be relevant for us. For one pair the effective Hamiltonian is simply a hopping Hamiltonian.

### 2.1.5 Interpretation of the Schrieffer-Wolff transformation

We have derived the limit $J/|U| \to 0$ by looking at two different aspects: the eigenstates and eigenvalues of the Hamiltonian and by means of perturbation theory. What is the connection of both ways?

[7] We will use this compact notation to denote Taylor expansions throughout the thesis.

[8] In fact up to a numerical constant the Hamiltonian is equivalent to a XXZ model.

Most often one thinks of the Schrieffer-Wolff transformation simply as a way to derive an effective Hamiltonian. What is left out is the actual interpretation of the block-diagonalization induced by $\mathbf{W}_\alpha$, namely that the $\mathbf{W}_\alpha$ maps an eigenstate of the effective model onto an eigenstate of the original model [16]. For simplicity restrict again to two particles and think of the system as a 2D layer. An eigenstate of the effective Hamiltonian in the **P** sector is given by a plane wave which is only non-zero at the diagonal, i.e. $|\phi\rangle \sim \sum_n e^{ikn} |n,n\rangle$. The transformation $\mathbf{W}_\alpha$ maps this state to the corresponding eigenstate of the original model $|\psi\rangle \sim \sum_{n,m} e^{iK(n+m)} e^{-\gamma|n-m|} |n,m\rangle$ where $K = k/2$. Note the fundamental difference between both states: $|\phi\rangle$ is completely restricted to the diagonal, while $|\psi\rangle$ also includes the exponential tails into the direction orthogonal to the diagonal. While the latter state $|\psi\rangle$ has a complicated dependence on the actual value of $J/|U|$, the state $|\phi\rangle$ does not depend on $J/|U|$ at all. Therefore if $J/|U|$ is non-zero it is actually much more simpler (both mathematical and interpretation-wise) to use the transformed state $|\phi\rangle$ .

The interpretation goes as follows: Let $J/|U|$ be finite but still close to zero. If we pick a state in the **P** sector it will correspond to some state made out of bound pair states. If we instead have a state from the **Q** sector it will correspond to a state where both particles are free. For example let us say we would like to describe a pair which is localized at one particular site $n$. In the effective model we would describe it by the simple and intuitive state $|n,n\rangle$. For finite $J/|U|$ this is of course not the state we would observe in the lab. To calculate it we need to apply $\mathbf{W}_\alpha$ to $|n,n\rangle$ and obtain a complicated superposition of bound pair states at different momenta (but exclusively those, no free states mixed into it). This superposition of course will not be localized at one specific site, however it will somehow describe the closest possible combination of paired states to such a localized state at a specific value of $J/|U|$. Since $\mathbf{W}_\alpha \to 1$ for $\alpha \to 0$ in this limit the superposition will indeed converge to $|n,n\rangle$.

To summarize, it is important to keep in mind that while the effective model makes accurate predictions for the dynamics of the system even for $\alpha$ finite but close to zero, the resulting wavefunctions only coincide with the actually observed ones in the ultimate limit $\alpha = 0$. This is more a feature than a bug and we can always calculate the 'real' wavefunction by applying $\mathbf{W}_\alpha$ to the wavefunction in the effective model. We are not going to repeat this interpretation in the later part of this thesis, but we will make implicit use of it.

## 2.2 Floquet theory

Floquet theory deals with the description of quantum systems with a time-periodic Hamiltonian $\mathbf{H}(\omega t)$. Here $\omega = \frac{2\pi}{T}$ is the driving frequency. Good introductions can be found in [17] and [18]. A more in-depth introduction, especially into the extended Hilbert space framework, is given in [19].

We will quickly summarize the main ideas behind Floquet theory following [17]: The time evolution operator satisfies the Schrödinger equation

$$i\frac{\mathrm{d}}{\mathrm{d}t}\mathbf{U}(t) = \mathbf{H}(\omega t)\mathbf{U}(t). \tag{2.18}$$

It has the following interesting property when shifting the time by a full period:

$$i\frac{\mathrm{d}}{\mathrm{d}t}\mathbf{U}(t+T) = \mathbf{H}(\omega(t+T))\mathbf{U}(t+T) = \mathbf{H}(\omega t)\mathbf{U}(t+T). \tag{2.19}$$

Due to the time-periodicity of the Hamiltonian the equations for $\mathbf{U}(t)$ and $\mathbf{U}(t+T)$ are equal. Since

the solution to such a differential equation is unique we immediately find:

$$\mathbf{U}(t+T) = \mathbf{U}(t)\mathbf{U}(T). \tag{2.20}$$

In particular by repeating this argumentation $n$ times we find that:

$$\mathbf{U}(nT) = \mathbf{U}(T)^n. \tag{2.21}$$

We can rewrite this formula in a more intuitive form by introducing the Floquet Hamiltonian[9] $\mathbf{H}_\mathrm{F}$ given by $\mathbf{U}(T) = e^{-i\mathbf{H}_\mathrm{F}T}$:

$$\mathbf{U}(nT) = e^{-i\mathbf{H}_\mathrm{F}(nT)}. \tag{2.22}$$

Therefore if we only look at the system at full periods the time evolution seems to be generated by an effective static Hamiltonian $\mathbf{H}_\mathrm{F}$. Of course this is not true for times in between a full period. The full time evolution can be written as

$$\mathbf{U}(t) = \mathbf{U}^\mathrm{micro}(t)e^{-i\mathbf{H}_\mathrm{F}t}. \tag{2.23}$$

The so called micromotion operator $\mathbf{U}^\mathrm{micro}(t) = \mathbf{U}(t)e^{i\mathbf{H}_\mathrm{F}t}$ can easily be seen to be time-periodic. In particular $\mathbf{U}^\mathrm{micro}(T) = 1$. The above findings are called Floquet's theorem [17] and are the basis for Floquet theory. Floquet's theorem can be thought of as a time-like version of Bloch's theorem (see for example chapter 7 of [20]). To see this apply the time evolution operator of equation (2.23) to an eigenstate $|\psi\rangle$ of $\mathbf{H}_\mathrm{F}$:

$$\mathbf{U}(t)\,|\psi\rangle = \mathbf{U}^\mathrm{micro}(t)\,|\psi\rangle\, e^{-i\varepsilon t}. \tag{2.24}$$

The time-evolution is given by a time-periodic state $|\psi(t)\rangle = \mathbf{U}^\mathrm{micro}(t)\,|\psi\rangle$ and an additional phase factor which multiplies the wavefunction by $e^{-i\varepsilon T}$ after each period $T$. The so called quasienergy $\varepsilon$ is the analogue of the quasimomentum and is the eigenvalue of $\mathbf{H}_\mathrm{F}$ corresponding to $|\psi\rangle$.

Most often when dealing with Floquet systems one tries to calculate the Floquet Hamiltonian $\mathbf{H}_\mathrm{F}$, which in some sense incorporates the time-averaged behaviour, and then ignores the micromotion. Unfortunately apart from a few special cases one cannot calculate the Floquet Hamiltonian exactly but only using perturbation theory [21, 19, 22]. We will use these perturbative expansions, like the high-frequency expansion [21, 19] or the Floquet-Schrieffer-Wolff transformation [22], later on. However in this section we would like to introduce another way of thinking about these systems which is particularly suited for scattering theory. It consists of mapping the system onto a (much more complicated) time-independent one. Unlike computing the Floquet Hamiltonian this strategy does not neglect the micromotion, so no approximation or averaging is done.

Imagine we would have been able to compute the Floquet Hamiltonian $\mathbf{H}_\mathrm{F}$ exactly. Then we could diagonalize it and obtain the eigenstates of the Floquet Hamiltonian. Pick one eigenstate $|\psi\rangle$ with quasi-energy $\varepsilon$. The full time evolution acting on this state gives $\mathbf{U}^\mathrm{micro}(t)\,|\psi\rangle\, e^{-i\varepsilon t}$. We define $|\psi(t)\rangle = \mathbf{U}^\mathrm{micro}(t)\,|\psi\rangle$ which is a time-periodic state and can therefore be decomposed into Fourier

[9] Note that $\mathbf{H}_\mathrm{F}$ is not uniquely defined.

components

$$|\psi(t)\rangle = \mathbf{U}^{\text{micro}}(t)\,|\psi\rangle = \sum_a |\psi_a\rangle\, e^{-ia\omega t}. \tag{2.25}$$

Differentiating this expression with respect to time and using the Schroedinger equation (2.18) gives

$$i\frac{\mathrm{d}}{\mathrm{d}t}\left(\sum_a |\psi_a\rangle\, e^{-ia\omega t} e^{-i\varepsilon t}\right) = \sum_a (a\omega+\varepsilon)\,|\psi_a\rangle\, e^{-ia\omega t} e^{-i\varepsilon t} = \mathbf{H}(\omega t)\left(\sum_a |\psi_a\rangle\, e^{-ia\omega t} e^{-i\varepsilon t}\right). \tag{2.26}$$

We can also expand the Hamiltonian $\mathbf{H}(\omega t) = \sum_a \mathbf{H}_a e^{-ia\omega t}$ and match the corresponding Fourier components on both sides. This gives

$$(a\omega+\varepsilon)\,|\psi_a\rangle = \sum_b \mathbf{H}_{a-b}\,|\psi_b\rangle \tag{2.27}$$

which is just an eigenvalue equation for a big block matrix consisting of block entries $\mathbf{H}_{a-b}$ with eigenvalue $\varepsilon$ and block eigenvectors $|\psi_a\rangle$. It can be thought of as the time-independent Schrödinger equation of an abstract system with one extra artificial dimension. The Hilbert space of the abstract system is often called the extended Hilbert space [19] (in [17] the above equation (2.27) is called the Shirley-Floquet form of the Schrödinger equation).

Without going into further mathematical detail we will conclude this section by describing the extended system [6]. Take the original system and copy it infinitely many times, labelling each copy by an integer $a$. We think about these copies to be arranged in an infinite stack and we will usually refer to such copy as a layer. The Hamiltonian on each layer is given by the time-independent part of the Hamiltonian, i.e. the Fourier component $\mathbf{H}_0$. Furthermore each layer $a$ has an extra energy offset of $-a\omega$. So far these layers are uncoupled. We couple them with the Fourier components of the Hamiltonian. Consider two layers $a$, $b$. These two layers are coupled via $\mathbf{H}_{b-a}$, which describes a transition from layer $b$ to layer $a$.

Using this construction we can map the time-dependent system onto a time-independent one which can be treated as a usual quantum system. What is the the interpretation of these other layers? Think about a scattering problem with a driven impurity. The incoming particle is in layer 0 and 'does not know' about all the other layers. As it hits the impurity it can either stay in layer 0 or transfer to another layer $a$. Physically speaking during the latter process the particle absorbs or emits $a$ energy quanta of size $\omega$. This is reflected in the energy offset $-a\omega$ of each layer. In the new layer $a$ the particle behaves as usual only with a different energy. If the energy still corresponds to a free state the particle can propagate away towards infinity in layer $a$. This corresponds physically to a particle propagating away with a different energy. Therefore one should not think about the other layers as physical but simply as a nice way to keep track of the current energy of the particle.

The scattering situation is also a good example to discuss resonant and non-resonant behaviour in Floquet theory. Imagine that the non-interacting system consists of several energy bands with a certain bandwidth. The incoming state will then be a state in one of these bands. Non-resonant behaviour of the interacting systems means that by adding or subtracting any number of energy quanta $\omega$ we never hit the energy of an eigenstate of the (non-interacting) system. In the extended system this means that all other layers than the 0'th layer are classically forbidden, or in other words the particle cannot escape to infinity in these layers, but will eventually come back to the 0'th layer. Therefore the incoming and

outgoing state will be in layer 0 and the other layers are only involved during the scattering process. In this case we can remove the other layers and replace the impurity in the 0'th layer by an effective impurity which includes all possible excitations to other layers. The last step is exactly the idea behind those perturbative expansions, like the high-frequency expansion. In particular the high-frequency expansion considers the case $\omega \to \infty$. This case is always non-resonant since whenever the frequency is bigger than the difference of the highest and the lowest energy of the non-interacting system, we of course cannot reach any other eigenstate by adding or subtracting $\omega$. The high-frequency expansion therefore is going to break down as soon as the frequency becomes lower than the highest energy scale in the system. The same is true for other methods too: They only work in the non-resonant case.

The resonant case is any other case where one can reach another eigenstate by adding or subtracting $\omega$. In this case the standard perturbative methods will not work and we cannot hope to derive an effective Hamiltonian for layer 0[10]. We will see that for pairs the resonant case is often linked to pair breaking (i.e. the pair absorbs energy from the driving and then breaks into two single particles.). In experiments where one tries to manipulate pairs as a whole one usually prefers to avoid pair breaking (unless of course one wants to study this pair breaking process explicitly). Therefore the non-resonant case is much more relevant, both experimentally and analytically.

## 2.3 Description of the numerical methods

In the thesis we will also use numerical methods to study the scattering at the impurity. In particular we would like to compute the transmission amplitude. In this section we would like to introduce the method we are going to work with. The treatment here will be completely general and applies to an arbitrary 1D system with a static impurity. We will later explain in section 3.4 how to apply it to a Floquet driven impurity with incoming pairs.

Calculating the transmission amplitude numerically is not straight-forward because a well defined scattering problem works on an infinite system, while any computer is of course only able to handle finite size systems. Note that we will work with open boundary conditions. We can think of the finite size systems in the following way: The system scatters at the impurity like in the infinite system. The difference is whenever the system hits the boundary it will reflect from the boundary. We therefore need a method which can handle these extra reflections but is also computationally fast, allows to extract the transmission amplitude and becomes exact in the limit $L \to \infty$ ($L$ is the system size). Furthermore, in order to not bias the method, we would like to include as little information about the impurity as possible.

One very basic method is to do real-time simulations. The problem is that, due to the finite size of the system, we cannot choose a plane wave as initial state, but rather need to fix an initial wavepacket (for example a Gaussian in position and momentum space) on one side of the impurity. The final time of the simulation must be chosen carefully such that the wavefunction was able to scatter from the impurity but has not been reflected at the boundary yet. This is complicated since the initial wave packet is a superposition of momentum states which evolve with different velocities. Also while we are able to determine the transmission coefficient, due to the initial superposition, we only get a smeared transmission coefficient which is an average over the transmission amplitudes for several

[10] Of course this is not exactly true. The Floquet Hamiltonian in equation (2.23) still exists and (if we were able to calculate it) would also work as an effective Hamiltonian. However the Floquet Hamiltonian might be totally different from the original non-driven Hamiltonian, for example including strange couplings between states far away from the impurity.

momentum states. As the system size increases we can widen the initial state in position space which corresponds to a narrowing in momentum space. Therefore the momentum accuracy increases for larger systems. So in principle this method becomes exact in the limit. But as we increase the system size we do not only increase the Hilbert space dimension but also have to repeat the simulations for more and more initial momenta in order to cover the whole Brillouin zone. This is what makes this method quite expensive.

We will therefore use a different way to obtain the transmission amplitude. The idea is that in principle all information about scattering can be read off from the eigenstates of the system. If we can establish a way to approximate the transmission probability from the eigenstates of the finite system, we only need to diagonalize the system once.

Let us have a look at the infinite system first. The idea is along the lines of [23][11], but we are going to use a different notation which is more applicable in our situation. Consider a free 1D system with an additional (time-independent) impurity. The impurity can have any size $2S + 1$ but it has to vanish outside of a certain region $|n| > S$[12]. We will also assume that the system conserves parity and time reversal symmetry (in other words, the Hamiltonian contains only real entries [24]).

So let us fix an energy $E$ and discuss how the corresponding scattering eigenstates of the system look like[13]. For the free system the eigenstates are plane waves $e^{ikn}$ and $e^{-ikn}$ where the momentum $k > 0$ is uniquely determined by the energy (for example $k = \arccos\left(\frac{-E}{2J}\right)$ for a hopping Hamiltonian). Outside of the impurity the eigenstate is given by a superposition of these two plane waves. There are two (relevant) ways to form such a superposition. The first one has a more direct interpretation and consists of eigenstates, which correspond to a particle coming from left $\psi^{\mathrm{L}}$ or right $\psi^{\mathrm{R}}$ and being reflected and transmitted at the impurity:

$$\psi^{\mathrm{L}}_n = \begin{cases} e^{ikn} + r_k e^{-ikn} & n < -S \\ t_k e^{ikn} & n > S \end{cases} \tag{2.28}$$

$$\psi^{\mathrm{R}}_n = \begin{cases} t_k e^{-ikn} & n < -S \\ e^{-ikn} + r_k e^{ikn} & n > S. \end{cases} \tag{2.29}$$

From these superpositions we can directly read off the transmission amplitude $t_k$ and reflection amplitude $r_k$. But they are not the ones which would be outputted by an eigensolver (on the finite system). We know that due to time reversal symmetry there exist purely real eigenstates and we can imply from parity that these have to be either even or odd functions. The two eigenstates are given by

$$\psi^{\mathrm{s}}_{|n|>S} = A_k \cos(k|n|) + B_k \sin(k|n|) \tag{2.30}$$

$$\psi^{\mathrm{a}}_{|n|>S} = \mathrm{sgn}(n)\big(C_k \cos(k|n|) + D_k \sin(k|n|)\big). \tag{2.31}$$

Both are real and are either symmetric $\psi^{\mathrm{s}}$ or antisymmetric $\psi^{\mathrm{a}}$. All four parameters $A_k, B_k, C_k, D_k$ are real and will later be obtained by fitting $\psi^{\mathrm{s}}$ or $\psi^{\mathrm{a}}$ to the eigenstate[14]. Note that we could have written

[11] It considers a continuous system while we are using discrete systems. For this analysis however it does not matter.

[12] Note that the impurity does not need to be a potential, but can basically be any hermitian operator. It is only important that its action is restricted to a finite spatial region.

[13] Scattering eigenstates are those that do not vanish at infinity. Of course there might also be bound states around the impurity, but these are irrelevant for scattering.

[14] Note that the parameters are only unique up to a sign. For example we can always replace $A_k, B_k \to -A_k, -B_k$ and the

the wavefunctions equivalently with an amplitude and a phase shift

$$\psi^{\mathrm{s}}_{|n|>S} = E_k \cos\big(k|n| - \theta^{\mathrm{s}}_k\big) \tag{2.32}$$
$$\psi^{\mathrm{a}}_{|n|>S} = F_k \cos\big(k|n| - \theta^{\mathrm{a}}_k\big), \tag{2.33}$$

but in this way it is more complicated to numerically fit them to data.

Now we have two different basis sets of wavefunctions for the eigenspace of energy $E$; one which can be easily interpreted $\psi^{\mathrm{L}}, \psi^{\mathrm{R}}$ and one which is numerically relevant $\psi^{\mathrm{s}}, \psi^{\mathrm{a}}$. Imagine we know the latter eigenstates how can be obtain the former ones? This can be done by expressing the states of one basis by the other basis. In particular calculate the symmetric and antisymmetric superposition of $\psi^{\mathrm{L}}, \psi^{\mathrm{R}}$ and compare to $\psi^{\mathrm{s}}, \psi^{\mathrm{a}}$ for $|n| > S$:

$$\frac{\psi^{\mathrm{L}}_n + \psi^{\mathrm{R}}_n}{\sqrt{2}} = \frac{(t_k + r_k)e^{ik|n|} + e^{-ik|n|}}{\sqrt{2}} = \frac{t_k + r_k + 1}{\sqrt{2}} \cos(k|n|) + i\frac{t_k + r_k - 1}{\sqrt{2}} \sin(k|n|) \tag{2.34}$$
$$\frac{\psi^{\mathrm{L}}_n - \psi^{\mathrm{R}}_n}{\sqrt{2}} = \mathrm{sgn}(n)\frac{(t_k - r_k)e^{ik|n|} - e^{-ik|n|}}{\sqrt{2}} = \mathrm{sgn}(n)\left(\frac{t_k - r_k - 1}{\sqrt{2}} \cos(k|n|) + i\frac{t_k - r_k + 1}{\sqrt{2}} \sin(k|n|)\right). \tag{2.35}$$

The symmetric combination has to be a multiple of $\psi^{\mathrm{s}}$ with coefficient $\alpha^{\mathrm{s}}_k$ and the antisymmetric one is a multiple of $\psi^{\mathrm{a}}$ with coefficient $\alpha^{\mathrm{a}}_k$. We therefore can read off

$$\alpha^{\mathrm{s}}_k A_k = \frac{t_k + r_k + 1}{\sqrt{2}} \tag{2.36}$$
$$\alpha^{\mathrm{s}}_k B_k = i\frac{t_k + r_k - 1}{\sqrt{2}} \tag{2.37}$$
$$\alpha^{\mathrm{a}}_k C_k = \frac{t_k - r_k - 1}{\sqrt{2}} \tag{2.38}$$
$$\alpha^{\mathrm{a}}_k D_k = i\frac{t_k - r_k + 1}{\sqrt{2}}. \tag{2.39}$$

These equations can be solved quite easily and we find:

$$\alpha^{\mathrm{s}}_k = \frac{\sqrt{2}}{A_k + iB_k} \tag{2.40}$$
$$\alpha^{\mathrm{a}}_k = -\frac{\sqrt{2}}{C_k + iD_k} \tag{2.41}$$
$$t_k = \frac{1}{2}\left(\frac{A_k - iB_k}{A_k + iB_k} - \frac{C_k - iD_k}{C_k + iD_k}\right) \tag{2.42}$$
$$r_k = \frac{1}{2}\left(\frac{A_k - iB_k}{A_k + iB_k} + \frac{C_k - iD_k}{C_k + iD_k}\right). \tag{2.43}$$

Especially formula (2.42) is going to be important. We can see that the transmission and reflection

result would be an eigenstate too.

amplitudes only depend on the phases $\frac{A_k - iB_k}{A_k + iB_k} = e^{-2i\theta_k^{\mathrm{s}}}$ and $\frac{C_k - iD_k}{C_k + iD_k} = e^{-2i\theta_k^{\mathrm{a}}}$, where we defined $A_k + iB_k = \sqrt{A_k^2 + B_k^2}e^{i\theta_k^{\mathrm{s}}}$ and $C_k + iD_k = \sqrt{C_k^2 + D_k^2}e^{i\theta_k^{\mathrm{a}}}$ (which indeed are the same phase shifts as in equations (2.32) and (2.33)).

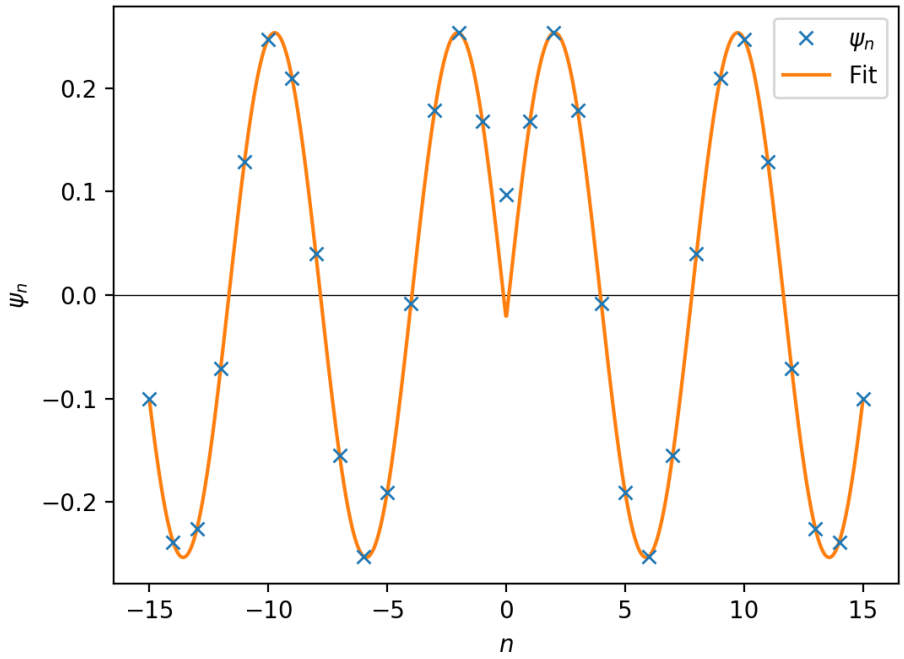


Figure 2.3: An example of a fit $\psi_n^{\mathrm{s}} = A_k \cos(k|n|) + B_k \sin(k|n|)$ to data $\psi_n$ obtained from an eigenstate which describes a pair (for details see section 3.4). The theoretically calculated momentum is $k = 0.817$. The three sites around the center $-1, 0, 1$ were excluded from the fit. The physical parameters are $N = 4, L = 31, J/\omega = 0.001, |U|/\omega = 0.5, \lambda = 1$.

So far we only treated the infinite system. What happens when we restrict the system to a certain length $L > S$ (For simplicity we will only consider odd $L$ and the system reaching from $\frac{L-1}{2}$ to $\frac{L-1}{2}$). Recall that we consider open boundary conditions. Open boundary conditions effectively mean that one takes the infinite system and imposes $\psi_{\pm\frac{L+1}{2}} = 0$. Therefore eigenstates $\psi^{\mathrm{s}}, \psi^{\mathrm{a}}$ of the finite system are given by eigenstates of the infinite system whenever they also satisfy $\psi_{\pm\frac{L+1}{2}} = 0$. This is of course only true for a finite number of $k$ and therefore the momentum is quantized. But it is crucial that other than that the eigenfunctions are not changed. In particular whenever we fit $A_k$ and $B_k$ (or $C_k$ and $D_k$) for a particular value of $k$ in the finite system that the result will be exact for the infinite system at this specific $k$ (up to their sign, which can be chosen freely by, for example $A_k, B_k \to -A_k, -B_k$). This is a really nice feature of the method. However when we want to calculate $t_k$ in the finite system there is still a big problem: Although we might have the exact values of $A_k, B_k$ for some set of sampling points $\{k\}_{\mathrm{s}}$ and the exact values of $C_k, D_k$ for some set of sampling points $\{k\}_{\mathrm{a}}$, but in general both sets will not be equal and we cannot combine them as required by formula (2.42).

We need to interpolate the parameters $A_k, B_k, C_k$ and $D_k$ for momenta $k$ where we do not know their exact values. For our purposes it is enough to use linear interpolation (a straight line between neighboring sampling points). Recall that the parameters are only specified up to a sign (in the sense

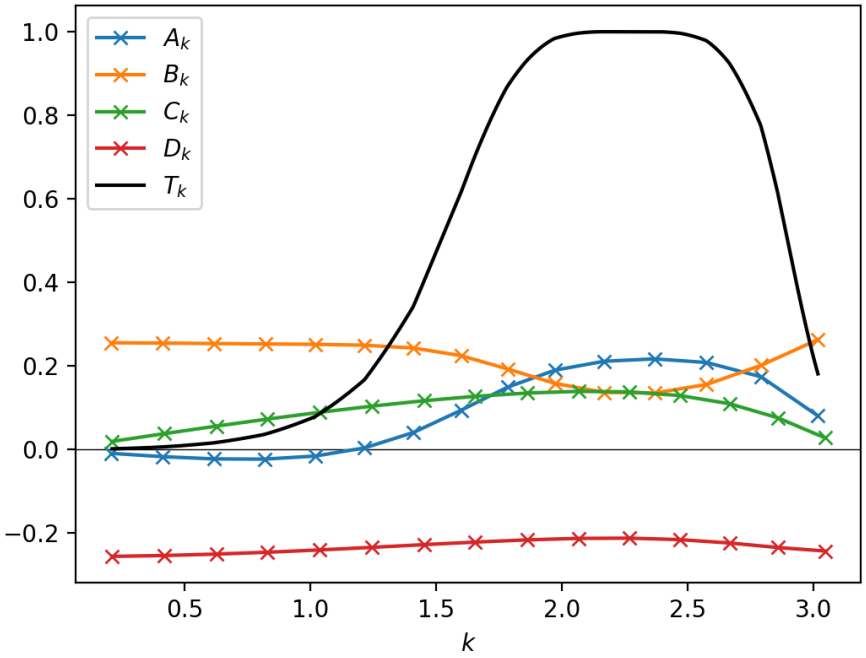


Figure 2.4: Example for the result of the interpolation. We mark the obtained values of $A_k, B_k, C_k$ and $D_k$ as crosses and also show their linear interpolation. The resulting transmission $T_k$ is shown in black. The physical parameters are $N = 4, L = 31, J/\omega = 0.001, |U|/\omega = 0.5, \lambda = 1$.

that $A_k, B_k \to -A_k, -B_k$ and $C_k, D_k \to -C_k, -D_k$). In order to obtain a good interpolation, we need to guess the correct sign of $A_k, B_k$ and $C_k, D_k$ for each sampling point. We will use a very simple method here. We iterate through the sampling points in ascending order of $k$. The sign of the first sampling point is adopted as it is. For any other point we compare both possibilities $A_k, B_k$ and $-A_k, -B_k$ with their values at the previous point and choose the one with the smaller (Euclidean) distance. For example if at the previous point $A_k = 1, B_k = 1$ and at the current point we have $A_k = 2, B_k = 1$ we have two possibilities: either the combination $2, 1$ or the combination $-2, -1$. Since the first one has the smaller (euclidean) distance from $A_k = 1, B_k = 1$ we will choose it. The same procedure is repeated for $C_k, D_k$.

To summarize, we will use the following method to calculate the transmission amplitude: First diagonalize the Hamiltonian, collect all unbounded states and sort them into symmetric or antisymmetric. Second for each state calculate the momentum $k$ from its energy $E$ and fit either $\psi^{\mathrm{s}}$ or $\psi^{\mathrm{a}}$ to it[15]. Note that, since we already know $k$, the fit can actually be performed as a linear fit (we will use the standard least square method in this thesis). The output of such a fit is a sampling point for either $A_k, B_k$ or $C_k, D_k$ at momentum $k$. Third perform a linear interpolation between these sampling points for both the symmetric $A_k, B_k$ and antisymmetric $C_k, D_k$ sector (and choosing the signs as described earlier). In the last step use equation (2.42) to compute the transmission probability $T_k = |t_k|^2$. Note that this method gives us an approximation of the transmission probability $T_k$ not just for one $k$ but for (almost) the whole Brillouin zone $0 \leq k \leq \pi$ in one go. This is not completely true because interpolation only

[15] Of course we only fit the wavefunction away from the impurity. The values of the wavefunction will simply be ignored.

works between two sampling points. We are therefore not able to compute $T_k$ for small or large $k$ outside of the minimal or maximal sampling point. In the figures we will leave this region blank.

To conclude, we have a method that allows us to numerically calculate the transmission through an impurity in a one dimensional chain from the eigenstates of the finite size system. The impurity has the following requirements: First it has to be localized. Second it has to be such that parity and time reversal symmetry are fulfilled. Third it has to be described by a hermitian operator (i.e. no particle loss). The last part is trivially fulfilled by any impurity as long as we indeed have a one-dimensional system. However one can also apply this method to a 1D subsystem of a much bigger system where the (effective) impurity can also include particle losses into other parts of the system (this is exactly what we are going to do for the pairs in section 3.4).

In figures 2.3 and 2.4 we give one example of a fit to an eigenstate and also of the interpolation. The black curve in figure 2.4 is the resulting transmission and the other curves are the interpolated curves of $A_k, B_k, C_k$ and $D_k$. We will later explain the meaning of all the physical parameters and how exactly we can apply this method to obtain pair transmission in section 3.4. In appendix E we also give a short discussion of the potential sources of errors when using this method.

CHAPTER 3

# Scattering in the non-resonant case

## 3.1 Model description

In this section we will add a single impurity into the Fermi-Hubbard model given by a periodically shaken chemical potential:

$$\mathbf{H} = -J\mathbf{H}_{\mathrm{H}} + U\mathbf{H}_{\mathrm{U}} + \lambda\omega\mathbf{V}\cos(\omega t). \tag{3.1}$$

Here $\lambda$ is the driving strength (in units of $\omega$), $\omega$ is the driving frequency and $\mathbf{V}$ describes the impurity:

$$\mathbf{V} = \mathbf{n}_{0\uparrow} + \mathbf{n}_{0\downarrow}. \tag{3.2}$$

The time-dependent Schroedinger equation reads

$$i\frac{\mathrm{d}}{\mathrm{d}t}\mathbf{U} = \left[-J\mathbf{H}_{\mathrm{H}} + U\mathbf{H}_{\mathrm{U}} + \lambda\omega\mathbf{V}\cos(\omega t)\right]\mathbf{U}. \tag{3.3}$$

We can obtain a unit free version of this by rescaling time $\phi = \omega t$:

$$i\frac{\mathrm{d}}{\mathrm{d}\phi}\mathbf{U} = \left[-\frac{J}{\omega}\mathbf{H}_{\mathrm{H}} + \frac{U}{\omega}\mathbf{H}_{\mathrm{U}} + \lambda\mathbf{V}\cos(\phi)\right]\mathbf{U}. \tag{3.4}$$

The above system is a Floquet system. As described in the section 2.3 we can think of such a Floquet system as an infinite collection of coupled layers. Each layer is labelled by an integer $a$ and has an energy offset $-a\omega$. For a single particle and two particles such a layer corresponds to a 1D chain or a 2D lattice respectively (see figures 3.1(a) and 3.1(b)). The Hamiltonian on each layer is given by a Fermi-Hubbard Hamiltonian which consists of a hopping Hamiltonian and, for two particles, also includes the Hubbard interaction at the diagonal (where both particles are at the same position). These layers are coupled to their neighboring layers whenever one particle is at site 0. For a single particle this gives only a coupling at a single site. For two particles however there is a coupling to neighboring layers whenever one of the particles is a site 0 which corresponds to the 'coordinate axes' of the 2D lattice (see figure 3.2(a) where all sites which are connected to other layers are marked blue). The coupling strength between the layers is $\frac{\lambda\omega}{2}$, because the driving has the following Fourier decomposition $\lambda\omega\cos(\omega t) = \frac{\lambda\omega}{2}\left(e^{i\omega t} + e^{-i\omega t}\right)$. For two particles there is a special case, namely

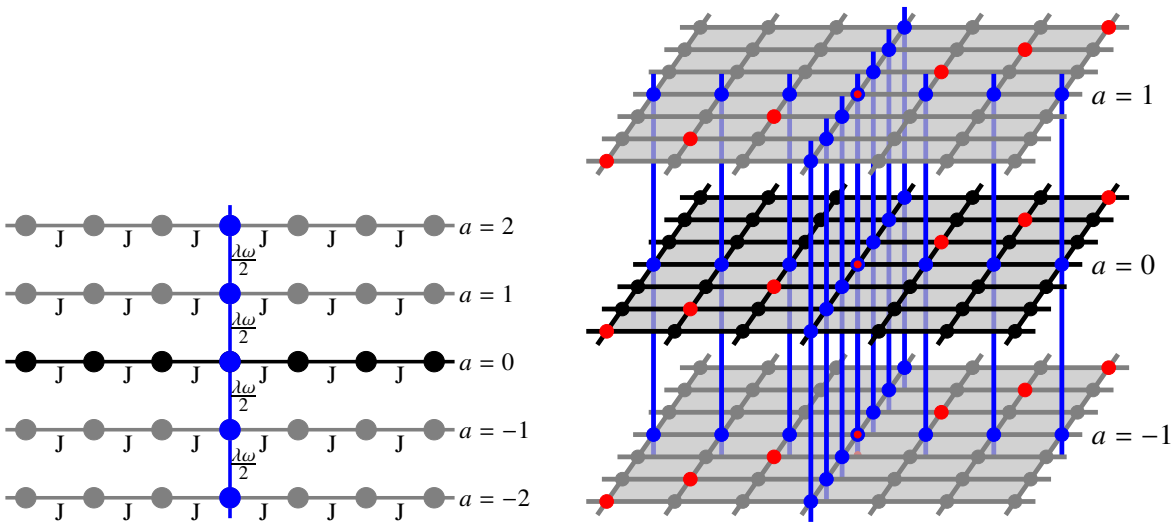


Figure 3.1: Sketches of the Hamiltonians in the extended Hilbert space: (a) For one particle (figure adopted from [6]) it consists of a stack of chains labelled by $a$, each having an energy offset of $-a\omega$ (gray). The original system is drawn in black. Neighboring chains are coupled at site 0 with coupling strength $\frac{\lambda\omega}{2}$ (blue). (b) For two particles it consists of a stack of 2D lattices labelled by $a$, each having an energy offset of $-a\omega$ (gray). In such a layer the x and y components are the position of the first and second particle respectively. We also marked the diagonal where the Hubbard interaction acts (red). Neighboring layers are coupled whenever one particle is at site 0, with coupling strength $\frac{\lambda\omega}{2}$ (blue). A single layer of this system is shown in figure 3.2(a).

when both particles are at site 0. Then the coupling strength is doubled and therefore given by $\lambda\omega$.

We could work directly with the above Hamiltonian, but in our case it is actually more convenient to first perform a gauge transformation. This gauge transformation will remove the extra driven potential and replace the static hopping parameter $J$ with a time-dependent one. The gauge transformation is given by

$$\mathbf{U}_0 = e^{-i\lambda\mathbf{V}\sin\phi}. \tag{3.5}$$

The transformed time evolution operator $\mathbf{U}^{\text{gauge}} = \mathbf{U}_0^\dagger\mathbf{U}$ satisfies the Schrödinger equation

$$i\frac{\mathrm{d}}{\mathrm{d}\phi}\mathbf{U}^{\text{gauge}} = \mathbf{H}^{\text{gauge}}\mathbf{U}^{\text{gauge}} \tag{3.6}$$

where

$$\mathbf{H}^{\text{gauge}} = \mathbf{U}_0^\dagger\hat{\mathbf{H}}_{\text{FH}}\mathbf{U}_0 = -\frac{J}{\omega}\mathbf{U}_0^\dagger\hat{\mathbf{H}}_{\text{H}}\mathbf{U}_0 + \frac{U}{\omega}\mathbf{H}_{\text{U}}. \tag{3.7}$$

Note that the Hubbard interaction is unaffected by the gauge transformation. It only affects the hopping from and to site 0. We can write this as (for a detailed derivation see appendix D.1):

$$\mathbf{H}^{\text{gauge}} = -\frac{J}{\omega}\left[\sum_{n\sigma} g_n(\phi)\mathbf{c}^\dagger_{n\sigma}\mathbf{c}_{n+1\sigma} + g^*_n(\phi)\mathbf{c}^\dagger_{n+1\sigma}\mathbf{c}_{n\sigma}\right] + \frac{U}{\omega}\mathbf{H}_{\text{U}} \tag{3.8}$$

with

$$g_n(\phi) = \begin{cases} e^{-i\lambda\sin(\phi)} & n = -1 \\ e^{i\lambda\sin(\phi)} & n = 0 \\ 1 & \text{else} \end{cases}. \tag{3.9}$$

The gauge transformation removes the extra driving term and thereby replaces the hopping by a time-dependent hopping from and to site 0. Note that the gauge transformation vanishes at full periods, i.e. $\mathbf{U}_0(2\pi \cdot k) = 1$ for integer $k$. This means the transformation will not change the wavefunction at full periods but only during a period. In fact in between full periods the wavefunction is only changed at the impurity site but not away from it. Therefore all scattering properties will not be affected by the transformation.

We can rewrite the time-dependent couplings into Fourier modes $g_n(\phi) = \sum_a g_{na}e^{-ia\phi}$ using the Jacobi–Anger expansion $e^{iz\sin\phi} = \sum_{a=-\infty}^{\infty} J_a(\phi)e^{ia\phi}$ (see [25] §10.12):

$$g_{na} = \begin{cases} J_a(\lambda) & n = -1 \\ (-1)^a J_a(\lambda) & n = 0 \\ \delta_{a,0} & \text{else} \end{cases} \tag{3.10}$$

and by inserting into the Hamiltonian $\mathbf{H}^{\text{gauge}} = \sum_a \mathbf{H}^{\text{gauge}}_a e^{-ia\phi}$:

$$\mathbf{H}^{\text{gauge}}_a = -\frac{J}{\omega}\left[\sum_{n\sigma} g_{na}\mathbf{c}^\dagger_{n\sigma}\mathbf{c}_{n+1\sigma} + g^*_{n,-a}\mathbf{c}^\dagger_{n+1\sigma}\mathbf{c}_{n\sigma}\right] + \frac{U}{\omega}\mathbf{H}_{\text{U}}\delta_{a,0}. \tag{3.11}$$

Here $J_a(\lambda)$ is the $a$'th Bessel function.

Let us discuss the effects of the gauge transformation in the extended Hilbert space. Before the gauge transformation the layers in the extended system were coupled at site 0 to the previous and next layer. In figure 3.2(a) we sketch such a layer for the two particle case. The blue dots represent points which are coupled to the neighboring layers. After the gauge transformation the situation is much more complicated. Instead of a driven potential we now have a driven hopping which involves sites $-1, 0$ and 1 (see figure 3.2(b)). Furthermore the layers are now not only coupled to their neighbors, but rather at sites $-1, 0, 1$ every layer $a$ is coupled to every other layer $b$ with coupling strength $g_{n,a-b} \sim J_{a-b}(\lambda)$. In particular this is even true for $a = b$, which means that the hopping from and to site 0 is renormalized to $JJ_0(\lambda)$ (indicated by dashed lines in figure 3.2(b)).

On the first sight the gauge transformation made the problem dramatically more complicted. So what have we gained from performing the gauge transformation? The answer to this is that we would like to take the limit $J/|U| \to 0$ as in the plain Fermi-Hubbard model (see section 2.1.4) and find an effective Hamiltonian for pair dynamics in a single layer. The original Hamiltonian had the driving term which resulted in a strong coupling between the layers at site 0. The gauge transformation removed this term and replaced it by a complicated hopping term coupling to all layers. But no matter

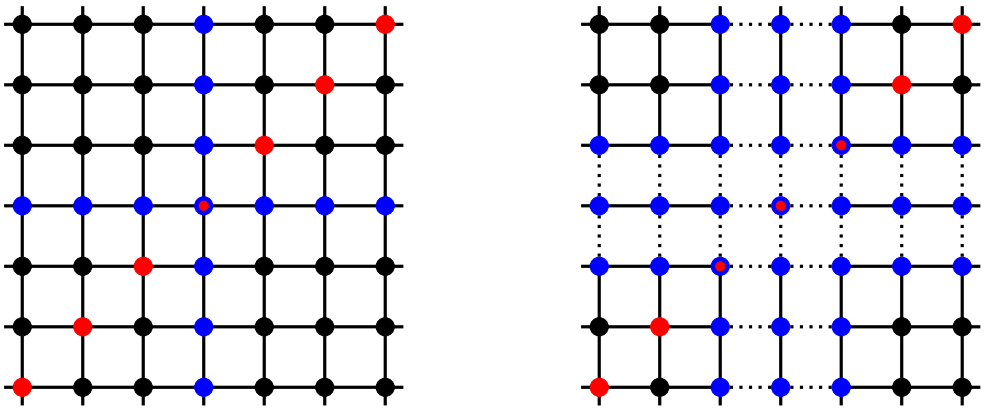

(a) (b)

Figure 3.2: View from top onto a single layer for two particles. The x and y components are the position of the first and second particle respectively. The Hubbard interaction $U$ acts on the sites marked in red: (a) Layer for the original Hamiltonian (3.1). The blue sites are coupled to neighboring layers. See figure 3.1(b) for the full system. (b) Layer for the gauge transformed Hamiltonian (3.8). At the blue sites the layer is coupled to all other layers. Solid lines describe normal hopping $J$ and dashed lines describe scaled hopping $JJ_0(\lambda)$.

how complicated this hopping term might be, it will still be proportional to $J$. In the limit $J/|U| \to 0$ it will become small and can therefore be treated via perturbation theory. This is the reason for introducing the gauge transformation.

### A remark on the non-resonant case

In this chapter we will focus only on the non-resonant case. Here the frequency $\omega$ is so large that any energetically allowed outgoing state must remain in the same layer as the incoming state. For one particle this means $\omega > 4J$ or $\alpha = J/\omega < 0.25$. For two particles it is a bit more complicated since we have a free and a bound particle band. In addition to avoiding excitations in the same band we need to make sure that by adding any multiple of $\omega$ to the lower bound pair band we can never end up in the upper free particle band. From the first requirement we find $\omega > 8J$. The second one implies that for any integer $a$ we need to satisfy:

$$a\omega \notin \left[|U| - 4J, \sqrt{|U|^2 + 16J^2} + 4J\right]. \tag{3.12}$$

If $J/|U|$ is small we can replace the square root in the upper bound by $|U|$ and find

$$a\omega \notin [|U| - 4J, |U| + 4J]. \tag{3.13}$$

In other words if we express all quantities in multiples of $\omega$, i.e. $\alpha = J/\omega$ and $u = U/\omega$, we need that $\alpha$ is so small s.t. the distance between $|u|$ and the nearest integer is bigger than $4\alpha$. For example for $u = -0.5$ the maximal possible value of $\alpha$ is $\alpha = 0.125$. If $\alpha$ is below this threshold we will be in the non-resonant case. In a later chapter 5 we will also consider the resonant case.

## 3.2 Analytical results in the limit $J/\omega \to 0$

The problem is too complicated to solve in general. However as we want to study bound pairs we could try to find a suitable limiting case where the calculation simplifies. In section 2.1.4 we learned that there is sort of a 'natural' limit for studying bound pairs namely $U/J \to -\infty$. In this limit the two particles form a localized pair which lives on an effective 1D system. Therefore this seems to be the correct limit to study pairs scattering off the impurity. There is however a new energy scale $\omega$ in the system. Before we can study the limit we need to fix how $\omega$ scales. From the above considerations for the non-resonant case we know $\alpha = J/\omega$ can be at maximum $\alpha < 0.125$, while there is no restriction on $u = U/\omega$. Since 0.125 is already a small number the limit $\alpha \to 0$, while keeping $u$ finite, seems to be quite promising. Note that this limit can either be thought of as keeping $U$ and $\omega$ fixed and letting $J$ go to 0 or as keeping $J$ fixed and letting $U$ and $\omega$ go to $\infty$.

### 3.2.1 Single particle case

For a single particle the Hubbard interaction is irrelevant. We can derive the limiting Hamiltonian by means of a high-frequency expansion as done in appendix A.1. It is given as the average of the time-dependent Hamiltonian over one period:

$$\mathbf{H}^{\text{single}} = -\frac{J}{\omega}\left[\sum_{n\neq -1,0}\left(\mathbf{c}_n^\dagger \mathbf{c}_{n+1} + \mathbf{c}_{n+1}^\dagger \mathbf{c}_n\right) + J_0(\lambda)\sum_{n=-1,0}\left(\mathbf{c}_n^\dagger \mathbf{c}_{n+1} + \mathbf{c}_{n+1}^\dagger \mathbf{c}_n\right)\right]. \tag{3.14}$$

The impurity in the effective model is not given as an extra potential but rather by a different hopping at the center site.

### 3.2.2 Particle pair

Here we also need to take into account $U$. Since $\alpha = J/\omega \to 0$ we are automatically in the non-resonant case as long as $u = U/\omega$ is not an integer. The procedure to arrive at the limiting model is similar to the Schrieffer-Wolff transformation in the plain Fermi-Hubbard model. The difference here is that we have to deal with a time-dependent hopping. We will use an extension of the Schrieffer-Wolff transformation called the Floquet-Schrieffer-Wolff transformation [22]. It simultaneously performs the Schrieffer-Wolff transformation and the time-averaging of the high-frequency expansion. The detailed derivation is given in appendix A.3.

We insert the Fourier components (3.10) into (A.33). The resulting effective Hamiltonian again only lives in the **P** sector (that is the subspace where all particles are paired) and has the following form

$$\mathbf{H}^{\text{pair}} = \sum_n \left[W_n \frac{1}{2}\left(\eta_n^+ \eta_{n+1}^- + \eta_{n+1}^+ \eta_n^-\right) + Z_n \hat{\mathbf{n}}_{n\uparrow}\hat{\mathbf{n}}_{n+1\uparrow} - \mu_n \hat{\mathbf{n}}_{n\uparrow}\right]. \tag{3.15}$$

The parameters are given by

$$W_n = \begin{cases} -\frac{4J^2}{\omega^2} \sum_a \frac{(-1)^a J_a(\lambda)^2}{|u|-a} & n = -1, 0 \\ -\frac{4J^2}{|u|\omega^2} & \text{else} \end{cases} \tag{3.16}$$

$$Z_n = \begin{cases} \frac{4J^2}{\omega^2} \sum_a \frac{J_a(\lambda)^2}{|u|-a} & n = -1, 0 \\ \frac{4J^2}{|u|\omega^2} & \text{else} \end{cases} \tag{3.17}$$

$$\mu_n = \begin{cases} \frac{2J^2}{|u|\omega^2} + \frac{2J^2}{\omega^2} \sum_a \frac{J_a(\lambda)^2}{|u|-a} & n = -1, 1 \\ \frac{4J^2}{\omega^2} \sum_a \frac{J_a(\lambda)^2}{|u|-a} & n = 0 \\ \frac{4J^2}{|u|\omega^2} & \text{else} \end{cases} . \tag{3.18}$$

These parameters are not defined if $|u|$ is an integer, which underlines that they are only valid in the non-resonant case. We can easily see that away from the impurity the model reduces to the result for the plain Fermi-Hubbard model in equation (2.15). Around the impurity we find different pair hoppings, pair interactions and potentials. Again we can ignore the pair interaction term $Z_n$ since we only consider a single pair. For two particles, i.e. one pair, this system reduces to a hopping Hamiltonian with a different hopping and an external potential around the impurity.

Before we go on to calculating the transmission amplitudes, we would like to state the result for the first order correction to this Hamiltonian. As we explain in appendix A.4 one can easily see that it vanishes. This implies that the transmission amplitude will not have a linear dependence on $\alpha$, but at most a quadratic dependence. Since we, in order to stay in the non-resonant case, only deal with relatively small $\alpha < 0.125$ we can expect that the quadratic term is negligible even at the highest $\alpha = 0.125$. Therefore we can expect that the transmission amplitude derived from (3.15) will be a good approximation throughout the non-resonant case.

### 3.2.3 Calculating the transmission in the effective models

In the limit where $J/\omega \to 0$ for one and two particles we found that the system is equivalent to a hopping Hamiltonian with an impurity consisting of a different hopping and a potential (see figure 3.3 for a detailed sketch of the system). In both cases the system can be rewritten as a model on a 1D lattice with the following Hamiltonian

$$\begin{aligned} \mathbf{H}^{\text{abstract}} = -J_{\text{eff}} \Big[ & \sum_{n \neq -1,0} \Big( |n\rangle \langle n+1| + |n+1\rangle \langle n| \Big) + \gamma \sum_{n=-1,0} \Big( |n\rangle \langle n+1| + |n+1\rangle \langle n| \Big) \\ & + v_0 |0\rangle \langle 0| + v_1 \Big( |-1\rangle \langle -1| + |1\rangle \langle 1| \Big) \Big]. \end{aligned} \tag{3.19}$$

We can take this abstract Hamiltonian and solve the scattering problem with an incoming plane wave $\sim e^{ikn}$. The derivation is again done in the appendix D.2. The transmission amplitude is

$$t_k = \frac{\gamma^2}{1 - v_1 e^{ik}} \frac{-2i \sin k}{(2\cos k - v_0)(1 - v_1 e^{ik}) - 2\gamma^2 e^{ik}}. \tag{3.20}$$

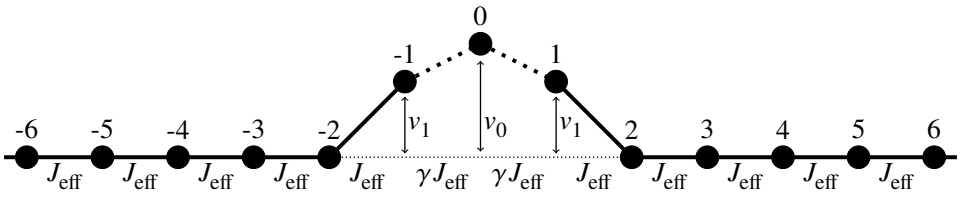


Figure 3.3: Sketch of the abstract Hamiltonian which describes the scattering situation. Away from the impurity the system is an ordinary hopping Hamiltonian with hopping $J_{\text{eff}}$ (indicated by solid lines). The effective impurity consists of two parts. First there is a different hopping $\gamma J_{\text{eff}}$ between sites $-1$ and 0 and between 0 and 1 (indicated by dashed lines). Second at sites $-1, 0$ and 1 there is also an additional potential $v_1$ or $v_0$ (indicated by the different height of the sites).

Note that the result does not depend on $J_{\text{eff}}$, because it is an overall factor which is irrelevant for scattering. The transmission probability for $v_0 = 2v_1$ (which is the only case we are going to need) is then given by $T_k = |t_k|^2$:

$$T_k = \frac{\gamma^4}{1 + \left(\frac{\cos k - v_1}{\sin k}\right)^2} \frac{1}{\left[\left(\cos k - v_1\right)^2 - \gamma^2\right]^2 + \left(\cos k - v_1\right)^2 \sin^2 k}. \tag{3.21}$$

#### Single particle case

For a single particle we can directly compare equations (3.14) and (3.19) to find

$$J_{\text{eff}} = J \tag{3.22}$$

$$\gamma = J_0(\lambda) \tag{3.23}$$

$$v_0 = v_1 = 0. \tag{3.24}$$

This means that the hopping around site 0 is scaled by a factor $J_0(\lambda)$ and the potential terms vanish. The later observation allows to simplify the transmission probability to (see appendix D.2)

$$T_k = |t_k|^2 = \frac{1}{1 + \left(\frac{1}{\gamma^2} - 1\right)^2 \cot^2 k}. \tag{3.25}$$

Note that this result has already been derived in [7]. We give a plot of it in figure 3.4. As a function of momentum $k$ the transmission can be described as follows: It is always zero for $k = 0$ or $k = \pi$ and always one for $k = \pi/2$. It looks like a symmetric peak around $k = \pi/2$ where the peak width depends on $\gamma = J_0(\lambda)$. For $\gamma = 1$ there is perfect transmission while for $\gamma = 0$ there is no transmission. Since the Bessel function is always below 1 the driven impurity can only reduce the transmission (we give a plot of $J_0(\lambda)$ in figure C.1). For some values of $\lambda$, namely at the zeros of the Bessel function, the transmission completely vanishes and therefore all incoming particles will be reflected.

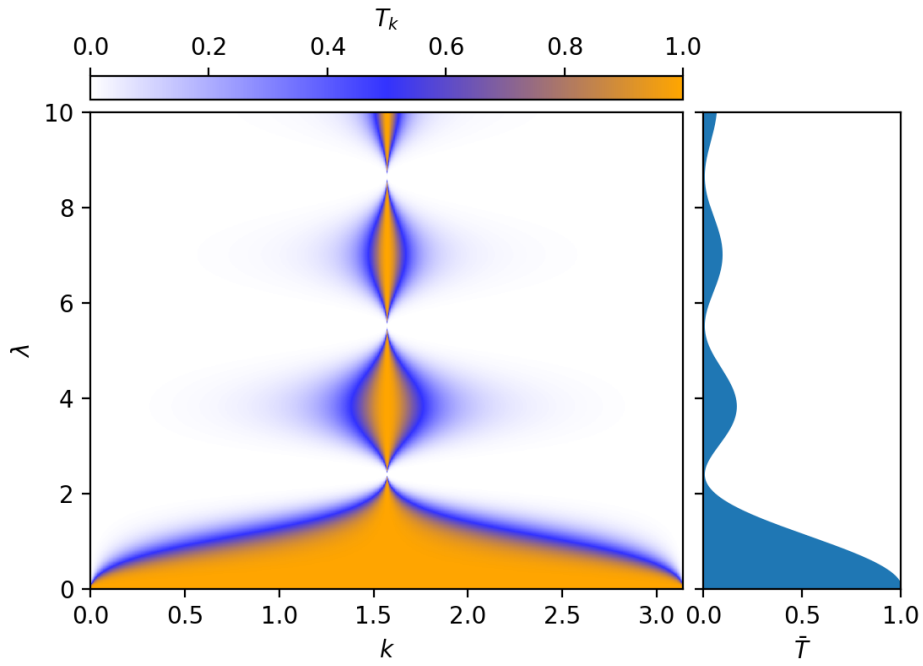


Figure 3.4: Single particle transmission $T_k$ as function of momentum $k$ and driving strength $\lambda$. The plot on the right displays the momentum averaged transmission $\bar{T}$.

#### Particle pair case

For a particle pair (3.15) we can read of the parameters for the abstract model (3.19) to be

$$J_{\text{eff}} = -\frac{1}{2}W_\infty = \frac{2J^2}{|u|\omega^2} \tag{3.26}$$

$$\gamma = \frac{-\frac{1}{2}W_0}{J_{\text{eff}}} = \sum_a \frac{|u|(-1)^a J_a(\lambda)^2}{|u| - a} \tag{3.27}$$

$$v_1 = \frac{\mu_1 - \mu_\infty}{J_{\text{eff}}} = \sum_a \frac{|u| J_a(\lambda)^2}{|u| - a} - 1 \tag{3.28}$$

$$v_0 = \frac{\mu_0 - \mu_\infty}{J_{\text{eff}}} = 2\left(\sum_a \frac{|u| J_a(\lambda)^2}{|u| - a} - 1\right) = 2v_1. \tag{3.29}$$

Note that in the last two equations we subtracted the overall constant potential $\mu_\infty = \frac{4J^2}{|u|\omega^2}$ from the model.

In contrast to the single particle case the transmission probability for a pair is more complicated. Again it is always zero for $k = 0$ or $k = \pi$, but it neither is a symmetric shape nor does it have to reach 1 for some value of $k$. The general shape can roughly be described as an asymmetric peak of varying width and height. As in the single particle case there are parameters for which the transmission completely vanishes. However in this case we are also able to find parameters where the transmission

is almost one for almost the full range of $k$. There are even some isolated parameter combinations where perfect transmission occurs. This happens when both $v_1 = 0$ and $\gamma = \pm 1$, which is rather rare.

## 3.3 Discussion of the pair transmission

Since the transmission probability for a pair is rather complicated we would like to discuss it further and at least roughly understand its features. We will split the discussion into two parts. First we will consider the effective model (3.21) with parameters $\gamma$ and $v_1$. Second we will express $\gamma$ and $v_1$ through $\lambda$ and $|u|$.

### 3.3.1 Discussion of the effective model

Instead of directly trying to understand the transmission as a function of $\lambda$ and $|u|$ it is actually more instructive to first consider the transmission as a function of $\gamma$ and $v_1$.

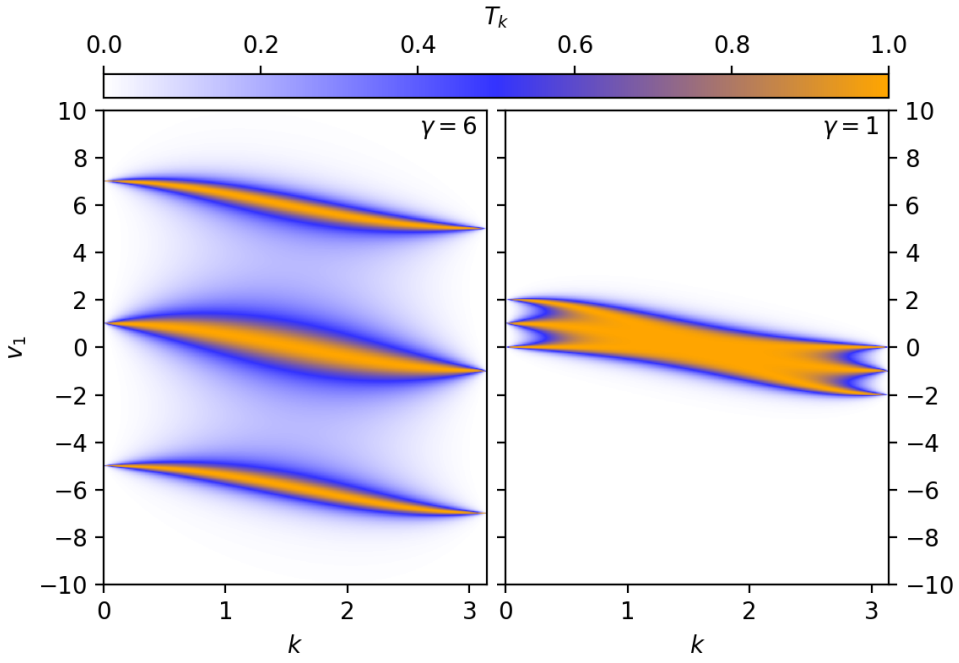


Figure 3.5: Transmission in the effective model for $\gamma = 6$ and $\gamma = 1$ as function of momentum $k$ and parameter $v_1$.

In figure 3.5 we give the transmission as a function of $k$ and $v_1$ for $\gamma = 6$ and $\gamma = 1$. The plot for $\gamma = 6$ is very representative for all $|\gamma| > 1$. The transmission mostly vanishes apart from three branches where it goes even up to full transmission $T_k = 1$. The position of the branches lie around $v_1 = 0, \pm|\gamma|$. Their form can be described by $v_1 = \cos k$ or $v_1 = \pm|\gamma| + \cos k$. Note that for $k = 0, \pi$ the transmission always vanishes expect at the branches $v_1 = \pm 1$ and $v_1 = \pm|\gamma| \pm 1$.

Imagine we would keep $\gamma$ fixed and sweep $v_1$ starting from well below $-|\gamma|$ up to well above $|\gamma|$. How will the transmission as a function of $k$ look like (i.e. a horizontal cut in the left plot of figure 3.5)? For $v_1 < -|\gamma| - 1$ the transmission will mostly vanish. Then for $v_1 \approx -|\gamma| - 1$ a transmission

peak will emerge for high momenta. As we increase $v_1$ further the peak will move its position from high momenta to low momenta and finally disappear above $v_1 \approx -|\gamma| + 1$. The emergence of such a peak which moves from high momenta to low momenta will happen two more times, one time for $-1 < v_1 < 1$ and a another time for $|\gamma| - 1 < v_1 < |\gamma| + 1$.

The discussion so far considered $|\gamma| > 1$. As we decrease $|\gamma|$ to 1 the three branches will no longer be separate. They will start to overlap as can be seen in the right plot of figure 3.5. The value $|\gamma| = 1$ is a very special value. The left side of the lower branch and the right side of the higher branch overlap such that we get at $v_1 = 0$ full transmission $T_k = 1$ for all values of $k$. Note that one can directly see this from the effective model (see figure 3.3) where $\gamma = 1, v_0 = v_1 = 0$ describes a free chain without an impurity. Furthermore because only the absolute value of $\gamma$ enters the transmission probability (3.21) both $\gamma = \pm 1$ lead to perfect transmission.

If we decrease $|\gamma|$ even further the three branches overlap even more, but become thinner and thinner and eventually vanish for $\gamma = 0$. Again one can directly see from the effective model (see figure 3.3) that the transmission has to vanish at $\gamma = 0$, because $\gamma$ describes the hopping parameter at the impurity.

To see the appearance of the three branches from the formula (3.21) first note that $v_1$ only appears in the combination $w_k = v_1 - \cos k$. This already explains the cosine shape of the branches:

$$T_k = \frac{\gamma^4}{1 + \frac{w_k^2}{\sin^2 k}} \frac{1}{\left[w_k^2 - \gamma^2\right]^2 + w_k^2 \sin^2 k}. \tag{3.30}$$

In a second step introduce $w_k = \xi_k |\gamma|$ and $\tilde{\gamma}_k = \frac{|\gamma|}{\sin k}$:

$$T_k = \frac{\gamma^4}{\left[\xi_k^2 - 1\right]^2 \gamma^4 + \xi_k^2 \gamma^2 \sin^2 k + \frac{\gamma^6}{\sin^2 k} \xi_k^2 \left[\xi_k^2 - 1\right]^2 + \xi_k^4 \gamma^4} \tag{3.31}$$

$$= \frac{1}{\left[\xi_k^2 - 1\right]^2 + \frac{\xi_k^2}{\tilde{\gamma}_k^2} + \tilde{\gamma}_k^2 \xi_k^2 \left[\xi_k^2 - 1\right]^2 + \xi_k^4}. \tag{3.32}$$

Although being written down using strange parameters the last equation is actually very useful because it only depends on two parameters $\xi_k$ and $\tilde{\gamma}_k$ unlike (3.21) which depends on the three parameters $\gamma, v_1$ and $k$. Now consider the case where $\xi_k$ is fixed (i.e. the ratio between $v_1$ and $\gamma$ is fixed) while $\tilde{\gamma}_k \to \infty$. The transmission will vanish unless $\xi_k = 0$ or $\xi_k^2 = 1$, where $T_k \to 1$. Recall that $\tilde{\gamma}_k = \frac{|\gamma|}{\sin k} \to \infty$ either means that $|\gamma|$ is large or that $\sin k \to 0$, in other words for small $k \to 0$ or large momenta $k \to \pi$. Therefore whenever $|\gamma|$ is large or $k$ is close to the boundary of the Brillouin zone transmission is only possible if $\xi_k \approx 0, -1, 1$. In the original parameters this translates to $v_1 \approx \cos k$ or $v_1 \approx \pm|\gamma| + \cos k$, which explains the appearance of the three branches in the transmission $T_k$.

In figure 3.6 we give a plot of $T_k$ as a function of $\xi_k$ and $\tilde{\gamma}_k$. We can see that the transmission vanishes outside of $-1 < \xi_k < 1$ independently of $\tilde{\gamma}_k$. For $\tilde{\gamma}_k \gtrsim 2$ we have that transmission only occurs for $\xi_k \approx -1, 0, 1$ as discussed before. For $\tilde{\gamma}_k < 2$ the three regions merge and we have transmission throughout $-1 < \xi_k < 1$.

To conclude, the transmission $T_k$ is only significantly above zero in three branches $v_1 \approx \cos k$ and $v_1 \approx \pm|\gamma| + \cos k$. At fixed parameters $\gamma$ and $v_1$ they lead to a peak in the transmission profile, which

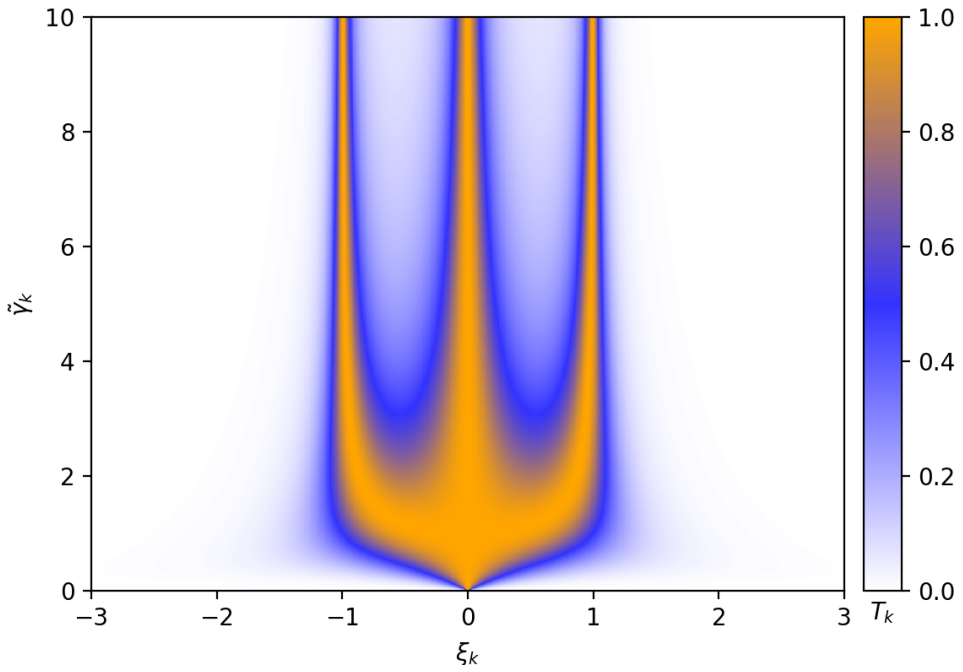


Figure 3.6: Transmission in the effective model as function of $\xi_k$ and $\tilde{\gamma}_k$.

position depends on $v_1$. If $|\gamma|$ becomes of order $|\gamma| \approx 1$ these branches merge and lead to a more complicated transmission profile as a function of $k$. In the special case $\gamma = \pm 1$ and $v_1 = 0$ the merging is such that there is full transmission $T_k = 1$ for all $k$.

### 3.3.2 Discussion of the parameters for $|u| > 1$

Now we understand how the transmission depends on the effective parameters $\gamma$ and $v_1$. But the experimentally accessible parameters are $\lambda$ and $u$ from which one can calculate $\gamma$ and $v_1$ using equations (3.27) and (3.28):

$$\gamma = \sum_a \frac{|u|(-1)^a J_a(\lambda)^2}{|u| - a} \tag{3.33}$$

$$v_1 = \sum_a \frac{|u| J_a(\lambda)^2}{|u| - a} - 1. \tag{3.34}$$

Both are given by sums over all Bessel functions (we give plots and an overview over their relevant properties in appendix C). The main difference is that $\gamma$ includes an alternating factor $(-1)^a$ in each term.

Since infinite sums are not easy to analyze we would like to approximate them somehow. The Bessel functions can roughly be thought as oscillating functions with an amplitude $\sim 1/\sqrt{\lambda}$ that are somehow regularized for $\lambda \to 0$. Since the amplitude does not depend on $a$ all terms $J_a(\lambda)^2$ will have roughly the same size. Luckily in each term there is a factor $\frac{1}{|u|-a}$. This factor goes to zero as $a \to \pm\infty$ and has is maximum at the two integers closest to $|u|$. Especially if $|u|$ is close to one of

these integers, then the factor will become very large and so we can approximate the full sum by this one term (this case will be considered in more detail later in section 3.3.4). If $|u|$ is between both integers we need to take both terms corresponding to the two closest integers into account. We will therefore make the approximation:

$$\gamma \approx |u| \frac{(-1)^{\lfloor |u| \rfloor} J_{\lfloor |u| \rfloor}(\lambda)^2}{|u| - \lfloor |u| \rfloor} + |u| \frac{(-1)^{\lceil |u| \rceil} J_{\lceil |u| \rceil}(\lambda)^2}{|u| - \lceil |u| \rceil} \tag{3.35}$$

$$v_1 \approx |u| \frac{J_{\lfloor |u| \rfloor}(\lambda)^2}{|u| - \lfloor |u| \rfloor} + |u| \frac{J_{\lceil |u| \rceil}(\lambda)^2}{|u| - \lceil |u| \rceil} - 1 \tag{3.36}$$

where $\lfloor |u| \rfloor$ and $\lceil |u| \rceil$ are the integer below and above $|u|$. We will now compare this approximation to the actual values for $\gamma$ and $v_1$ separately. In this section we will use $|u| = 10.5$ as an example. This might be quite a high value, but the figures nicely show all relevant features which appear for all $|u| > 1$. Later we will also consider the case $|u| < 1$ separately because the behaviour there is a bit different.

#### Approximation for $\gamma$ for $|u| > 1$

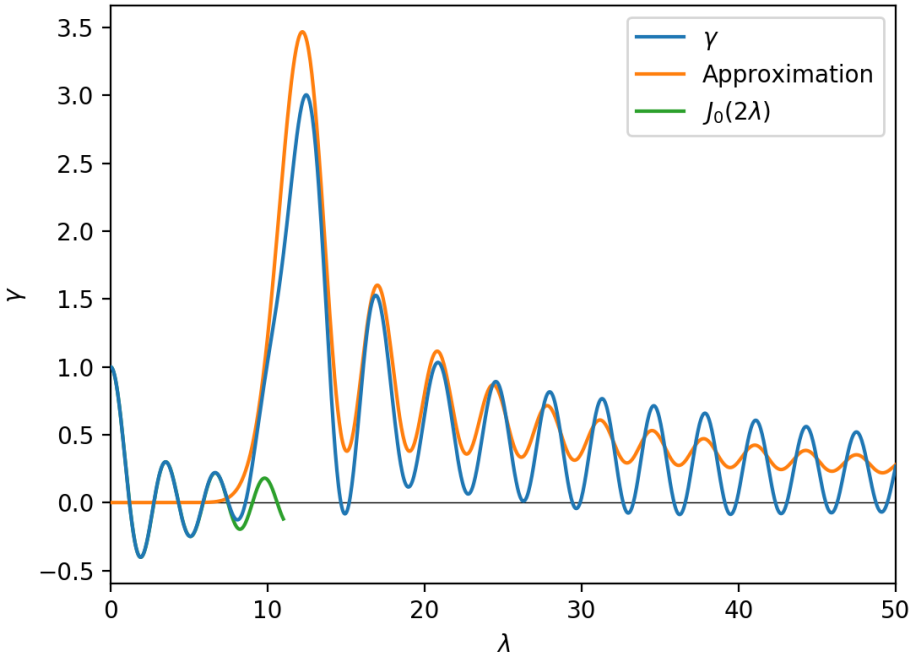


Figure 3.7: Value of $\gamma$ as function of driving strength $\lambda$ for $|U|/\omega = 10.5$ (blue) and its approximation using two terms (orange). Also we give $J_0(2\lambda)$ (green) which is an approximation for $\lambda < |u|$.

In figure 3.7 we show $\gamma$ as a function of $\lambda$ for $|u| = 10.5$ (blue). Let us describe the typical behaviour of $\gamma$ as a function of a $\lambda$. At $\lambda = 0$ we start at $\gamma = 1$ which then decreases. Then the function starts to oscillate around $\gamma = 0$ until there is a prominent peak at $\lambda \approx |u| + 1.5$. The sign of this peak is positive for $\lfloor |u| \rfloor = 0, 2, 4, \ldots$ and negative for $\lfloor |u| \rfloor = 1, 3, 5, \ldots$. After this peak $\lambda > |u| + 1.5$,

$\gamma$ slowly decays and oscillates while staying (mostly) either on the positive or negative side. The amplitude of oscillations decays roughly as $\sim 1/\lambda$.

From figure 3.7 we can see that our approximation using the closest two integers (orange) is completely off for $\lambda < |u|$, but nicely fits the peak at $\lambda = |u| + 1.5$. For $\lambda > |u| + 1.5$ the approximation also decays while oscillating. Even though the amplitudes of oscillations are not the same we find that the frequency of oscillations matches.

Let us try to understand what we see. We will start with $\lambda < |u|$ where our approximation completely fails since, instead of an oscillating function, it gives a flat function. This is because the Bessel function has the following Taylor expansion for $\lambda \to 0$:

$$J_a(\lambda) = \frac{1}{a!}\left(\frac{\lambda}{2}\right)^a + O\left(\lambda^{a+2}\right). \tag{3.37}$$

If $|u|$ is sufficiently large $J_{\lfloor|u|\rfloor}(\lambda)$ and $J_{\lceil|u|\rceil}(\lambda)$ are going to grow only very slowly around $\lambda = 0$. The oscillations for small $\lambda$ have to originate from terms with small $a$. To estimate them let us assume that $|u| \gg 1$ and split the sum into two parts with a cutoff $A \ll |u|$:

$$\gamma = \sum_{a=-A}^{A} \frac{|u|(-1)^a J_a(\lambda)^2}{|u| - a} + \sum_{|a|>A} \frac{|u|(-1)^a J_a(\lambda)^2}{|u| - a} = \sum_{a=-A}^{A} \frac{|u|(-1)^a J_a(\lambda)^2}{|u| - a} + O\left(\lambda^{2A+2}\right). \tag{3.38}$$

For $\lambda$ being small enough the right sum is going to be negligible (unless $|u|$ is really close to an integer). In the first sum, since $A \ll |u|$ we can approximate $\frac{|u|}{|u|-a} = 1 + O(1/|u|)$:

$$\gamma \approx \sum_{a=-A}^{A} (-1)^a J_a(\lambda)^2 + O\left(\frac{1}{|u|}\right) + O\left(\lambda^{2A+2}\right) \tag{3.39}$$

$$\approx \sum_{a=-\infty}^{\infty} (-1)^a J_a(\lambda)^2 + O\left(\frac{1}{|u|}\right) + O\left(\lambda^{2A+2}\right) \tag{3.40}$$

$$= J_0(2\lambda) + O\left(\frac{1}{|u|}\right) + O\left(\lambda^{2A+2}\right). \tag{3.41}$$

where in the second step we added the missing terms into the sum and thereby making another error of $O\left(\lambda^{2A+2}\right)$. In the last step we used Neumann's addition theorem from appendix C.5. The derivation above shows that for small $\lambda$ and large $|u|$ we can approximate $\gamma \approx J_0(2\lambda)$[1]. We also add a plot of this function into figure 3.7 (green) to show that it indeed describes the first oscillatory part, up to the prominent peak, quite well.

Let us go on to the prominent peak. For $\lambda < |u|$ we alternately add and subtract the $J_a(\lambda)^2$ from each other, thereby cancelling each other and creating the oscillations around 0. Now for $\lambda \approx |u| + 1.5$ three important things happen. First of all at $\lambda \approx |u| + 1.5$ the two closest Bessel functions $J_{\lfloor|u|\rfloor}(\lambda)$ and $J_{\lceil|u|\rceil}(\lambda)$ have their first (and highest) maximum as discussed in appendix C.4. Second the prefactor $\frac{1}{|u|-a}$ also has a maximum here. Third and most important these two terms do not cancel each other,

[1] The reader might wonder why the result is the same as for a single particle: We can also think of this limit as $|u| \to \infty$. In this limit both particles are always on the same site and therefore behave as a single localized particle. The only difference is that it is driven with twice the coupling strength, which explains why $\lambda$ is replaced by $2\lambda$.

because the prefactor $\frac{1}{|u|-a}$ switches sign and therefore cancels the $(-1)^a$:

$$\gamma \approx (-1)^{\lfloor |u| \rfloor} |u| \left( \frac{J_{\lfloor |u| \rfloor}(\lambda)^2}{|u| - \lfloor |u| \rfloor} + \frac{J_{\lceil |u| \rceil}(\lambda)^2}{\lceil |u| \rceil - |u|} \right). \tag{3.42}$$

Note this also shows that the sign of the peak depends only on whether $\lfloor |u| \rfloor$ is an even or an odd number.

Because the terms corresponding to the two closest integers to $|u|$ have the highest prefactor, they will still dominate for $\lambda > |u| + 1.5$. However as we increase $\lambda > |u| + 1.5$ more and more Bessel functions will start oscillating with the same amplitude $\sim 1/\sqrt{\lambda}$ and so more and more terms in the sum will become relevant. Since the prefactor $\frac{1}{|u|-a}$ decreases only slowly, there is the extra $(-1)^a$ and the amplitudes of these oscillations are comparable, the whole sum is going to be quite complicated with a lot of near cancellations. In other words it is going to converge slowly and so it is also hard to predict it accurately. We will therefore only summarize the main features. We know that, since all Bessel functions decay as $\sim 1/\sqrt{\lambda}$, that the envelope of $\gamma$ will decay as $\sim 1/\lambda$. Also since the two terms of (3.42) still dominate the sum we can expect that $\gamma$ will also either stay positive or negative (this is not exactly true as can be seen in figure 3.7, but still holds in a big range). We can also observe that (roughly) the period of oscillations of $\gamma$ (blue) follows the period of oscillations of the approximation (orange).

#### Approximation for $v_1$ for $|u| > 1$

Let us repeat the steps we did for $\gamma$ also for $v_1$:

$$v_1 = \sum_a \frac{|u| J_a(\lambda)^2}{|u| - a} - 1. \tag{3.43}$$

In figure 3.8 we plot $v_1$ (blue) and its approximation by two terms (orange) for $|u| = 10.5$. For small $\lambda$ the function starts at $v_1 = 0$ and then slowly grows. Around $\lambda \approx |u| + 1.5$ we first have a peak $v_1 > 0$ and then a rapid switch of sign to another peak $v_1 < 0$. After this peak we again find an oscillating decay to $v_1 \to -1$. For most values of $|u|$ the function stays completely negative above $\lambda > 1.5$, however it can also become positive at the peaks.

The approximation by the two closest terms of the sum (orange) is again completely off for $\lambda \approx 0$, where it predicts $v_1 = -1$ instead of $v_1 = 0$. Apart from that for $\lambda > |u| + 1.5$ the approximation captures the oscillatory behaviour quite well. Compared to $\gamma$ where for $|u| = 10.5$ the approximation was only able to explain the frequency but not the amplitude, the approximation of $v_1$ captures both.

Let us again go through the features one by one. The approximation fails for $\lambda \approx 0$, which, as for $\gamma$, is not surprising. For small $\lambda$ we also need to take the Bessel functions for low $a \ll |u|$ into account. We can redo the argumentation which led to (3.41):

$$v_1 \approx \sum_{a=-\infty}^{\infty} J_a(\lambda)^2 - 1 + O\left(\frac{1}{|u|}\right) + O\left(\lambda^{2A+2}\right) \tag{3.44}$$

$$= 0 + O\left(\frac{1}{|u|}\right) + O\left(\lambda^{2A+2}\right). \tag{3.45}$$

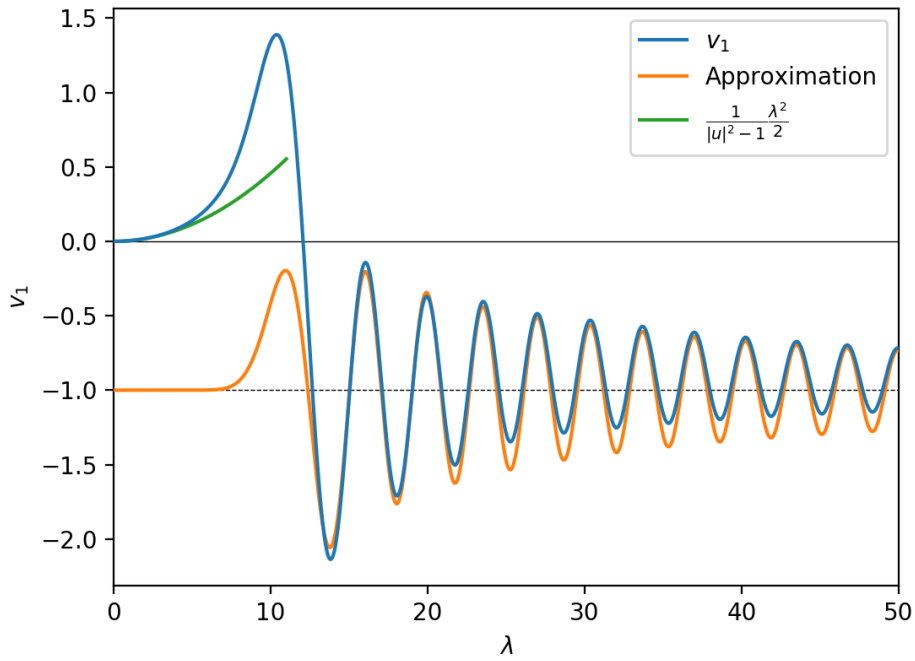


Figure 3.8: Value of $v_1$ as function of driving strength $\lambda$ for $|U|/\omega = 10.5$ (blue) and its approximation using two terms (orange). Also we give the second order Taylor approximation of $v_1$ at $\lambda = 0$ (green). For large $\lambda$, $v_1$ converges towards $-1$ (dashed line).

This time the sum gives $\sum_a J_a(\lambda)^2 = 1$ (see appendix C.5) instead of a complicated function, which cancels the $-1$ in the definition of $v_1$ and therefore shows $v_1 = 0$ at $\lambda = 0$. We can even go one step further and calculate the Taylor expansion of $v_1$ up to the second order in $\lambda$ (green curve in figure 3.8). It is given by (calculation done in the appendix C.6):

$$v_1 = \frac{1}{|u|^2 - 1}\frac{\lambda^2}{2} + O\left(\lambda^4\right). \tag{3.46}$$

Since $\frac{1}{|u|^2-1} > 0$ we find that for all $|u| > 1$ the function $v_1$ grows around $\lambda = 0$.

Now let us turn our attention to the two peaks at $\lambda \approx |u| + 1.5$. We can rewrite the approximation to:

$$v_1 \approx |u|\left(\frac{J_{\lfloor|u|\rfloor}(\lambda)^2}{|u| - \lfloor|u|\rfloor} - \frac{J_{\lceil|u|\rceil}(\lambda)^2}{\lceil|u|\rceil - |u|}\right) - 1. \tag{3.47}$$

Note that now, because the $(-1)^a$ are missing there is a minus sign between the two terms. This means instead of adding up, both terms are actually subtracted. Since the first maximum of $J_{\lfloor|u|\rfloor}(\lambda)$ comes a bit before the first maximum of $J_{\lceil|u|\rceil}(\lambda)$, we observe first the positive maximum of $J_{\lfloor|u|\rfloor}(\lambda)$ which then is quickly followed by the negative maximum of $J_{\lceil|u|\rceil}(\lambda)$. This explains the quick sign change of $v_1$ around $|u| + 1.5$. After the two peaks we have again the oscillatory behaviour with a decay $\sim 1/\lambda$, because all Bessel functions decay equally fast $\sim 1/\sqrt{\lambda}$. Contrary to $\gamma$ where due to the $(-1)^a$ many terms of the sum cancelled each other, for $v_1$ all these terms add up. In other words the sum converges

much faster, which also explains why the approximation is much better than for $\gamma$. Note that due to the overall $-1$ outside of the sum $v_1$ goes to $-1$ for $\lambda \to \infty$.

#### Transmission depending on $\lambda$ and $u$

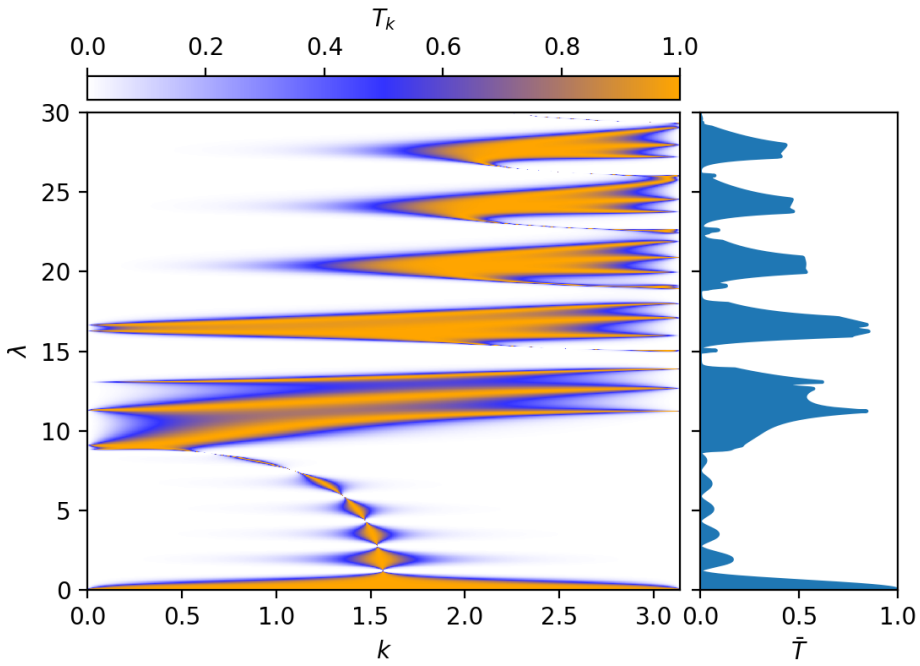


Figure 3.9: Pair transmission as function of momentum $k$ and driving strength $\lambda$ for $|U|/\omega = 10.5$. The plot on the right displays the momentum averaged transmission $\bar{T}$.

We now understand how the transmission behaves as a function of $\gamma$ and $v_1$ and we also understand how $\gamma$ and $v_1$ depend on $\lambda$ and $u$. We only need to put both behaviours together to get the full picture.

In figure 3.9 we give the transmission as a function of $k$ and $\lambda$ for fixed $|u| = 10.5$. Like for the parameters we find three distinct regimes. For $\lambda < |u| + 1.5$ we have a 'chain' of small connected parts where the transmission is locally high. This chain starts at $k = \pi/2$ and then slowly bends towards smaller $k$. Around $\lambda \approx |u| + 1.5$ we then have a region of quite high transmission throughout the whole Brillouin zone. After that there are alternating regions with transmission and without transmission. The regions with transmission are mainly concentrating on high momenta $k$. Also while the frequency of the appearance of these regions is roughly constant, their size in $k$ become smaller as $\lambda$ grows.

Before we start analyzing we would like to recall that the transmission always vanishes for $k = 0, \pi$, except when $v_1 = |\gamma| + 1, 1, -|\gamma| + 1$ (for $k = 0$) or $v_1 = |\gamma| - 1, -1, -|\gamma| - 1$ (for $k = \pi$). These situations can easily be identified in figure 3.9 as they are the distinct values of $\lambda$ where the transmission reaches the boundary of the figure. We will use this to explain the behaviour of the transmission. Let

us define:

$$\xi_0 = \frac{v_1 - 1}{|\gamma|} \tag{3.48}$$

$$\xi_\pi = \frac{v_1 + 1}{|\gamma|}. \tag{3.49}$$

Whenever $\xi_0 = 1, 0, -1$ we find a finite transmission for $k = 0$. Analogously if $\xi_\pi = 1, 0, -1$ we find a finite transmission for $k = \pi$. Even more note that we have $\xi_0 \leq \xi_k \leq \xi_\pi$, where $\xi_k = \frac{v_1 - \cos k}{|\gamma|}$. In particular whenever both $\xi_0, \xi_\pi$ are above 1 or below $-1$ the transmission will be low for all $k$ (recall figure 3.6). Therefore we will mostly study when $\xi_0$ and $\xi_\pi$ pass $\pm 1$, which can then be translated into whether transmission occurs or not.

From our previous considerations we can expect that the three regimes in figure 3.9 are linked to the different regimes of $\gamma$ and $v_1$. Let us go through them one by one. For $\lambda < |u| + 1.5$ we found that $\gamma = J_0(2\lambda)$ and $v_1 = \frac{1}{|u|^2 - 1}\frac{\lambda^2}{2}$, which grows quite slow. Without doing any complicated calculation we can immediately see that $v_1 \approx 0$ reduces to the single particle case. There we have $\gamma = J_0(\lambda)$ which is now replaced by $\gamma = J_0(2\lambda)$. The behaviour for $\lambda \approx 0$ is therefore similar to figure 3.4, only with twice the frequency. In particular this explains the small regions around $k = \pi/2$, where we have transmission. As we move away from $\lambda = 0$ we find that

$$\xi_0 = \frac{-1 + \frac{1}{|u|^2 - 1}\frac{\lambda^2}{2}}{|J_0(2\lambda)|} < -1 \tag{3.50}$$

$$\xi_\pi = \frac{1 + \frac{1}{|u|^2 - 1}\frac{\lambda^2}{2}}{|J_0(2\lambda)|} > 1 \tag{3.51}$$

where the last inequalities hold because $|J_0(2\lambda)| < 1$ (strictly speaking the inequality for $\xi_0 < -1$ only holds for $|u| > \frac{\sqrt{5}}{2} \approx 1.12$). Since $\xi_k$ can range from $\xi_0$ to $\xi_\pi$ it passes the full region $-1 < \xi_k < 1$ and we therefore find a small region around $k = \pi/2$ where the transmission does not vanish. This region is small because $|\gamma| = |J_0(2\lambda)| \ll 1$ and therefore transmission only occurs around $\xi_k \approx 0$ (see lower part of figure 3.6). In fact the size of the region is given by $J_0(2\lambda)$. In particular whenever $J_0(2\lambda) = 0$ the transmission vanishes completely. Because both $\xi_0, \xi_\pi$ grow with growing $\lambda$ the position of the small region with transition is not centred at $\pi/2$ any more, but rather shifts to smaller $k$, which leads to the arc structure to the left in figure 3.9. This can be seen from the definition of $\xi_k = \frac{v_1 - \cos k}{|\gamma|}$. Transmission only occurs around $\xi_k \approx 0$ and so the central momentum is given by $\cos k = v_1$. Using the Taylor expansion (3.46) of $v_1$ we find:

$$k = \arccos(v_1) \approx \frac{\pi}{2} - \frac{1}{|u|^2 - 1}\frac{\lambda^2}{2} + O\left(\lambda^4\right). \tag{3.52}$$

We would like to point out again that this is only valid for $\lambda \ll |u| + 1.5$ and is in particular only applicable for $|u| > 1$.

Let us go on to $\lambda \approx |u| + 1.5$. There we found that $\gamma$ had a prominent maximum, while $v_1$ quickly changed its sign from positive to negative. As a very rough approximation we can think of $\gamma$ being constant around $\lambda \approx |u| + 1.5$ and of $v_1$ as a linear function going from a high positive value to a low

negative one. The emerging picture is therefore a mirror version of figure 3.5 (with the distance of the branches according to $\gamma$). Of course the actual image in figure 3.9 looks a bit distorted, but one can clearly see three values of $\lambda$ on each side where the transmission reaches the boundary.

The third regime is the oscillatory part for $\lambda > |u| + 1.5$. We can see a periodic pattern which is, of course, due to the periodicity of $\gamma$ and $v_1$. We can use the approximations (3.42) and (3.47) to find

$$\xi_0 \approx \frac{\frac{J_{\lfloor|u|\rfloor}(\lambda)^2}{|u|-\lfloor|u|\rfloor} - \frac{J_{\lceil|u|\rceil}(\lambda)^2}{\lceil|u|\rceil-|u|} - 2}{\frac{J_{\lfloor|u|\rfloor}(\lambda)^2}{|u|-\lfloor|u|\rfloor} + \frac{J_{\lceil|u|\rceil}(\lambda)^2}{\lceil|u|\rceil-|u|}} \tag{3.53}$$

$$\xi_\pi \approx \frac{\frac{J_{\lfloor|u|\rfloor}(\lambda)^2}{|u|-\lfloor|u|\rfloor} - \frac{J_{\lceil|u|\rceil}(\lambda)^2}{\lceil|u|\rceil-|u|}}{\frac{J_{\lfloor|u|\rfloor}(\lambda)^2}{|u|-\lfloor|u|\rfloor} + \frac{J_{\lceil|u|\rceil}(\lambda)^2}{\lceil|u|\rceil-|u|}} = \frac{1 - \frac{|u|-\lfloor|u|\rfloor}{\lceil|u|\rceil-|u|}\frac{J_{\lceil|u|\rceil}(\lambda)^2}{J_{\lfloor|u|\rfloor}(\lambda)^2}}{1 + \frac{|u|-\lfloor|u|\rfloor}{\lceil|u|\rceil-|u|}\frac{J_{\lceil|u|\rceil}(\lambda)^2}{J_{\lfloor|u|\rfloor}(\lambda)^2}}. \tag{3.54}$$

We can immediately see that $|\xi_\pi| < 1$. Due to the oscillatory nature of the Bessel functions it will therefore oscillate between $-1$ and 1. In particular we find $\xi_\pi = 1$ whenever $J_{\lceil|u|\rceil}(\lambda) = 0$ and $\xi_\pi = -1$ whenever $J_{\lfloor|u|\rfloor}(\lambda) = 0$. Since all Bessel functions have infinitely many zeros both cases will happen infinitely often. This explains why the transmission reaches the boundary for $k = \pi$ so often (which happens for $\xi_\pi = -1, 0, 1$). Because for $\xi_\pi < -1$ the transmission vanishes completely the values of $\lambda$ with no transmission are given by the zeros of the Bessel function $J_{\lfloor|u|\rfloor}(\lambda) = 0$ (in case of $|u| = 10.5$ these are $\lambda = 14.5, 18.5, 22.0, 25.5, \ldots$).

We can easily estimate $\xi_0$ for large $\lambda$ because all Bessel functions decay as $\mathcal{O}\left(1/\sqrt{\lambda}\right)$. This leads to

$$\xi_0 \approx -\frac{2}{\frac{J_{\lfloor|u|\rfloor}(\lambda)^2}{|u|-\lfloor|u|\rfloor} + \frac{J_{\lceil|u|\rceil}(\lambda)^2}{\lceil|u|\rceil-|u|}} \sim -2\lambda \tag{3.55}$$

which shows that $\xi_0$ is well below $-1$ for large $\lambda$. This means that the transmission cannot reach to $k = 0$ anymore which explains why transmission only occurs for $k$ close to $\pi$. Also because $\xi_0$ goes to minus infinity the regions of transmission become smaller in $k$ as $\lambda$ grows.

This finishes our discussion of the case $|u| > 1$. Before we end this section we would like to note that especially the last approximations only give a qualitative understanding of the observed features. For quantitative estimates they are too rough and one has to numerically evaluate the exact values.

### 3.3.3 Discussion for $|u| < 1$

While the above discussion is valid for all $|u| > 1$, for $|u| < 1$ there are some differences. That is why we would like to quickly treat this case separately.

In figure 3.10 we give $\gamma$ and $v_1$ as well as their approximations by two terms. We can see that there is an oscillatory decay part as for $|u| > 1$, but the other two parts are missing. This is not surprising since they were located below $\lambda < |u|$ which is not possible for $|u| < 1$. Especially note that, contrary to $|u| > 1$, the approximation now also well describes $\lambda \approx 0$ (because $J_0(\lambda)$ is included into the approximation).

The transmission amplitude is given in figure 3.11. Again we can see that the first part, where the function looks similar to the single particle result, is completely missing. Instead we directly start

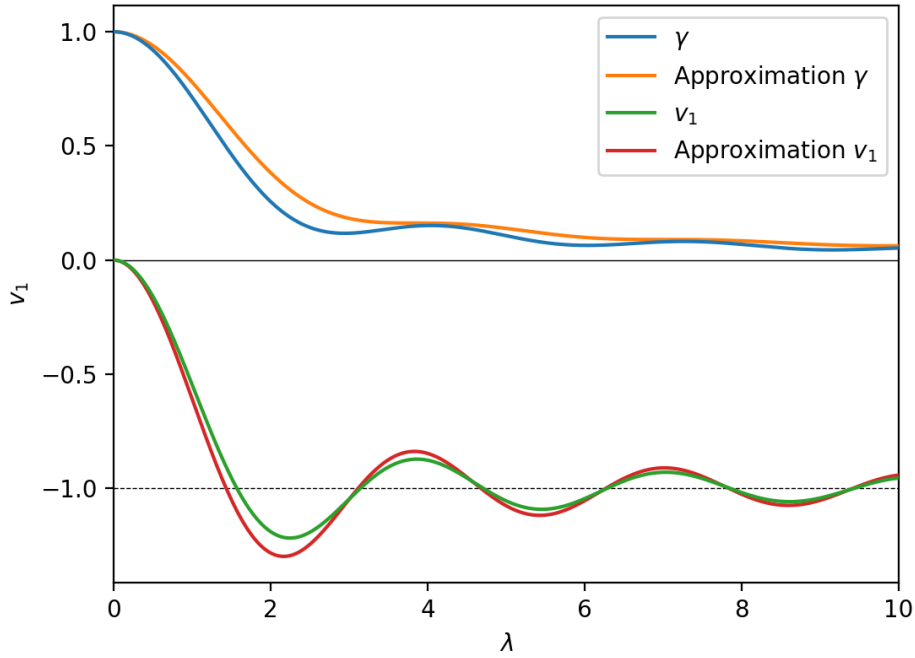


Figure 3.10: Values of $\gamma$ (blue) and $v_1$ (green) as function of driving strength $\lambda$ for $|U|/\omega = 0.5$. Also we give their approximations by two terms (orange, red).

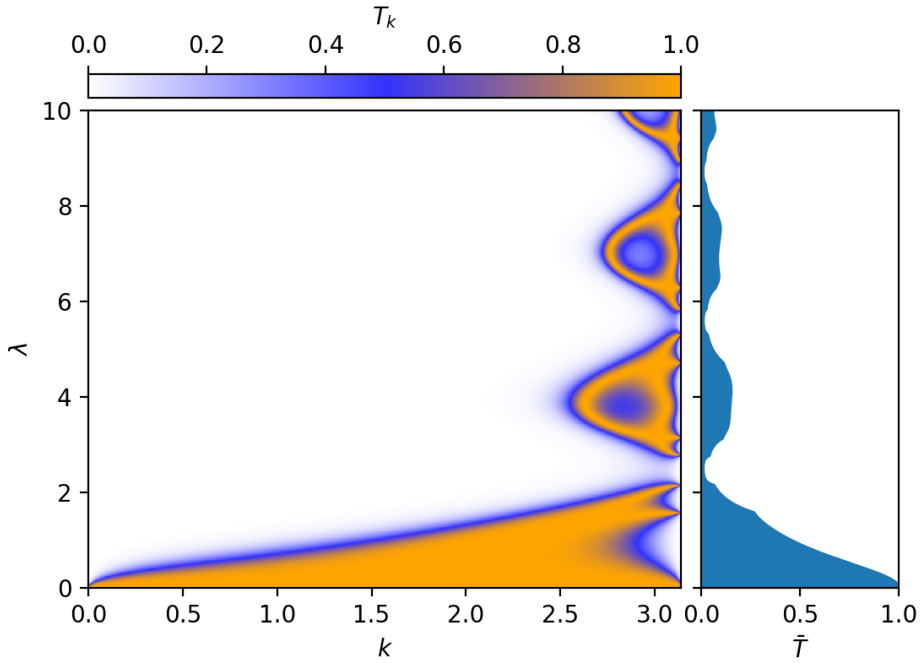


Figure 3.11: Pair transmission as function of momentum $k$ and driving strength $\lambda$ for $|U|/\omega = 0.5$. The plot on the right displays the momentum averaged transmission $\bar{T}$.

with the oscillating part where the transmission periodically appears for large $k$ as $\lambda$ grows.

### 3.3.4 Discussion for $|u|$ close to an integer

Before completing this section let us have a closer look on the case where $|u|$ is close to an integer. Let us call $u_0$ the closest integer to $u$ and write $|u| = |u_0| + \varepsilon$. $\varepsilon > 0$ means that $|u|$ is slightly above an integer and $\varepsilon < 0$ means that $|u|$ is slightly below one. For $|u|$ close to an integer $|u_0|$ the usual approximation with two terms is not necessary and we can instead approximate it using only one term corresponding to $|u_0|$:

$$\gamma = \sum_a \frac{|u|(-1)^a J_a(\lambda)^2}{|u| - a} \approx \frac{|u_0|(-1)^{|u_0|} J_{|u_0|}(\lambda)^2}{\varepsilon} + \left( (-1)^{|u_0|} J_{|u_0|}(\lambda)^2 + \sum_{a \neq |u_0|} \frac{|u_0|(-1)^a J_a(\lambda)^2}{|u_0| - a} \right) + O(\varepsilon) \tag{3.56}$$

$$v_1 = \sum_a \frac{|u| J_a(\lambda)^2}{|u| - a} - 1 \approx \frac{|u_0| J_{|u_0|}(\lambda)^2}{\varepsilon} + \left( J_{|u_0|}(\lambda)^2 + \sum_{a \neq |u_0|} \frac{|u_0| J_a(\lambda)^2}{|u_0| - a} - 1 \right) + O(\varepsilon) \tag{3.57}$$

where we already include the next order correction for later convenience. One can see that both diverge as $\varepsilon \to 0$. From this we can calculate $\xi_k$ up to first order in $\varepsilon$:

$$\xi_k = \frac{v_1 - \cos k}{|\gamma|} = \operatorname{sgn}(\varepsilon) + \frac{|\varepsilon|}{J_{|u_0|}(\lambda)^2} \left( s_{|u_0|}(\lambda) - \frac{1 + \cos k}{|u_0|} \right) + O\left(\varepsilon^2\right) \tag{3.58}$$

where

$$s_{|u_0|}(\lambda) = \sum_{a \neq |u_0|} \frac{1 - (-1)^{|u_0| - a}}{|u_0| - a} J_a(\lambda)^2. \tag{3.59}$$

Depending on $|u_0|$ the sum in $s_{|u_0|}(\lambda)$ either contains only even or odd terms. We have

$$\left(\xi_k^2 - 1\right)^2 = \left( \frac{2}{J_{|u_0|}(\lambda)^2} \left( s_{|u_0|}(\lambda) - \frac{1 + \cos k}{|u_0|} \right) \right)^2 \varepsilon^2 + O\left(\varepsilon^3\right) \tag{3.60}$$

and by using (3.32) and (3.56) we find:

$$T_k = \frac{1}{1 + \left( \frac{2}{\sin k} \left( |u_0| s_{|u_0|}(\lambda) - (1 + \cos k) \right) \right)^2} + O(\varepsilon). \tag{3.61}$$

We plot this limiting transmission in figure 3.13 for $|u| = 10$ (Apart from small $\lambda$ it looks similar to figure 3.12. Exactly at integer $|u|$ the range of validity of approximations (3.41) and (3.45) shrink to $\lambda = 0$ and so the transmission behaves differently for small $\lambda$). Surprisingly even though $\gamma$ and $v_1$ diverge as $\varepsilon \to 0$ the transmission is continuous across integer values of $|u|$.

This might seem rather surprising because if one compares plots of the actual transmission above and below integer $|u|$ they look different (compare figures 3.12 and 3.14 which are for $|u| = 9.9$ and

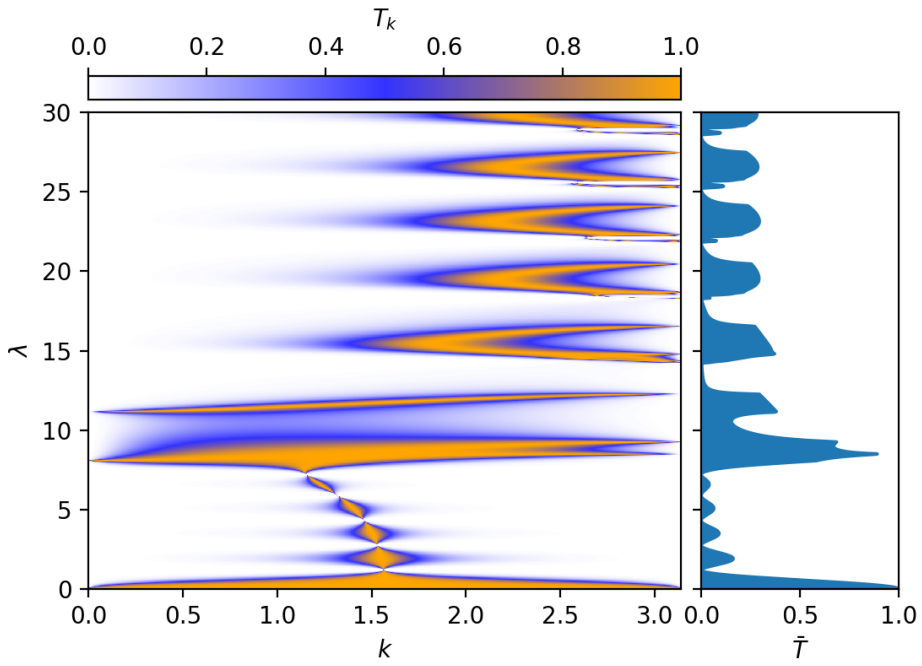


Figure 3.12: Pair transmission as function of momentum $k$ and driving strength $\lambda$ for $|U|/\omega = 9.9$. The plot on the right displays the momentum averaged transmission $\bar{T}$.

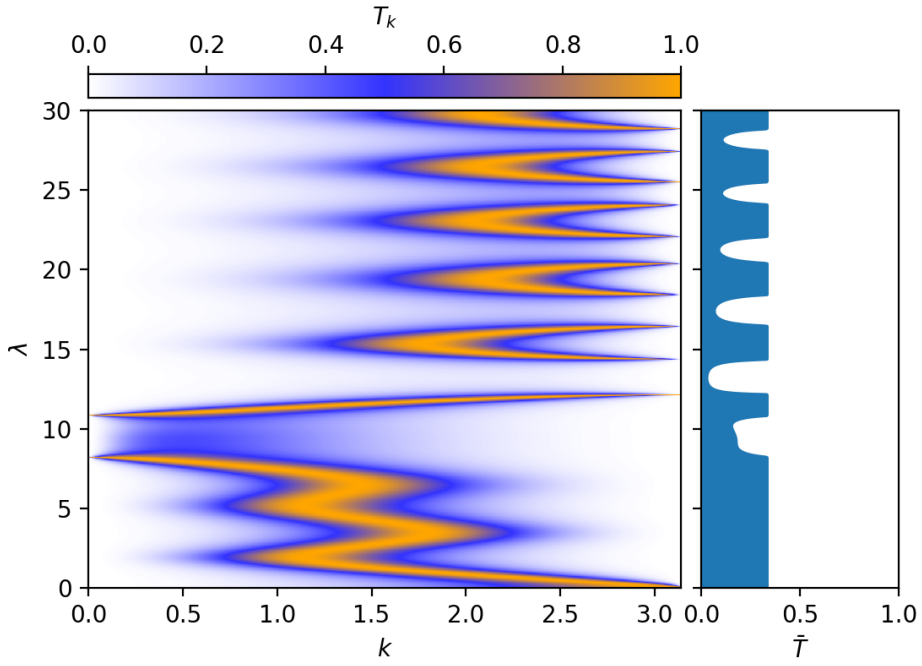


Figure 3.13: Pair transmission as function of momentum $k$ and driving strength $\lambda$ for $|U|/\omega \to 10.0$. The plot on the right displays the momentum averaged transmission $\bar{T}$.

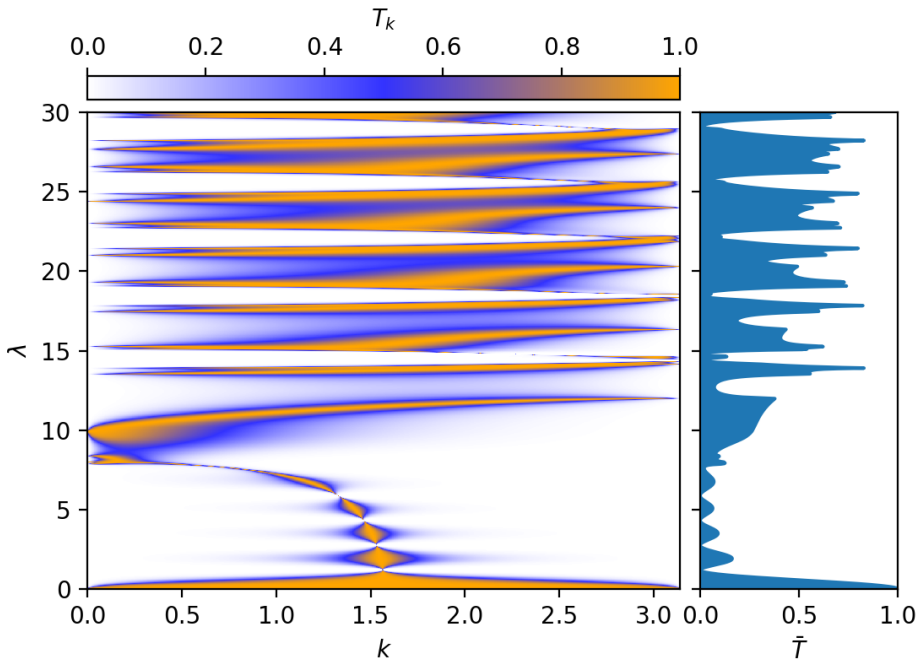


Figure 3.14: Pair transmission as function of momentum $k$ and driving strength $\lambda$ for $|U|/\omega = 10.1$. The plot on the right displays the momentum averaged transmission $\bar{T}$.

$|u| = 10.1$ respectively). In particular for $|u| = 9.9$ the transmission concentrates mainly on high $k$, while for $|u| = 10.1$ it also reaches to low $k$. In the following we will see that the reason for this behaviour is that $\xi_k$ jumps from $-1$ to 1 as $\varepsilon$ passes 0[2]:

Recall that we always have $\xi_0 \leq \xi_k \leq \xi_\pi$ where $\xi_0$ and $\xi_\pi$ are given by

$$\xi_0 = \frac{v_1 - 1}{|\gamma|} = \operatorname{sgn}(\varepsilon) + \frac{|\varepsilon|}{J_{|u_0|}(\lambda)^2}\left(\frac{s_{|u_0|}(\lambda)}{|u_0|} - \frac{2}{|u_0|}\right) + O\left(\varepsilon^2\right) \tag{3.62}$$

$$\xi_\pi = \frac{v_1 + 1}{|\gamma|} = \operatorname{sgn}(\varepsilon) + \frac{|\varepsilon|}{J_{|u_0|}(\lambda)^2}\frac{s_{|u_0|}(\lambda)}{|u_0|} + O\left(\varepsilon^2\right). \tag{3.63}$$

Because $\gamma$ diverges as $\varepsilon \to 0$ from plot 3.6 we know that we will only find transmission if $\xi_k = -1, 0, 1$. Depending on how often $\xi_k$ actually crosses one of these values the transmission is organized in either 1, 2 or 3 branches. Due to the zeroth order result in $\varepsilon$ we expect to always have exactly one branch because either all $\xi_k \to 1$ or all $\xi_k \to -1$.

Let us now also include the first order correction. The first order correction is symmetric for $\varepsilon > 0$ and $\varepsilon < 0$. It consists of two parts: We have the part including $s_{|u_0|}(\lambda)$. Recall that $s_{|u_0|}(\lambda)$ is given by a complicated sum over Bessel functions (3.59). The terms for $a < |u_0|$ have a positive sign while the for $a > |u_0|$ the sign is negative. Thus it is hard to predict the sign of $s_{|u_0|}(\lambda)$. We can however bound

[2] Or in other words: The transmission is continuous as $\varepsilon \to 0$, but its derivative jumps.

its absolute value by

$$\left|s_{|u_0|}(\lambda)\right| \leq \sum_{a\neq|u_0|}\left|\frac{1-(-1)^{|u_0|-a}}{|u_0|-a}J_a(\lambda)^2\right| \leq 2\sum_a J_a(\lambda)^2 = 2 \tag{3.64}$$

where in the last step we again used Neumann's addition theorem (see appendix C.5). We achieved this bound by ignoring the sign change and also $\frac{1}{|u_0|-a} \leq 1$. Because the sign change will yield a partial cancellation of terms and also usually $\frac{1}{|u_0|-a} \ll 1$we can expect $\left|s_{|u_0|}(\lambda)\right| \ll 2$.

For $\xi_0$ there is also another term $-\frac{2}{|u|}$. Because we expect $s_{|u_0|}(\lambda)$ to be small this term is dominant (unless of course $|u|$ is too large):

$$\xi_0 \approx \operatorname{sgn}(\varepsilon) - \frac{2|\varepsilon|}{|u_0|J_{|u_0|}(\lambda)^2}. \tag{3.65}$$

As we increase $|\varepsilon|$ away from zero $\xi_0$ starts either at $\pm1$ and then quite rapidly grows into the negative direction (It grows fast because $J_{|u_0|}(\lambda)^2$ is usually small).

Now let us consider the cases $\varepsilon < 0$ and $\varepsilon > 0$ separately. For $\varepsilon < 0$ we expect that $\xi_0 < -1$. Depending on the unknown sign of $s_{|u_0|}(\lambda)$ we have two cases: If also $s_{|u_0|}(\lambda) < 0$, then $\xi_k$ will be below $-1$ for all $k$ and so we do not observe transmission. If on the other hand $s_{|u_0|}(\lambda) > 0$ then $\xi_k$ ranges from slightly below $-1$ to above $-1$ and therefore includes one branch of the transmission. This one-branch-behaviour can be nicely seen in figure 3.12.

For $\varepsilon > 0$ the situation is different. Here $\xi_0$ starts at 1, but then we expect it to quickly grow into the negative direction. This means above a certain small value of $\varepsilon$ we also have $\xi_0 < -1$. Now because $\xi_\pi \approx 1$, depending on the sign of $s_{|u_0|}(\lambda)$ we will observe either two (for $s_{|u_0|}(\lambda) < 0$) or three (for $s_{|u_0|}(\lambda) > 0$) branches. In any case we can expect much transmission than for $\varepsilon < 0$. This can be easily seen by comparing figure 3.14 to figure 3.12. Especially note that the transmission also reaches $k = 0$ in figure 3.14. This happens whenever $\xi_0$ crosses $-1, 0$ or 1 which is expected to happen much more often for $\varepsilon > 0$ than for $\varepsilon < 0$.

Before we end this section let us note that the exact form of the transmission depends on the behaviour (and in particular the sign) of $s_{|u_0|}(\lambda)$. We will not go into detail here, but we will only note that it is also given by a sum similar to $\gamma$ and $v_1$. We could basically repeat the analysis of section 3.3.2. In particular the dominating terms will be again given by the two closest terms to $|u_0|$. Since these are also Bessel functions we again find similar regimes: One regime for $\lambda < |u_0|$, a peak for $\lambda \approx |u_0| + 1.5$ and an oscillating decay for $\lambda > |u_0| + 1.5$. This explains why figures 3.12 and 3.14 look so similar to figure 3.9. In fact the positions of the features as function of $\lambda$ are almost the same in all figures. The only difference is how pronounced the regions with transmission are. For $|u| = 9.9$ the transmission is mostly contained in thin single separated branches, while for $|u| = 10.1$ we can see patterns with two or three thin branches (The branches are thin because $\gamma$ is quite large for $|u|$ close to an integer, see figure 3.6). Because $\gamma$ is smaller for $|u| = 10.5$, the branches are thicker in figure 3.9 which makes the image of the transmission less filigree.

## 3.4 Numerical results

In this section we would like to check the analytical results with numerical results. For single particles there have already been numerical studies [6]. Therefore we will concentrate on numerical simulations for the pairs here. The method we want to use is outlined in section 2.3 which is a general method for numerically calculating transmission coefficients in 1D systems.

However our system consists of a stack of layers, each layer being a 2D lattice, which is far from a 1D system. Therefore we will apply the method not on the system as a whole but only on the diagonal of layer 0. This is of course a one dimensional subsystem, but we should explain carefully why applying the method onto this subsystem gives the right result.

Consider only layer 0 first and ignore the existence of all other layers. The idea is based on the fact that pairs are given by plane waves on the diagonal and decay quite quickly perpendicular to it (as discussed in section 2.1.4). This means that already for relatively small system sizes the wavefunction between the impurity and the boundary is given by an unperturbed eigenstate of the plain Fermi-Hubbard model. Only close to the impurity around site 0 and close to the boundary the wavefunction will get perturbed. In order to make sure that the influence of the boundary is neglectable we need that the size of the pair is well below 1. In section 2.1.4 we found that this is true for $U/J > 4.7$, which is automatically satisfied in the non-resonant case. So the boundary will not perturb the eigenstate significantly. How about the impurity? For the procedure to work we need the impurity to be confined to a finite sized region. This might seem obvious but when looking at one layer as in figure 3.2(b) we actually find that the impurity extends to infinity. Again we can argue that, due to the small size of the pair, as soon as we are a few steps away from the center site 0 the pair state will not be affected by the impurity anymore and thus the impurity is effectively localized.

Now let us take the other layers into account. That is actually not very complicated as there is no restriction on the complexity of the impurity. We will simply combine all other layers apart from layer 0 together with their couplings into one very complicated effective impurity. The two requirements, parity conservation and time reversal symmetry, are fulfilled. We also need to make sure that this effective impurity is given by a hermitian operator, i.e. that there is no particle loss to other layers. Particle losses to other layers are automatically prohibited as long as we are in the non-resonant case (basically this is the definition of the non-resonant case). In the resonant case this method is not applicable.

The Hilbert space of a system with $N$ layers of size $L$ has dimension $NL^2$. From these states only $\approx L$ states will correspond to paired states in layer 0. We therefore first need to filter these paired states from the eigenstates of the system. This is done by adding the modulus squared of the wavefunction along the diagonal of layer 0. As this number is only large for paired states we will choose the $L$ states with the highest number as potential candidates for paired states. After that we can fit either $\psi_n^{\mathrm{s}}$ or $\psi_n^{\mathrm{a}}$ of equations (2.30) and (2.31) to it (depending on whether the state is symmetric or antisymmetric). The momentum $k = 2K$ of the pair can be calculated from the eigenenergy of the eigenstate by inverting (2.10). Note that we exclude sites $-1, 0, 1$ from the fitting process because the impurity acts on these sites. If either the momentum cannot be computed or the error of the fit is too large (if the squared distance is above $0.001L$) we exclude this state from the fitting procedure.

After we obtained the fitting parameters $A_k, B_k, C_k, D_k$ we interpolate between them and calculate the transmission as described in section 2.3.

To illustrate that it is enough to consider the diagonal of layer 0 we plot a typical layer 0 of such an eigenstate in figure 3.15. We can see that the wavefunction is almost completely concentrated on the

diagonal. All other parts of the layer are therefore not relevant for us. The diagonal of figure 3.15 together with a fit is shown in figure 2.3.

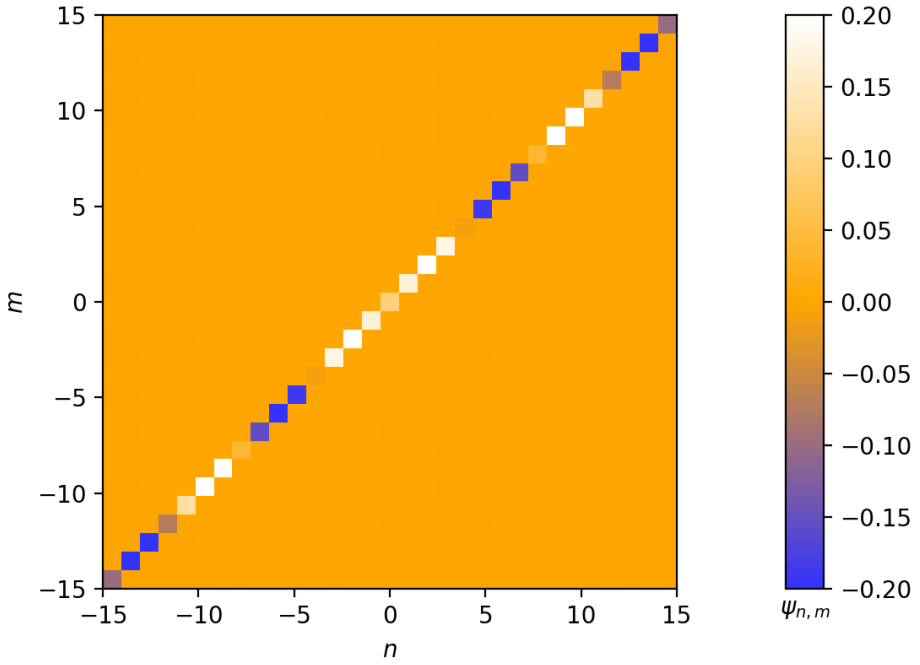


Figure 3.15: Layer 0 of a pair eigenstate for $J/\omega = 0.001, |U|/\omega = 0.5, \lambda = 1, N = 4, L = 31$. $n$ and $m$ denote the position of the first and second particle respectively. The wavefunction $\psi_{n,m}$ concentrates on the diagonal where both particles are at the same site. The diagonal is shown in figure 2.3.

Combining all these arguments we can see that it is indeed valid to apply the procedure of section 2.3 to the diagonal of layer 0. Note again that this procedure is only applicable in the non-resonant case.

### 3.4.1 Numerical results in the limit $J/\omega \to 0$

We first want to confirm the results of the numerical calculations. Of course we cannot consider the total limit $J/\omega \to 0$, but we can choose a small $J/\omega = 0.001$. Also we have to restrict the system size $L$ and the number of layers $N$ to finite numbers. For convenience we will only choose odd system sizes $L$ and label the sites $-\frac{L-1}{2}, \ldots, \frac{L-1}{2}$. The $N$ layers are chosen such that layer 0 is in the middle, i.e. they are labelled by $-\lfloor \frac{N-1}{2} \rfloor, \ldots, \lceil \frac{N-1}{2} \rceil$. For example if we choose $N = 3$ we have layers $a = -1, 0, 1$, or if we choose $N = 4$ we have layers $a = -1, 0, 1, 2$.

We will perform the simulations using the gauge transformed version of the Hamiltonian (3.8). Although much simpler to implement, the original Hamiltonian (3.1) has a major drawback: The layers are coupled quite strongly due to the possibly large $\lambda$ independent of $\alpha$ and $|u|$. This means we need a relatively large number of layers $N$ until we reach convergence. On the other hand the gauge transformed Hamiltonian 3.8 couples to other layers only with $\alpha = J/\omega$ which is quite small. We also know that in the limit the dominant contribution to the scattering comes from the two layers closest to $|u|$. This means we should already get a good approximation by choosing $N > 2|u|$.

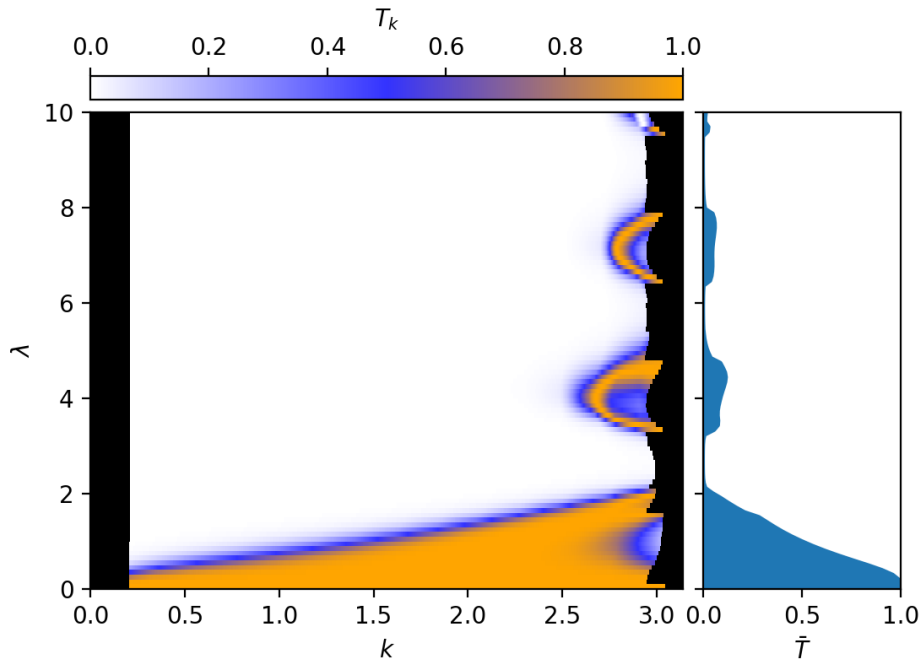


Figure 3.16: Numerically calculated pair transmission for $J/\omega = 0.001, |U|/\omega = 0.5, N = 4, L = 31$ as function of momentum $k$ and driving strength $\lambda$. The black regions at the boundary are outside of the scope of the numerical method (see section 2.3). The plot on the right displays the momentum averaged transmission $\bar{T}$.

In figure 3.16 we give the numerical results for $|u| = 0.5$. We have chosen $L = 31$ and $N = 4$. The figure looks similar to the expected theoretical result shown in 3.11. Unfortunately we are not able to access the transmission for large and low $k$, because the numerical method cannot provide it (see section 2.3). For a better comparison we plot a vertical cut at constant $k = 0.85\pi$ in figure 3.17. Note that we have chosen $k = 0.85\pi$ instead of a more apparent value, like $k = \pi/2$, in order to be in the more interesting region on the right side.

In figure 3.17 we also give two theoretical results: First the full result determined by (3.27) and (3.28) and second another variant where the sums in $\gamma$ and $v_1$ only include the four terms corresponding to the four layers $a = -1, 0, 1, 2$. The later transmission amplitude is the theoretically expected one in the limit $L \to \infty$ while keeping $N = 4$ fixed. This helps to distinguish whether the difference between the numerical and theoretical result is due to a too small value of $L$ or $N$. One can see that while the numerically calculated transmission nicely matches the result for four layers, it is a bit off for infinite layers. It still shows the main important features also seen in the result for infinite layers, like the position of the peaks, but the details of the peaks are not well approximated. We can see that this is completely due to the fact that we only use four layers $N = 4$. If we would include more layers the numerical results as well as the expected theoretical result for this number of layers would converge to the actual result. We would like to remark that already the good agreement with the four layer theoretical result shows the applicability of the limiting model obtained via the Schrieffer-Wolff transformation and verifies our derivations as a whole. The only missing piece is to further increase $N$ (which is restricted to $N \leq 4$ due to limited computational power), but this will only change the parameters $\gamma$ and $v_1$ of the effective model and not the model itself.

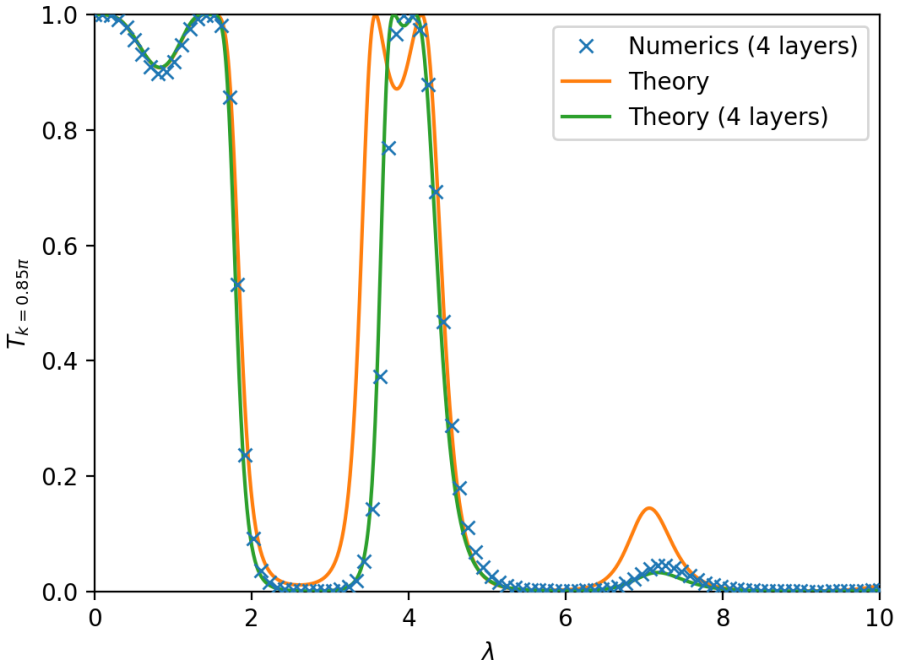


Figure 3.17: Numerically calculated pair transmission with momentum $k = 0.85\pi$ for $J/\omega = 0.001, |U|/\omega = 0.5, N = 4, L = 31$ as function of driving strength $\lambda$. We also give the theoretical result for infinite and four layers.

### 3.4.2 Numerical results for finite $J/\omega$

After we checked the prediction of our analytical result in the limit $J/\omega \to 0$, we can go on to also compute the transmission for higher values of $J/\omega$.

In figure 3.18 we give the pair transmission as a function of $k$ and $J/\omega$. Recall that $J/\omega < 0.125$ is required for the non-resonant case. We can see that in this range the transmission does not change significantly as a function of $J/\omega$. For better comparison we also give a vertical cut at constant $k = 0.85\pi$ in figure 3.19. Here we see that the transmission at the maximum value $J/\omega = 0.125$ is about 2% away from the value at $J/\omega \to 0$.

From the theoretical discussion in section 3.2.2 we already expected that the transmission will not depend significantly on $J/\omega$, because its first order correction (i.e. the linear term) vanishes. Therefore we can conclude that the analytical result for the transmission still is a good approximation also for $J/\omega$ up to it maximum value $J/\omega < 0.125$.

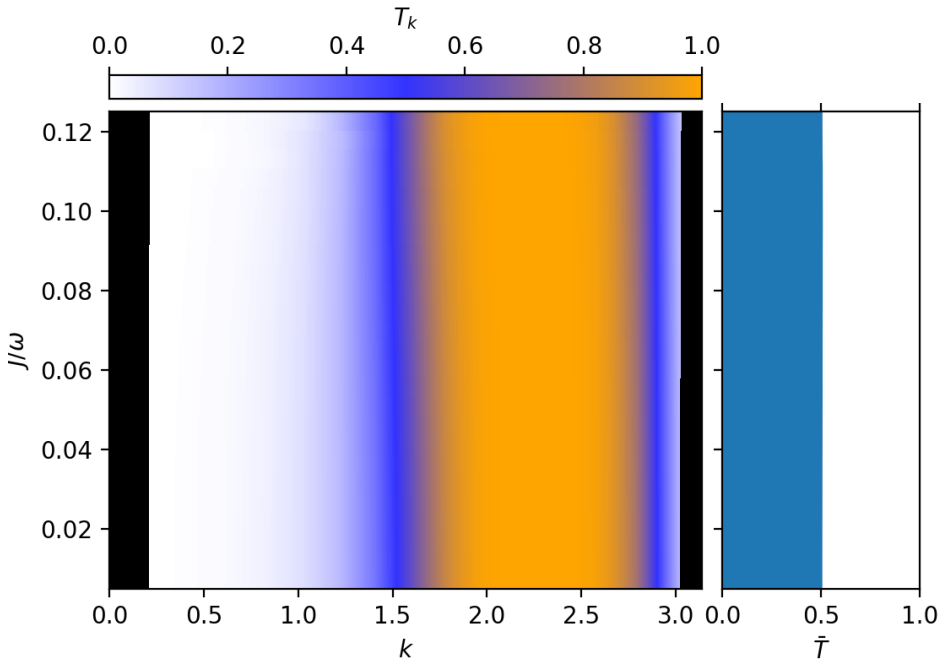


Figure 3.18: Numerically calculated pair transmission for $|U|/\omega = 0.5, \lambda = 1, N = 4, L = 31$ as function of momentum $k$ and hopping parameter $J/\omega$. The black regions at the boundary are outside of the scope of the numerical method (see section 2.3). The plot on the right displays the momentum averaged transmission $\bar{T}$.

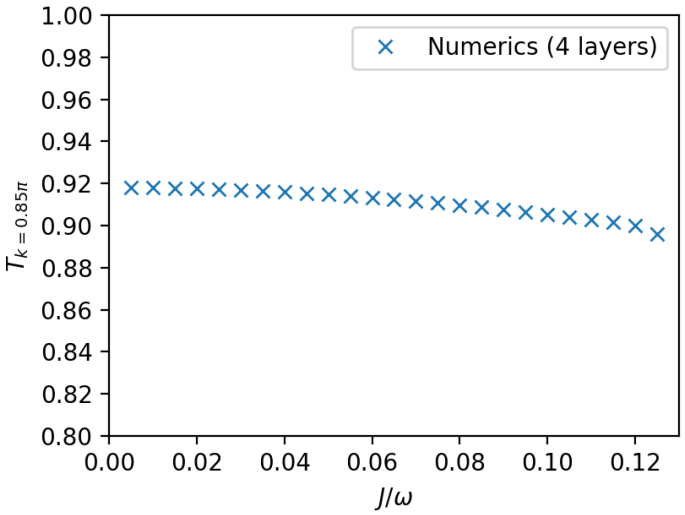


Figure 3.19: Numerically calculated pair transmission with momentum $k = 0.85\pi$ for $|U|/\omega = 0.5, \lambda = 1, N = 4, L = 31$ as function of hopping parameter $J/\omega$.

CHAPTER 4

# Applications

We have seen that single particles are treated differently by the impurity than pairs. This allows for applications where we would like to manipulate either single particles or pairs. In chapter 3 we have calculated the transmission in the limit $J/\omega \to 0$. Also we expect that the transmission of the pairs is not influenced significantly for finite $J/\omega$ as long as we stay in the non-resonant case $J/\omega < 0.125$ (this maximum value is for $|u|$ being half integer. If $|u|$ is more closer to an integer it is given by one fourth of the distance to the nearest integer). The same is true for single particles [7]. Therefore it will be enough to work with the results obtained for $J/\omega \to 0$.

In particular we have seen that transmissions for single particles vanishes at the zeros for the Bessel function $J_0(\lambda)$. At these points only pairs will go through the barrier, i.e. the driven impurity acts as a pair filter. In this section we will take a closer look at this situation and also give other applications of the impurity.

## 4.1 Average transmission

We have seen that the transmission is a complicated function of $k, |u|$ and $\lambda$. In order to simplify the discussion we will average the transmission over all momenta:

$$\bar{T} = \frac{1}{\pi} \int_0^\pi T_k \, \mathrm{d}k \, . \tag{4.1}$$

This quantity can be interpreted as the probability that a particle with randomly chosen momentum will penetrate the impurity. Note that if either $\bar{T} = 1$ or $\bar{T} = 0$ we can conclude $T_k = 1$ or $T_k = 0$ for all $k$.

In figures 4.1 and 4.2 we give the average transmission for a single particle and a pair respectively. Note that the averaged transmission for a single particle (3.25) can be explicitly calculated (for example using mathematica):

$$\bar{T} = \frac{1}{\pi} \int_0^\pi \frac{1}{1 + \left( \frac{1}{J_0(\lambda)^2} - 1 \right)^2 \cot^2 k} \, \mathrm{d}k = J_0(\lambda)^2. \tag{4.2}$$

This shows that the averaged single particle transmission is relatively small unless $\lambda \approx 0$. The

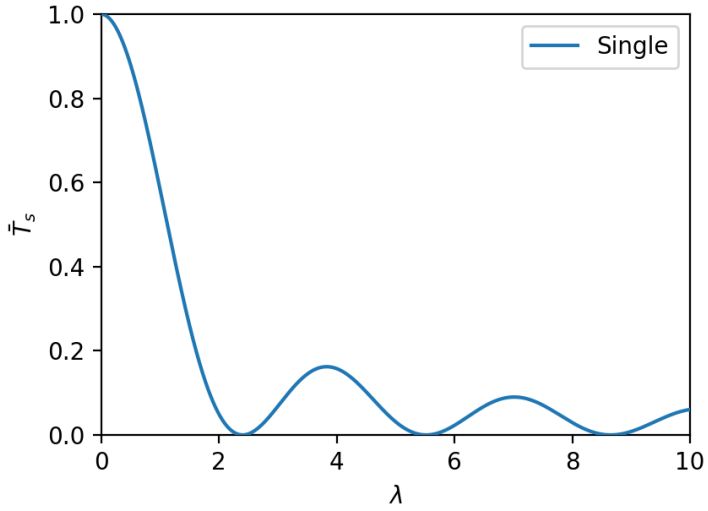


Figure 4.1: Averaged single particle transmission $\bar{T}_\mathrm{s}$ as function of driving strength $\lambda$.

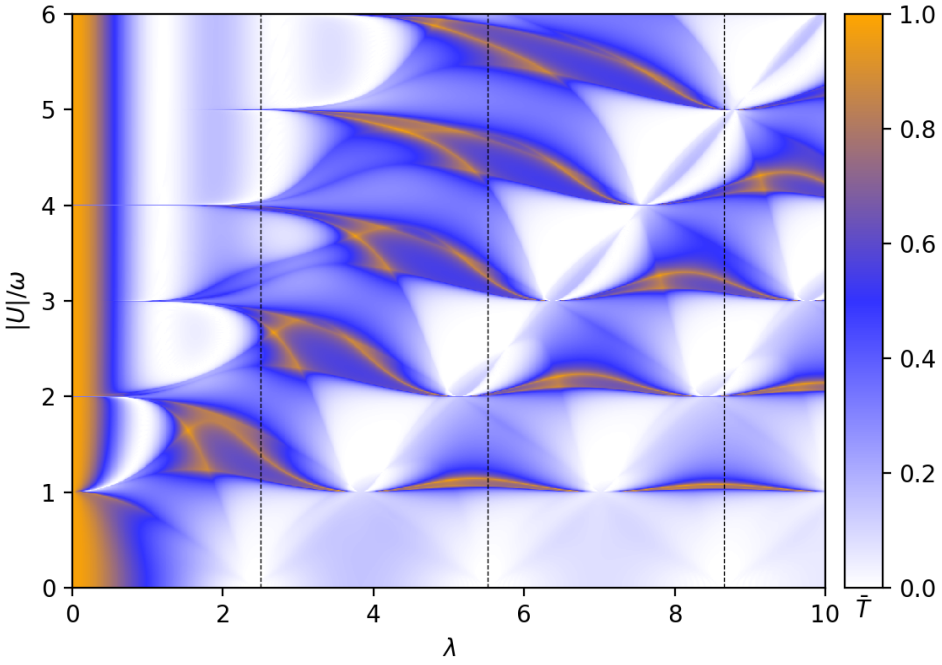


Figure 4.2: Averaged pair transmission $\bar{T}_\mathrm{p}$ as function of driving strength $\lambda$ and Hubbard interaction $|U|/\omega$. The vertical lines are drawn at the zeros of the single particle transmission $\bar{T}_\mathrm{s} = J_0(\lambda)^2$.

transmission vanishes completely at the zeros of the Bessel function $J_0(\lambda)$.

The picture is more complicated for the pairs (see figure 4.2). We already discussed the behaviour of the transmission in section 3.3. In figure 4.2 one can clearly see the first maximum of the transmission around $\lambda \approx |u| + 1$ and the periodic decay afterwards. We would like to draw the attention of the reader to two features: First that in the upper left corner $\lambda < |u|$ the averaged transmission becomes

independent of $|u|$ as expected by the discussion in section 3.3. Second that we can often see a sudden increase of the averaged transmission above an integer value of $|u|$ which is also expected from section 3.3.4.

## 4.2 Pair filter

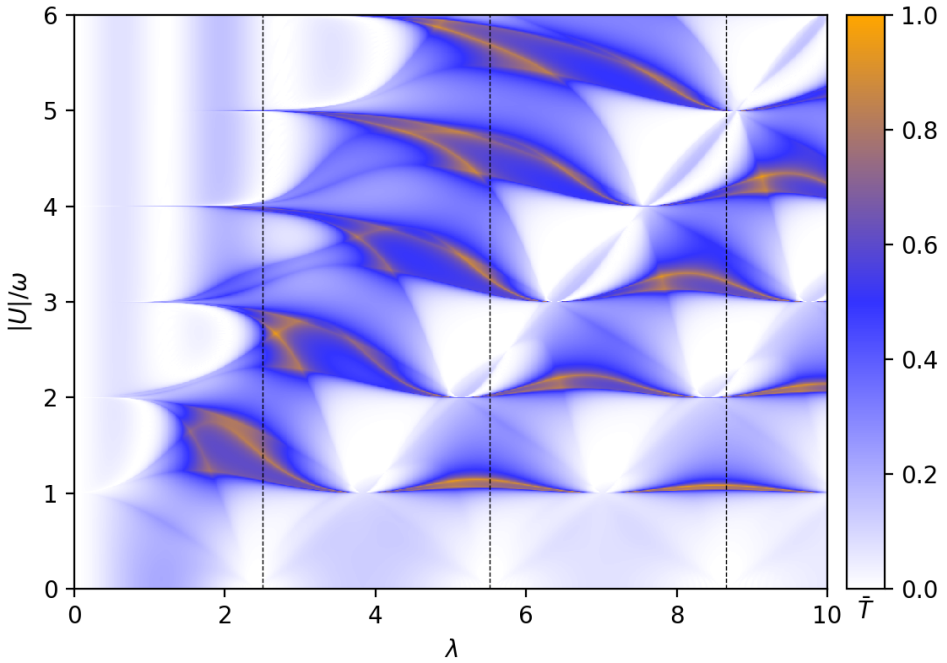


Figure 4.3: $r_1 = \bar{T}_p(1 - \bar{T}_s)$ as function of driving strength $\lambda$ and Hubbard interaction $|U|/\omega$. The vertical lines are drawn at the zeros of the single particle transmission $\bar{T}_s = J_0(\lambda)^2$.

Our aim is to maximize the pair transmission $\bar{T}_p$ while at the same time minimizing the single particle transmission $\bar{T}_s$. To combine both into one quantity we are going to use the following formula:

$$r_1 = \bar{T}_p\big(1 - \bar{T}_s\big). \tag{4.3}$$

This quantity grows when either $\bar{T}_p$ rises or $\bar{T}_s$ shrinks. It lies between 0 and 1 and is only 1 if both $\bar{T}_p = 1$ and $\bar{T}_s = 0$. We can think of $r_1$ in the following way: Imaging a single particle and a pair are simultaneously send to the impurity. Then $r_1$ is the probability that exactly the event occurs which we want, i.e. the pair is transmitted while the single particle is reflected. In fact if $\bar{T}_s = 0$ then $r_1$ reduces simply to $\bar{T}_p$. This is why figure 4.3 looks so similar to figure 4.2.

From figure 4.3 we can see that the regions with high $r_1$ are those with $\lambda \approx |u| + 1.5$ and the regions in the oscillating part $\lambda > |u| + 1.5$. In general the region for $\lambda \approx |u| + 1.5$ is bigger in size than those in the oscillating part, which makes $\lambda \approx |u| + 1.5$ a good choice for experiments. Also, because we would like to minimize the single particle transmission $\bar{T}_s = J_0(\lambda)^2$, it is natural to choose $\lambda$ as a zero of the Bessel function $J_0(\lambda)$, i.e. $\lambda = 2.4, 5.5, \ldots$. For a better comparison we plot the averaged transmission $\bar{T}_p$ at these values of $\lambda$ as a function of $|u|$ in figure 4.4.

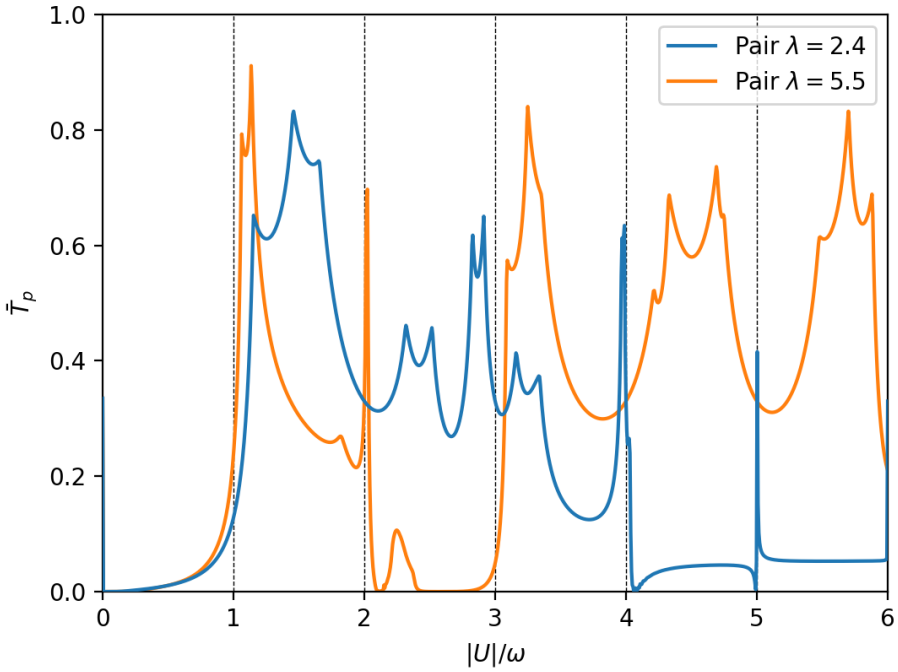


Figure 4.4: Averaged pair transmission $\bar{T}_\mathrm{p}$ as function of Hubbard interaction $|U|/\omega$ for $\lambda = 2.4$ (blue) and $\lambda = 5.5$ (orange). In order to stay in the non-resonant case one should avoid to be too close to integer values of $|U|/\omega$ (dashed lines).

From these plots one can try to find high values of average pair transmission. For $\lambda = 2.4$ we have one apparent maximum at $|u| = 1.5$ with $\bar{T}_\mathrm{p} = 0.794$. For $\lambda = 5.5$ we have more possible values of $|u|$ for which the average transmission is high. However many of them are close to integer values, which, for finite $J/\omega$, we would like to avoid in order to stay in the non-resonant case. A good value here is $|u| = 5.7$, where the average transmission reaches $\bar{T}_\mathrm{p} = 0.842$.

## 4.3 Single particle filter

The question arises whether it is also possible to achieve the opposite situation, namely a filter which blocks pairs but lets single particles pass. Analogously to the pair filter we will define the quantity

$$r_2 = \bar{T}_\mathrm{s}\left(1 - \bar{T}_\mathrm{p}\right), \tag{4.4}$$

which describes the probability of a single particle passing, while a pair is blocked. In figure 4.5 we give a plot of $r_2$. One can easily see that it is mostly small which is a direct consequence of $\bar{T}_\mathrm{s}$ being small in general. Only for $\lambda \approx 1.2$ we find a relatively high value. Let us explain how this value comes about. We know that the single particle transmission amplitude is determined by $\gamma = J_0(\lambda)$, $v_1 = 0$. We also know that for small $\lambda$ we can describe the pair scattering by $\gamma = J_0(2\lambda)$, $v_1 = 0$. The averaged transmission amplitude is in both cases given by $\gamma^2$. Although $J_0(\lambda)^2$ is mostly quite small for small values of $\lambda$ it is actually relatively large for small $\lambda$. That is why at the first zero of the pair transmission $J_0(2\lambda)$, with $\lambda \approx 1.2$, the single particle transmission is still $\bar{T}_\mathrm{s} = J_0(1.2) \approx 0.45$.

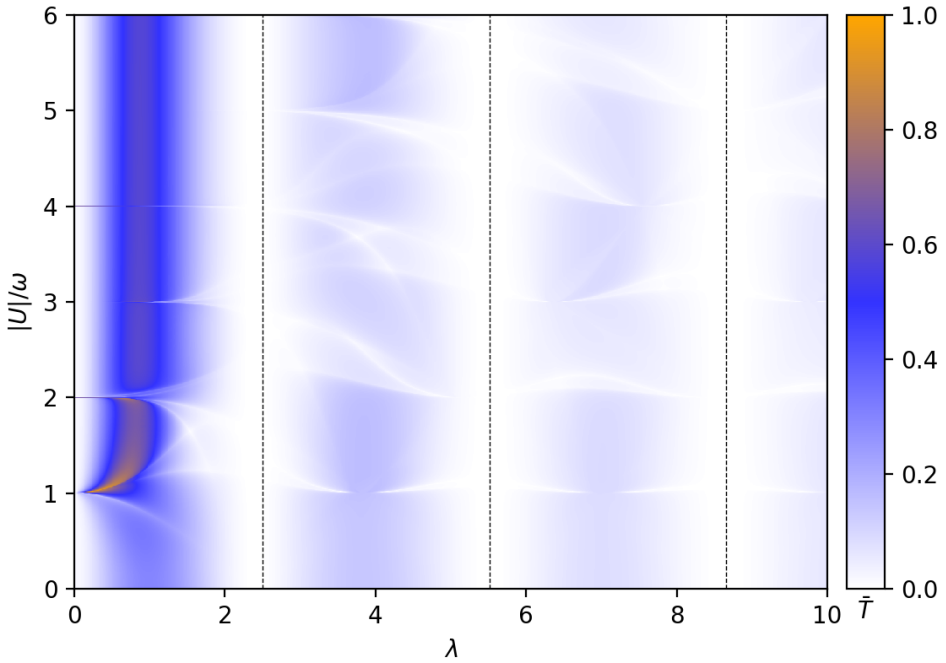


Figure 4.5: $r_2 = \bar{T}_s(1 - \bar{T}_p)$ as function of driving strength $\lambda$ and Hubbard interaction $|U|/\omega$. The vertical lines are drawn at the zeros of the single particle transmission $\bar{T}_s = J_0(\lambda)^2$.

In other words all pairs are blocked but almost half of the single particles can penetrate. Especially note that this result is independent of $|u|$ (as long as $|u| > 2$). One drawback is that the transmission probability is not uniform in momentum, but rather prefers momenta around $\pi/2$ (see figure 3.4).

## 4.4 Blocking transmission for both pairs and single particles

Another possibility of using the driven impurity is to make sure that both single particles and pairs cannot penetrate the impurity. The respective quantity here is

$$r_3 = \left(1 - \bar{T}_s\right)\left(1 - \bar{T}_p\right), \tag{4.5}$$

which gives the probability that both single particles and pairs are reflected. It is plotted in figure 4.6. For the oscillating part $\lambda > |u| + 1.5$ it looks like an inverse image of $r_1$ in figure 4.3. This is not surprising since now we want to find regions where the pair transmission is as low as possible. We are able to find many possible regions of low transmission both for pairs and single particles for $\lambda > |u| + 1.5$. However there is also the possibility to achieve this for $\lambda < |u| + 1.5$ as long as $|u|$ is large enough. We know that in this case $\bar{T}_s = J_0(\lambda)^2$ and $\bar{T}_p = J_0(2\lambda)^2$. The resulting $r_3$ is given in figure 4.7. It has the first maximum at $\lambda \approx 2.65$, where $r_3 \approx 0.98$ is almost 1. In particular for $\lambda = 2.65$ we have $\bar{T}_s \approx 0.014$ and $\bar{T}_p \approx 0.006$ which is quite small. Note that $\lambda = 2.65$ will always lead to almost complete blocking as long as $|u| > 4$.

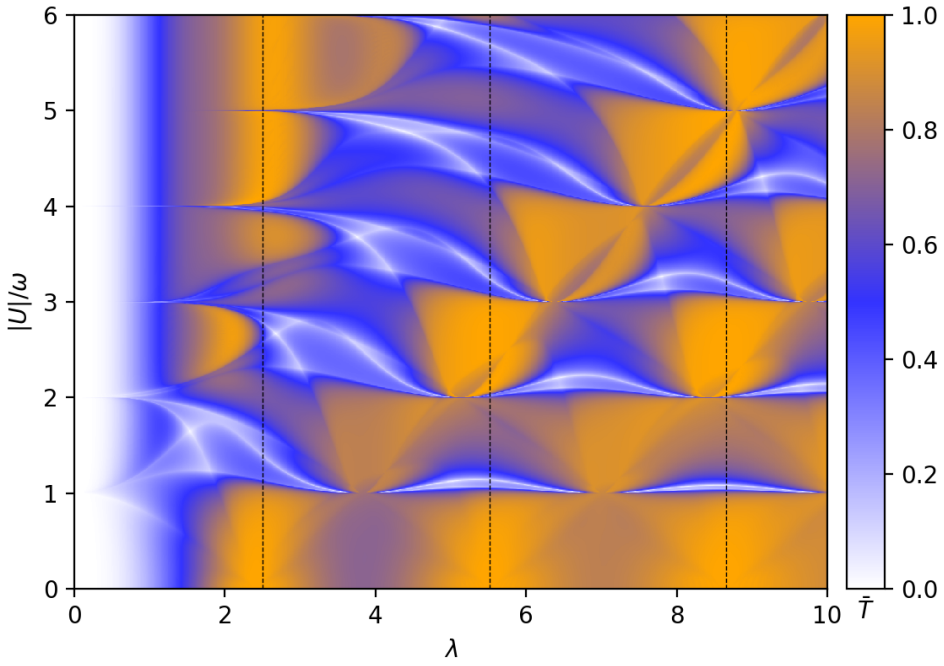


Figure 4.6: $r_3 = \bar{T}_s(1 - \bar{T}_p)$ as function of driving strength $\lambda$ and Hubbard interaction $|U|/\omega$. The vertical lines are drawn at the zeros of the single particle transmission $\bar{T}_s = J_0(\lambda)^2$.

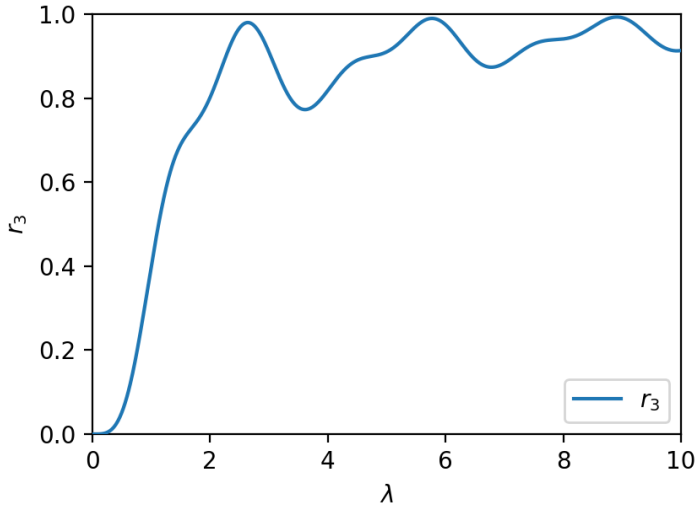


Figure 4.7: Limiting $r_3 = \left(1 - J_0(\lambda)^2\right)\left(1 - J_0(2\lambda)^2\right)$ as function of driving strength $\lambda$ in the limit $\lambda \ll |U|/\omega$.

## 4.5 Parameter proposal for a tunable impurity

Before we conclude this discussion we would like to propose two values of $|u| = |U|/\omega$ for experiments. They are $|u| = 1.5$ and $|u| = 5.7$. By changing the driving strength $\lambda$ these values allow to tune the impurity in all possible ways.

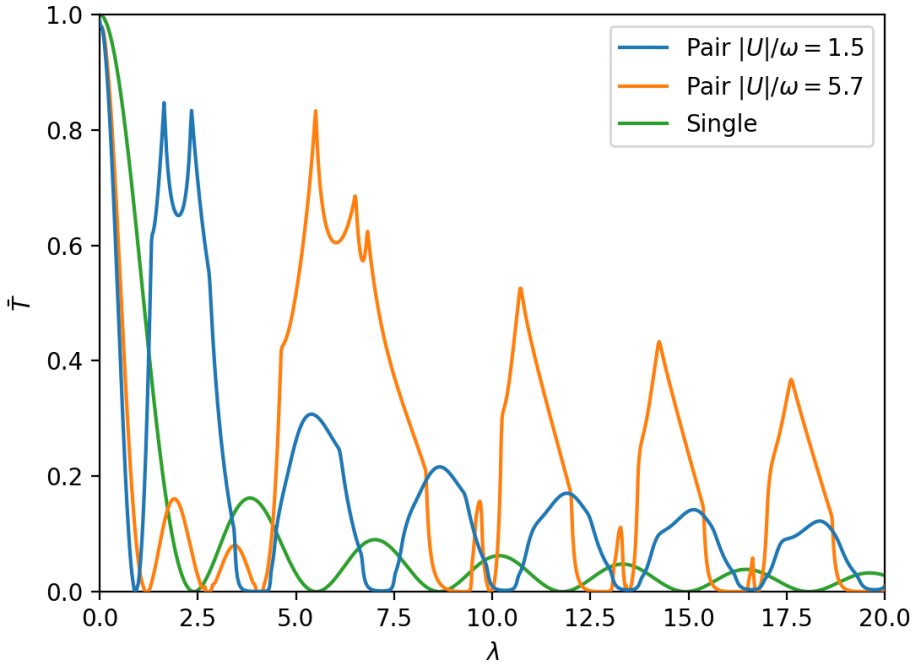


Figure 4.8: Averaged pair transmission $\bar{T}_\mathrm{p}$ for Hubbard interaction $|U|/\omega = 1.5$ (blue) and $|U|/\omega = 5.7$ (orange) and averaged single particle transmission $\bar{T}_\mathrm{s}$ (green) as function of driving strength $\lambda$.

| Situation | $\lambda$ | $\bar{T}_\mathrm{s}$ | $\bar{T}_\mathrm{p}$ |
|---|---|---|---|
| No impurity | 0 | 1 | 1 |
| Single particle filter | 0.9 | 0.652 | 0.001 |
| Both blocked | – | – | – |
| Pair filter | 2.4 | $< 10^{-3}$ | 0.794 |

Table 4.1: Averaged single particle transmission $\bar{T}_\mathrm{s}$ and averaged pair transmission $\bar{T}_\mathrm{p}$ at specific values of driving strength $\lambda$ for Hubbard interaction $|U|/\omega = 1.5$.

| Situation | $\lambda$ | $\bar{T}_\mathrm{s}$ | $\bar{T}_\mathrm{p}$ |
|---|---|---|---|
| No impurity | 0 | 1 | 1 |
| Single particle filter | 1.2 | 0.450 | $< 10^{-3}$ |
| Both blocked | 2.65 | 0.014 | 0.004 |
| Pair filter | 5.5 | $< 10^{-3}$ | 0.842 |

Table 4.2: Averaged single particle transmission $\bar{T}_\mathrm{s}$ and averaged pair transmission $\bar{T}_\mathrm{p}$ at specific values of driving strength $\lambda$ for Hubbard interaction $|U|/\omega = 5.7$.

In figure 4.8 we give the averaged transmission for both single particles and pairs for these values. We see that there is a wide variety of possibilities for different behaviour. In tables 4.1 and 4.2 we summarized some optimal values of $\lambda$ at certain configurations of the impurity. Note that for $|u| = 1.5$

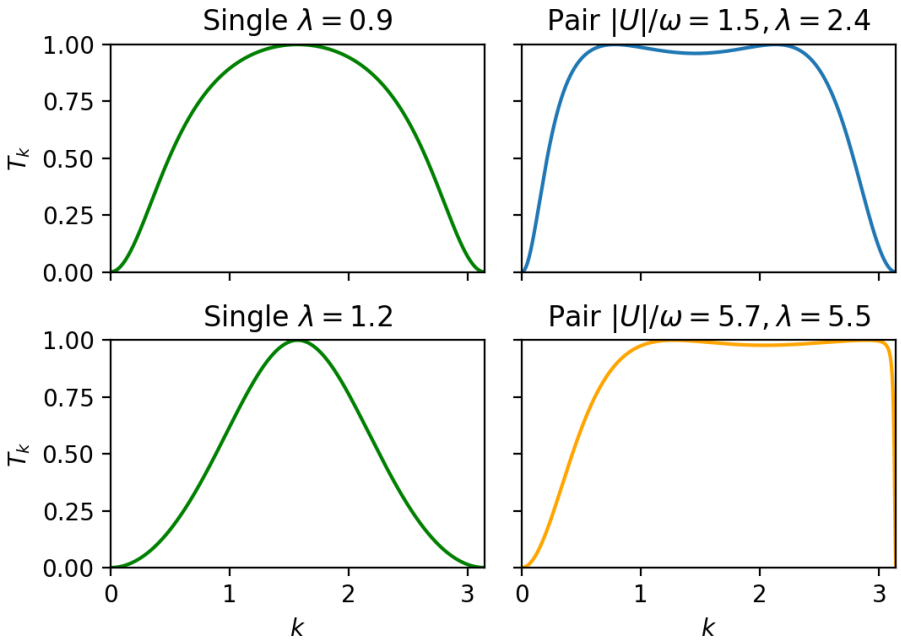


Figure 4.9: Single particle and pair transmission as function of momentum $k$ at certain optimal values of driving strength $\lambda$ and Hubbard interaction $|U|/\omega$ according to tables 4.1 and 4.2 (colors chosen correspondingly to figure 4.8).

we cannot find a configuration where both types of particles are blocked, but if necessary one can always go to high $\lambda$ where both averaged transmissions slowly decay to zero. On the other hand $|u| = 1.5$ has the advantage that it admits a higher single particle transmission at the first zero of the averaged pair transmission.

One should keep in mind that the transmittance of the pair and single particle filter depends on the momentum. Therefore we give plots of its momentum dependence in figure 4.9 for both the pair and single particle filter. Especially the pair filter for $|u| = 5.7$ and $\lambda = 5.5$ allows almost all momenta except low ones to penetrate.

We also want to point out that while this discussion only included $|u|$ and $\lambda$ there is still an implicit restriction for $J/\omega$. Since $|u| = 1.5$ ($|u| = 5.7$) have a distance of 0.5 (0.3) to the next integer, we need $J/\omega < 0.125$ ($J/\omega < 0.075$) to stay in the non-resonant case. In other words it only works for systems with $|U|/J > 12$ ($|U|/J > 76$).

One could also go to higher values of $|u|$ to find more parameters for a tunable impurity. However one should keep in mind that then also the required minimum value of $|U|/J$ grows. For half integers $|u|$ we have $|U|/J > 8|u|$, but the minimum value is even higher if $|u|$ is closer to an integer.

## 4.6 Pair momentum filter

So far we compared the averaged transmission of the pairs to those of the single particles. However we have seen that for most parameters the transmission is not uniformly throughout the Brillouin zone, but rather prefers certain momenta over others. In this section we would like to also distinguish

whether dominantly high or low momenta are transmitted.

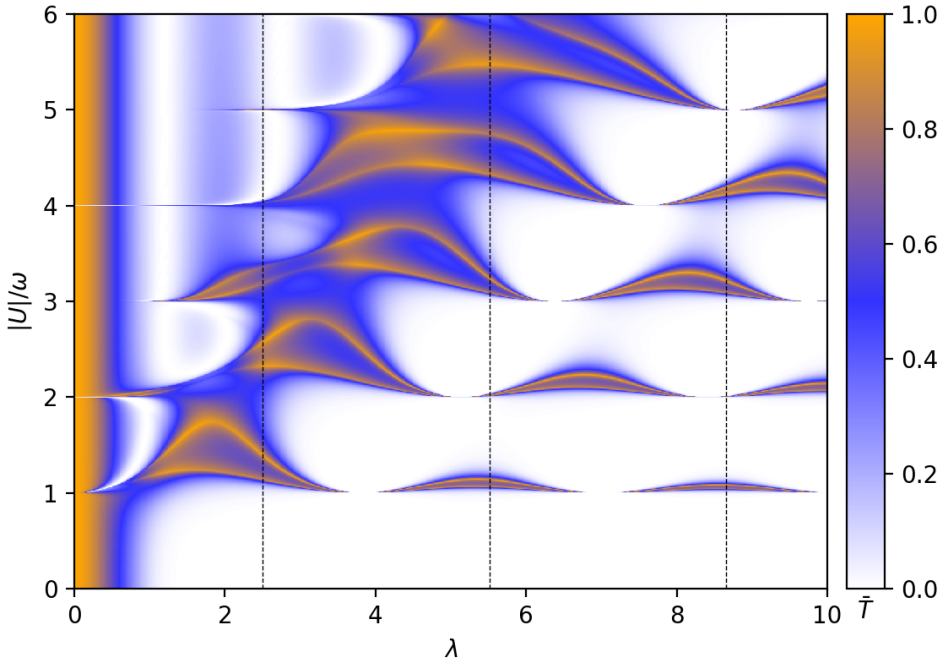


Figure 4.10: Pair transmission averaged over low momenta $k \in [0, \pi/2]$ as function of driving strength $\lambda$ and Hubbard interaction $|U|/\omega$. The vertical lines are drawn at the zeros of the single particle transmission $\bar{T}_s = J_0(\lambda)^2$.

In figures 4.10 and 4.11 we give two plots similar to figure 4.2, only that this time we do not average over the whole Brillouin zone, but only over low momenta $k \in [0, \pi/2]$ or high momenta $k \in [\pi/2, \pi]$. By comparing both figures one can find regions where only low or high momenta are transmitted. Let us again go through the regimes $\lambda < |u| + 1.5$, $\lambda \approx |u| + 1.5$ and $\lambda > |u| + 1.5$ one by one: For $\lambda < |u| + 1.5$ we know from the discussion in section 3.3 that the transmission is mainly located around $k = \pi/2$ for small $\lambda$ and as $\lambda$ increases shifts to smaller $k$ (see for example figure 3.9). This is why in the upper left corner of figure 4.10 there is generally more transmission than in figure 4.11.

In the regime $\lambda \approx |u| + 1.5$ we find that the transmission is mostly dominated by small momenta. Only for larger $\lambda \gtrsim |u| + 1.5$ high momenta are also transmitted.

In the third regime $\lambda > |u| + 1.5$ the regions with high total transmission are mostly dominated by high momenta. In general low momenta are not transmitted at all. This is not surprising but follows from our discussion in section 3.3 where we found that the transmission in this regime concentrates on high momenta (see again figure 3.9). Only for $|u|$ slightly above an integer we found that the transmission also reaches up to low $k$ (see discussion in section 3.3.4 and figure 3.14). This is responsible for the small isolated regions above integer values of $|u|$ where the low momentum transmission is also high.

Usually the distribution of the transmission over the momenta is quite broad. Therefore one can only use the impurity to filter broad regions of momenta (i.e. either high or low momenta). If one wants to filter low momenta one should choose $\lambda \approx |u| + 1.5$. If one wants to filter high momenta one can use many possible values of $\lambda > |u| + 1.5$.

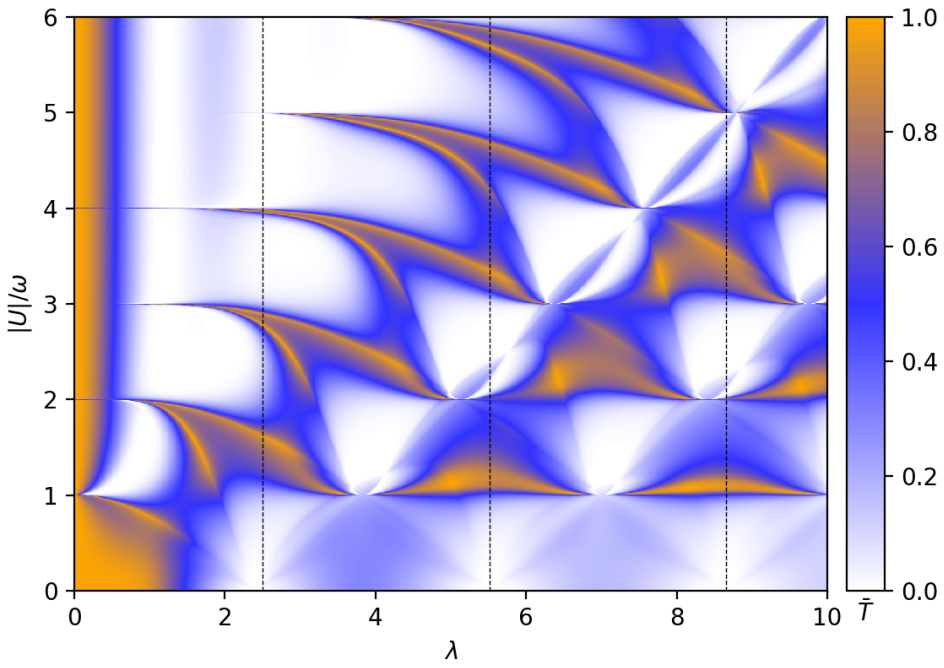


Figure 4.11: Pair transmission averaged over low momenta $k \in [\pi/2, \pi]$ as function of driving strength $\lambda$ and Hubbard interaction $|U|/\omega$. The vertical lines are drawn at the zeros of the single particle transmission $\bar{T}_s = J_0(\lambda)^2$.

If one is interested in filtering specific momenta one can use the regime $\lambda < |u| + 1.5$ where the transmission is concentrated in a rather narrow peak of width $\sim J_0(2\lambda)$. For small $\lambda$ this peak is centered around $k = \pi/2$. As $\lambda$ increases the center shifts to smaller $k$ (see again figure 3.9). Using this one can in principle create a narrow filter for a specific momentum $k < \pi/2$. The central momentum of this filter is given by equation (3.52) as $k = \arccos(v_1)$.

Unfortunately $v_1$ is always positive for small $\lambda$ and therefore we cannot build filters for $k > \pi/2$. Recall that this $v_1$ describes the effective chemical potential at site 1 (and the potential $v_0 = 2v_1$ at site 0) in the effective model (3.19). We can imagine that by adding an extra (negative) static potential around the driven impurity one can also reach negative $v_1$ at small $\lambda$. This impurity would then allow to also filter a specific momentum $k > \pi/2$. However one should first carefully redo the calculations done in section 3.2 which is outside of the scope of this thesis.

CHAPTER 5

# Scattering in the resonant case

## 5.1 Description of the situation

In chapter 3 we analyzed how paired fermions scatter off the driven impurity in the limit $J/\omega \to 0$ while keeping $u = U/\omega$ fixed. We concentrated on the non-resonant case, $|u| \notin \mathbb{N}$, where we knew for certain that the only possible outgoing states are either a transmitted or a reflected pair with the same energy, but no pair breaking (or other forms of absorbing energy from the driving) occured. This allowed us to compute an effective (static) Hamiltonian governing the pair dynamics and replacing the driven impurity with an effective static one in the limit $J/\omega \to 0$. We also compared these analytical results to numerical simulations and found that they are a good approximation for all $J/\omega < 0.125$ where $J/\omega = 0.125$ is the threshold above which resonant behaviour occurs.

In this chapter we would like to go beyond the non-resonant case. In particular we would like to study pair breaking due to the external driving. This process destroys a pair and should be avoided when trying to manipulate pairs with Floquet systems. Therefore we do not expect this chapter to be relevant for applications, but studying these resonance effects is still interesting for the general understanding of Floquet theory. In particular we would like to report some interesting and unintuitive behaviour of the Floquet system in this setting.

We will still consider a small $\alpha = J/\omega \ll 1$ but this time $u = U/\omega$ will be close to an integer $|u| \approx |u_0| \in \mathbb{N}$, where $u_0$ denotes the closest integer to $u$. By close to an integer we understand $|u| \in \left[|u_0| - 4\alpha, |u_0| + 4\alpha\right]$ which implies we are in the resonant case. Since $J/\omega$ is still a small quantity the bands are quite narrow and the absorption of energy quanta $\omega$ will only transfer the system from the bound pair band to the free single particle band (i.e. pair breaking). Note that no other effects, like excitations inside a single band, will occur.

Note also that this case does not affect the single particle case at all (since $U$ is not relevant there). Therefore the whole analysis will concentrate on the pairs.

## 5.2 Analytical results in the limit $J/\omega \to 0$

As $J/\omega$ is a small number the limit $\alpha = J/\omega \to 0$ is still a promising limit to obtain analytical results. Since the situation is more complicated than in the non-resonant case, before we start it is a good idea to think about what are the most important parts of the system. We will again think about the Floquet

system in the extended Hilbert space formalism, where it consists of a stack of 2D lattices labelled by an integer $a$ (recall figure 3.1(b)).

Of course an essential part is the layer 0 which corresponds to the original system. In this layer we have the initial state before the scattering. The final state long time after the scattering event will consist of three parts: a transmitted pair in layer 0, a reflected pair in layer 0 and a broken pair given by two single particles in layer $|u_0|$. All other layers expect 0 and $|u_0|$ are energetically not allowed and can therefore only play a role during the scattering event, but not afterwards. Therefore let us concentrate in our discussion on pair states in layer 0 and on free particle states in layer $|u_0|$.

### 5.2.1 Expected behaviour

First we want to qualitatively discuss what we expect. In the limit $\alpha = J/\omega \to 0$ there are two timescales in the system. The pairs move slowly on timescales $\frac{|U|}{4J^2} \sim \frac{1}{\alpha^2}$ while the single particles move comparatively faster on timescales $\frac{1}{J} \sim \frac{1}{\alpha}$. So what is our expectation in the limit $\alpha \to 0$?

As $\alpha \to 0$ the incoming pair will become slower and slower. During the scattering event it will spend an increasingly longer time at the impurity. As long as it is there the pair breaking process will break the pair into single particles. These single particles move much faster than the pair and can propagate away to infinity quickly and are therefore observed as pair loss. Since the time spend at the impurity becomes increasingly longer there is more possibility for the pair breaking process to break the pair. Therefore our expectation is that for small $\alpha$ almost the whole pair breaks into single particles and only a minor fraction is transmitted. However as it turns out this expectation is completely wrong: Actually pair breaking vanishes in the limit $\alpha \to 0$.

Analytical results for systems with several timescales are much harder to obtain than for systems with only one (dominating) timescale. In the next section we will discuss such problems in more detail.

### 5.2.2 Discussion of the different timescales

Recall that we have to deal with two different timescales: the pairs move slowly on timescales $1/\alpha^2$ and the single particles move faster on timescales $1/\alpha$. This would not be a problem if we would mostly be interested in single particle dynamics. Then the pairs move so slow that they in fact become immobile and we could ignore them and write down an effective Hamiltonian on timescale $1/\alpha$. However we are interested in pairs. If we would only consider timescales $1/\alpha$ pairs would not move at all and we could not study their scattering at the impurity. Therefore we are forced to look at long timescales $1/\alpha^2$ but also take into account the shorter ones $1/\alpha$. Writing down an effective Hamiltonian for slow parts of a system which also couples to fast parts is a complicated matter because one usually needs a non-perturbative solution for the fast parts which can then be reinserted into the dynamics of the slow scales.

Let us illustrate that in the present problem. We expect that an effective Hamiltonian for the slow pairs would be given by a hopping Hamiltonian with some kind of effective impurity around site 0. In the non-resonant case this impurity contains excitations to all other layers which then quickly decay back into layer 0. Note that this effective impurity was given by a hermitian operator because pairs cannot get lost during the scattering. In the resonant case however the effective impurity will contain two parts: a hermitian one as before for all layers other than $|u_0|$ and a non-hermitian part encoding the

loss of pairs due to pair breaking into layer $|u_0|$. Unfortunately not all pairs that break propagate away as free particles in layer $|u_0|$, but there is also the possibility of both of them coming back together at the impurity and recombining to a pair. This requires a detailed solution of the dynamics in the first layer[1].

But even if we would be able to compute such an effective Hamiltonian this might not be what we actually want. The effective Hamiltonian would give us the effective dynamics on the timescale $1/\alpha^2$. But we are not interested in analyzing these timescales, we actually would like to study the scattering properties. All results in scattering theory are implicitly based on the limit where the time $t \to \pm\infty$. So when we derive an effective Hamiltonian and then derive its scattering properties what we really do is to perform two limits: First we let $\alpha \to 0$ and then $t \to \pm\infty$. What we should actually do is to take the limits in the opposite order: First let $t \to \pm\infty$ and then let $\alpha \to 0$. Most often both limits can be interchanged, especially when there is only one dominating timescale in the system. But for two or more timescales this is not a priori clear. Therefore instead of trying to find an effective Hamiltonian it is more careful (and, as it turns out, also more analytically useful) to first consider scattering theory and then perform the limit $\alpha \to 0$ inside its equations.

### 5.2.3 A quick overview about scattering theory

Consider an arbitrary Hamiltonian $\mathbf{H} = \mathbf{H}_0 + \mathbf{V}$, where $\mathbf{H}_0$ is a free Hamiltonian with a continuous spectrum and $\mathbf{V}$ a scattering impurity. The basic equation of scattering theory is the Lippman-Schwinger equation [26] (see [27] chapter 'The Formal Theory of Scattering' for an overview over scattering theory and its connection to the Lippmann-Schwinger equation):

$$\left|\psi^+\right\rangle = |\phi\rangle + \frac{1}{E - \mathbf{H}_0 + i\epsilon}\mathbf{V}\left|\psi^+\right\rangle. \tag{5.1}$$

Here we imply the limit $\epsilon \to 0$. It describes a specific eigenstate $\left|\psi^+\right\rangle$ of $\mathbf{H}$ with energy $E$. There is usually more than one eigenstate with energy $E$, so the Lippman-Schwinger equation picks out the correct one for scattering. It can be interpreted as follows: imagine an incoming particle at time $t \to -\infty$ far away from the impurity. Its wavefunction is an eigenstate $|\phi\rangle$ of the unperturbed Hamiltonian $\mathbf{H}_0$ with energy $E$ (typically a plane wave). The Lippman-Schwinger equation now picks out the eigenstate $\left|\psi^+\right\rangle$ with energy $E$ for which its incoming part, when evaluated far away from the impurity, is given by $|\phi\rangle$. Note that this does not mean that the wavefunction itself reduces to $|\phi\rangle$ far away from the impurity. Far away from the impurity $\left|\psi^+\right\rangle$ is given by a superposition of the incoming wave $|\phi\rangle$ and several outgoing waves $\left|\psi^+\right\rangle - |\phi\rangle = \frac{1}{E-\mathbf{H}_0+i\epsilon}\mathbf{V}\left|\psi^+\right\rangle$. The small regulator $\epsilon$ in the Greens function $\frac{1}{E-\mathbf{H}_0+i\epsilon}$ is introduced in order to make sure that it will only produce outgoing states.

Once we have found the solution $\left|\psi^+\right\rangle$ of the Lippmann-Schwinger equation we can easily read off the transmission amplitudes into various parts of the system as the prefactors in front of the corresponding outgoing plane waves.

If a system contains several parts one can either write down a very big vectorized Lippmann-Schwinger equation or one can write down several coupled Lippmann-Schwinger equations, one for

[1] which would be possible, though still complicated, if the Hamiltonian in layer $|u_0|$ would be a simple Fermi-Hubbard Hamiltonian. But as one can see in figure 3.2(b) even when ignoring the coupling to other layers there is still a renormalized hopping around the impurity, which breaks translation symmetry and drastically complicates the calculation.

each part of the system. Our aim is to study the Lippman-Schwinger equation in a situation where two parts of the system evolve on different timescales. Especially we are interested in a situation where the incoming state evolves very slowly in time and the possible outgoing states in the other parts of the system evolve much faster. In order to get used to such situations it is good to first look at a much simpler toy model which can be explicitly solved.

### 5.2.4 Intermezzo: A simple toy model

Note that the toy model is not connected to our actual problem in any way. We study it because it is an instructive and simple example of what happens if there are two different timescales in the system.

The toy model consists of two hopping chains called P and Q (see figure 5.1). The Q chain has hopping parameter $J_1 = J$ while the P chain has hopping parameter $J_2 = \alpha J$, where $\alpha$ is a small positive number (i.e. the states on the P chain only evolve slowly in time). We denote the state where a particle is at site $n$ in the P chain or in the Q chain by $\left|n_\mathrm{P}\right\rangle$ or $\left|n_\mathrm{Q}\right\rangle$ respectively. The two chains are coupled at site zero by $\mathbf{V} = \lambda\Big(\left|0_\mathrm{P}\right\rangle\left\langle 0_\mathrm{Q}\right| + \left|0_\mathrm{P}\right\rangle\left\langle 0_\mathrm{Q}\right|\Big)$. We want to calculate how an incoming wave $|\phi\rangle$ in the P chain scatters from this impurity in the limit $\alpha \to 0$. Note that this system contains the main important features we also have in our original problem: We have two parts of the system, a slow one P and a fast one Q, and the incoming state is in the slow part P.

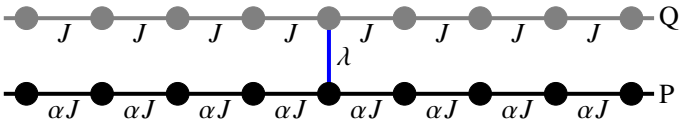


Figure 5.1: Sketch of the toy model. It consists of two hopping chains: a slow one P (black) with hopping parameter $\alpha J$ and a fast one Q (gray) with hopping parameter $J$. Both chains are coupled at site 0 with coupling strength $\lambda$ (blue).

A very important observation is that by changing the hopping parameter $J_2 = \alpha J$ of the slow system, we also change the energy of the incoming plane wave $E = \alpha\varepsilon$ where $\varepsilon = -2J\cos(k)$.

Denote the projector on the P chain by $\mathbf{P}$ and the one on the Q chain by $\mathbf{Q} = 1 - \mathbf{P}$. The two coupled Lippmann-Schwinger equations read

$$\mathbf{P}\left|\psi^+\right\rangle = |\phi\rangle + \frac{\lambda}{\alpha\varepsilon + \alpha J\mathbf{H}_\mathrm{H} + i\epsilon}\left|0_\mathrm{P}\right\rangle\left\langle 0_\mathrm{Q}\right|\mathbf{Q}\left|\psi^+\right\rangle \tag{5.2}$$

$$\mathbf{Q}\left|\psi^+\right\rangle = \frac{\lambda}{\alpha\varepsilon + J\mathbf{H}_\mathrm{H} + i\epsilon}\left|0_\mathrm{Q}\right\rangle\left\langle 0_\mathrm{P}\right|\mathbf{P}\left|\psi^+\right\rangle. \tag{5.3}$$

The second equation (5.3) can be immediately inserted into the first one and gives:

$$\mathbf{P}\left|\psi^+\right\rangle = |\phi\rangle + \frac{1}{\alpha}\left(\frac{\lambda}{\varepsilon + J\mathbf{H}_\mathrm{H} + i\epsilon}\left|0_\mathrm{P}\right\rangle\left\langle 0_\mathrm{Q}\right|\frac{\lambda}{\alpha\varepsilon + J\mathbf{H}_\mathrm{H} + i\epsilon}\left|0_\mathrm{Q}\right\rangle\right)\left\langle 0_\mathrm{P}\right|\mathbf{P}\left|\psi^+\right\rangle. \tag{5.4}$$

The last equation can be thought of as an effective Lippmann-Schwinger equation in the $\mathbf{P}$ sector with an effective potential $\mathbf{V}^\mathrm{eff} = \left(\lambda^2\left\langle 0_\mathrm{Q}\right|\frac{1}{\alpha\varepsilon + J\mathbf{H}_\mathrm{H} + i\epsilon}\left|0_\mathrm{Q}\right\rangle\right)\left|0_\mathrm{P}\right\rangle\left\langle 0_\mathrm{P}\right|$.

How can we solve this equation? Note that the right hand side only depends on the value of the wavefunction at the impurity. Therefore if we multiply equation (5.4) by $\left\langle 0_\mathrm{P}\right|$ we find an equation

solely for $\langle 0_\mathrm{P}| \mathbf{P} |\psi^+\rangle$:

$$\langle 0_\mathrm{P}| \mathbf{P} |\psi^+\rangle = \langle 0_\mathrm{P}|\phi\rangle + \frac{\lambda^2}{\alpha} \langle 0_\mathrm{P}| \frac{1}{\varepsilon + J\mathbf{H}_\mathrm{H} + i\epsilon} |0_\mathrm{P}\rangle \langle 0_\mathrm{Q}| \frac{1}{\alpha\varepsilon + J\mathbf{H}_\mathrm{H} + i\epsilon} |0_\mathrm{Q}\rangle \langle 0_\mathrm{P}| \mathbf{P} |\psi^+\rangle \tag{5.5}$$

which can be easily solved:

$$\langle 0_\mathrm{P}| \mathbf{P} |\psi^+\rangle = \frac{1}{1 - \frac{\lambda^2}{\alpha} \langle 0_\mathrm{P}| \frac{1}{\varepsilon + J\mathbf{H}_\mathrm{H} + i\epsilon} |0_\mathrm{P}\rangle \langle 0_\mathrm{Q}| \frac{1}{\alpha\varepsilon + J\mathbf{H}_\mathrm{H} + i\epsilon} |0_\mathrm{Q}\rangle} \langle 0_\mathrm{P}|\phi\rangle \,. \tag{5.6}$$

Reinserting this into the above equations (5.2) and (5.3) gives the full solution to the Lippmann-Schwinger equation. Now it is finally time to study the limit $\alpha \to 0$. We find[2]:

$$\langle 0_\mathrm{P}| \mathbf{P} |\psi^+\rangle = -\frac{\alpha}{\lambda^2 \langle 0_\mathrm{P}| \frac{1}{\varepsilon + J\mathbf{H}_\mathrm{H} + i\epsilon} |0_\mathrm{P}\rangle \langle 0_\mathrm{Q}| \frac{1}{J\mathbf{H}_\mathrm{H} + i\epsilon} |0_\mathrm{Q}\rangle} \langle 0_\mathrm{P}|\phi\rangle + O\left(\alpha^2\right). \tag{5.7}$$

Inserting back into the above equations (5.2) and (5.3) gives:

$$\mathbf{P} |\psi^+\rangle = |\phi\rangle - \frac{1}{\varepsilon + J\mathbf{H}_\mathrm{H} + i\epsilon} |0_\mathrm{P}\rangle \frac{1}{\langle 0_\mathrm{Q}| \frac{1}{\varepsilon + J\mathbf{H}_\mathrm{H} + i\epsilon} |0_\mathrm{Q}\rangle} \langle 0_\mathrm{P}|\phi\rangle + O(\alpha) \tag{5.8}$$

$$\mathbf{Q} |\psi^+\rangle = -\alpha \frac{\lambda}{J\mathbf{H}_\mathrm{H} + i\epsilon} |0_\mathrm{Q}\rangle \frac{1}{\lambda^2 \langle 0_\mathrm{P}| \frac{1}{\varepsilon + J\mathbf{H}_\mathrm{H} + i\epsilon} |0_\mathrm{P}\rangle \langle 0_\mathrm{Q}| \frac{1}{J\mathbf{H}_\mathrm{H} + i\epsilon} |0_\mathrm{Q}\rangle} \langle 0_\mathrm{P}|\phi\rangle + O\left(\alpha^2\right). \tag{5.9}$$

In particular look at equation (5.9) which tells us how much scatters from the slow chain P to the fast chain Q. We expected, as for the pairs, that in the limit $\alpha \to 0$ scattering into Q should be dominant. Surprisingly we find quite the opposite – scattering into the Q chain is suppressed. What is the reason for that? Take a look at equation (5.7). The wavefunction at the impurity site vanishes in the limit $\langle 0_\mathrm{P}| \mathbf{P} |\psi^+\rangle \to 0$. Therefore no more scattering into the Q chain can happen. There is also another interesting feature. The solution in the P chain does not depend on any property of the Q system. It does not even depend on the coupling strength between both chains $\lambda$. At first this might seem strange because for $\lambda = 0$ the system should be completely unperturbed, but in fact it does only mean that the limits $\alpha \to 0$ and $\lambda \to 0$ do not commute[3].

By taking a closer look at equation (5.8) we find that the incoming wave is fully reflected and no more transmission occurs. This can be either verified by explicit calculation or by observing that the pinning of the wavefunction at the impurity $\langle 0_\mathrm{P}| \mathbf{P} |\psi^+\rangle \to 0$ acts as an artificial boundary condition. This artificial boundary condition disconnects both sides of the P chain and therefore transmission is no longer possible.

Although for the pairs the situation is much more complicated in several aspects, seeing the full treatment of the Lippmann-Schwinger equation once for a simple toy model helps to understand the general features in the limit $\alpha \to 0$. In particular we will find that pair breaking, which is scattering from a slow to a fast part of the system, vanishes in the limit. This is directly connected to the pinning

[2] The limit is of course only correct if $\left\langle 0_\mathrm{Q}\right| \frac{1}{\varepsilon + J\mathbf{H}_\mathrm{H} + i\epsilon} \left|0_\mathrm{Q}\right\rangle \neq 0$, which can be checked by explicit calculation for a hopping Hamiltonian.

[3] Or in other words the results are only applicable if $\alpha \ll \lambda$.

of the wavefunction to 0 at all points where the potential 'acts' (we will later explain what we mean by that). Interestingly the third feature, namely that the wavefunction gets fully reflected in the limit, is not there for pairs. Instead we will find a finite transmission which depends non-trivially on $\lambda$.

### 5.2.5 The Lippmann-Schwinger equation for the pairs

Let us come back to the pairs. Recall how we describe the system for a pair in the extended Hilbert space: The system consists of an infinite stack of copies $a$ of the original model each having an energy offset of $-a$. Each layer is a 2D lattice with an extra potential due to the Hubbard interaction at the diagonal. The driving induces couplings between the layers. We will now cast this complicated model into a scattering problem.

The free Hamiltonian is simply given by uncoupled Fermi-Hubbard Hamiltonians $-\frac{J}{\omega}\mathbf{H}_{\mathrm{H}}+\frac{U}{\omega}\mathbf{H}_{\mathrm{U}}-a$ on each layer $a$ with an extra energy offset $-a$. We will use the gauge transformed version of the Hamiltonian (3.8). In order to get the potential we need to subtract the Fermi-Hubbard model from it and then express it in Fourier components. This gives the following Fourier component of the potential (compare to formula (3.11))

$$\mathbf{V}_a = -\frac{J}{\omega}\left[\sum_{n\sigma}(g_{na}-\delta_{a,0})\mathbf{c}^\dagger_{n\sigma}\mathbf{c}_{n+1\sigma}+(g^*_{n,-a}-\delta_{a,0})\mathbf{c}^\dagger_{n+1\sigma}\mathbf{c}_{n\sigma}\right] \tag{5.10}$$

$$= \begin{cases} -\frac{J}{\omega}J_a(\lambda)\left[\sum_\sigma \mathbf{c}^\dagger_{-1\sigma}\mathbf{c}_{0\sigma}+(-1)^a\mathbf{c}^\dagger_{0\sigma}\mathbf{c}_{-1\sigma}+(-1)^a\mathbf{c}^\dagger_{0\sigma}\mathbf{c}_{1\sigma}+\mathbf{c}^\dagger_{1\sigma}\mathbf{c}_{0\sigma}\right] & a\neq 0 \\ -\frac{J}{\omega}\big(J_0(\lambda)-1\big)\left[\sum_\sigma \mathbf{c}^\dagger_{-1\sigma}\mathbf{c}_{0\sigma}+\mathbf{c}^\dagger_{0\sigma}\mathbf{c}_{-1\sigma}+\mathbf{c}^\dagger_{0\sigma}\mathbf{c}_{1\sigma}+\mathbf{c}^\dagger_{1\sigma}\mathbf{c}_{0\sigma}\right] & a=0 \end{cases} \tag{5.11}$$

where the $g_{na}$ are the Fourier components of the time-depending hopping. The extra $-\delta_{a,0}$ appear because we had to subtract the Fermi-Hubbard model from the full Hamiltonian. These Fourier components $\mathbf{V}_a$ couple a layer $b$ to layer $b-a$. In order to keep track of the current layer $a$ we will introduce the creation operators $\mathbf{c}^\dagger_{n\sigma;a}$ which creates a particle of spin $\sigma$ on site $n$ on layer $a$. The potential connecting layer $b$ and $a$ is given by

$$\mathbf{V}_{a\leftarrow b} = \begin{cases} -\frac{J}{\omega}J_{b-a}(\lambda)\left[\sum_\sigma \mathbf{c}^\dagger_{-1\sigma;a}\mathbf{c}_{0\sigma;b}+(-1)^{b-a}\left(\mathbf{c}^\dagger_{0\sigma;a}\mathbf{c}_{-1\sigma;b}+\mathbf{c}^\dagger_{0\sigma;a}\mathbf{c}_{1\sigma;b}\right)+\mathbf{c}^\dagger_{1\sigma;a}\mathbf{c}_{0\sigma;b}\right] & a\neq b \\ -\frac{J}{\omega}\big(J_0(\lambda)-1\big)\left[\sum_\sigma \mathbf{c}^\dagger_{-1\sigma;a}\mathbf{c}_{0\sigma;a}+\mathbf{c}^\dagger_{0\sigma;a}\mathbf{c}_{-1\sigma;a}+\mathbf{c}^\dagger_{0\sigma;a}\mathbf{c}_{1\sigma;a}+\mathbf{c}^\dagger_{1\sigma;a}\mathbf{c}_{0\sigma;a}\right] & a=b \end{cases}. \tag{5.12}$$

We can now write down the Lippmann-Schwinger equations (with a preliminary notation):

$$\left|\psi^+_a\right\rangle = |\phi\rangle\,\delta_{a,0}+\frac{1}{E-\left(-\frac{J}{\omega}\mathbf{H}_{\mathrm{H}}+\frac{U}{\omega}\mathbf{H}_{\mathrm{U}}\right)+a+i\varepsilon}\left[\sum_b \mathbf{V}_{a\leftarrow b}\left|\psi^+_b\right\rangle\right]. \tag{5.13}$$

Here $|\phi\rangle$ is an incoming pair state in layer 0 and $E$ is its energy. We would like to study the limit $\alpha=\frac{J}{\omega}\to 0$. We know that in this limit, by using the Schrieffer-Wolff transformation $\mathbf{W}_\alpha$, the Hamiltonian on each layer block diagonalizes into two parts: A Hamiltonian for pairs and one for free particles. As $\alpha\to 0$ we have:

$$-\frac{J}{\omega}\mathbf{H}_{\mathrm{H}}+\frac{U}{\omega}\mathbf{H}_{\mathrm{U}} = \mathbf{W}_\alpha\Big(-|u|\mathbf{P}+\alpha^2\mathbf{P}\mathbf{h}^{\mathrm{P}}_\alpha\mathbf{P}+\alpha\mathbf{Q}\mathbf{h}^{\mathrm{Q}}_\alpha\mathbf{Q}\Big)\mathbf{W}^\dagger_\alpha. \tag{5.14}$$

Here we denote $u = U/\omega$ and define $\mathbf{P}$ and $\mathbf{Q}$ as the subspaces for pairs and single particles respectively. The Hamiltonian $\mathbf{h}_\alpha^{\mathrm{P}}$ becomes in the limit the effective Hamiltonian from the Schrieffer-Wolff transformation (2.15):

$$\mathbf{h}_\alpha^{\mathrm{P}} \to \frac{-4}{|u|}\left[\sum_n \frac{1}{2}\left(\eta_n^+\eta_{n+1}^- + \eta_{n+1}^+\eta_n^-\right) - 1\right]. \tag{5.15}$$

The form of the free particle Hamiltonian $\mathbf{h}_\alpha^{\mathrm{Q}}$ will not be relevant. By applying $\mathbf{W}_\alpha^\dagger$ to both sides of the Lippmann-Schwinger equation (5.13) and defining $\left|\tilde{\psi}^+\right\rangle = \mathbf{W}_\alpha^\dagger \left|\psi^+\right\rangle$ and $\left|\tilde{\phi}\right\rangle = \mathbf{W}_\alpha^\dagger \left|\phi\right\rangle$ we find:

$$\left|\tilde{\psi}_a^+\right\rangle = \left|\tilde{\phi}\right\rangle \delta_{a,0} + \frac{1}{E + |u|\mathbf{P} - \alpha^2 \mathbf{P}\mathbf{h}_\alpha^{\mathrm{P}}\mathbf{P} - \alpha \mathbf{Q}\mathbf{h}_\alpha^{\mathrm{Q}}\mathbf{Q} + a + i\epsilon}\left[\sum_b \mathbf{W}_\alpha^\dagger \mathbf{V}_{a\leftarrow b}\mathbf{W}_\alpha \left|\tilde{\psi}_b^+\right\rangle\right]. \tag{5.16}$$

In this version the denominator of the Lippmann-Schwinger equation block diagonalizes into $\mathbf{P}$ and $\mathbf{Q}$ spaces. In order to keep track of the layer $a$ we define $\mathbf{P}_a$ and $\mathbf{Q}_a$ as the projectors onto pairs and free states in layer $a$ (also we will soon need $\mathbf{P}$ and $\mathbf{Q}$ for other purposes). From now on we will drop the tilde over the wavefunctions. In this new notation we can write the Lippmann-Schwinger equations (5.16) as

$$\mathbf{P}_a \left|\psi^+\right\rangle = |\phi\rangle \delta_{a,0} + \frac{1}{E + |u| - \alpha^2 \mathbf{h}_\alpha^{\mathrm{P}} + a + i\epsilon}\left[\sum_b \mathbf{W}_\alpha^\dagger \mathbf{V}_{a\leftarrow b}\mathbf{W}_\alpha \mathbf{P}_b \left|\psi^+\right\rangle + \mathbf{W}_\alpha^\dagger \mathbf{V}_{a\leftarrow b}\mathbf{W}_\alpha \mathbf{Q}_b \left|\psi^+\right\rangle\right] \tag{5.17}$$

$$\mathbf{Q}_a \left|\psi^+\right\rangle = \frac{1}{E - \alpha \mathbf{h}_\alpha^{\mathrm{Q}} + a + i\epsilon}\left[\sum_b \mathbf{W}_\alpha^\dagger \mathbf{V}_{a\leftarrow b}\mathbf{W}_\alpha \mathbf{P}_b \left|\psi^+\right\rangle + \mathbf{W}_\alpha^\dagger \mathbf{V}_{a\leftarrow b}\mathbf{W}_\alpha \mathbf{Q}_b \left|\psi^+\right\rangle\right]. \tag{5.18}$$

Let us perform a few minor changes here. First, in order to make the order of $\alpha$ explicit, let us redefine the potential (5.12) as $\alpha \mathbf{V}_a$. Second the energy of the incoming pair with momentum $k$ is $E = -|u| - \alpha^2 \frac{2}{|u|}(\cos(k) - 1) + O\left(\alpha^2\right) = -|u| + \alpha^2 \varepsilon_\alpha$. Inserting this into the formulas (5.17) and (5.18) yields:

$$\mathbf{P}_a \left|\psi^+\right\rangle = |\phi\rangle \delta_{a,0} + \frac{\alpha}{\alpha^2 \varepsilon_\alpha - \alpha^2 \mathbf{h}_\alpha^{\mathrm{P}} + a + i\epsilon}\left[\sum_b \mathbf{W}_\alpha^\dagger \mathbf{V}_{a\leftarrow b}\mathbf{W}_\alpha \mathbf{P}_b \left|\psi^+\right\rangle + \mathbf{W}_\alpha^\dagger \mathbf{V}_{a\leftarrow b}\mathbf{W}_\alpha \mathbf{Q}_b \left|\psi^+\right\rangle\right] \tag{5.19}$$

$$\mathbf{Q}_a \left|\psi^+\right\rangle = \frac{\alpha}{\alpha^2 \varepsilon_\alpha - \alpha \mathbf{h}_\alpha^{\mathrm{Q}} + (a - |u|) + i\epsilon}\left[\sum_b \mathbf{W}_\alpha^\dagger \mathbf{V}_{a\leftarrow b}\mathbf{W}_\alpha \mathbf{P}_b \left|\psi^+\right\rangle + \mathbf{W}_\alpha^\dagger \mathbf{V}_{a\leftarrow b}\mathbf{W}_\alpha \mathbf{Q}_b \left|\psi^+\right\rangle\right]. \tag{5.20}$$

This will be the final form of the Lippmann-Schwinger equations we are going to use. Before we continue let us quickly give a summary of all appearing quantities:

- $\mathbf{P}_a$ projects onto paired states (i.e. the diagonal) in layer $a$.
- $\mathbf{Q}_a$ projects onto free states (i.e. everything except the diagonal) in layer $a$.

- $\mathbf{h}_\alpha^{\mathrm{P}}$ is the effective Hamiltonian for pairs. In the limit $\alpha \to 0$ it is equivalent to a hopping Hamiltonian $\frac{-2}{|u|}\big(\mathbf{H}_{\mathrm{H}} - 2\big)$.

- $\mathbf{h}_\alpha^{\mathrm{Q}}$ is the effective Hamiltonian for free particles.

- $|\phi\rangle$ incoming plane wave with momentum $k$ in $\mathbf{P}_0$ (i.e. a pair in layer 0).

- The energy of the incoming pair: $\varepsilon_\alpha = -\frac{4}{|u|}(\cos(k) - 1) + O(\alpha)$

- The potential coupling the layers

$$\mathbf{V}_{a\leftarrow b} = \begin{cases} -J_{b-a}(\lambda)\Big[\sum_\sigma \mathbf{c}^\dagger_{-1\sigma;a}\mathbf{c}_{0\sigma;b} + (-1)^{b-a}\Big(\mathbf{c}^\dagger_{0\sigma;a}\mathbf{c}_{-1\sigma;b} + \mathbf{c}^\dagger_{0\sigma;a}\mathbf{c}_{1\sigma;b}\Big) + \mathbf{c}^\dagger_{1\sigma;a}\mathbf{c}_{0\sigma;b}\Big] & a \neq b \\ -\big(J_0(\lambda) - 1\big)\Big[\sum_\sigma \mathbf{c}^\dagger_{-1\sigma;a}\mathbf{c}_{0\sigma;a} + \mathbf{c}^\dagger_{0\sigma;a}\mathbf{c}_{-1\sigma;a} + \mathbf{c}^\dagger_{0\sigma;a}\mathbf{c}_{1\sigma;a} + \mathbf{c}^\dagger_{1\sigma;a}\mathbf{c}_{0\sigma;a}\Big] & a = b \end{cases}. \tag{5.21}$$

- The Schrieffer-Wolff transformation $\mathbf{W}_\alpha$. It was introduced s.t. the Hamiltonian decouples into bound pairs on the diagonal and free particles elsewhere (see section 2.1.4). It acts on each layer $a$ separately and has the expansion $\mathbf{W}_\alpha = 1 + \alpha\frac{1}{|u|}\mathbf{Q}_a\mathbf{H}_{\mathrm{H}}\mathbf{P}_a + O\Big(\alpha^2\Big)$.

### 5.2.6 Applying the theorem

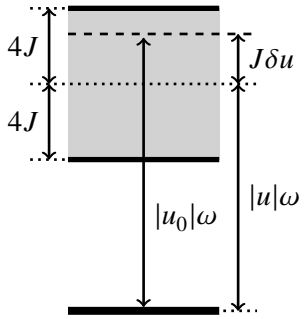


Figure 5.2: Sketch of relevant energy levels involved in pair breaking. The interaction $U = u_0\omega + J\delta u$ is decomposed into an integer multiple of omega $u_0\omega$ and a remainder $J\delta u$ which determines the energy of the broken pair (dashed) inside the single particle band (gray). Note also that the pair band (lowest line) has a width, which is not shown because it is of order $(J/\omega)^2$.

As said before we are interested in situations where $u \approx u_0$ and $u_0$ is an integer. We will make the approximation precise by writing $u = u_0 + \alpha\delta u$. This means we give $u$ the freedom to approach $u_0$ in different ways as $\alpha \to 0$. The situation is depicted in figure 5.2. In order to stay in the resonant case we need $|\delta u| < 4$.

Inserting this into the Lippmann-Schwinger equations (5.19) and (5.20) gives:

$$\mathbf{P}_a \left|\psi^+\right\rangle = |\phi\rangle\, \delta_{a,0} + \frac{1}{\alpha\varepsilon_\alpha - \alpha\mathbf{h}_\alpha^{\mathrm{P}} + \frac{a}{\alpha} + i\epsilon}\left[\sum_b \mathbf{W}_\alpha^\dagger \mathbf{V}_{a\leftarrow b}\mathbf{W}_\alpha \mathbf{P}_b \left|\psi^+\right\rangle + \mathbf{W}_\alpha^\dagger \mathbf{V}_{a\leftarrow b}\mathbf{W}_\alpha \mathbf{Q}_b \left|\psi^+\right\rangle\right] \tag{5.22}$$

$$\mathbf{Q}_a \left|\psi^+\right\rangle = \frac{1}{\alpha\varepsilon_\alpha - \left(\mathbf{h}_\alpha^{\mathrm{Q}} - \delta u\right) + \frac{a-|u_0|}{\alpha} + i\epsilon}\left[\sum_b \mathbf{W}_\alpha^\dagger \mathbf{V}_{a\leftarrow b}\mathbf{W}_\alpha \mathbf{P}_b \left|\psi^+\right\rangle + \mathbf{W}_\alpha^\dagger \mathbf{V}_{a\leftarrow b}\mathbf{W}_\alpha \mathbf{Q}_b \left|\psi^+\right\rangle\right]. \tag{5.23}$$

where we also cancelled an $\alpha$ in both equations (in order to bring them into the form for theorem 1). We can easily see that, by looking at the denominator, as $\alpha \to 0$ the wavefunction $\mathbf{P}_a \left|\psi^+\right\rangle$ and $\mathbf{Q}_a \left|\psi^+\right\rangle$ vanishes for almost all parts of the system. Only in the spaces $\mathbf{P}_{a=0}$ and $\mathbf{Q}_{a=|u_0|}$ the wavefunction will not go to zero as $\alpha \to 0$. We deal with such situations in theorem 1 of appendix B. Define the subspaces

$$\mathbf{P} = \mathbf{P}_0 \tag{5.24}$$

$$\mathbf{Q} = 1 - \mathbf{P} = \sum_{a\neq 0} \mathbf{P}_a + \sum_a \mathbf{Q}_a. \tag{5.25}$$

$\mathbf{P}$ is the subspace of the incoming pair, which evolves by a factor $\alpha$ slower than all other subspaces $\mathbf{Q}$. Theorem 1 gives us some important conclusions about the scattering wavefunction $\mathbf{P}\left|\psi^+\right\rangle$ in the $\mathbf{P}$ sector in the limit $\alpha \to 0$. It does not directly predict anything in the $\mathbf{Q}$ sector. But as we will see we can use the information about $\mathbf{P}_0 \left|\psi^+\right\rangle$ to calculate the full wavefunction.

#### Properties of the Greens function

The central object of Theorem 1 is the effective potential

$$\mathbf{V}_\alpha^{\mathrm{eff}} = \mathbf{P}\mathbf{V}_\alpha\mathbf{P} + \mathbf{P}\mathbf{V}_\alpha\mathbf{Q}\mathbf{G}_\alpha^{\mathrm{Q}}\mathbf{Q}\mathbf{V}_\alpha\mathbf{P} \tag{5.26}$$

where in our case the potential $\mathbf{V}_\alpha$ can be thought of as a big block matrix in the extended Hilbert space with entries $\mathbf{W}_\alpha^\dagger \mathbf{V}_{a\leftarrow b}\mathbf{W}_\alpha$ coupling layer $b$ to $a$. The Greens function $\mathbf{G}_\alpha^{\mathrm{Q}}$ is defined in the following way: Assume that we already know the wavefunction in the $\mathbf{P}$ sector. Then the solution to the Lippmann-Schwinger equation in the $\mathbf{Q}$ sector is given by:

$$\mathbf{Q}\left|\psi^+\right\rangle = \mathbf{G}_\alpha^{\mathrm{Q}}\left(\mathbf{Q}\mathbf{V}_\alpha\mathbf{P}\left|\psi^+\right\rangle\right). \tag{5.27}$$

We could try to give a general formula for it, but it is actually more instructive to directly evaluate it in the limit $\alpha \to 0$. Let us assume we fix the wavefunction in the sector $\mathbf{P} = \mathbf{P}_0$. Now consider the Lippmann-Schwinger equation for all the other subspaces. If $a \neq 0$ equation (5.19) shows that as $\alpha \to 0$ the wavefunction in $\mathbf{P}_a$ vanishes (recall $\mathbf{W}_\alpha \to 1$):

$$\mathbf{P}_a \left|\psi^+\right\rangle = \frac{\alpha}{\alpha^2\varepsilon_\alpha - \alpha^2\mathbf{h}_\alpha^{\mathrm{P}} + a + i\varepsilon}\left[\sum_b \mathbf{W}_\alpha^\dagger \mathbf{V}_{a\leftarrow b}\mathbf{W}_\alpha \mathbf{P}_b \left|\psi^+\right\rangle + \mathbf{W}_\alpha^\dagger \mathbf{V}_{a\leftarrow b}\mathbf{W}_\alpha \mathbf{Q}_b \left|\psi^+\right\rangle\right] \tag{5.28}$$

$$= \frac{\alpha}{a}\left[\sum_b \mathbf{V}_{a\leftarrow b}\mathbf{P}_b \left|\psi^+\right\rangle + \mathbf{V}_{a\leftarrow b}\mathbf{Q}_b \left|\psi^+\right\rangle\right] + \mathcal{O}\left(\alpha^2\right) \to 0 \tag{5.29}$$

and similar if $a \neq |u_0|$ equation (5.20) shows in $\mathbf{Q}_a$:

$$\mathbf{Q}_a \left|\psi^+\right\rangle = \frac{\alpha}{\alpha^2\varepsilon_\alpha - \alpha\mathbf{h}_\alpha^{\mathrm{Q}} + (a - |u|) + i\varepsilon}\left[\sum_b \mathbf{W}_\alpha^\dagger \mathbf{V}_{a\leftarrow b}\mathbf{W}_\alpha \mathbf{P}_b \left|\psi^+\right\rangle + \mathbf{W}_\alpha^\dagger \mathbf{V}_{a\leftarrow b}\mathbf{W}_\alpha \mathbf{Q}_b \left|\psi^+\right\rangle\right] \tag{5.30}$$

$$= \frac{\alpha}{a - |u_0|}\left[\sum_b \mathbf{V}_{a\leftarrow b}\mathbf{P}_b \left|\psi^+\right\rangle + \mathbf{V}_{a\leftarrow b}\mathbf{Q}_b \left|\psi^+\right\rangle\right] + \mathcal{O}\left(\alpha^2\right) \to 0. \tag{5.31}$$

The only non-trivial sector is $\mathbf{Q}_{|u_0|}$:

$$\mathbf{Q}_{|u_0|} \left|\psi^+\right\rangle = \frac{1}{\alpha\varepsilon_\alpha - \left(\mathbf{h}_\alpha^{\mathrm{Q}} - \delta u\right) + i\epsilon}\left[\sum_b \mathbf{W}_\alpha^\dagger \mathbf{V}_{|u_0|\leftarrow b}\mathbf{W}_\alpha \mathbf{P}_b \left|\psi^+\right\rangle + \mathbf{W}_\alpha^\dagger \mathbf{V}_{|u_0|\leftarrow b}\mathbf{W}_\alpha \mathbf{Q}_b \left|\psi^+\right\rangle\right] \tag{5.32}$$

$$\to \frac{1}{-\left(\mathbf{h}_0^{\mathrm{Q}} - \delta u\right) + i\epsilon}\left[\sum_b \mathbf{V}_{|u_0|\leftarrow b}\mathbf{P}_b \left|\psi^+\right\rangle + \mathbf{V}_{|u_0|\leftarrow b}\mathbf{Q}_b \left|\psi^+\right\rangle\right] \tag{5.33}$$

$$= \frac{1}{-\left(\mathbf{h}_0^{\mathrm{Q}} - \delta u\right) + i\epsilon}\left[\mathbf{V}_{|u_0|\leftarrow 0}\mathbf{P}_0 \left|\psi^+\right\rangle + \mathbf{V}_{|u_0|\leftarrow |u_0|}\mathbf{Q}_{|u_0|} \left|\psi^+\right\rangle\right]. \tag{5.34}$$

where we used in the last step that all other parts of the wavefunction vanish as $\alpha \to 0$. This equation can be solved:

$$\mathbf{Q}_{|u_0|} \left|\psi^+\right\rangle = \frac{1}{-\left(\mathbf{h}_\alpha^{\mathrm{Q}} - \delta u\right) - \mathbf{V}_{|u_0|\leftarrow |u_0|} + i\epsilon}\mathbf{V}_{|u_0|\leftarrow 0}\mathbf{P}_0 \left|\psi^+\right\rangle. \tag{5.35}$$

By comparing with the definition (5.27) we conclude that in the limit $\alpha \to 0$ the Greens function acts only in $\mathbf{Q}_{|u_0|}$ and is given by:

$$\mathbf{G}_0^{\mathrm{Q}} = \mathbf{Q}_{|u_0|}\mathbf{G}_0^{\mathrm{Q}}\mathbf{Q}_{|u_0|} = \frac{1}{-\left(\mathbf{h}_\alpha^{\mathrm{Q}} - \delta u\right) - \mathbf{V}_{|u_0|\leftarrow |u_0|} + i\epsilon}. \tag{5.36}$$

In order to obtain higher orders of the Greens function $\mathbf{G}_\alpha^{\mathrm{Q}} = \mathbf{G}_0^{\mathrm{Q}} + \alpha\mathbf{G}_1^{\mathrm{Q}} + \mathcal{O}\left(\alpha^2\right)$ we can plug equation (5.35) back into the other ones. We find that for $a \neq 0$ (and $a \neq |u_0|$) up to first order:

$$\mathbf{P}_a \left|\psi^+\right\rangle = \frac{\alpha}{a}\left[\mathbf{V}_{a\leftarrow 0}\mathbf{P}_0 \left|\psi^+\right\rangle + \mathbf{V}_{a\leftarrow |u_0|}\mathbf{Q}_{|u_0|}\left|\psi^+\right\rangle\right] + \mathcal{O}\left(\alpha^2\right) \tag{5.37}$$

$$= \frac{\alpha}{a}\left[\mathbf{V}_{a\leftarrow 0}\mathbf{P}_0 \left|\psi^+\right\rangle + \mathbf{V}_{a\leftarrow |u_0|}\mathbf{Q}_{|u_0|}\mathbf{G}_0^{\mathrm{Q}}\mathbf{Q}_{|u_0|}\mathbf{V}_{|u_0|\leftarrow 0}\mathbf{P}_0 \left|\psi^+\right\rangle\right] + \mathcal{O}\left(\alpha^2\right) \tag{5.38}$$

$$\mathbf{Q}_a \left|\psi^+\right\rangle = \frac{\alpha}{a-|u_0|}\left[\mathbf{V}_{a\leftarrow 0}\mathbf{P}_0 \left|\psi^+\right\rangle + \mathbf{V}_{a\leftarrow |u_0|}\mathbf{Q}_{|u_0|}\left|\psi^+\right\rangle\right] + \mathcal{O}\left(\alpha^2\right) \tag{5.39}$$

$$= \frac{\alpha}{a-|u_0|}\left[\mathbf{V}_{a\leftarrow 0}\mathbf{P}_0 \left|\psi^+\right\rangle + \mathbf{V}_{a\leftarrow |u_0|}\mathbf{Q}_{|u_0|}\mathbf{G}_0^{\mathrm{Q}}\mathbf{Q}_{|u_0|}\mathbf{V}_{|u_0|\leftarrow 0}\mathbf{P}_0 \left|\psi^+\right\rangle\right] + \mathcal{O}\left(\alpha^2\right) \tag{5.40}$$

and so

$$\mathbf{P}_a\mathbf{G}_1^{\mathrm{Q}}\mathbf{P}_a = \frac{1}{a} \qquad \mathbf{P}_a\mathbf{G}_1^{\mathrm{Q}}\mathbf{Q}_{|u_0|} = \frac{\alpha}{a}\mathbf{V}_{a\leftarrow |u_0|}\mathbf{Q}_{|u_0|}\mathbf{G}_0^{\mathrm{Q}} \tag{5.41}$$

$$\mathbf{Q}_a\mathbf{G}_1^{\mathrm{Q}}\mathbf{Q}_a = \frac{1}{a-|u_0|} \qquad \mathbf{Q}_a\mathbf{G}_1^{\mathrm{Q}}\mathbf{Q}_{|u_0|} = \frac{\alpha}{a-|u_0|}\mathbf{V}_{a\leftarrow |u_0|}\mathbf{Q}_{|u_0|}\mathbf{G}_0^{\mathrm{Q}}. \tag{5.42}$$

All other parts of $\mathbf{G}_1^{\mathrm{Q}}$ will vanish, expect $\mathbf{Q}_{|u_0|}\mathbf{G}_1^{\mathrm{Q}}\mathbf{Q}_{|u_0|}$, which is given by a quite complicated expression (we will not compute it, because we do not need it). The full effective potential (5.26) in the limit $\alpha \to 0$ is therefore:

$$\mathbf{V}_0^{\mathrm{eff}} = \mathbf{P}\mathbf{V}_{0\leftarrow |u_0|}\mathbf{Q}_{|u_0|}\mathbf{G}_0^{\mathrm{Q}}\mathbf{Q}_{|u_0|}\mathbf{V}_{|u_0|\leftarrow 0}\mathbf{P} \tag{5.43}$$

while its first order is a bit more complicated:

$$\begin{aligned}\mathbf{V}_1^{\mathrm{eff}} =& \mathbf{P}\mathbf{W}_1^{\dagger}\mathbf{V}_{0\leftarrow 0}\mathbf{P} + \mathbf{P}\mathbf{V}_{0\leftarrow 0}\mathbf{W}_1\mathbf{P} \\ &+ \mathbf{P}\mathbf{W}_1^{\dagger}\mathbf{V}_{0\leftarrow |u_0|}\mathbf{Q}_{|u_0|}\mathbf{G}_0^{\mathrm{Q}}\mathbf{Q}_{|u_0|}\mathbf{V}_{|u_0|\leftarrow 0}\mathbf{P} + \mathbf{P}\mathbf{V}_{0\leftarrow |u_0|}\mathbf{W}_1\mathbf{Q}_{|u_0|}\mathbf{G}_0^{\mathrm{Q}}\mathbf{Q}_{|u_0|}\mathbf{V}_{|u_0|\leftarrow 0}\mathbf{P} \\ &+ \mathbf{P}\mathbf{V}_{0\leftarrow |u_0|}\mathbf{Q}_{|u_0|}\mathbf{G}_1^{\mathrm{Q}}\mathbf{Q}_{|u_0|}\mathbf{V}_{|u_0|\leftarrow 0}\mathbf{P} \\ &+ \mathbf{P}\mathbf{V}_{0\leftarrow |u_0|}\mathbf{Q}_{|u_0|}\mathbf{G}_0^{\mathrm{Q}}\mathbf{Q}_{|u_0|}\mathbf{W}_1^{\dagger}\mathbf{V}_{|u_0|\leftarrow 0}\mathbf{P} + \mathbf{P}\mathbf{V}_{0\leftarrow |u_0|}\mathbf{Q}_{|u_0|}\mathbf{G}_0^{\mathrm{Q}}\mathbf{Q}_{|u_0|}\mathbf{V}_{|u_0|\leftarrow 0}\mathbf{W}_1\mathbf{P} \\ &+ \sum_{b\neq |u_0|}\mathbf{P}\mathbf{V}_{0\leftarrow b}\mathbf{Q}_b\mathbf{G}_1^{\mathrm{Q}}\mathbf{Q}_b\mathbf{V}_{b\leftarrow 0}\mathbf{P} \\ &+ \sum_{b\neq |u_0|}\mathbf{P}\mathbf{V}_{0\leftarrow b}\mathbf{Q}_b\mathbf{G}_1^{\mathrm{Q}}\mathbf{Q}_{|u_0|}\mathbf{V}_{|u_0|\leftarrow 0}\mathbf{P}\end{aligned} \tag{5.44}$$

where we carefully expanded all terms up to first order.

#### Properties of the effective potential

In this section we will have a more closer look at $\mathbf{V}_0^{\mathrm{eff}}$ because we need its properties to make use of theorem 1. We already know how $\mathbf{G}_0^{\mathrm{Q}}$ looks like, let us now consider $\mathbf{Q}_{|u_0|}\mathbf{V}_{|u_0|\leftarrow 0}\mathbf{P}$. Recall that it is basically a hopping Hamiltonian for sites $-1, 0$ and $1$:

$$\mathbf{V}_{|u_0|\leftarrow 0} = -J_{-|u_0|}(\lambda)\left[\sum_\sigma \mathbf{c}^\dagger_{-1\sigma;|u_0|}\mathbf{c}_{0\sigma;0} + (-1)^{|u_0|}\left(\mathbf{c}^\dagger_{0\sigma;|u_0|}\mathbf{c}_{-1\sigma;0} + \mathbf{c}^\dagger_{0\sigma;|u_0|}\mathbf{c}_{1\sigma;0}\right) + \mathbf{c}^\dagger_{1\sigma;|u_0|}\mathbf{c}_{0\sigma;0}\right] \tag{5.45}$$

$$= -(-1)^{|u_0|}J_{|u_0|}(\lambda)\begin{cases}\mathbf{A}_{\text{odd}} & |u_0| = 1,3,5,\ldots \\ \mathbf{A}_{\text{even}} & |u_0| = 2,4,6,\ldots\end{cases} \tag{5.46}$$

where we define

$$\mathbf{A}_{\text{odd}} = \sum_\sigma \mathbf{c}^\dagger_{-1\sigma;|u_0|}\mathbf{c}_{0\sigma;0} - \mathbf{c}^\dagger_{0\sigma;|u_0|}\mathbf{c}_{-1\sigma;0} - \mathbf{c}^\dagger_{0\sigma;|u_0|}\mathbf{c}_{1\sigma;0} + \mathbf{c}^\dagger_{1\sigma;|u_0|}\mathbf{c}_{0\sigma;0} \tag{5.47}$$

$$\mathbf{A}_{\text{even}} = \sum_\sigma \mathbf{c}^\dagger_{-1\sigma;|u_0|}\mathbf{c}_{0\sigma;0} + \mathbf{c}^\dagger_{0\sigma;|u_0|}\mathbf{c}_{-1\sigma;0} + \mathbf{c}^\dagger_{0\sigma;|u_0|}\mathbf{c}_{1\sigma;0} + \mathbf{c}^\dagger_{1\sigma;|u_0|}\mathbf{c}_{0\sigma;0}. \tag{5.48}$$

We can see that depending on $|u_0|$, $\mathbf{V}_{|u_0|\leftarrow 0}$ has two versions: If $|u_0|$ is an odd number $|u_0| = 1,3,5,\ldots$ then $\mathbf{V}_{|u_0|\leftarrow 0}$ is an antisymmetric hopping $\mathbf{A}_{\text{odd}}$, while if $|u_0|$ is even $|u_0| = 2,4,6,\ldots$ it is a symmetric hopping $\mathbf{A}_{\text{even}}$. Apart from being even or odd $|u_0|$ only determines the prefactor $J_{|u_0|}(\lambda)$ in front of the operator. Note that we will exclude the case $J_{|u_0|}(\lambda) = 0$, where the full operator vanishes. In this case there is therefore no pair breaking for $\alpha \to 0$. As said before the operator $\mathbf{V}_{|u_0|\leftarrow 0}$ only interacts with the three sites $-1, 0$ and 1. It is instructive to write the operators $\mathbf{A}_{\text{odd}}$ and $\mathbf{A}_{\text{even}}$ as a matrix. As basis in $\mathbf{P}$ we will choose the vectors

$$|-1,-1\rangle = \mathbf{c}^\dagger_{-1\uparrow;0}\mathbf{c}^\dagger_{-1\downarrow;0}|\Omega\rangle \qquad |0,0\rangle = \mathbf{c}^\dagger_{0\uparrow;0}\mathbf{c}^\dagger_{0\downarrow;0}|\Omega\rangle \qquad |1,1\rangle = \mathbf{c}^\dagger_{1\uparrow;0}\mathbf{c}^\dagger_{1\downarrow;0}|\Omega\rangle \tag{5.49}$$

and as basis in $\mathbf{Q}_{|u_0|}$ the vectors

$$\frac{|-1,0\rangle + |0,-1\rangle}{\sqrt{2}} = \frac{1}{\sqrt{2}}\left(\mathbf{c}^\dagger_{0\uparrow;|u_0|}\mathbf{c}^\dagger_{-1\downarrow;|u_0|}|\Omega\rangle + \mathbf{c}^\dagger_{-1\uparrow;|u_0|}\mathbf{c}^\dagger_{0\downarrow;|u_0|}|\Omega\rangle\right) \tag{5.50}$$

$$\frac{|0,1\rangle + |1,0\rangle}{\sqrt{2}} = \frac{1}{\sqrt{2}}\left(\mathbf{c}^\dagger_{1\uparrow;|u_0|}\mathbf{c}^\dagger_{0\downarrow;|u_0|}|\Omega\rangle + \mathbf{c}^\dagger_{0\uparrow;|u_0|}\mathbf{c}^\dagger_{1\downarrow;|u_0|}|\Omega\rangle\right). \tag{5.51}$$

In this basis the two operators have the following matrix representation:

$$\mathbf{A}_{\text{odd}} = \sqrt{2}\begin{pmatrix}-1 & 1 & 0\\ 0 & 1 & -1\end{pmatrix} \tag{5.52}$$

$$\mathbf{A}_{\text{even}} = \sqrt{2}\begin{pmatrix}1 & 1 & 0\\ 0 & 1 & 1\end{pmatrix}. \tag{5.53}$$

Define the vectors

$$|a\rangle_{\text{odd}} = \frac{1}{\sqrt{2}}\begin{pmatrix}1\\0\\-1\end{pmatrix} \qquad |b\rangle_{\text{odd}} = \frac{1}{\sqrt{6}}\begin{pmatrix}1\\-2\\1\end{pmatrix} \qquad |c\rangle_{\text{odd}} = \frac{1}{\sqrt{3}}\begin{pmatrix}1\\1\\1\end{pmatrix} \tag{5.54}$$

$$|a\rangle_{\text{even}} = \frac{1}{\sqrt{2}}\begin{pmatrix}1\\0\\-1\end{pmatrix} \qquad |b\rangle_{\text{even}} = \frac{1}{\sqrt{6}}\begin{pmatrix}1\\2\\1\end{pmatrix} \qquad |c\rangle_{\text{even}} = \frac{1}{\sqrt{3}}\begin{pmatrix}1\\-1\\1\end{pmatrix} \tag{5.55}$$

which are chosen s.t. $\mathbf{A}|c\rangle = 0$, $|a\rangle$ is antisymmetric and $|b\rangle$ is the remaining orthogonal vector. In the following we will only add the index 'odd' and 'even' where it is necessary to distinguish between the two cases. Note that $\mathbf{V}_{|u_0|\leftarrow 0} \sim \mathbf{A}$ restricted to $|a\rangle$ and $|b\rangle$ is an invertible $2\times 2$ matrix. If we use the basis spanned by $\mathbf{A}|a\rangle$ and $\mathbf{A}|b\rangle$ for the $\mathbf{Q}_{|u_0|}$ subspace, the matrix will even be diagonal due to parity conservation, because $|a\rangle$ is antisymmetric and $|b\rangle$ symmetric. Similar when restricted to these two states $\mathbf{G}_0^{\mathrm{Q}}$ will also be a diagonal $2\times 2$ matrix. Since $\mathbf{G}_0^{\mathrm{Q}}$ is a rather complicated non-local operator we can expect that both diagonal entries are non-zero[4], or in other words $\mathbf{G}_0^{\mathrm{Q}}$ restricted to the basis is invertible. Since all three matrices are invertible (recall $\mathbf{P}\mathbf{V}_{0\leftarrow|u_0|}\mathbf{Q}_{|u_0|} = \left(\mathbf{Q}_{|u_0|}\mathbf{V}_{|u_0|\leftarrow 0}\mathbf{P}\right)^\dagger$), the combination

$$\mathbf{V}_0^{\text{eff}} = \mathbf{P}\mathbf{V}_{0\leftarrow|u_0|}\mathbf{Q}_{|u_0|}\mathbf{G}_0^{\mathrm{Q}}\mathbf{Q}_{|u_0|}\mathbf{V}_{|u_0|\leftarrow 0}\mathbf{P} \tag{5.56}$$

is also invertible in the basis $|a\rangle, |b\rangle$. On all other states $\mathbf{V}_0^{\text{eff}}$ vanishes. This means the projector $\mathbf{K} := |a\rangle\langle a| + |b\rangle\langle b|$ describes the subspace on which the effective potential $\mathbf{V}_0^{\text{eff}}$ acts (i.e. it is the complement of the kernel of $\mathbf{V}_0^{\text{eff}}$). The projector $\mathbf{K}$ plays a central role in theorem 1 as we will explain soon.

For actual computations we also need to consider the first order of the effective potential (5.44). Luckily we only need to think about its restricted version to the remaining parts of $\mathbf{P}$: $\bar{\mathbf{K}}\mathbf{V}_1^{\text{eff}}\bar{\mathbf{K}}$ where $\bar{\mathbf{K}} = \mathbf{P} - \mathbf{K}$ contains $|c\rangle$ as well as all other states in $\mathbf{P}$ without $|a\rangle, |b\rangle$. Note that by definition:

$$\bar{\mathbf{K}}\mathbf{V}_{0\leftarrow|u_0|} = \mathbf{V}_{|u_0|\leftarrow 0}\bar{\mathbf{K}} = 0 \tag{5.57}$$

$$\bar{\mathbf{K}}\mathbf{V}_0^{\text{eff}} = \mathbf{V}_0^{\text{eff}}\bar{\mathbf{K}} = 0 \tag{5.58}$$

where the latter is an important prerequisite for theorem 1. The first one is extremely helpful since it drastically reduces the number of terms in (5.44):

$$\bar{\mathbf{K}}\mathbf{V}_1^{\text{eff}}\bar{\mathbf{K}} = \bar{\mathbf{K}}\mathbf{W}_1^\dagger\mathbf{V}_{0\leftarrow 0}\bar{\mathbf{K}} + \bar{\mathbf{K}}\mathbf{V}_{0\leftarrow 0}\mathbf{W}_1\bar{\mathbf{K}} + \sum_{b\neq|u_0|}\bar{\mathbf{K}}\mathbf{V}_{0\leftarrow b}\mathbf{Q}_b\mathbf{G}_1^{\mathrm{Q}}\mathbf{Q}_b\mathbf{V}_{b\leftarrow 0}\bar{\mathbf{K}}. \tag{5.59}$$

Even more since up to a prefactor all odd or even potentials $\mathbf{V}_{b\leftarrow 0}$ are the same all even or odd terms in the sum drop out as well.

**Case 1: $|u_0|$ odd** If $|u_0| = 1, 3, 5, \ldots$ is an odd number we get from (5.59):

$$\bar{\mathbf{K}}\mathbf{V}_1^{\text{eff}}\bar{\mathbf{K}} = \bar{\mathbf{K}}\mathbf{W}_1^\dagger\mathbf{V}_{0\leftarrow 0}\bar{\mathbf{K}} + \bar{\mathbf{K}}\mathbf{V}_{0\leftarrow 0}\mathbf{W}_1\bar{\mathbf{K}} + \sum_{b \text{ even}}\bar{\mathbf{K}}\mathbf{V}_{0\leftarrow b}\mathbf{Q}_b\mathbf{G}_1^{\mathrm{Q}}\mathbf{Q}_b\mathbf{V}_{b\leftarrow 0}\bar{\mathbf{K}} \tag{5.60}$$

$$= v\,|c\rangle_{\text{odd}}\langle c|_{\text{odd}}\,. \tag{5.61}$$

[4] Of course it could be that one of them accidentally vanishes for some isolated values of $\delta u$ or $\lambda$. But then we can expect that even the smallest change of $\lambda$ will move them away from 0.

The operator is proportional to $|c\rangle_{\text{odd}}\langle c|_{\text{odd}}$ because it still only acts on sites $-1, 0$ and $1$ and the vectors $|a\rangle_{\text{odd}}, |b\rangle_{\text{odd}}$ are already excluded. In the above basis we can write[5]

$$\mathbf{V}_{0\leftarrow 0} = -(J_0(\lambda) - 1)\mathbf{A}_{\text{even}} \tag{5.62}$$

$$\mathbf{V}_{b\leftarrow 0} = -J_b(\lambda)\mathbf{A}_{\text{even}} \qquad b \neq 0 \tag{5.63}$$

$$\mathbf{W}_1 = -\frac{1}{|u_0|}\mathbf{A}_{\text{even}} \tag{5.64}$$

$$\mathbf{Q}_b\mathbf{G}_1^{\text{Q}}\mathbf{Q}_b = \frac{1}{b - |u_0|} \tag{5.65}$$

and by using $\langle c|_{\text{odd}}\mathbf{A}_{\text{even}}^\dagger\mathbf{A}_{\text{even}}|c\rangle_{\text{odd}} = \frac{16}{3}$ we find:

$$v = \langle c|_{\text{odd}}\bar{\mathbf{K}}\mathbf{V}_1^{\text{eff}}\bar{\mathbf{K}}|c\rangle_{\text{odd}} \tag{5.66}$$

$$= \left[\sum_{b\neq 0}\frac{J_{2b}(\lambda)^2}{2b - |u_0|} - \frac{(J_0(\lambda) - 1)^2}{|u_0|} - \frac{2}{|u_0|}(J_0(\lambda) - 1)\right]\langle c|_{\text{odd}}\mathbf{A}_{\text{even}}^\dagger\mathbf{A}_{\text{even}}|c\rangle_{\text{odd}} \tag{5.67}$$

$$= \frac{16}{3}\left[\sum_b \frac{J_{2b}(\lambda)^2}{2b - |u_0|} + \frac{1}{|u_0|}\right]. \tag{5.68}$$

**Case 2: $|u_0|$ even** The calculation for $|u_0| = 2, 4, 6, \ldots$ is similar to the odd case. We can ignore all terms in (5.59) that contain even $\mathbf{V}_{b\leftarrow 0}$, and also those which contain the Schrieffer-Wolff transformation $\mathbf{W}_1$ (since it is also given by a symmetric hopping). This time we need the formula for the odd potentials:

$$\mathbf{V}_{b\leftarrow 0} = J_b(\lambda)\mathbf{A}_{\text{odd}} \tag{5.69}$$

$$\mathbf{Q}_b\mathbf{G}_1^{\text{Q}}\mathbf{Q}_b = \frac{1}{b - |u_0|}. \tag{5.70}$$

This gives

$$\bar{\mathbf{K}}\mathbf{V}_1^{\text{eff}}\bar{\mathbf{K}} = v\,|c\rangle_{\text{even}}\langle c|_{\text{even}} \tag{5.71}$$

since this time $|c\rangle_{\text{even}}$ is the only remaining state in $\bar{\mathbf{K}}$. Here $v$ is given by

$$v = \langle c|_{\text{even}}\bar{\mathbf{K}}\mathbf{V}_1^{\text{eff}}\bar{\mathbf{K}}|c\rangle_{\text{even}} = \left[\sum_b \frac{J_{2b+1}(\lambda)^2}{2b + 1 - |u_0|}\right]\langle c|_{\text{even}}\mathbf{A}_{\text{odd}}^\dagger\mathbf{A}_{\text{odd}}|c\rangle_{\text{even}} \tag{5.72}$$

$$= \frac{16}{3}\left[\sum_b \frac{J_{2b+1}(\lambda)^2}{2b + 1 - |u_0|}\right] \tag{5.73}$$

where again $\langle c|_{\text{even}}\mathbf{A}_{\text{odd}}^\dagger\mathbf{A}_{\text{odd}}|c\rangle_{\text{even}} = \frac{16}{3}$.

[5] Note that $\mathbf{W}_1 \sim \mathbf{A}_{\text{even}}$, because it is also given by a symmetric hopping.

#### Implications of the theorem

In appendix B we proof the following theorem[6]:

**Theorem 1′** *Consider the scattering problem given by the free Hamiltonian* $\mathbf{H}_0 = \alpha \mathbf{h}_\alpha^{\mathrm{P}}$ *with (not necessarily hermitian) potential* $\mathbf{V}_\alpha^{\mathrm{eff}}$*. Assume that this scattering problem is such that we can apply the Lippmann-Schwinger equation for all finite* $\alpha$*. Choose as incoming state an eigenstate* $|\phi\rangle$ *of* $\mathbf{h}_\alpha^{\mathrm{P}}$ *with an energy* $\alpha\varepsilon_\alpha$*. Furthermore assume that* $\mathbf{h}_\alpha^{\mathrm{P}}$ *has a well defined limit for* $\alpha \to 0$ *and that the Taylor expansion of* $\mathbf{V}_\alpha^{\mathrm{eff}}$ *exists at least up to first order.*

*In case that* $\mathbf{V}_\alpha^{\mathrm{eff}} \not\to 0$ *and the operators satisfy the additional technical assumptions (a), (b) we find in the limit* $\alpha \to 0$*:*

1. $\mathbf{K}\left|\psi^+\right\rangle \to 0$

There are two more conclusions one can obtain under the assumptions of theorem 1′. However they will not be relevant in this section and also contain notation we have not introduced yet. The interested reader can find them in theorem 1 in appendix B.

Since we already established all necessary properties of $\mathbf{V}_\alpha^{\mathrm{eff}}$ we can directly apply theorem 1′ in the limit $\alpha \to 0$. We will now discuss the interesting consequences of $\mathbf{K}\left|\psi^+\right\rangle \to 0$.

What is the intuitive meaning of $\mathbf{K}\left|\psi^+\right\rangle \to 0$? Recall that $\mathbf{K} = |a\rangle\langle a| + |b\rangle\langle b|$ and so we have $\left\langle a\middle|\psi^+\right\rangle \to 0$ and $\left\langle b\middle|\psi^+\right\rangle \to 0$. The two vectors $|a\rangle$ and $|b\rangle$ are the ones on which the potential acts. In the limit $\alpha \to 0$ the wavefunction vanishes where the potential acts. Note that this is similar to the toy model (5.7), where we have $\left\langle 0_{\mathrm{P}}\middle|\mathbf{P}\middle|\psi^+\right\rangle \to 0$. We interpreted this as adding an artificial boundary condition to the system. The same happens for the pairs, with one major difference. While in the toy model the artificial boundary condition decoupled the system and therefore led to total reflection, for the pairs the system does not decouple. In fact because $|c\rangle$ does not couple to the zeroth order potential, $\left\langle c\middle|\psi^+\right\rangle$ is allowed to have any value. Since $|c\rangle$ spreads over sites $-1, 0$ and 1 there is still a connection between the two sides of the system and therefore transmission is still possible. Because only $|c\rangle$ is allowed, the system will have the interesting feature that the probability of the pair being on sites $-1, 0$ and 1 is equal, a feature we will encounter in the numerics.

Let us come to the most important conclusion of this chapter. So far we only considered the intact pair in sector **P**. But we actually wanted to study what fraction of the pair breaks, i.e. how does the wavefunction look like in the $\mathbf{Q}_{|u_0|}$ sector[7]. We can calculate this using the Greens function (5.27):

$$\mathbf{Q}_{|u_0|}\left|\psi^+\right\rangle \to \mathbf{Q}_{|u_0|}\mathbf{G}_0^{\mathrm{Q}}\mathbf{Q}_{|u_0|}\mathbf{V}_{|u_0|\leftarrow 0}\mathbf{P}\left|\psi^+\right\rangle \tag{5.74}$$

$$= \mathbf{Q}_{|u_0|}\mathbf{G}_0^{\mathrm{Q}}\mathbf{Q}_{|u_0|}\mathbf{V}_{|u_0|\leftarrow 0}\mathbf{K}\left|\psi^+\right\rangle = 0 \tag{5.75}$$

where we used $\mathbf{Q}_{|u_0|}\mathbf{V}_{|u_0|\leftarrow 0}\mathbf{P} = \mathbf{Q}_{|u_0|}\mathbf{V}_{|u_0|\leftarrow 0}\mathbf{K}$ due to the definition of $\mathbf{K}$. We see that the wavefunction in the $\mathbf{Q}_{|u_0|}$ sector vanishes in the limit $\alpha \to 0$, or in other words: Pair breaking is suppressed as $\alpha \to 0$. Intuitively speaking the limit $\alpha \to 0$ adds the artificial boundary conditions $\mathbf{K}\left|\psi^+\right\rangle = 0$, wherever the potential acts. But because the same potential is also responsible for pair breaking, pair

[6] The two technical assumptions (a) and (b) can be found in appendix B.1 (we expect them to hold almost always as discussed in appendix B.4).

[7] Recall that sector $\mathbf{Q}_{|u_0|}$ is the only one where it is energetically possible that free particles escape to infinity.

breaking itself cannot occur anymore. Note that this is completely contrary to our original expectation, where we expected almost full pair breaking (see section 5.2.1).

We would like to stress that this does not seem to be case only for the pairs, but rather seems to happen in quite generality when one considers scattering from slow modes of a system into fast modes. Theorem 1 shows that $\mathbf{K}\left|\psi^{+}\right\rangle \to 0$ for a huge variety of systems. Apart from some technical requirements the only important requirement is that $\mathbf{V}_{\alpha}^{\text{eff}}$ does not vanish as $\alpha \to 0$. From $\mathbf{K}\left|\psi^{+}\right\rangle \to 0$ it then follows that the full wavefunction in the $\mathbf{Q}$ sector vanishes $\mathbf{Q}\left|\psi^{+}\right\rangle \to 0$.

#### Pair transmission in the limit $\alpha \to 0$

We use the other two conclusions of theorem 1 in appendix B to calculate the transmission amplitude in appendix (D.74):

$$T_k = \frac{1}{1 + \left(\frac{3|u_0|v \mp 8 + 8\cos k}{4\sin k}\right)^2} \tag{5.76}$$

where the upper sign is for $|u_0| = 1, 3, 5, \ldots$ odd and the lower sign for $|u_0| = 2, 4, 6, \ldots$ even. $v$ was calculated before in section 5.2.6:

$$v = \begin{cases} \frac{16}{3}\left[\sum_b \frac{J_{2b}(\lambda)^2}{2b-|u_0|} + \frac{1}{|u_0|}\right] & |u_0| = 1, 3, 5, \ldots \\ \frac{16}{3}\left[\sum_b \frac{J_{2b+1}(\lambda)^2}{2b+1-|u_0|}\right] & |u_0| = 2, 4, 6, \ldots \end{cases}. \tag{5.77}$$

The two sums in $v$ look similar to $s_{|u_0|}(\lambda)$ defined in (3.59). In fact we have

$$3|u_0|v \mp 8 + 8\cos k = -8\Big(|u_0| s_{|u_0|}(\lambda) - (1 + \cos k)\Big) \tag{5.78}$$

and by inserting this into (5.76) we find that $T_k$ is given exactly by the same result already obtained in section 3.3.4 (see equation (3.61)). There we computed the limit where $|u|$ approaches an integer from the results in the non-resonant case. It might seem obvious that both results should be equal, however recall that the physical situation in the resonant and non-resonant case is rather different. In particular there will be major differences as we move away from the limit and consider higher order corrections. Already in first order in $\alpha$ we find a linear increase of the pair breaking in the resonant case while the first order completely vanishes in the non-resonant case.

Before we move on we want to stress two important facts. First that we get, contrary to the toy model, a non-trivial transmission even in the limit $\alpha \to 0$. Second recall that we gave ourselves the freedom to choose how $u$ approaches $u_0$ by defining $u = u_0 + \alpha\delta u$. Interestingly the transmission does not depend on the parameter $\delta u$ at all. Since we absorbed the $\delta u$ into the $\mathbf{Q}$ sector this again demonstrates that the details in the $\mathbf{Q}$ sector are not relevant for the transmission amplitude in the limit $\alpha \to 0$.

In figure 5.3 we plot the transmission as a function of $k$ and $\lambda$ for $|u_0| = 1$. We are now going to to verify this result using numerics.

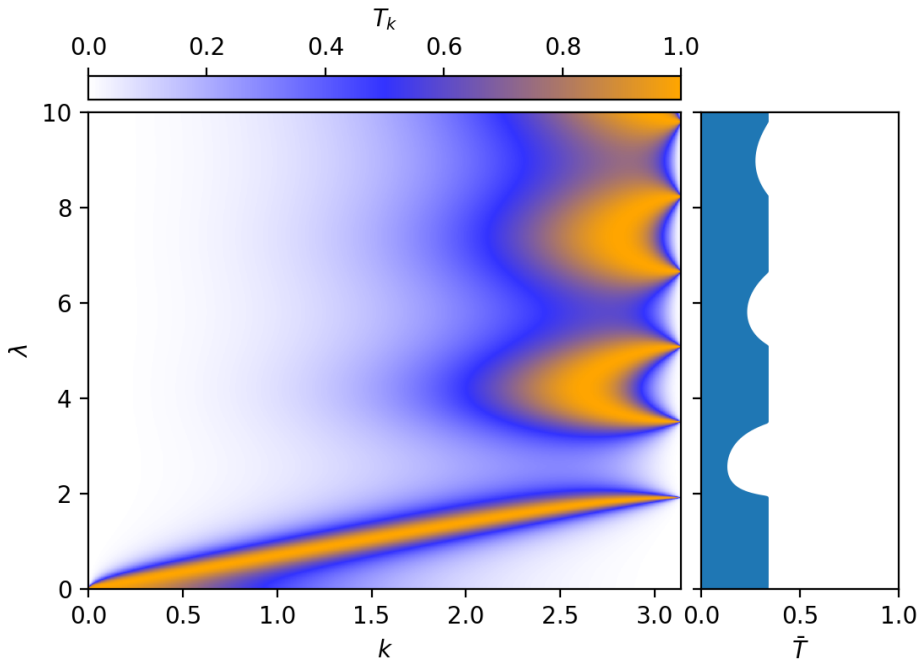


Figure 5.3: Pair transmission as function of momentum $k$ and driving strength $\lambda$ for $|U|/\omega = 1$. The plot on the right displays the momentum averaged transmission $\bar{T}$.

## 5.3 Numerical results

In this section we would like to show that we can indeed find the non-trivial transmission amplitude also from the numerics. We are again going to use the method explained in section 2.3 which determines the transmission directly from the eigenstates[8]. Note that this method is not able to capture any pair breaking at all because it only analyzes the diagonal of layer 0. Also even the transmission calculated from the diagonal of layer 0 will not be correct since the method crucially depends on the assumption that the impurity does not allow for particles losses. Therefore we cannot trust its results as long as we cannot neglect the pair breaking. But luckily for $J/\omega \to 0$ the pair breaking vanishes and we can apply the method to check the limiting transmission amplitude. Note that by checking the transmission amplitude we also implicitly validate the other analytical results such as that pair breaking vanishes in the limit.

Before we give the result for the transmission let us verify an implication of the theorem, namely that the wavefunction at sites $-1, 0, 1$ is restricted to be a multiple of $|c\rangle$. In figure 5.4 we give an example for a layer 0 of an eigenstate for $|u| = 1$. There $|c\rangle = |c\rangle_{\text{odd}}$ is given by (5.54) and so the wavefunction on all three sites should be equal. We can see in figure 5.4 that this is indeed the case. This is a first verification of the analytical results.

Unfortunately it is not easy to have a more direct proof that the pair breaking vanishes as $\alpha \to 0$. The problem can be best explained with a real-time simulation: Imagine an incoming pair state in layer 0 that scatters off the impurity. As it moves really slow we need to simulate long times. Imagine that a part of the state gets excited into layer $|u_0|$ and breaks into two single particles. The single

[8] In fact only from the diagonal of layer 0.

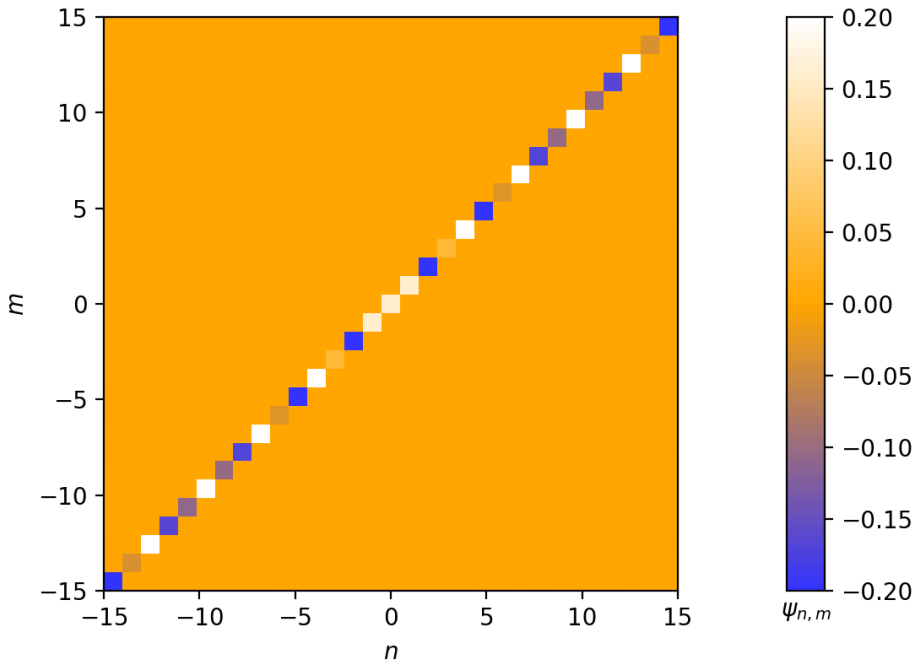


Figure 5.4: Layer 0 of a pair eigenstate for $J/\omega = 0.001, |U|/\omega = 0.9997$ (i.e. $u_0 = -1, \delta u = 0.3$), $\lambda = 1, N = 4, L = 31$. $n$ and $m$ denote the position of the first and second particle respectively. The wavefunction $\psi_{n,m}$ concentrates on the diagonal where both particles are at the same site. In particular observe that the value of the wavefunction is the constant on sites $-1, 0, 1$ which is an important prediction of section 5.2.6.

particles will move much faster. But due to the finite size $L$ of the system they will quickly reach the boundary, bounce back and re-enter the impurity while the incoming pair basically did not move. Due to the strong coupling there is a high probability that both single particles will recombine into a pair. This spoils the overall pair breaking probability as well as the transmission probability of the pair. The only way out would be to scale the system size $L \sim 1/\alpha$, so that single particles will only reach the boundary after the scattering has finished. Since we are at most able to simulate $L \approx 50$ (if we restrict the system to $N = 2$ layers), but would like to reach $\alpha = 0.001$, this is clearly not realistic. Therefore it is not possible for us to directly observe the pair breaking in numerical simulations. The discussion was done for a real-time simulation, but of course there is a similar effect on the eigenstates.

In figure 5.5 we give the numerically calculated transmission for $N = 4$ layers and $|u_0| = 1$ analogously to figure 5.3. Note that we used a system size of $L = 31$ and restricted the number of layers to $N = 4$ which includes layers $-1, 0, 1, 2$. Up to small regions around $\lambda = 0, 4$ and 7 the transmission behaves similarly as the theoretical result from figure 5.3. Figure 5.7 shows a vertical cut at constant $k = \pi/2$ through figure 5.5. For comparison we also give the expected theoretical result, both for infinite layers and for four layers (this means we only include the terms $b = 0, 1$ in the sum of (5.68)). If we again exclude $\lambda = 0, 4, 7$ we find that the numerical result follows the theoretical result for four layers nicely. It differs a bit from the theoretical result for the infinite layer system, but this is already due to the difference between the two theoretical results. If we would include more layers into the simulation we could also include more terms in the sum (5.68) and therefore reach a better approximation for the theoretical transmission amplitude.

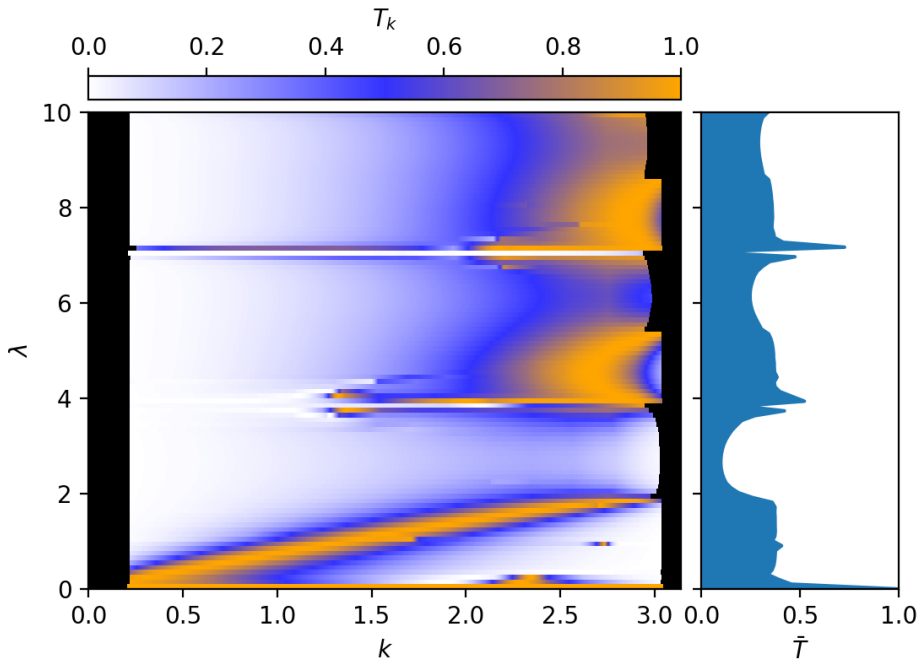


Figure 5.5: Numerically calculated pair transmission for $J/\omega = 0.001, |U|/\omega = 0.9997$ (i.e. $u_0 = -1, \delta u = 0.3$), $N = 4, L = 31$ as function of momentum $k$ and driving strength $\lambda$. The black regions at the boundary are outside of the scope of the numerical method (see section 2.3). The plot on the right displays the momentum averaged transmission $\bar{T}$.

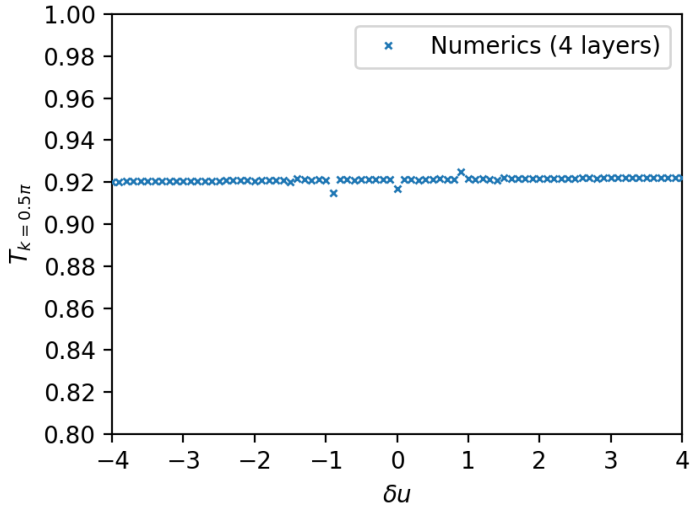


Figure 5.6: Numerically calculated pair transmission with momentum $k = 0.5\pi$ for $J/\omega = 0.0001, |U|/\omega = 1 - 0.0001\delta u$ (i.e. $u_0 = -1$), $\lambda = 1, N = 4, L = 31$ as function of $\delta u$.

Let us now explain why the numerics fail at $\lambda = 0, 4$ and 7. These values are close to the zeros of the first Bessel function $J_1(\lambda)$ which are approximately $0, 3.8, 7.0, \ldots$. Recall that the major observation in the limit of $\alpha \to 0$ was that the parts of the wavefunction, on which the potential connecting layer 0

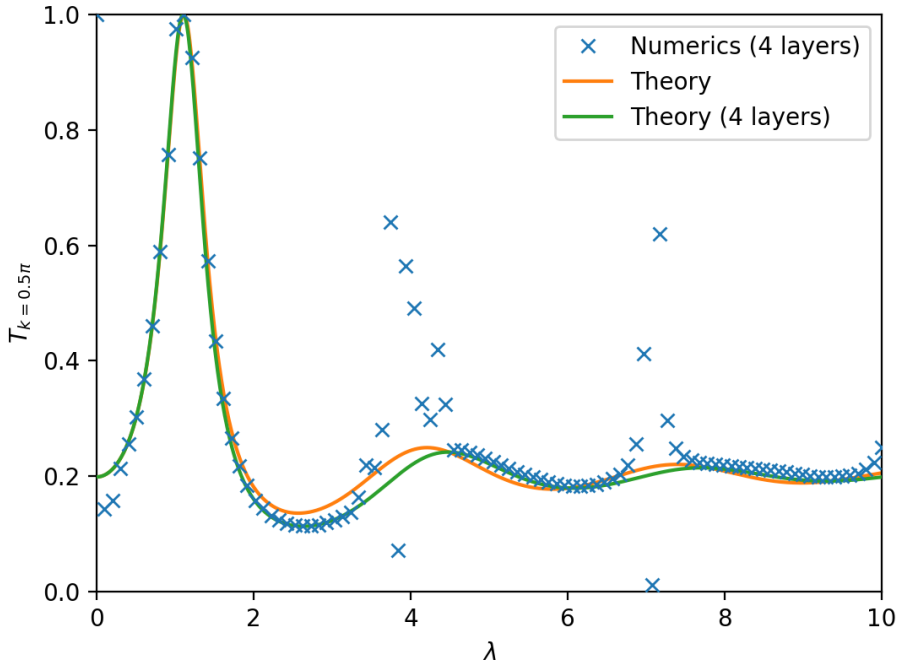


Figure 5.7: Numerically calculated pair transmission with momentum $k = 0.5\pi$ for $J/\omega = 0.001, |U|/\omega = 0.9997$ (i.e. $u_0 = -1, \delta u = 0.3$), $N = 4, L = 31$ as function of driving strength $\lambda$. We also give the theoretical results for infinite and four layers.

and 1 acts, vanish. This potential is given by $\mathbf{V}_{1\leftarrow 0}$ (see equation equation (5.21)):

$$\mathbf{V}_{1\leftarrow 0} = J_1(\lambda)\left[\sum_\sigma \mathbf{c}^\dagger_{-1\sigma;1}\mathbf{c}_{0\sigma;0} - \mathbf{c}^\dagger_{0\sigma;1}\mathbf{c}_{-1\sigma;0} - \mathbf{c}^\dagger_{0\sigma;1}\mathbf{c}_{1\sigma;0} + \mathbf{c}^\dagger_{1\sigma;1}\mathbf{c}_{0\sigma;0}\right]. \tag{5.79}$$

The derived limit for $\alpha \to 0$ is applicable if the prefactor $\alpha$ is much smaller than the size of $\mathbf{V}_{1\leftarrow 0}$, i.e. much smaller than $J_1(\lambda)$. If $\lambda$ is away from a zero of $J_1(\lambda)$ this is satisfied for $\alpha = 0.001$. But if $\lambda$ is close to a zero of $J_1(\lambda)$ then $J_1(\lambda)$ will be comparable to $\alpha = 0.001$ and therefore we cannot apply the result we found in the limit $\alpha \to 0$. This explains why the numerical results do not match the theoretical ones there. We could get a better approximation by further decreasing $\alpha$, however a narrow region where the limit does not apply will always remain around the zeros of $J_1(\lambda)$.

### Dependence on $\delta u$

Recall that the analytical result for $\alpha = J/\omega \to 0$ also predicted another feature, namely that the transmission is independent of $\delta u$. We introduced $\delta u$ to give us more freedom how $u = U/\omega$ approaches an integer. We defined $u = u_0 + \alpha\delta u$, with $u_0$ being an integer, where $-4 < \delta u < 4$. In figure 5.6 we plot the transmission as a function of $\delta u$. We can see that the transmission is not affected by $\delta u$. This verifies another prediction in the limit $\alpha \to 0$.

CHAPTER 6

# Conclusion

In this thesis we studied the scattering of bound pairs of fermions in a Fermi-Hubbard chain at a driven impurity. The model was described by the hopping parameter $J$, the on-site Hubbard interaction $U$, the driving frequency $\omega$ and the driving strength $\lambda$. In the non-resonant case, where $U$ is not an integer multiple of $\omega$, we were able to derive an effective Hamiltonian with an effective impurity for the pair in the limit $J/\omega \to 0$ while keeping $U/\omega$ fixed. The resulting transmission probability through the impurity shows a complicated dependence on the parameters which yields a wide range of possible transmission profiles. We checked the analytical work with numerical studies in which we extract the transmission directly from the eigenstates of the system.

We compared the transmission of the pairs to the one of the single particles. This led us to several ideas of how the driven impurity could be used, most prominently as a pair filter. We found some sets of parameters where the pair transmits through the impurity but the transmission of single particles is highly suppressed. One can also tune the parameters such that the pairs are filtered out and single particles are transmitted to have a single particle filter.

To complete the discussion about the driven impurity we also considered the resonant case, i.e. where $U$ is an integer multiple of $\omega$. This case allowed for pair breaking. Quite surprisingly pair breaking is not the dominant process for $J/\omega \to 0$, but it is suppressed. We have argued that this suppression is a general feature for systems which have scattering from a slow to a fast subspace. We explained this behaviour with a simple toy model and proved a general theorem which applies to a huge variety of systems.

To go away from the limit $J/\omega \to 0$ we also numerically calculated the transmission for finite values of $J/\omega$ where the driving was still non-resonant. We found that the result for $J/\omega \to 0$ is a good approximation throughout the whole non-resonant case. However as soon as $J/\omega$ is greater than a certain cutoff, which depends on the distance of $U/\omega$ to the nearest integer value, one is automatically in the resonant case. Due to the high complexity of possible final states after the scattering our analytical and numerical methods are not applicable in the general resonant case. One could try to study other limits like the low frequency limit $\omega \ll J, |U|$ or to do a perturbative expansion in the driving strength $\lambda$. Apart from these limiting scenarios however we expect that studying the resonant case in general requires more sophisticated analytical and numerical methods. We will leave this problem for future work.

We discussed how one could use the rich behaviours of the impurity to tailor specific filters. However one can only achieve specific configurations of the impurity at special parameter values.

We expect that adding an extra static chemical potential around the impurity site will lead to even richer behaviour and thus to more flexibility for choosing the parameters. Such a potential should be unaffected by the Schrieffer-Wolff transformation and therefore the analytical calculations should be very similar.

Another idea for future work is to shake a whole region instead of a single site. This will lead to an effective extended impurity which is again given by a scaled hopping and an extra potential. If the scaled hopping is smaller than the actual hopping the bandwidth inside the driven region will be smaller than outside. Therefore, for a sufficiently long impurity, only states which lie inside this bandwidth will be transmitted. This could be used to tailor specific momentum filters for single particles and pairs.

# Bibliography


[1] André Eckardt. "Colloquium: Atomic quantum gases in periodically driven optical lattices". In: *Rev. Mod. Phys.* 89 (1 2017), p. 011004. DOI: 10.1103/RevModPhys.89.011004. URL: https://link.aps.org/doi/10.1103/RevModPhys.89.011004.

[2] H. Lignier et al. "Dynamical Control of Matter-Wave Tunneling in Periodic Potentials". In: *Phys. Rev. Lett.* 99 (22 2007), p. 220403. DOI: 10.1103/PhysRevLett.99.220403. URL: https://link.aps.org/doi/10.1103/PhysRevLett.99.220403.

[3] M. Aidelsburger et al. "Experimental Realization of Strong Effective Magnetic Fields in an Optical Lattice". In: *Phys. Rev. Lett.* 107 (25 2011), p. 255301. DOI: 10.1103/PhysRevLett.107.255301. URL: https://link.aps.org/doi/10.1103/PhysRevLett.107.255301.

[4] Alessandro Zenesini et al. "Coherent Control of Dressed Matter Waves". In: *Phys. Rev. Lett.* 102 (10 2009), p. 100403. DOI: 10.1103/PhysRevLett.102.100403. URL: https://link.aps.org/doi/10.1103/PhysRevLett.102.100403.

[5] Sota Kitamura and Hideo Aoki. "$\eta$-pairing superfluid in periodically-driven fermionic Hubbard model with strong attraction". In: *Phys. Rev. B* 94 (17 2016), p. 174503. DOI: 10.1103/PhysRevB.94.174503. URL: https://link.aps.org/doi/10.1103/PhysRevB.94.174503.

[6] Daniel Thuberg, Sebastián A. Reyes and Sebastian Eggert. "Quantum resonance catastrophe for conductance through a periodically driven barrier". In: *Phys. Rev. B* 93 (18 2016), p. 180301. DOI: 10.1103/PhysRevB.93.180301. URL: https://link.aps.org/doi/10.1103/PhysRevB.93.180301.

[7] Sebastián A Reyes et al. "Transport through an AC-driven impurity: Fano interference and bound states in the continuum". In: *New Journal of Physics* 19.4 (2017), p. 043029. DOI: 10.1088/1367-2630/aa66fe. URL: https://doi.org/10.1088/1367-2630/aa66fe.

[8] Daniel Thuberg et al. "Perfect Spin Filter by Periodic Drive of a Ferromagnetic Quantum Barrier". In: *Phys. Rev. Lett.* 119 (26 2017), p. 267701. DOI: 10.1103/PhysRevLett.119.267701. URL: https://link.aps.org/doi/10.1103/PhysRevLett.119.267701.

[9] C. F. Chan et al. "Pair correlations in the attractive Hubbard model". In: *Phys. Rev. Research* 2 (2 2020), p. 023210. DOI: 10.1103/PhysRevResearch.2.023210. URL: https://link.aps.org/doi/10.1103/PhysRevResearch.2.023210.

[10] Peter T. Brown et al. "Angle-resolved photoemission spectroscopy of a Fermi–Hubbard system". In: *Nature Physics* 16 (2019), pp. 26–31.

[11] Niels Strohmaier et al. "Interaction-Controlled Transport of an Ultracold Fermi Gas". In: *Phys. Rev. Lett.* 99 (22 2007), p. 220601. DOI: 10.1103/PhysRevLett.99.220601. URL: https://link.aps.org/doi/10.1103/PhysRevLett.99.220601.

[12] Thomas Hartke et al. “Doublon-Hole Correlations and Fluctuation Thermometry in a Fermi-Hubbard Gas”. In: *Phys. Rev. Lett.* 125 (11 2020), p. 113601. DOI: 10.1103/PhysRevLett.125.113601. URL: https://link.aps.org/doi/10.1103/PhysRevLett.125.113601.

[13] Fabian H. L. Essler et al. *The One-Dimensional Hubbard Model*. Cambridge University Press, 2005. DOI: 10.1017/CBO9780511534843.

[14] M Valiente and D Petrosyan. “Two-particle states in the Hubbard model”. In: *Journal of Physics B: Atomic, Molecular and Optical Physics* 41.16 (2008), p. 161002. DOI: 10.1088/0953-4075/41/16/161002. URL: https://doi.org/10.1088/0953-4075/41/16/161002.

[15] J. R. Schrieffer and P. A. Wolff. “Relation between the Anderson and Kondo Hamiltonians”. In: *Phys. Rev.* 149 (2 1966), pp. 491–492. DOI: 10.1103/PhysRev.149.491. URL: https://link.aps.org/doi/10.1103/PhysRev.149.491.

[16] Sergey Bravyi, David P. DiVincenzo and Daniel Loss. “Schrieffer–Wolff transformation for quantum many-body systems”. In: *Annals of Physics* 326.10 (2011), pp. 2793–2826. ISSN: 0003-4916. DOI: https://doi.org/10.1016/j.aop.2011.06.004. URL: https://www.sciencedirect.com/science/article/pii/S0003491611001059.

[17] Giuseppe E. Santoro. *Lecture notes - Introduction to Floquet*. 2019.

[18] Martin Holthaus. “Floquet engineering with quasienergy bands of periodically driven optical lattices”. In: 49.1 (2015), p. 013001. DOI: 10.1088/0953-4075/49/1/013001. URL: https://doi.org/10.1088/0953-4075/49/1/013001.

[19] André Eckardt and Egidijus Anisimovas. “High-frequency approximation for periodically driven quantum systems from a Floquet-space perspective”. In: *New Journal of Physics* 17.9 (2015), p. 093039. DOI: 10.1088/1367-2630/17/9/093039. URL: https://doi.org/10.1088/1367-2630/17/9/093039.

[20] N.W. Ashcroft et al. *Solid State Physics*. HRW international editions. Holt, Rinehart and Winston, 1976. ISBN: 9780030839931.

[21] K. Takegoshi et al. “Comparison among Magnus/Floquet/Fer expansion schemes in solid-state NMR”. In: *The Journal of Chemical Physics* 142.13 (2015), p. 134201. DOI: 10.1063/1.4916324. eprint: https://doi.org/10.1063/1.4916324. URL: https://doi.org/10.1063/1.4916324.

[22] Marin Bukov, Michael Kolodrubetz and Anatoli Polkovnikov. “Schrieffer-Wolff Transformation for Periodically Driven Systems: Strongly Correlated Systems with Artificial Gauge Fields”. In: *Phys. Rev. Lett.* 116 (12 2016), p. 125301. DOI: 10.1103/PhysRevLett.116.125301. URL: https://link.aps.org/doi/10.1103/PhysRevLett.116.125301.

[23] A. H. Kahn. “Phase-Shift Method for One-Dimensional Scattering”. In: *American Journal of Physics* 29.2 (1961), pp. 77–80. DOI: 10.1119/1.1937700. eprint: https://doi.org/10.1119/1.1937700. URL: https://doi.org/10.1119/1.1937700.

[24] Florian Schäfer. “Time-Reversal Symmetry Breaking in Quantum Billiards”. PhD thesis. Darmstadt: Technische Universität, 2009. URL: http://tuprints.ulb.tu-darmstadt.de/1329/.

[25] *NIST Digital Library of Mathematical Functions*. http://dlmf.nist.gov/, Release 1.1.2 of 2021-06-15. F. W. J. Olver, A. B. Olde Daalhuis, D. W. Lozier, B. I. Schneider, R. F. Boisvert, C. W. Clark, B. R. Miller, B. V. Saunders, H. S. Cohl, and M. A. McClain, eds. URL: http://dlmf.nist.gov/.

[26] B. A. Lippmann and Julian Schwinger. "Variational Principles for Scattering Processes. I". In: *Phys. Rev.* 79 (3 1950), pp. 469–480. DOI: 10.1103/PhysRev.79.469. URL: https://link.aps.org/doi/10.1103/PhysRev.79.469.

[27] S.S. Schweber. *An Introduction to Relativistic Quantum Field Theory*. Dover Publications, 2011. ISBN: 9780486139609.

[28] M. Abusini. "The first-order optical potential evaluation for the elastic scattering of neutron on the bound system using the impulse approximation method". In: *International Journal of Modern Physics E* 28.10 (2019), p. 1950091. DOI: 10.1142/S0218301319500915. eprint: https://doi.org/10.1142/S0218301319500915. URL: https://doi.org/10.1142/S0218301319500915.

[29] Encyclopedia of Mathematics. *Linear interpolation*. URL: http://encyclopediaofmath.org/index.php?title=Linear_interpolation&oldid=27068.

APPENDIX A

# Perturbative expansions in Floquet theory

## A.1 The high-frequency expansion

The high-frequency expansion allows to calculate the Floquet Hamiltonian as a series expansion in $1/\omega$. We will only calculate the dominant term. For higher order terms see [21]. Consider a Floquet system given by a Hamiltonian $\mathbf{H}(\omega t)$. The Schroedinger equation reads

$$i\frac{\mathrm{d}}{\mathrm{d}t}\mathbf{U} = \mathbf{H}(\omega t)\mathbf{U}. \tag{A.1}$$

Now change the time variable to $\phi = \omega t$. The Schrödinger equation transforms to

$$i\frac{\mathrm{d}}{\mathrm{d}\phi}\mathbf{U} = \frac{1}{\omega}\mathbf{H}(\phi)\mathbf{U}. \tag{A.2}$$

If we consider the ultimate limit $\omega \to \infty$ the right hand side vanishes and the time evolution becomes trivial. Therefore we can do a perturbative expansion in $1/\omega$. The first order correction of the time evolution operator after one period is

$$\mathbf{U}(2\pi) = 1 - i\frac{1}{\omega}\int_0^{2\pi} \mathrm{d}\phi\, \mathbf{H}(\phi) + O\left(1/\omega^2\right) \tag{A.3}$$

$$= 1 - i\frac{2\pi}{\omega}\mathbf{H}_0 + O\left(1/\omega^2\right). \tag{A.4}$$

In the last step we used the Fourier expansion of the Hamiltonian $\mathbf{H}(\phi) = \sum_a \mathbf{H}_a e^{-ia\phi}$. From general Floquet theory we know that the time evolution operator after a full period relates to the Floquet Hamiltonian according to

$$\mathbf{U}(2\pi) = e^{-i\mathbf{H}_\mathrm{F}\frac{2\pi}{\omega}} = 1 - i\frac{2\pi}{\omega}\mathbf{H}_{\mathrm{F}_0} + O\left(1/\omega^2\right) \tag{A.5}$$

where we also expand $\mathbf{H}_\mathrm{F} = \mathbf{H}_{\mathrm{F}_0} + O(1/\omega)$. By comparing both expressions we find immediately

$$\mathbf{H}_\mathrm{F} = \mathbf{H}_0 + O(1/\omega). \tag{A.6}$$

In the same manner we can also calculate the Floquet Hamiltonian to any order. The result for the zero'th order is particularly interesting because it is given by the time-average of the Hamiltonian over one period $\mathbf{H}_0 = \int \frac{\mathrm{d}\phi}{2\pi}\mathbf{H}(\phi)$. The high-frequency expansion can be applied to any system, whenever the frequency is much larger than any intrinsic energy scale of the system. However sometimes we also want to consider other parameters to be of the same size as $\omega$ too (in case of the pairs we have $U \sim \omega$). In this case we need to structure the perturbation theory a bit differently as explained in the next two sections.

## A.2 The Schrieffer-Wolff transformation

Before we apply it to the Floquet setting we want to first introduce the Schrieffer-Wolff transformation in the usual (and more simpler) time-independent setting. We could simply give a reference to publications like [16] which already include a detailed derivation and analysis. But because we are going to use a non-standard notation and also the Schrieffer-Wolff transformation is going to play a central role in this thesis, we will quickly repeat the main steps of the derivation:

Consider a general system with a Hamiltonian

$$\mathbf{H} = \mathbf{F} + \alpha\mathbf{G}. \tag{A.7}$$

Here $\alpha\mathbf{G}$ is a small perturbation to $\mathbf{F}$. We would like to study this system in the limit $\alpha \to 0$. For finite $\alpha$ the system can be diagonalized into eigenstates $\left|\psi_i\right\rangle_\alpha$. Now for each of these states define their limit as $\alpha \to 0$ as $\left|\psi_i\right\rangle_\alpha \to \left|\phi_i\right\rangle$, where the $\left|\phi_i\right\rangle$ are an eigenbasis of $\mathbf{F}$. The idea behind the Schrieffer-Wolff transformation is to introduce an unitary transformation $\mathbf{W}_\alpha$ which maps the limiting eigenstates onto the real eigenstates at finite $\alpha$:

$$\mathbf{W}_\alpha \left|\phi_i\right\rangle = \left|\psi_i\right\rangle_\alpha . \tag{A.8}$$

From the definition we know that $\mathbf{W}_0 = 1$. Soon we will expand $\mathbf{W}_\alpha = 1 + \alpha\mathbf{W}_1 + \alpha^2\mathbf{W}_2 + O\left(\alpha^3\right)$ in a Taylor series. Such an expansion suffers from the problem that a truncated approximation to $\mathbf{W}_\alpha$ will not be unitary. That is why in [16], as well as in most other publications, they instead define $\mathbf{W}_\alpha = e^{-\mathbf{S}_\alpha}$ and then expand $\mathbf{S}_\alpha$. This expansion is then guaranteed to be unitary even at finite order. But since this is not important for us and the derivation with $\mathbf{W}_\alpha$ is more direct we will stick to it.

The $\mathbf{W}_\alpha$ allow us to describe eigenstates of the total Hamiltonian in terms of eigenstates of $\mathbf{F}$. Consider the transformed Hamiltonian $\mathbf{W}_\alpha^\dagger\mathbf{H}\mathbf{W}_\alpha$. Its eigenstates are given by eigenstates of $\mathbf{F}$. In particular in any eigenbasis of $\mathbf{F}$ the transformed Hamiltonian is block diagonal. Each block describes the effective Hamiltonian for finite $\alpha$ governing the dynamics in this subspace.

Our aim is to compute such an effective Hamiltonian for a specific subspace perturbatively. Fix a (possibly degenerate) eigenspace of $\mathbf{F}$ given by a projector $\mathbf{P}$ which projects on an eigenspace of $\mathbf{F}$ (usually one takes the ground states, but in principle any eigenspace is possible). For simplicity we will assume that the eigenvalue of this eigenspace is 0[1], i.e. $\mathbf{PF} = \mathbf{FP} = 0$. For convenience define $\mathbf{Q} = 1 - \mathbf{P}$ as the remaining parts of the system. It is shown in [16] that $\mathbf{S}_\alpha$ is block off-diagonal which translates to $\mathbf{PW}_1\mathbf{P} = \mathbf{QW}_1\mathbf{Q} = 1$. For simplicity we will also assume that $\mathbf{PGP} = 0$[2].

[1] Otherwise subtract a constant from the Hamiltonian.

[2] This is the case for the Fermi-Hubbard model and dramatically simplifies the calculations.

As said before due to the definition of $\mathbf{W}_\alpha$ the transformed Hamiltonian is block diagonal, i.e.

$$\mathbf{Q}\mathbf{W}_\alpha^\dagger(\mathbf{F}+\alpha\mathbf{G})\mathbf{W}_\alpha\mathbf{P}=0. \tag{A.9}$$

By expanding $\mathbf{W}_\alpha = 1+\alpha\mathbf{W}_1+\alpha^2\mathbf{W}_2+O\left(\alpha^3\right)$ and equating each order separately we find:

$$\mathbf{Q}\mathbf{W}_1\mathbf{P}=-\frac{1}{\mathbf{F}}\mathbf{Q}\mathbf{G}\mathbf{P} \tag{A.10}$$

$$\mathbf{Q}\mathbf{W}_2\mathbf{P}=-\frac{1}{\mathbf{F}}\mathbf{Q}\mathbf{G}\mathbf{Q}\mathbf{Q}\mathbf{W}_1\mathbf{P}. \tag{A.11}$$

The inverse operator $\frac{1}{\mathbf{F}}$ exists because it is only applied on the $\mathbf{Q}$ subspace where $\mathbf{F}$ has only non-zero eigenvalues. By also expanding the effective Hamiltonian

$$\mathbf{H}_\alpha^{\text{eff}}=\mathbf{P}\mathbf{W}_\alpha^\dagger(\mathbf{F}+\alpha\mathbf{G})\mathbf{W}_\alpha\mathbf{P} \tag{A.12}$$

in a Taylor series $\mathbf{H}_\alpha^{\text{eff}}=\alpha\mathbf{H}_1^{\text{eff}}+\alpha^2\mathbf{H}_2^{\text{eff}}+\alpha^3\mathbf{H}_\alpha^{\text{eff}}+O\left(\alpha^4\right)$ we find:

$$\mathbf{H}_1^{\text{eff}}=0 \tag{A.13}$$

$$\mathbf{H}_2^{\text{eff}}=-\mathbf{P}\mathbf{G}\mathbf{Q}\frac{1}{\mathbf{F}}\mathbf{Q}\mathbf{G}\mathbf{P} \tag{A.14}$$

$$\mathbf{H}_3^{\text{eff}}=\mathbf{P}\mathbf{G}\mathbf{Q}\frac{1}{\mathbf{F}}\mathbf{Q}\mathbf{G}\mathbf{Q}\frac{1}{\mathbf{F}}\mathbf{Q}\mathbf{G}\mathbf{P}. \tag{A.15}$$

Note that the first order vanishes because $\mathbf{PGP}=0$. We are not going to use the third order formula very much. We will only need it to explain why $\mathbf{H}_3^{\text{eff}}$ vanishes for the Fermi-Hubbard model.

## A.3 The Floquet-Schrieffer-Wolff transformation

Consider a general system with a Hamiltonian given by

$$\mathbf{H}=\mathbf{F}+\alpha\mathbf{G}(\phi) \tag{A.16}$$

where $\mathbf{H}(\phi)$ is $2\pi$ periodic. We can therefore use Floquet theory to describe the system. Note that $\mathbf{F}$ is the part of the system which has energy scales about the same size as $\omega$ and $\alpha\mathbf{G}(\phi)$ is the part with energy scales much smaller than $\omega$. Our aim is to find an effective (static) Hamiltonian describing the limit $\alpha\to 0$[3]. In particular we again fix a degenerate eigenspace of $\mathbf{F}$ which is described by a projector $\mathbf{P}$ and assume that the eigenvalue of this eigenspace is 0. We will denote $\mathbf{Q}=1-\mathbf{P}$ and further assume that $\mathbf{PG}(\phi)\mathbf{P}=0$ for all $\phi$.

Under these conditions we can use the Floquet-Schrieffer-Wolff transformation [22] to obtain an effective Hamiltonian for $\alpha\to 0$. It simultaneously applies two procedures. First it performs a time-average over the time-dependent part as the high-frequency expansion. Second it also restricts the system to the subspace $\mathbf{P}$ as the Schrieffer-Wolff transformation. There are many ways

[3] We will not call it the Floquet Hamiltonian due to the different idea behind the expansion. But it is essentially the same. In particular it will predict the true time evolution of the system only at full periods.

to derive it. We could try to perform a perturbative expansion of both the time evolution operator and the Floquet Hamiltonian as we did for the high-frequency expansion. However this turns out to be quite cumbersome. The easiest derivation in our setting is to use the extended Hilbert space framework. Recall that we can think about the driven system as a static system which consists of an infinite stack of copies of the original system. These copies are coupled by the corresponding Fourier component of the Hamiltonian. If we expand $\mathbf{G} = \sum_a \mathbf{G}_a e^{-ia\phi}$ then the coupling between layer $a$ and $b$ is given by $\mathbf{G}_{a-b}$. Also recall that the $a$'th copy of the system has an extra energy offset $-a$.

The ordinary Schrieffer-Wolff transformation for a static system results in an effective Hamiltonian which is given by (A.14):

$$\mathbf{H}_2^{\text{eff}} = -\alpha^2 \mathbf{PGQ}\frac{1}{\mathbf{F}}\mathbf{QGP}. \tag{A.17}$$

In the driven case we need to apply this formula to the extended static system. This means we need to think about $\mathbf{P}$ as the original $\mathbf{P}$, but restricted to layer 0. On the other hand the new $\mathbf{Q}$ now does not only include the $\mathbf{Q}$ subspaces, but in principle also all $\mathbf{P}$ apart from the one in layer 0. In order to not confuse ourselves let us introduce the notation $\mathbf{P}_a$ and $\mathbf{Q}_a$ for the respective subspaces in layer $a$. We would like to derive an effective Hamiltonian in the subspace $\mathbf{P} = \mathbf{P}_0$. It is given by

$$\mathbf{H}_2^{\text{eff}} = -\alpha^2 \left[ \sum_a \mathbf{P}_0 \mathbf{G}_a \mathbf{Q}_a \frac{1}{\mathbf{F} - a} \mathbf{Q}_a \mathbf{G}_{-a} \mathbf{P}_0 + \sum_{a \neq 0} \mathbf{P}_0 \mathbf{G}_a \mathbf{P}_a \frac{1}{\mathbf{F} - a} \mathbf{P}_a \mathbf{G}_{-a} \mathbf{P}_0 \right] \tag{A.18}$$

where the Fourier components $\mathbf{G}_{-a}$, $\mathbf{G}_a$ also implicitly include a change of layer from 0 to $a$ or from layer $a$ to 0 respectively. Note that we do not only also sum over the $\mathbf{Q}_a$, but also over the $\mathbf{P}_a$ subspaces for $a \neq 0$, because they are not part of $\mathbf{P} = \mathbf{P}_0$. Also note that the denominator $\frac{1}{\mathbf{F}}$ got replaced by $\frac{1}{\mathbf{F}-a}$. This is due to the extra energy offset in layer $a$. Already from this denominator we can see that the method is not suited to describe resonant situations, i.e where there exists a eigenvalue of $\mathbf{F}$ which is an integer multiple of the frequency (which is $\omega = 1$ in this case). We can simplify formula (A.18) by observing that the second part actually vanishes. This follows from the condition $\mathbf{PG}(\phi)\mathbf{P} = 0$:

$$\mathbf{H}_2^{\text{eff}} = -\alpha^2 \sum_a \mathbf{P}_0 \mathbf{G}_a \mathbf{Q}_a \frac{1}{\mathbf{F} - a} \mathbf{Q}_a \mathbf{G}_{-a} \mathbf{P}_0. \tag{A.19}$$

Note that this formula reduces to the usual Schrieffer-Wolff transformation formula (A.14) when all Fourier components $\mathbf{G}_a$ vanish for $a \neq 0$ (which is the static case).

## A.4 Application to the Fermi-Hubbard model

In this section we will apply the above formulas to the Fermi-Hubbard model

$$\mathbf{H} = -\frac{J}{\omega} \left[ \sum_{n\sigma} g_n(\phi) \mathbf{c}_{n\sigma}^\dagger \mathbf{c}_{n+1\sigma} + g_n^*(\phi) \mathbf{c}_{n+1\sigma}^\dagger \mathbf{c}_{n\sigma} \right] + \frac{U}{\omega} \mathbf{H}_{\text{U}} \tag{A.20}$$

where the $g_n(\phi)$ describe the time-periodic hopping between site $n$ and $n+1$.

### Single particle

For a single particle we can ignore the Hubbard interaction term. The only energy scale in the system is $J$ which is supposed to be much smaller than $\omega$. We will therefore use the high-frequency expansion (A.6) which predicts:

$$\mathbf{H}_{\mathrm{F}} = \mathbf{H}_0 = \int \frac{\mathrm{d}\phi}{2\pi}\mathbf{H}(\phi) = -\frac{J}{\omega}\left[\sum_{n\sigma} g_{n,0}\mathbf{c}^\dagger_{n\sigma}\mathbf{c}_{n+1\sigma} + g_{n,0}\mathbf{c}^\dagger_{n+1\sigma}\mathbf{c}_{n\sigma}\right]. \tag{A.21}$$

Here we have used the definition of the Fourier components $g_n(\phi) = \sum_a g_{n,a}e^{-ia\phi}$. The result is given by a hopping Hamiltonian with hopping parameter given by $Jg_{n,0}$.

### Particle pair

Since the derivation is the same we will not consider only one pair but rather any numbers of pairs. We will only require an equal number of particles in both spin species $N_\uparrow = N_\downarrow$. Since $\frac{U}{\omega}$ is supposed to stay finite while $\alpha = \frac{J}{\omega} \to 0$ we use the Floquet-Schrieffer-Wolff transformation (A.19): $\mathbf{F}$ is given by $\mathbf{F} = \frac{U}{\omega}\Big(\mathbf{H}_{\mathrm{U}} - N_\uparrow\Big)$. $\mathbf{P}$ is the subspace where all particles are paired. We added the extra constant to $\mathbf{F}$ to make sure that $\mathbf{F}$ is zero on the subspace $\mathbf{P}$. We have

$$\mathbf{G}(\phi) = -\left[\sum_{n\sigma} g_n(\phi)\mathbf{c}^\dagger_{n\sigma}\mathbf{c}_{n+1\sigma} + g^*_n(\phi)\mathbf{c}^\dagger_{n+1\sigma}\mathbf{c}_{n\sigma}\right]. \tag{A.22}$$

or expressed in Fourier components

$$\mathbf{G}_a = -\left[\sum_{n\sigma} g_{na}\mathbf{c}^\dagger_{n\sigma}\mathbf{c}_{n+1\sigma} + g^*_{n,-a}\mathbf{c}^\dagger_{n+1\sigma}\mathbf{c}_{n\sigma}\right]. \tag{A.23}$$

Here we denote $g_n(\phi) = \sum_a g_{na}e^{-ia\phi}$. We need to check the requirement $\mathbf{P}\mathbf{G}_a\mathbf{P} = 0$. This can be easily seen because each $\mathbf{H}_a$ will move exactly one particle. When acting on a fully paired state of $\mathbf{P}$ it will lead to one broken pair and therefore the result will be annihilated by the projector $\mathbf{P}$.

The last observation, namely that $\mathbf{G}_a$ breaks exactly one pair, also shows that the Hubbard-interaction energy will be raised by $|U|/\omega$ and that we can replace denominator $\frac{1}{\mathbf{F}-a}$ by $\frac{1}{|U|/\omega-a} = \frac{1}{|u|-a}$:

$$\mathbf{H}^{\mathrm{pair}} = -\alpha^2 \sum_a \mathbf{P}_0\mathbf{G}_a\mathbf{Q}_a\frac{1}{|u|-a}\mathbf{Q}_a\mathbf{G}_{-a}\mathbf{P}_0. \tag{A.24}$$

What remains is to calculate $\mathbf{P}_0\mathbf{G}_a\mathbf{Q}_a\mathbf{G}_{-a}\mathbf{P}_0$. Both operators will move exactly one particle. There are two possibilities of starting and also ending with only pairs: Either both operators act on opposite spin and move the two particles of one pair in the same direction, or both operators act on the same

spin and move one particle out of the pair and back again.:

$$\mathbf{H}^{\text{pair}} = -\alpha^2 \sum_a \frac{1}{|u|-a}\Big[\sum_{n\sigma} \mathbf{P}_0 (g_{na} g_{n,-a} \mathbf{c}^\dagger_{n\bar{\sigma}} \mathbf{c}_{n+1\bar{\sigma}} \mathbf{c}^\dagger_{n\sigma} \mathbf{c}_{n+1\sigma} \tag{A.25}$$

$$+ g^*_{na} g^*_{n,-a} \mathbf{c}^\dagger_{n+1\bar{\sigma}} \mathbf{c}_{n\bar{\sigma}} \mathbf{c}^\dagger_{n+1\sigma} \mathbf{c}_{n\sigma} \tag{A.26}$$

$$+ g^*_{n,-a} g_{n,-a} \mathbf{c}^\dagger_{n+1\sigma} \mathbf{c}_{n\sigma} \mathbf{c}^\dagger_{n\sigma} \mathbf{c}_{n+1\sigma} \tag{A.27}$$

$$+ g_{na} g^*_{na} \mathbf{c}^\dagger_{n\sigma} \mathbf{c}_{n+1\sigma} \mathbf{c}^\dagger_{n+1\sigma} \mathbf{c}_{n\sigma}) \mathbf{P}_0 \Big]. \tag{A.28}$$

We denote the opposite spin with $\bar{\sigma}$. Since both spins are treated equally we can replace the spin sum by an overall factor of 2. We define the 'creation' and 'annihilation' operators of a pair as

$$\eta^+_n = \mathbf{c}^\dagger_{n\uparrow} \mathbf{c}^\dagger_{n\downarrow} \tag{A.29}$$

$$\eta^-_n = \mathbf{c}_{n\downarrow} \mathbf{c}_{n\uparrow}. \tag{A.30}$$

By rearranging the creation and annihilation operators and using their commutation relations we can simplify the expressions. For example we have

$$\mathbf{c}^\dagger_{n\downarrow} \mathbf{c}_{n+1\downarrow} \mathbf{c}^\dagger_{n\uparrow} \mathbf{c}_{n+1\uparrow} = \eta^+_n \eta^-_{n+1} \tag{A.31}$$

$$\mathbf{c}^\dagger_{n+1\uparrow} \mathbf{c}_{n\uparrow} \mathbf{c}^\dagger_{n\uparrow} \mathbf{c}_{n+1\uparrow} = \mathbf{n}_{n+1\uparrow} - \mathbf{n}_{n+1\uparrow} \mathbf{n}_{n\uparrow}. \tag{A.32}$$

We finally find

$$\mathbf{H}^{\text{pair}} = \sum_n \left[ W_n \frac{1}{2} \left( \eta^+_n \eta^-_{n+1} + \eta^+_{n+1} \eta^-_n \right) + Z_n \hat{\mathbf{n}}_{n\uparrow} \hat{\mathbf{n}}_{n+1\uparrow} - \mu_n \hat{\mathbf{n}}_{n\uparrow} \right]. \tag{A.33}$$

The parameters are given by:

$$W_n = -4\alpha^2 \sum_a \frac{g_{na} g_{n,-a}}{|u|-a} \tag{A.34}$$

$$Z_n = 2\alpha^2 \sum_m \frac{|g_{na}|^2 + |g_{n,-a}|^2}{|u|-a} \tag{A.35}$$

$$\mu_n = 2\alpha^2 \sum_a \frac{|g_{n-1,-a}|^2 + |g_{n,a}|^2}{|u|-a}. \tag{A.36}$$

The first term describes the pair hopping. The second term is the nearest neighbour pair interaction term. The third term adds an extra chemical potential. Note that instead of $\mathbf{n}_{n\uparrow}$ we could have equivalently used $\mathbf{n}_{n\downarrow}$ (both are necessary equal in the $\mathbf{P}$ sector and equal to either 0 or 1).

#### A remark on the next order correction

In this section we will quickly show that the next order correction vanishes. For simplicity we will explain it with the static Schrieffer-Wolff transformation (the argument is completely the same also in

the Floquet case). In general the next order is given by equation (A.15):

$$\mathbf{H}_3^{\text{eff}} = \mathbf{PGQ}\frac{1}{\mathbf{F}}\mathbf{QGQ}\frac{1}{\mathbf{F}}\mathbf{QGP}. \tag{A.37}$$

The reason why it vanishes is because if we start with a completely paired state in **P** then by hopping three times via **G** we can never end up in a completely paired state again. To see this denote the sum of all positions of the particles by $s$. For a completely paired state $s$ is an even number. Now each time we apply **G**, which is a hopping Hamiltonian, it moves exactly one particle and therefore $s$ changes by one. This means when we apply **G** three times $s$ is going to be an odd number and therefore the state cannot be completely paired, i.e. $\mathbf{H}_3^{\text{eff}} = 0$.

APPENDIX B

# A general theorem about scattering from slow to fast modes

In this chapter we will establish a general theorem for a huge variety of systems and thereby show that the unintuitive result we found for the pair breaking in the limit $\alpha \to 0$ is not unusual.

In the following consider a general system with a small positive parameter $\alpha$. As $\alpha \to 0$ a part of the system, described by projector $\mathbf{P}$, evolves slower and slower in time, while the timescales of the other part of the system $\mathbf{Q}$ are fixed (and therefore $\mathbf{Q}$ evolves faster than $\mathbf{P}$).

## B.1 General considerations

Consider a system with two subsystems: a slow one $\mathbf{P}$ with Hamiltonian $\alpha\mathbf{h}_\alpha^{\mathrm{P}}$ and a fast one $\mathbf{Q}$ with Hamiltonian $\mathbf{h}_\alpha^{\mathrm{Q}}$. Additionally we also have a potential $\mathbf{V}_\alpha$ which couples both subsystems. We consider an incoming wave in the slow subsystem $\mathbf{P}$ and would like to study how it scatters at the potential in the limit $\alpha \to 0$. In particular we are interested in what fraction of the wavefunction ends up in subsystem $\mathbf{Q}$.

The Lippmann-Schwinger equations of such a system are given by:

$$\mathbf{P}\left|\psi^+\right\rangle = \left|\phi_\alpha\right\rangle + \frac{1}{\alpha\varepsilon_\alpha - \alpha\mathbf{h}_\alpha^{\mathrm{P}} + i\epsilon}\left(\mathbf{P}\mathbf{V}_\alpha\mathbf{P}\left|\psi^+\right\rangle + \mathbf{P}\mathbf{V}_\alpha\mathbf{Q}\left|\psi^+\right\rangle\right) \tag{B.1}$$

$$\mathbf{Q}\left|\psi^+\right\rangle = \frac{1}{\alpha\varepsilon_\alpha - \mathbf{h}_\alpha^{\mathrm{Q}} + i\epsilon}\left(\mathbf{Q}\mathbf{V}_\alpha\mathbf{P}\left|\psi^+\right\rangle + \mathbf{Q}\mathbf{V}_\alpha\mathbf{Q}\left|\psi^+\right\rangle\right). \tag{B.2}$$

We can solve the second equation (B.2)

$$\mathbf{Q}\left|\psi^+\right\rangle = \mathbf{G}_\alpha^{\mathrm{Q}}\mathbf{Q}\mathbf{V}_\alpha\mathbf{P}\left|\psi^+\right\rangle \tag{B.3}$$

using the Greens operator of the system in the $\mathbf{Q}$ sector:

$$\mathbf{G}_\alpha^{\mathrm{Q}} = \mathbf{Q}\frac{1}{\alpha\varepsilon_\alpha - \mathbf{h}_\alpha^{\mathrm{Q}} - \mathbf{Q}\mathbf{V}_\alpha\mathbf{Q} + i\epsilon}\mathbf{Q}. \tag{B.4}$$

The interpretation of this operator is as follows: Assume we somehow know the complete wavefunction

in **P** sector. Then we can compute the wavefunction in the **Q** sector by applying the Greens operator to $\mathbf{QV}_\alpha\mathbf{P}\left|\psi^+\right\rangle$. The Greens operator will play an important role as its contains all knowledge about the **Q** sector which will be relevant for us. In particular we do not need that $\mathbf{h}_\alpha^{\mathrm{Q}}$ behaves nicely as $\alpha \to 0$, as long as $\mathbf{G}_\alpha^{\mathrm{Q}}$ has a well defined limit for $\alpha \to 0$ (This is in particular important for our bound pair case. Actually $\mathbf{h}_\alpha^{\mathrm{Q}}$ diverges for the pairs as $\alpha \to 0$, but $\mathbf{G}_\alpha^{\mathrm{Q}}$ has a well defined limit.).

Inserting back into the Lippmann-Schwinger equation (B.1) gives:

$$\mathbf{P}\left|\psi^+\right\rangle = |\phi\rangle + \frac{1}{\alpha}\frac{1}{\varepsilon_\alpha - \mathbf{h}_\alpha^{\mathrm{P}} + i\epsilon}\left(\mathbf{PV}_\alpha\mathbf{P}\left|\psi^+\right\rangle + \mathbf{PV}_\alpha\mathbf{QG}_\alpha^{\mathrm{Q}}\mathbf{QV}_\alpha\mathbf{P}\left|\psi^+\right\rangle\right) \tag{B.5}$$

$$= |\phi\rangle + \frac{1}{\alpha}\frac{1}{\varepsilon_\alpha - \mathbf{h}_\alpha^{\mathrm{P}} + i\epsilon}\mathbf{V}_\alpha^{\mathrm{eff}}\mathbf{P}\left|\psi^+\right\rangle. \tag{B.6}$$

The last equation is again a Lippmann-Schwinger equation involving only the **P** sector with the effective potential[1]

$$\mathbf{V}_\alpha^{\mathrm{eff}} = \mathbf{PV}_\alpha\mathbf{P} + \mathbf{PV}_\alpha\mathbf{QG}_\alpha^{\mathrm{Q}}\mathbf{QV}_\alpha\mathbf{P}. \tag{B.7}$$

Note that this $\mathbf{V}_\alpha^{\mathrm{eff}}$ is not a hermitian operator, since it also includes particle loss from **P** into **Q**. Recall that our aim is to study the limit $\alpha \to 0$. In this limit we can expect that the effective potential has a non-zero limit $\mathbf{V}_\alpha^{\mathrm{eff}} \to \mathbf{V}_0^{\mathrm{eff}} \neq 0$.

Because the effective Lippmann-Schwinger equation (B.6) reduces the problem to only one sector **P** it is enough to study how scattering in subsystem **P** behaves for $\alpha \to 0$. This will be part of the first theorem. The second theorem then makes the connection to the **Q** subsystem.

For clarity we will remind the reader of the following subspaces connected to a linear operator **A**:

- The kernel $\mathrm{Ker}\mathbf{A} = \{|x\rangle : \mathbf{A}|x\rangle = 0\}$ is the subspace which is annihilated by **A**.
- The image $\mathrm{Im}\mathbf{A} = \{\mathbf{A}|x\rangle\}$ is the subspace of all possible outcomes of **A**.
- The space on which **A** acts[2] is the orthogonal complement of the kernel. Intuitively speaking it is the subspace on which **A** does not vanish.

Before trying to understand the whole proofs we advise the reader to first have a look at the simple toy model (see section 5.2.4) which already includes many ideas of the proofs. Since the proofs are quite messy and require the definition of many quantities (especially lots of projectors) we will stick to the same notation in both proofs. We give an overview over all occurring quantities in tables B.1 and B.2.

**A remark on projectors** The reader might wonder why we define so many projectors. In short they will pick out small relevant subspaces of the infinite dimensional Hilbert space, which are in most practical applications finite dimensional[3]. This allows us to reduce the Lippmann-Schwinger equation to basically a matrix equation which is much easier to handle.

We will also use projectors to 'invert' non-invertible operators/matrices (like the potential). For an arbitrary operator/matrix **A** we can define two projectors **X** (the projector on the image of **A**) and **Y**

[1] In the context of particle physics this effective potential is often called the optical potential [28].

[2] We are not aware of a commonly accepted name for it.

[3] We will often call them finite dimensional, even though the theorem also works if they are not.

(the projector onto the space where **A** acts), s.t. **XAY** is invertible (when restricted to **X** and **Y**).

During the proofs we are going to need some technical assumptions. They state that certain operators on these finite dimensional subspaces are invertible. In section B.4 we will argue why we can expect them to almost always hold. Although we have not described the involved quantities yet we will now state them here so that we have a compact list we can refer to.

The technical assumptions are:

(a) $\bar{\mathbf{K}} - \frac{1}{\alpha}\bar{\mathbf{K}}\mathbf{G}_\alpha^{\mathrm{P}}\mathbf{V}_\alpha^{\mathrm{eff}}\bar{\mathbf{K}}$ is invertible for all $\alpha$ and its limit $\bar{\mathbf{K}} - \bar{\mathbf{K}}\mathbf{G}_0^{\mathrm{P}}\mathbf{V}_1^{\mathrm{eff}}\bar{\mathbf{K}}$ is also invertible.

(b) $\mathbf{K} - \frac{1}{\alpha}\mathbf{K}\mathbf{G}_\alpha^{\mathrm{P}}\mathbf{V}_\alpha^{\mathrm{eff}}\mathbf{K} - \frac{1}{\alpha}\mathbf{K}\mathbf{G}_\alpha^{\mathrm{P}}\mathbf{V}_\alpha^{\mathrm{eff}}\bar{\mathbf{K}}\frac{1}{\bar{\mathbf{K}}-\frac{1}{\alpha}\bar{\mathbf{K}}\mathbf{G}_\alpha^{\mathrm{P}}\mathbf{V}_\alpha^{\mathrm{eff}}\bar{\mathbf{K}}}\frac{1}{\alpha}\bar{\mathbf{K}}\mathbf{G}_\alpha^{\mathrm{P}}\mathbf{V}_\alpha^{\mathrm{eff}}\mathbf{K}$ is invertible for all $\alpha$ and its limit $\mathbf{K}\mathbf{G}_0^{\mathrm{P}}\mathbf{V}_0^{\mathrm{eff}}\mathbf{K} + \mathbf{K}\mathbf{G}_0^{\mathrm{P}}\mathbf{V}_1^{\mathrm{eff}}\bar{\mathbf{K}}\frac{1}{\bar{\mathbf{K}}-\bar{\mathbf{K}}\mathbf{G}_0^{\mathrm{P}}\mathbf{V}_1^{\mathrm{eff}}\bar{\mathbf{K}}}\bar{\mathbf{K}}\mathbf{G}_0^{\mathrm{P}}\mathbf{V}_0^{\mathrm{eff}}\mathbf{K}$ is also invertible.

(c) $\mathbf{K}^{\mathrm{Q}}\mathbf{G}_0^{\mathrm{Q}}\mathbf{K}^{\mathrm{Q}}$ is invertible.

(d) $\mathbf{K}\mathbf{G}_0^{\mathrm{P}}\mathbf{K}$ is invertible.

(e) $\mathbf{L} - \left(\mathbf{L} - \mathbf{L}\mathbf{G}_0^{\mathrm{P}}\mathbf{K}\frac{1}{\mathbf{K}\mathbf{G}_0^{\mathrm{P}}\mathbf{K}}\mathbf{K}\right)\mathbf{K}\mathbf{G}_0^{\mathrm{P}}\bar{\mathbf{K}}\mathbf{V}_1^{\mathrm{eff}}\mathbf{L}$ is invertible.

## B.2 Theorem for only one slow subspace

Let us go on to the first theorem. It concerns a system defined only on the subspace $\mathbf{P}$[4]. The free Hamiltonian on $\mathbf{P}$ scales as $\mathbf{H}_0 = \alpha\mathbf{h}_\alpha^{\mathrm{P}}$, in order words the dynamics become slower and slower as $\alpha \to 0$. The potential on the other hand $\mathbf{V}_\alpha^{\mathrm{eff}}$ is constant as $\alpha \to 0$. Note that we call the potential effective because it will play the role of the effective potential once we include the $\mathbf{Q}$ subspace and because it does not need to be a hermitian potential, i.e. it allows for particle loss. We will not require further properties of $\mathbf{V}_\alpha^{\mathrm{eff}}$, only that it is such that we can apply scattering theory (and by this we mean the Lippmann-Schwinger equation).

We would like to study how an incoming wave $|\phi\rangle$ scatters at this potential in the limit $\alpha \to 0$. In particular we aim to calculate the Lippmann-Schwinger wavefunction $|\psi^+\rangle$. Note that we require that $|\phi\rangle$ is an eigenstate of the free Hamiltonian $\alpha\mathbf{h}_\alpha^{\mathrm{P}}$ for all $\alpha$[5]. Therefore as $\alpha \to 0$ its form does not change but only its energy $\alpha\varepsilon_\alpha$.

**Theorem 1** *Consider the scattering problem given by the free Hamiltonian $\mathbf{H}_0 = \alpha\mathbf{h}_\alpha^{\mathrm{P}}$ with (not necessarily hermitian) potential $\mathbf{V}_\alpha^{\mathrm{eff}}$. Assume that this scattering problem is such that we can apply the Lippmann-Schwinger equation for all finite $\alpha$. Choose as incoming state an eigenstate $|\phi\rangle$ of $\mathbf{h}_\alpha^{\mathrm{P}}$ with an energy $\alpha\varepsilon_\alpha$. Furthermore assume that $\mathbf{h}_\alpha^{\mathrm{P}}$ has a well defined limit for $\alpha \to 0$ and that the Taylor expansion of $\mathbf{V}_\alpha^{\mathrm{eff}}$ exists at least up to first order.*

*In case that $\mathbf{V}_\alpha^{\mathrm{eff}} \not\to 0$ and the operators satisfy the additional technical assumptions (a), (b) we find in the limit $\alpha \to 0$:*

[4] For now one can think of $\mathbf{P}$ as the whole space. In the later theorems we will add another subspace $\mathbf{Q}$ to it.

[5] If this is not the case we can easily achieve this by first performing an $\alpha$ dependent unitary transformation which diagonalizes $\mathbf{h}_\alpha^{\mathrm{P}}$.

1. $\mathbf{K}\left|\psi^{+}\right\rangle \to 0$

2. *If additionally* $\bar{\mathbf{K}}\mathbf{V}_0^{\text{eff}} = 0$ *and (d), (e) hold:*

$$\mathbf{L}\left|\psi_0^{+}\right\rangle = \frac{1}{\mathbf{L} - \left(\mathbf{L} - \mathbf{L}\mathbf{G}_0^{\text{P}}\mathbf{K}\frac{1}{\mathbf{K}\mathbf{G}_0^{\text{P}}\mathbf{K}}\mathbf{K}\right)\mathbf{K}\mathbf{G}_0^{\text{P}}\bar{\mathbf{K}}\mathbf{V}_1^{\text{eff}}\mathbf{L}}\left(\mathbf{L} - \mathbf{L}\mathbf{G}_0^{\text{P}}\mathbf{K}\frac{1}{\mathbf{K}\mathbf{G}_0^{\text{P}}\mathbf{K}}\mathbf{K}\right)|\phi\rangle \tag{B.8}$$

3. *If additionally* $\bar{\mathbf{K}}\mathbf{V}_0^{\text{eff}} = 0$ *and (d) holds:*

$$\mathbf{P}\left|\psi_0^{+}\right\rangle = \left(1 - \mathbf{G}_0^{\text{P}}\mathbf{K}\frac{1}{\mathbf{K}\mathbf{G}_0^{\text{P}}\mathbf{K}}\mathbf{K}\right)\left(|\phi\rangle + \mathbf{G}_0^{\text{P}}\bar{\mathbf{K}}\mathbf{V}_1^{\text{eff}}\mathbf{L}\left|\psi_0^{+}\right\rangle\right) \tag{B.9}$$

We have not yet defined the various quantities appearing here. We give their definitions, as well as others, in tables B.1 and B.2. The first conclusion states that $\mathbf{K}\left|\psi^{+}\right\rangle \to 0$. As stated in table B.2 the projector $\mathbf{K}$ gives the subspace on which the potential $\mathbf{V}_0^{\text{eff}}$ acts. Therefore the first conclusion states that the wavefunction will vanish at the potential (as in the toy model), which we can think of as adding an additional boundary condition to the system. This is also the most important finding of this theorem. Conclusions 2 and 3 give the full (and quite complicated) solution of $\left|\psi^{+}\right\rangle$. They are only relevant if one would like to explicitly calculate scattering properties. Note that their extra requirement $\bar{\mathbf{K}}\mathbf{V}_0^{\text{eff}} = 0$ is automatically satisfied if $\mathbf{V}_0^{\text{eff}}$ is hermitian.

Proof: Let us start with the Lippmann-Schwinger equation

$$\mathbf{P}\left|\psi^{+}\right\rangle = |\phi\rangle + \frac{1}{\alpha}\frac{1}{\varepsilon_\alpha - \mathbf{h}_\alpha^{\text{P}} + i\epsilon}\mathbf{V}_\alpha^{\text{eff}}\mathbf{P}\left|\psi^{+}\right\rangle. \tag{B.10}$$

In the toy model this equation corresponds to (5.4).

**Step 1: Solving the Lippmann-Schwinger equation** The Lippmann-Schwinger equation is an implicit equation for the infinite dimensional vector $\mathbf{P}\left|\psi^{+}\right\rangle$. As such we cannot solve it directly. But note that in the limit $\alpha \to 0$ the right hand side does not depend on the whole $\mathbf{P}\left|\psi^{+}\right\rangle$, but only on the finite dimensional part of the wavefunction $\mathbf{K}\left|\psi^{+}\right\rangle$. $\mathbf{K}$ is the subspace of $\mathbf{P}$ on which the zeroth order potential $\mathbf{V}_0^{\text{eff}}$ acts. For later convenience define $\bar{\mathbf{K}} = \mathbf{P} - \mathbf{K}$. In the toy model the projector $\mathbf{K}$ projects on the subspace spanned by $\left|0_{\text{P}}\right\rangle$ (because the potential acts only on $\left\langle 0_{\text{P}}\right|\mathbf{P}\left|\psi^{+}\right\rangle$). Since we expect a different behaviour of the wavefunction in $\mathbf{K}$ and in $\bar{\mathbf{K}}$ as $\alpha \to 0$, it is a good a idea to split the Lippmann-Schwinger equation (B.10) into two equations for each subsystem:

$$\mathbf{K}\left|\psi^{+}\right\rangle = \mathbf{K}|\phi\rangle + \frac{1}{\alpha}\mathbf{K}\frac{1}{\varepsilon_\alpha - \mathbf{h}_\alpha^{\text{P}} + i\epsilon}\mathbf{V}_\alpha^{\text{eff}}\mathbf{K}\left|\psi^{+}\right\rangle + \frac{1}{\alpha}\mathbf{K}\frac{1}{\varepsilon_\alpha - \mathbf{h}_\alpha^{\text{P}} + i\epsilon}\mathbf{V}_\alpha^{\text{eff}}\bar{\mathbf{K}}\left|\psi^{+}\right\rangle \tag{B.11}$$

$$\bar{\mathbf{K}}\left|\psi^{+}\right\rangle = \bar{\mathbf{K}}|\phi\rangle + \frac{1}{\alpha}\bar{\mathbf{K}}\frac{1}{\varepsilon_\alpha - \mathbf{h}_\alpha^{\text{P}} + i\epsilon}\mathbf{V}_\alpha^{\text{eff}}\mathbf{K}\left|\psi^{+}\right\rangle + \frac{1}{\alpha}\bar{\mathbf{K}}\frac{1}{\varepsilon_\alpha - \mathbf{h}_\alpha^{\text{P}} + i\epsilon}\mathbf{V}_\alpha^{\text{eff}}\bar{\mathbf{K}}\left|\psi^{+}\right\rangle. \tag{B.12}$$

From now on we will abbreviate $\mathbf{G}_\alpha^{\mathrm{P}} = \frac{1}{\varepsilon_\alpha - \mathbf{h}_\alpha^{\mathrm{P}} + i\epsilon}$. The second equation (B.12) can be solved:

$$\bar{\mathbf{K}} \left|\psi^+\right\rangle = \frac{1}{\bar{\mathbf{K}} - \frac{1}{\alpha}\bar{\mathbf{K}}\mathbf{G}_\alpha^{\mathrm{P}}\mathbf{V}_\alpha^{\mathrm{eff}}\bar{\mathbf{K}}} \left( \bar{\mathbf{K}} \left|\phi\right\rangle + \frac{1}{\alpha}\bar{\mathbf{K}}\mathbf{G}_\alpha^{\mathrm{P}}\mathbf{V}_\alpha^{\mathrm{eff}}\mathbf{K} \left|\psi^+\right\rangle \right). \tag{B.13}$$

Here we need technical assumption (a) to ensure $\bar{\mathbf{K}} - \frac{1}{\alpha}\bar{\mathbf{K}}\mathbf{G}_\alpha^{\mathrm{P}}\mathbf{V}_\alpha^{\mathrm{eff}}\bar{\mathbf{K}}$ is indeed invertible. Reinserting this into equation (B.11) yields:

$$\mathbf{K} \left|\psi^+\right\rangle = \mathbf{K} \left|\phi\right\rangle + \frac{1}{\alpha}\mathbf{K}\mathbf{G}_\alpha^{\mathrm{P}}\mathbf{V}_\alpha^{\mathrm{eff}}\mathbf{K} \left|\psi^+\right\rangle + \frac{1}{\alpha}\mathbf{K}\mathbf{G}_\alpha^{\mathrm{P}}\mathbf{V}_\alpha^{\mathrm{eff}}\bar{\mathbf{K}} \frac{1}{\bar{\mathbf{K}} - \frac{1}{\alpha}\bar{\mathbf{K}}\mathbf{G}_\alpha^{\mathrm{P}}\mathbf{V}_\alpha^{\mathrm{eff}}\bar{\mathbf{K}}} \left( \bar{\mathbf{K}} \left|\phi\right\rangle + \frac{1}{\alpha}\bar{\mathbf{K}}\mathbf{G}_\alpha^{\mathrm{P}}\mathbf{V}_\alpha^{\mathrm{eff}}\mathbf{K} \left|\psi^+\right\rangle \right). \tag{B.14}$$

This is a complicated equation. But note that it depends only on the finite dimensional $\mathbf{K} \left|\psi^+\right\rangle$ and as such is simply a matrix equation. It is the equivalent of equation (5.5) for the toy model. We can directly solve this equation which gives:

$$\begin{aligned} \mathbf{K} \left|\psi^+\right\rangle = & \frac{1}{\mathbf{K} - \frac{1}{\alpha}\mathbf{K}\mathbf{G}_\alpha^{\mathrm{P}}\mathbf{V}_\alpha^{\mathrm{eff}}\mathbf{K} - \frac{1}{\alpha}\mathbf{K}\mathbf{G}_\alpha^{\mathrm{P}}\mathbf{V}_\alpha^{\mathrm{eff}}\bar{\mathbf{K}} \frac{1}{\bar{\mathbf{K}} - \frac{1}{\alpha}\bar{\mathbf{K}}\mathbf{G}_\alpha^{\mathrm{P}}\mathbf{V}_\alpha^{\mathrm{eff}}\bar{\mathbf{K}}} \frac{1}{\alpha}\bar{\mathbf{K}}\mathbf{G}_\alpha^{\mathrm{P}}\mathbf{V}_\alpha^{\mathrm{eff}}\mathbf{K}} \cdot \\ & \cdot \left( \mathbf{K} + \frac{1}{\alpha}\mathbf{K}\mathbf{G}_\alpha^{\mathrm{P}}\mathbf{V}_\alpha^{\mathrm{eff}}\bar{\mathbf{K}} \frac{1}{\bar{\mathbf{K}} - \frac{1}{\alpha}\bar{\mathbf{K}}\mathbf{G}_\alpha^{\mathrm{P}}\mathbf{V}_\alpha^{\mathrm{eff}}\bar{\mathbf{K}}} \bar{\mathbf{K}} \right) \left|\phi\right\rangle . \end{aligned} \tag{B.15}$$

This time we used technical assumption (b) to invert the first operator.

**Step 2: Performing the limit $\alpha \to 0$** So far we derived complicated expressions for finite $\alpha$. Now we are ready to reap the fruits of our work, namely we can perform the limit $\alpha \to 0$. Before we tackle the big formulas let us first determine the limits for smaller parts. In particular we have due to the definitions of the projectors:

$$\mathbf{G}_\alpha^{\mathrm{P}} \to \mathbf{G}_0^{\mathrm{P}} \tag{B.16}$$

$$\mathbf{V}_\alpha^{\mathrm{eff}}\mathbf{K} \to \mathbf{V}_0^{\mathrm{eff}}\mathbf{K} \tag{B.17}$$

$$\frac{1}{\alpha}\mathbf{V}_\alpha^{\mathrm{eff}}\bar{\mathbf{K}} \to \mathbf{V}_1^{\mathrm{eff}}\bar{\mathbf{K}} \tag{B.18}$$

where we Taylor expanded the potential $\mathbf{V}_\alpha^{\mathrm{eff}} = \mathbf{V}_0^{\mathrm{eff}} + \alpha\mathbf{V}_1^{\mathrm{eff}} + O\left(\alpha^2\right)$.

Now we only have to insert these limits into the equation (B.15):

$$\begin{aligned} \mathbf{K} \left|\psi^+\right\rangle = & \frac{\alpha}{\alpha\mathbf{K} - \mathbf{K}\mathbf{G}_\alpha^{\mathrm{P}}\mathbf{V}_\alpha^{\mathrm{eff}}\mathbf{K} - \left(\frac{1}{\alpha}\mathbf{K}\mathbf{G}_\alpha^{\mathrm{P}}\mathbf{V}_\alpha^{\mathrm{eff}}\bar{\mathbf{K}}\right) \frac{1}{\bar{\mathbf{K}} - \left(\frac{1}{\alpha}\bar{\mathbf{K}}\mathbf{G}_\alpha^{\mathrm{P}}\mathbf{V}_\alpha^{\mathrm{eff}}\bar{\mathbf{K}}\right)} \bar{\mathbf{K}}\mathbf{G}_\alpha^{\mathrm{P}}\mathbf{V}_\alpha^{\mathrm{eff}}\mathbf{K}} \cdot \\ & \cdot \left( \mathbf{K} + \left(\frac{1}{\alpha}\mathbf{K}\mathbf{G}_\alpha^{\mathrm{P}}\mathbf{V}_\alpha^{\mathrm{eff}}\bar{\mathbf{K}}\right) \frac{1}{\bar{\mathbf{K}} - \left(\frac{1}{\alpha}\bar{\mathbf{K}}\mathbf{G}_\alpha^{\mathrm{P}}\mathbf{V}_\alpha^{\mathrm{eff}}\bar{\mathbf{K}}\right)} \bar{\mathbf{K}} \right) \left|\phi\right\rangle \end{aligned} \tag{B.19}$$

where we have included brackets to group terms which will become finite in the limit. In the limit $\alpha \to 0$ (B.19) becomes:

$$\mathbf{K}\left|\psi^+\right\rangle \to -\frac{\alpha}{\mathbf{K}\mathbf{G}_0^{\mathrm{P}}\mathbf{V}_0^{\mathrm{eff}}\mathbf{K} + \mathbf{K}\mathbf{G}_0^{\mathrm{P}}\mathbf{V}_1^{\mathrm{eff}}\bar{\mathbf{K}}\frac{1}{\bar{\mathbf{K}}-\bar{\mathbf{K}}\mathbf{G}_0^{\mathrm{P}}\mathbf{V}_1^{\mathrm{eff}}\bar{\mathbf{K}}}\bar{\mathbf{K}}\mathbf{G}_0^{\mathrm{P}}\mathbf{V}_0^{\mathrm{eff}}\mathbf{K}}\left(\mathbf{K} + \mathbf{K}\mathbf{G}_0^{\mathrm{P}}\mathbf{V}_1^{\mathrm{eff}}\bar{\mathbf{K}}\frac{1}{\bar{\mathbf{K}}-\bar{\mathbf{K}}\mathbf{G}_0^{\mathrm{P}}\mathbf{V}_1^{\mathrm{eff}}\bar{\mathbf{K}}}\bar{\mathbf{K}}\right)|\phi\rangle \tag{B.20}$$

where again technical assumptions (a) and (b) make sure that the two operators are still invertible in the limit. In particular we have $\mathbf{K}\left|\psi^+\right\rangle \to 0$ as $\alpha \to 0$. This already shows the first finding.

**Step 3: Calculation of the full wavefunction in the limit** This step is not as important as the other ones before and only relevant for explicit calculations. It should merely been seen as an additional step to further analyze the limit $\alpha \to 0$. If the reader is more interested in qualitative results he can skip this part and go directly to theorem 2. So far we have seen that the wavefunction at the potential will vanish $\mathbf{K}\left|\psi^+\right\rangle \to 0$. This can be thought of as adding an additional boundary condition to the system. For the toy model we saw that this additional boundary condition leads to a full reflection of the wavefunction. Is this also true in general? Interestingly in general the answer is no. We are now going to show this.

We could obtain the full wavefunction by simply inserting the limit (B.20) into equation (B.13) where the $\alpha$ and $\frac{1}{\alpha}$ of both formulas cancel. The resulting equation would be correct, but quite complicated and not suitable for explicit calculations because we need to invert the infinite dimensional operator $\bar{\mathbf{K}} - \bar{\mathbf{K}}\mathbf{G}_0^{\mathrm{P}}\mathbf{V}_1^{\mathrm{eff}}\bar{\mathbf{K}}$. Interestingly there is a much simpler formula in case $\bar{\mathbf{K}}\mathbf{V}_0^{\mathrm{eff}} = 0$.

To see this let us go back to the original Lippmann-Schwinger equation (B.10):

$$\mathbf{P}\left|\psi^+\right\rangle = |\phi\rangle + \frac{1}{\alpha}\mathbf{G}_\alpha^{\mathrm{P}}\mathbf{V}_\alpha^{\mathrm{eff}}\mathbf{P}\left|\psi^+\right\rangle. \tag{B.21}$$

Due to the findings in the previous step we know that in the limit $\mathbf{K}\left|\psi^+\right\rangle = \alpha\mathbf{K}\left|\psi_1^+\right\rangle + O\left(\alpha^2\right)$, where $\mathbf{K}\left|\psi_1^+\right\rangle$ is the complicated expression of (B.20). We will now show that we can avoid computing $\mathbf{K}\left|\psi_1^+\right\rangle$ by doing some clever tricks. By Taylor expanding the Lippmann-Schwinger equation (B.21) itself and using $\mathbf{K}\left|\psi_0^+\right\rangle = 0$ we find that in the limit:

$$\mathbf{P}\left|\psi_0^+\right\rangle = |\phi\rangle + \mathbf{G}_0^{\mathrm{P}}\left(\mathbf{V}_0^{\mathrm{eff}}\mathbf{K}\left|\psi_1^+\right\rangle + \mathbf{V}_1^{\mathrm{eff}}\bar{\mathbf{K}}\left|\psi_0^+\right\rangle\right). \tag{B.22}$$

By the extra assumption $\bar{\mathbf{K}}\mathbf{V}_0^{\mathrm{eff}} = 0$ of the theorem we can expand this to

$$\mathbf{P}\left|\psi_0^+\right\rangle = |\phi\rangle + \mathbf{G}_0^{\mathrm{P}}\left(\mathbf{K}\mathbf{V}_0^{\mathrm{eff}}\mathbf{K}\left|\psi_1^+\right\rangle + \mathbf{K}\mathbf{V}_1^{\mathrm{eff}}\bar{\mathbf{K}}\left|\psi_0^+\right\rangle + \bar{\mathbf{K}}\mathbf{V}_1^{\mathrm{eff}}\bar{\mathbf{K}}\left|\psi_0^+\right\rangle\right). \tag{B.23}$$

Now multiply both sides by $\mathbf{K}$ from the left:

$$0 = \mathbf{K}\left|\psi_0^+\right\rangle = \mathbf{K}|\phi\rangle + \mathbf{K}\mathbf{G}_0^{\mathrm{P}}\mathbf{K}\left(\mathbf{K}\mathbf{V}_0^{\mathrm{eff}}\mathbf{K}\left|\psi_1^+\right\rangle + \mathbf{K}\mathbf{V}_1^{\mathrm{eff}}\bar{\mathbf{K}}\left|\psi_0^+\right\rangle\right) + \mathbf{K}\mathbf{G}_0^{\mathrm{P}}\bar{\mathbf{K}}\mathbf{V}_1^{\mathrm{eff}}\bar{\mathbf{K}}\left|\psi_0^+\right\rangle \tag{B.24}$$

and solve this equation using technical assumption (d):

$$\mathbf{K}\mathbf{V}_0^{\text{eff}}\mathbf{K}\left|\psi_1^+\right\rangle + \mathbf{K}\mathbf{V}_1^{\text{eff}}\bar{\mathbf{K}}\left|\psi_0^+\right\rangle = -\frac{1}{\mathbf{K}\mathbf{G}_0^{\text{P}}\mathbf{K}}\Big(\mathbf{K}\left|\phi\right\rangle + \mathbf{K}\mathbf{G}_0^{\text{P}}\bar{\mathbf{K}}\mathbf{V}_1^{\text{eff}}\bar{\mathbf{K}}\left|\psi_0^+\right\rangle\Big). \tag{B.25}$$

This can be directly reinserted into the Lippmann-Schwinger equation (B.21):

$$\mathbf{P}\left|\psi_0^+\right\rangle = \left(1 - \mathbf{G}_0^{\text{P}}\mathbf{K}\frac{1}{\mathbf{K}\mathbf{G}_0^{\text{P}}\mathbf{K}}\mathbf{K}\right)\Big(\left|\phi\right\rangle + \mathbf{G}_0^{\text{P}}\bar{\mathbf{K}}\mathbf{V}_1^{\text{eff}}\bar{\mathbf{K}}\left|\psi_0^+\right\rangle\Big). \tag{B.26}$$

Now we will define the projector $\mathbf{L}$ as the subspace of $\bar{\mathbf{K}}$ on which $\bar{\mathbf{K}}\mathbf{V}_1^{\text{eff}}\bar{\mathbf{K}}$ acts[6], i.e. $\bar{\mathbf{K}}\mathbf{V}_1^{\text{eff}}\bar{\mathbf{K}} = \bar{\mathbf{K}}\mathbf{V}_1^{\text{eff}}\mathbf{L}$. Using this we arrive at the third conclusion of the theorem:

$$\mathbf{P}\left|\psi_0^+\right\rangle = \left(1 - \mathbf{G}_0^{\text{P}}\mathbf{K}\frac{1}{\mathbf{K}\mathbf{G}_0^{\text{P}}\mathbf{K}}\mathbf{K}\right)\Big(\left|\phi\right\rangle + \mathbf{G}_0^{\text{P}}\bar{\mathbf{K}}\mathbf{V}_1^{\text{eff}}\mathbf{L}\left|\psi_0^+\right\rangle\Big). \tag{B.27}$$

Again we can solve this implicit equation by applying $\mathbf{L}$ to the equation from the left and assuming technical assumption (e):

$$\mathbf{L}\left|\psi_0^+\right\rangle = \left(\mathbf{L} - \mathbf{L}\mathbf{G}_0^{\text{P}}\mathbf{K}\frac{1}{\mathbf{K}\mathbf{G}_0^{\text{P}}\mathbf{K}}\mathbf{K}\right)\Big(\left|\phi\right\rangle + \mathbf{G}_0^{\text{P}}\bar{\mathbf{K}}\mathbf{V}_1^{\text{eff}}\mathbf{L}\left|\psi_0^+\right\rangle\Big) \tag{B.28}$$

and thus:

$$\mathbf{L}\left|\psi_0^+\right\rangle = \frac{1}{\mathbf{L} - \Big(\mathbf{L} - \mathbf{L}\mathbf{G}_0^{\text{P}}\mathbf{K}\frac{1}{\mathbf{K}\mathbf{G}_0^{\text{P}}\mathbf{K}}\mathbf{K}\Big)\mathbf{K}\mathbf{G}_0^{\text{P}}\bar{\mathbf{K}}\mathbf{V}_1^{\text{eff}}\mathbf{L}}\left(\mathbf{L} - \mathbf{L}\mathbf{G}_0^{\text{P}}\mathbf{K}\frac{1}{\mathbf{K}\mathbf{G}_0^{\text{P}}\mathbf{K}}\mathbf{K}\right)\left|\phi\right\rangle. \tag{B.29}$$

This finishes the proof of the first theorem. We would like to make a final remark on why the last step 3 was useful. Equation (B.29) might seem complicated but it has a major advantage: It depends only on the subspaces $\mathbf{K}$ and $\mathbf{L}$, which describe the subspaces on which $\mathbf{V}_0^{\text{eff}}$ and $\mathbf{V}_1^{\text{eff}}$ act. These subspaces will be comparatively small and in most cases be finite dimensional. This means equation (B.29) is in most cases not an operator equation, but a low dimensional matrix equation which can be solved either by hand or via computer. If we tried to use equation (B.13) instead, we would need to invert an infinite dimensional operator which is much more complicated.

## B.3 Theorem for a slow and a fast subspace

So far we only only considered one subsystem $\mathbf{P}$ in which the dynamics become slower and slower. Now we can go on to study what happens if we have two subsystems: a slow one $\mathbf{P}$ with Hamiltonian $\alpha\mathbf{h}_\alpha^{\text{P}}$ and a fast one $\mathbf{Q}$ with Hamiltonian $\mathbf{h}_\alpha^{\text{Q}}$. Additional we also have a potential $\mathbf{V}_\alpha$ which couples both subsystems. We consider an incoming wave in the slow subsystem $\mathbf{P}$ and would like to study how it scatters at the potential in the limit $\alpha \to 0$. In particular we are interested what fraction of the wavefunction ends up in subsystem $\mathbf{Q}$.

[6] Note that defining $\mathbf{L}$ using $\bar{\mathbf{K}}\mathbf{V}_1^{\text{eff}}\bar{\mathbf{K}}$ and not just $\mathbf{V}_1^{\text{eff}}$ is going to be important later.

Of course our plan is to reduce it to case of theorem 1. We therefore need to show that the effective potential (B.7) satisfies the required properties. This will be done in the following lemma. As the first theorem it does not require many properties of the system and as such applies to a huge variety of systems. Unfortunately due to some minor technicalities, which we will discuss later, it cannot be applied to the pairs. However we would like to state it anyway to convince the reader that the observed behaviour is quite general.

**Lemma 1** *Assume that* $\mathbf{G}_\alpha^{\mathrm{Q}}$ *and* $\mathbf{V}_\alpha$ *have a Taylor expansion at least up to first order. In case that* $\mathbf{G}_\alpha^{\mathrm{Q}} \not\to 0$, $\mathbf{PV}_\alpha\mathbf{P} \to 0$ *and* $\mathbf{QV}_\alpha\mathbf{P} \not\to 0$ *and the additional technical assumption (c) holds, we find in the limit* $\alpha \to 0$ *the effective potential* $\mathbf{V}_\alpha^{\mathrm{eff}}$ *has the following properties:*

- *It has a Taylor expansion up to first order* $\mathbf{V}_\alpha^{\mathrm{eff}} = \mathbf{V}_0^{\mathrm{eff}} + \alpha\mathbf{V}_1^{\mathrm{eff}} + \mathcal{O}\left(\alpha^2\right)$.
- $\mathbf{V}_\alpha^{\mathrm{eff}} \not\to 0$
- $\mathbf{K} = \mathbf{K}^{\mathrm{P}}$
- $\bar{\mathbf{K}}\mathbf{V}_0^{\mathrm{eff}} = 0$
- $\bar{\mathbf{K}}\mathbf{V}_1^{\mathrm{eff}}\bar{\mathbf{K}} = \bar{\mathbf{K}}\mathbf{V}_1\bar{\mathbf{K}}$

The lemma does not only provide the requirements for theorem 1, but also useful characterizations of the quantities appearing in theorem 1.

Proof: We start by explicitly computing the Taylor expansion of the effective potential (B.7):

$$\mathbf{V}_\alpha^{\mathrm{eff}} = \mathbf{PV}_0\mathbf{QG}_0^{\mathrm{Q}}\mathbf{QV}_0\mathbf{P} + \alpha\Big(\mathbf{PV}_1\mathbf{P} + \mathbf{PV}_1\mathbf{QG}_0^{\mathrm{Q}}\mathbf{QV}_0\mathbf{P} + \mathbf{PV}_0\mathbf{QG}_1^{\mathrm{Q}}\mathbf{QV}_0\mathbf{P} + \mathbf{PV}_0\mathbf{QG}_0^{\mathrm{Q}}\mathbf{QV}_1\mathbf{P}\Big) + \mathcal{O}\left(\alpha^2\right) \tag{B.30}$$

and so

$$\mathbf{V}_0^{\mathrm{eff}} = \mathbf{PV}_0\mathbf{QG}_0^{\mathrm{Q}}\mathbf{QV}_0\mathbf{P} \tag{B.31}$$

$$\mathbf{V}_1^{\mathrm{eff}} = \mathbf{PV}_1\mathbf{P} + \mathbf{PV}_1\mathbf{QG}_0^{\mathrm{Q}}\mathbf{QV}_0\mathbf{P} + \mathbf{PV}_0\mathbf{QG}_1^{\mathrm{Q}}\mathbf{QV}_0\mathbf{P} + \mathbf{PV}_0\mathbf{QG}_0^{\mathrm{Q}}\mathbf{QV}_1\mathbf{P}. \tag{B.32}$$

We need to show that $\mathbf{V}_0^{\mathrm{eff}} \neq 0$. To this end define the projectors $\mathbf{K}^{\mathrm{P}}$ and $\mathbf{K}^{\mathrm{Q}}$. They are defined in tabular B.2 as the subspace where $\mathbf{V}_0$ acts and the image of $\mathbf{V}_0$. As such $\mathbf{K}^{\mathrm{P}}$ plays the same role for $\mathbf{V}_0$ as $\mathbf{K}$ plays for $\mathbf{V}_0^{\mathrm{eff}}$. In a moment we will find that indeed $\mathbf{K} = \mathbf{K}^{\mathrm{P}}$. The definitions of $\mathbf{K}^{\mathrm{P}}$ and $\mathbf{K}^{\mathrm{Q}}$ are made such that $\mathbf{QV}_0\mathbf{P} = \mathbf{K}^{\mathrm{Q}}\mathbf{V}_0\mathbf{K}^{\mathrm{P}}$ and that we can think of $\mathbf{K}^{\mathrm{Q}}\mathbf{V}_0\mathbf{K}^{\mathrm{P}}$ as an invertible matrix. This means we can rewrite (B.31)

$$\mathbf{V}_0^{\mathrm{eff}} = \mathbf{K}^{\mathrm{P}}\mathbf{V}_0\mathbf{K}^{\mathrm{Q}}\mathbf{G}_0^{\mathrm{Q}}\mathbf{K}^{\mathrm{Q}}\mathbf{V}_0\mathbf{K}^{\mathrm{P}}. \tag{B.33}$$

This is a product of three matrices, which are all invertible due to technical assumption (c). Therefore the combination must also be invertible and in particular $\mathbf{V}_0^{\mathrm{eff}}$ cannot be 0. Because $\mathbf{V}_0^{\mathrm{eff}}$ is invertible it maps all vectors of $\mathbf{K}^{\mathrm{P}}$ onto non-zero vectors. Since this is exactly the definition of $\mathbf{K}$ we find

$$\mathbf{K} = \mathbf{K}^{\mathrm{P}}. \tag{B.34}$$

We can even go one step further and apply $\bar{\mathbf{K}} = \mathbf{P} - \mathbf{K}$ onto $\mathbf{V}_0^{\text{eff}}$ in (B.33):

$$\mathbf{V}_0^{\text{eff}}\bar{\mathbf{K}} = \mathbf{V}_0^{\text{eff}}\mathbf{P} - \mathbf{V}_0^{\text{eff}}\mathbf{K} = \mathbf{V}_0^{\text{eff}} - \mathbf{V}_0^{\text{eff}} = 0 \tag{B.35}$$

$$\bar{\mathbf{K}}\mathbf{V}_0^{\text{eff}} = (\mathbf{P} - \mathbf{K})\mathbf{K}^{\text{P}}\mathbf{V}_0\mathbf{K}^{\text{Q}}\mathbf{G}_0^{\text{Q}}\mathbf{K}^{\text{Q}}\mathbf{V}_0\mathbf{K}^{\text{P}} = \mathbf{K}^{\text{P}}\mathbf{V}_0\mathbf{K}^{\text{Q}}\mathbf{G}_0^{\text{Q}}\mathbf{K}^{\text{Q}}\mathbf{V}_0\mathbf{K}^{\text{P}} - \mathbf{K}^{\text{P}}\mathbf{V}_0\mathbf{K}^{\text{Q}}\mathbf{G}_0^{\text{Q}}\mathbf{K}^{\text{Q}}\mathbf{V}_0\mathbf{K}^{\text{P}} = 0. \tag{B.36}$$

The first result is trivially true for any operator due to the definitions of the projectors. The second one, though it seems equally trivial, is not automatically true[7], but only because $\mathbf{V}_0^{\text{eff}}$ has this special sandwich structure ($\mathbf{G}_0^{\text{Q}}$ between two $\mathbf{V}_0$). This is the important condition for conclusions 2 and 3 of theorem 1. Therefore in the case of two subsystems this condition is automatically fulfilled for all situations.

There is one final part of conclusion 3 missing, namely simplifying the first order of the effective potential $\mathbf{V}_1^{\text{eff}}$. The result can obtained directly by applying $\bar{\mathbf{K}}$ on both sides of the effective potential (B.32):

$$\bar{\mathbf{K}}\mathbf{V}_1^{\text{eff}}\bar{\mathbf{K}} = \bar{\mathbf{K}}\Big(\mathbf{P}\mathbf{V}_1\mathbf{P} + \mathbf{P}\mathbf{V}_1\mathbf{Q}\mathbf{G}_0^{\text{Q}}\mathbf{Q}\mathbf{V}_0\mathbf{P} + \mathbf{P}\mathbf{V}_0\mathbf{Q}\mathbf{G}_1^{\text{Q}}\mathbf{Q}\mathbf{V}_0\mathbf{P} + \mathbf{P}\mathbf{V}_0\mathbf{Q}\mathbf{G}_0^{\text{Q}}\mathbf{Q}\mathbf{V}_1\mathbf{P}\Big)\bar{\mathbf{K}} \tag{B.37}$$

$$= \bar{\mathbf{K}}\mathbf{V}_1\bar{\mathbf{K}}. \tag{B.38}$$

Here we used $\mathbf{V}_0\bar{\mathbf{K}} = \bar{\mathbf{K}}\mathbf{V}_0 = 0$. This finishes the lemma. We are now ready to formulate the final result in this section:

**Theorem 2** *Consider the scattering problem given by the free Hamiltonian* $\mathbf{H}_0 = \alpha\mathbf{P}\mathbf{h}_\alpha^{\text{P}}\mathbf{P} + \mathbf{Q}\mathbf{h}_\alpha^{\text{Q}}\mathbf{Q}$*, where* $\mathbf{P}$ *and* $\mathbf{Q}$ *are complementary projectors* $\mathbf{P} + \mathbf{Q} = 1$*, with potential* $\mathbf{V}_\alpha$*. Assume that this scattering problem is such that we can apply the Lippmann-Schwinger equations (B.1) and (B.2) for all finite* $\alpha$*. Choose as incoming state an eigenstate* $|\phi\rangle$ *of* $\mathbf{h}_\alpha^{\text{P}}$ *with an energy* $\alpha\varepsilon_\alpha$*. Furthermore assume that* $\mathbf{h}_\alpha^{\text{P}}$ *has a well defined limit for* $\alpha \to 0$ *and that Taylor expansions of* $\mathbf{G}_\alpha^{\text{Q}}$ *and* $\mathbf{V}_\alpha$ *exists at least up to first order.*

*In case that* $\mathbf{G}_\alpha^{\text{Q}} \not\to 0$*,* $\mathbf{P}\mathbf{V}_\alpha\mathbf{P} \to 0$ *and* $\mathbf{Q}\mathbf{V}_\alpha\mathbf{P} \not\to 0$ *and the operators satisfy the additional technical assumptions (a), (b), (c) we find in the limit* $\alpha \to 0$*:*

- *All findings of theorem 1*
- $\mathbf{Q}\left|\psi^+\right\rangle \to 0$

The second conclusion $\mathbf{Q}\left|\psi^+\right\rangle \to 0$ is the most important one. It shows that the wavefunction in the $\mathbf{Q}$ sector is going to vanish in the limit $\alpha \to 0$ which implies that scattering into the system $\mathbf{Q}$ vanishes.

Proof: We can apply theorem 1 directly due to lemma 1. We know from theorem 1 that $\mathbf{K}\left|\psi^+\right\rangle \to 0$. By the definition of the Greens function (B.3) the wavefunction in the $\mathbf{Q}$ sector is given by:

$$\mathbf{Q}\left|\psi^+\right\rangle = \mathbf{G}_\alpha^{\text{Q}}\mathbf{Q}\mathbf{V}_\alpha\mathbf{P}\left|\psi^+\right\rangle. \tag{B.39}$$

[7] It would be automatically true for hermitian operators, but recall that $\mathbf{G}_0^{\text{Q}}$ is not necessarily hermitian.

We can easily perform the limit $\alpha \to 0$. Recall that $\mathbf{V}_0 = \mathbf{V}_0\mathbf{K}^{\mathrm{P}}$ and that $\mathbf{K} = \mathbf{K}^{\mathrm{P}}$:

$$\mathbf{Q}\left|\psi^{+}\right\rangle \to \mathbf{G}_0^{\mathrm{Q}}\mathbf{Q}\mathbf{V}_0\mathbf{P}\left|\psi^{+}\right\rangle \tag{B.40}$$

$$= \mathbf{G}_0^{\mathrm{Q}}\mathbf{Q}\mathbf{V}_0\mathbf{K}\left|\psi^{+}\right\rangle = 0. \tag{B.41}$$

This concludes the theorem.

As promised this theorem applies to a huge variety of systems and shows that scattering into the **Q** subsystem is suppressed as $\alpha \to 0$. All we basically need are two subsystems, one which is slow **P** and one which is fast **Q**, and a non-vanishing coupling $\mathbf{QV}_0\mathbf{P}$ between them. But as said before unfortunately this theorem does not apply to the pairs. The problem is that the Greens operator in some parts of the system vanishes in the limit $\mathbf{Q}_b\mathbf{G}_\alpha^{\mathrm{Q}}\mathbf{Q}_b \to 0$ where $\mathbf{Q}_b$ is the projector on free particle states in layer $b \neq |u_0|$[8]. This implies that the effective potential $\mathbf{V}_0^{\mathrm{eff}} = \mathbf{PV}_0\mathbf{QG}_0^{\mathrm{Q}}\mathbf{QV}_0\mathbf{P}$ vanishes 'more often' than the original potential $\mathbf{QV}_0\mathbf{P}$. In the language of lemma 1 this means $\mathbf{K} \subset \mathbf{K}^{\mathrm{P}}$. In particular we have $\mathbf{K}^{\mathrm{P}} = |a\rangle\langle a| + |b\rangle\langle b| + |c\rangle\langle c|$ and $\mathbf{K} = |a\rangle\langle a| + |b\rangle\langle b|$ as shown in section 5.2.6. Mathematically speaking we cannot apply the theorem because the technical condition (c), namely that $\mathbf{K}^{\mathrm{Q}}\mathbf{G}_0^{\mathrm{Q}}\mathbf{K}^{\mathrm{Q}}$ is invertible, is not satisfied (because as said before the Greens function completely vanishes in some parts of the system). However even though the theorem fails, in practice we can basically repeat the same steps only restricting the definitions of $\mathbf{K}^{\mathrm{P}}$ and $\mathbf{K}^{\mathrm{Q}}$ to the subspaces where $\mathbf{G}_0^{\mathrm{Q}}$ does not vanish.

[8] This happens because these layers evolve ultra-fast, i.e. they evolve on timescales a factor $\alpha^2$ faster than the slow subspace **P**.

| Quantity | Definition | Taylor expansion | Toy model | Interpretation |
|---|---|---|---|---|
| $\mathbf{h}_\alpha^{\mathrm{P}}$ | | $\mathbf{h}_0^{\mathrm{P}} + O(\alpha)$ | $-J\mathbf{H}_{\mathrm{H}}$ | Hamiltonian in the **P** sector (up to a factor $\alpha$) |
| $\mathbf{h}_\alpha^{\mathrm{Q}}$ | | $\mathbf{h}_0^{\mathrm{Q}} + O(\alpha)$ | $-J\mathbf{H}_{\mathrm{H}}$ | Hamiltonian in the **Q** sector |
| $\mathbf{V}_\alpha$ | | $\mathbf{V}_0 + \alpha\mathbf{V}_1 + O\left(\alpha^2\right)$ | $\lambda\left(\left\|0_{\mathrm{P}}\right\rangle\left\langle 0_{\mathrm{Q}}\right\| + \left\|0_{\mathrm{Q}}\right\rangle\left\langle 0_{\mathrm{P}}\right\|\right)$ | Scattering potential coupling **P** and **Q** sectors |
| $\|\phi\rangle$ | | Constant | $e^{ikn}$ | Incoming wave, has to be eigenstate of $\mathbf{h}_\alpha^{\mathrm{P}}$ for all $\alpha$ |
| $\varepsilon_\alpha$ | | $\varepsilon_0 + O(\alpha)$ | $-2J\cos k$ | Energy of the incoming wave $\|\phi\rangle$ |
| $\mathbf{G}_\alpha^{\mathrm{P}}$ | $\frac{1}{\varepsilon_\alpha - \mathbf{h}_\alpha^{\mathrm{P}} + i\varepsilon}$ | $\mathbf{G}_0^{\mathrm{P}} + O(\alpha)$ | $\frac{1}{\varepsilon + J\mathbf{H}_{\mathrm{H}} + i\epsilon}$ | Free Greens function in **P** sector (up to a factor $\alpha$) |
| $\mathbf{G}_\alpha^{\mathrm{Q}}$ | $\frac{1}{\alpha\varepsilon_\alpha - \mathbf{h}_\alpha^{\mathrm{Q}} - \mathbf{Q}\mathbf{V}_\alpha\mathbf{Q} + i\epsilon}$ | $\mathbf{G}_0^{\mathrm{Q}} + \alpha\mathbf{G}_1^{\mathrm{Q}} + O\left(\alpha^2\right)$ | $\frac{1}{\alpha\varepsilon + J\mathbf{H}_{\mathrm{H}} + i\epsilon}$ | Perturbed Greens function in **Q** sector |
| $\mathbf{V}_\alpha^{\mathrm{eff}}$ | $\mathbf{P}\mathbf{V}_\alpha\mathbf{P} + \mathbf{P}\mathbf{V}_\alpha\mathbf{Q}\mathbf{G}_\alpha^{\mathrm{Q}}\mathbf{Q}\mathbf{V}_\alpha\mathbf{P}$ | $\mathbf{V}_0^{\mathrm{eff}} + \alpha\mathbf{V}_1^{\mathrm{eff}} + O\left(\alpha^2\right)$ | $\lambda^2\left\langle 0_{\mathrm{Q}}\right\| \frac{1}{\alpha\varepsilon + J\mathbf{H}_{\mathrm{H}} + i\epsilon} \left\|0_{\mathrm{Q}}\right\rangle \left\|0_{\mathrm{P}}\right\rangle \left\langle 0_{\mathrm{P}}\right\|$ | Effective potential in the **P** sector including what is induced by the **Q** sector |

Table B.1: Definitions of various quantities and operators. We give their definition and interpretation. Also we define their Taylor expansions and give the analogous quantity in the treatment of the toy model (see section 5.2.4).

| Projector | Subspace of | Definition | Dimension (typical) | Toy model | Interpretation |
|---|---|---|---|---|---|
| $\mathbf{P}$ | | | $\infty$ | Slow chain P | The slow subspace of the system, hosts the incoming particle |
| $\mathbf{Q}$ | | $1 - \mathbf{P}$ | $\infty$ | Fast chain Q | Fast subspace, everything which is not in $\mathbf{P}$ |
| $\bar{\mathbf{K}}$ | $\mathbf{P}$ | Kernel of $\mathbf{V}_0^{\text{eff}}$ | $\infty$ | Chain P without $\lvert 0_P \rangle$ | Everything which is unaffected by the zeroth order effective potential. |
| $\mathbf{K}$ | $\mathbf{P}$ | $\mathbf{P} - \bar{\mathbf{K}}$ | Finite | $\lvert 0_P \rangle \langle 0_P \rvert$ | All parts of $\mathbf{P}$ where the zeroth order effective potential acts. |
| $\mathbf{K}^P$ | $\mathbf{P}$ | Space where $\mathbf{QV}_0\mathbf{P}$ acts | Finite | $\lvert 0_P \rangle \langle 0_P \rvert$ | Parts of $\mathbf{P}$ where the zeroth order potential acts. |
| $\mathbf{K}^Q$ | $\mathbf{Q}$ | Image of $\mathbf{QV}_0\mathbf{P}$ | Finite | $\lvert 0_Q \rangle \langle 0_Q \rvert$ | The equivalent of $\mathbf{K}^P$ in the $\mathbf{Q}$ sector. |
| $\bar{\mathbf{L}}$ | $\bar{\mathbf{K}}$ | Kernel of $\bar{\mathbf{K}}\mathbf{V}_1^{\text{eff}}\bar{\mathbf{K}}$ | $\infty$ | Equals $\bar{\mathbf{K}}$ | The parts of $\mathbf{P}$ which are completely unaffected by $\mathbf{V}_\alpha^{\text{eff}}$ up to first order. |
| $\mathbf{L}$ | $\bar{\mathbf{K}}$ | $\bar{\mathbf{K}} - \bar{\mathbf{L}}$ | Finite | Vanishes | The space on which $\bar{\mathbf{K}}\mathbf{V}_1^{\text{eff}}\bar{\mathbf{K}}$ acts, i.e. the parts of $\mathbf{P}$ which are unaffected by $\mathbf{V}_0^{\text{eff}}$, but affected by the first order $\mathbf{V}_1^{\text{eff}}$. |

Table B.2: Definition of various projectors. We give their definition and interpretation. The second column specifies on which space the projectors are defined (which might be technical, but still quite important). The fourth column specifies whether these projectors are typical finite or infinite dimensional. Also we again give the analogous projectors in the treatment of the toy model (see section 5.2.4).

## B.4 Discussion of the technical assumptions

In this section we would like to discuss the technical assumptions of the above theorems. They state that certain operators are invertible. In particular we will argue why we expect these assumptions to be almost always fulfilled.

Before we start let us recall that typically the subspaces $\mathbf{K}, \mathbf{K}^{\mathrm{Q}}$ and $\mathbf{L}$ are relatively small and in particular finite dimensional. This is because they are only non-zero where the potential acts and the potential typically acts only on a small finite region.

Let us start with assumptions (b) and (e). The argument is the same for all of these operators, therefore we will explain it using simplest one (e): $\mathbf{L} - \left(\mathbf{L} - \mathbf{L}\mathbf{G}_0^{\mathrm{P}}\mathbf{K}\frac{1}{\mathbf{K}\mathbf{G}_0^{\mathrm{P}}\mathbf{K}}\mathbf{K}\right)\mathbf{K}\mathbf{G}_0^{\mathrm{P}}\bar{\mathbf{K}}\mathbf{V}_1^{\mathrm{eff}}\mathbf{L}$. Since $\mathbf{K}$ and $\mathbf{L}$ are low dimensional subspaces we can think about the operators from (b) and (e) as low dimensional matrices. Of course if the matrix elements of these matrices are finely tuned it is possible that they are not invertible. But because both operators depend non-linear on the potential $\mathbf{V}_0^{\mathrm{eff}}$ and the Greens function $\mathbf{G}_0^{\mathrm{P}}$ already a minor change of the parameters of the system, for example in the coupling strength, will destroy the fine tuning and the matrix becomes invertible. Therefore we expect that up to a few isolated parameter configurations these matrices are invertible.

A similar reasoning is also true for assumption (a). First discuss the operator for $\alpha \to 0$: $\bar{\mathbf{K}} - \bar{\mathbf{K}}\mathbf{G}_0^{\mathrm{P}}\mathbf{V}_1^{\mathrm{eff}}\bar{\mathbf{K}}$. At first it might seem that the operator acts on the infinite dimensional subspace $\bar{\mathbf{K}}$. But we can expect that $\mathbf{V}_1^{\mathrm{eff}}\bar{\mathbf{K}}$ acts only on a finite dimensional space (let us call it $\mathbf{R}$). On the remaining subspace $\bar{\mathbf{K}} - \mathbf{R}$ we have $\left(\bar{\mathbf{K}} - \bar{\mathbf{K}}\mathbf{G}_0^{\mathrm{P}}\mathbf{V}_1^{\mathrm{eff}}\bar{\mathbf{K}}\right) \cdot \left(\bar{\mathbf{K}} - \mathbf{R}\right) = \bar{\mathbf{K}} - \mathbf{R}$ and thus the operator just acts as identity operator on the subspace $\bar{\mathbf{K}} - \mathbf{R}$. In order to invert this operator we only need to invert it on the subspace $\mathbf{R}$, which is typically finite dimensional. Therefore we can apply the same reasoning as for assumptions (b) and (e) to conclude that we can expect, up to a few isolated parameter configurations, the operator to be invertible. We have just seen that for $\alpha \to 0$ the operator is given by unit operator combined with a low dimensional invertible matrix. Now its version for finite $\alpha$, the operator $\bar{\mathbf{K}} - \frac{1}{\alpha}\bar{\mathbf{K}}\mathbf{G}_\alpha^{\mathrm{P}}\mathbf{V}_\alpha^{\mathrm{eff}}\bar{\mathbf{K}}$, must be close to unit operator and a low dimensional invertible matrix (for small $\alpha$). Both the unit operator and the invertible matrix are far away from being non-invertible in the sense that a small perturbation of neither the unit operator nor the low dimensional invertible matrix will lead to an overall non-invertible operator. Therefore we can assume that also the finite $\alpha$ operator is invertible (at least for small values of $\alpha$, but that is all we need).

Finally let us deal with assumptions (c) and (d), namely that $\mathbf{K}^{\mathrm{Q}}\mathbf{G}_0^{\mathrm{Q}}\mathbf{K}^{\mathrm{Q}}$ and $\mathbf{K}\mathbf{G}_0^{\mathrm{P}}\mathbf{K}$ are invertible. First note that again we can think of both operators as finite dimensional matrices, because $\mathbf{K}$ and $\mathbf{K}^{\mathrm{Q}}$ are finite dimensional. In case the Hamiltonians have extra symmetries, for example parity, the matrices decouple into even smaller matrices. Typically Greens functions are highly non-local objects. If we apply them to one small part of the system they will yield non-zero results in all parts of the system (in the same symmetry sectors). Therefore if we look at one specific symmetry sector we can expect that the matrices $\mathbf{K}^{\mathrm{Q}}\mathbf{G}_0^{\mathrm{Q}}\mathbf{K}^{\mathrm{Q}}$ and $\mathbf{K}\mathbf{G}_0^{\mathrm{P}}\mathbf{K}$ will contain only non-zero entries. Again by our intuition we expect that such a low dimensional matrix with only non-zero entries is usually invertible.

APPENDIX C

# Useful properties of the Bessel functions

In this appendix we would like to summarize all properties of the Bessel functions $J_a(\lambda)$ which are relevant for us. We will cite them from [25] which is also a good source for many further interesting properties. Note that we will only consider integer Bessel functions with $a \geq 0$.

## C.1 Qualitative description

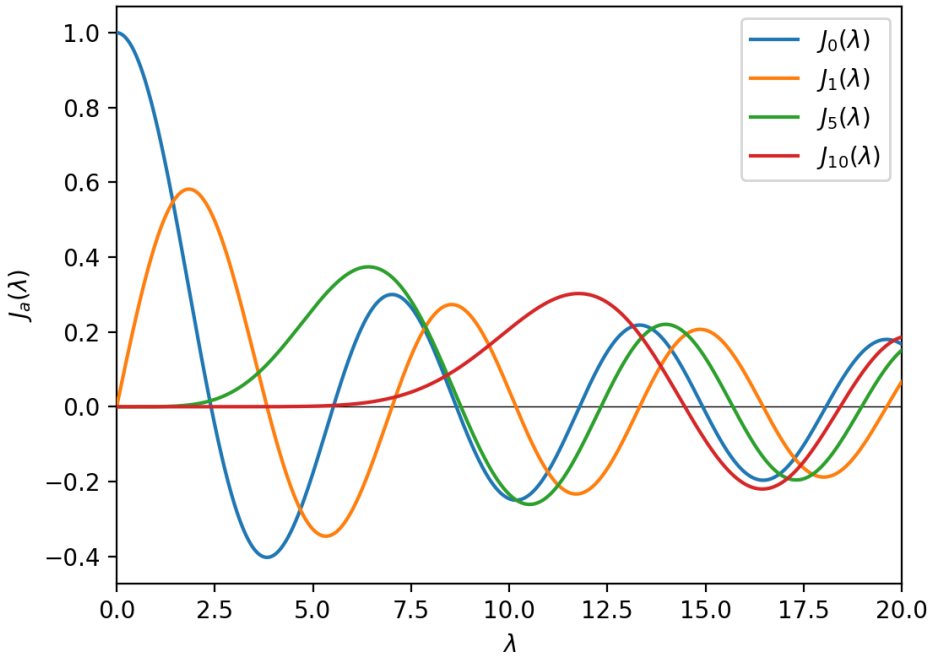


Figure C.1: Bessel functions $J_a(\lambda)$ for $a = 0, 1, 5, 10$.

In figure C.1 we plot the Bessel function $J_a(\lambda)$ for $a = 0, 1, 5, 10$. For large $\lambda$ they can all be described as oscillating functions whose envelopes decay like $\sim 1/\sqrt{\lambda}$. For small $\lambda \to 0$ however they do not explode, but rather decay to 0 (except $J_0(\lambda)$ which goes to 1). Apart from $J_0(\lambda)$ all other Bessel

functions start at zero and then slowly rise monotonic until they have their first maximum, which is located a bit above $\lambda = a$, and then decay in the oscillatory fashion.

## C.2 Definition and basic properties

The integer Bessel functions can be defined as

$$J_a(\lambda) = \frac{1}{2\pi} \int_{-\pi}^{\pi} e^{i(\lambda \sin t - at)} \, \mathrm{d}t \, . \tag{C.1}$$

All Bessel functions are bounded $|J_a(\lambda)| < 1$. Depending on whether $a$ is even or odd they are even or odd functions:

$$J_a(-\lambda) = (-1)^a J_a(\lambda). \tag{C.2}$$

Also the Bessel functions for negative $a$ equal those for positive $a$ up to a sign:

$$J_{-a}(\lambda) = (-1)^a J_a(\lambda). \tag{C.3}$$

The last formula allows us to consider only $a \geq 0$.

## C.3 Asymptotic formulas

There are two useful asymptotic formulas, one for $\lambda \to \infty$ and one for $\lambda \to 0$. As $\lambda \to \infty$ we have (see [25] §10.17(i)):

$$J_a(\lambda) = \sqrt{\frac{2}{\pi\lambda}} \Big( \cos\Big( \lambda - a\frac{\pi}{2} - \frac{\pi}{4} \Big) + O(1/\lambda) \Big). \tag{C.4}$$

This expansion shows directly the oscillatory decay of the Bessel function as $\lambda \to \infty$. While the envelope $\sqrt{\frac{2}{\pi\lambda}}$ works very well throughout the oscillatory part $\lambda > a$, one has to go to really high $\lambda$ to make sure that the phase of the cosine agrees with the phase of the Bessel function[1]. This is because the phase of the Bessel function slightly shifts as $\lambda$ grows.

The other asymptotic formula concerns $\lambda \to 0$, i.e. the first non-zero coefficient of its Taylor expansion (see [25] §10.2):

$$J_a(\lambda) = \frac{1}{a!} \left( \frac{\lambda}{2} \right)^a + O\Big( \lambda^{a+2} \Big). \tag{C.5}$$

We can see that as $a$ grows $J_a(\lambda)$ will also grow slower. For $a = 0$ the Taylor expansion is

$$J_0(\lambda) = 1 - \frac{\lambda^2}{4} + O\Big( \lambda^4 \Big). \tag{C.6}$$

[1] For example for $a = 10$ this is satisfied only for $\lambda \gtrsim 500$.

## C.4 Distribution of the first maximum of the Bessel functions

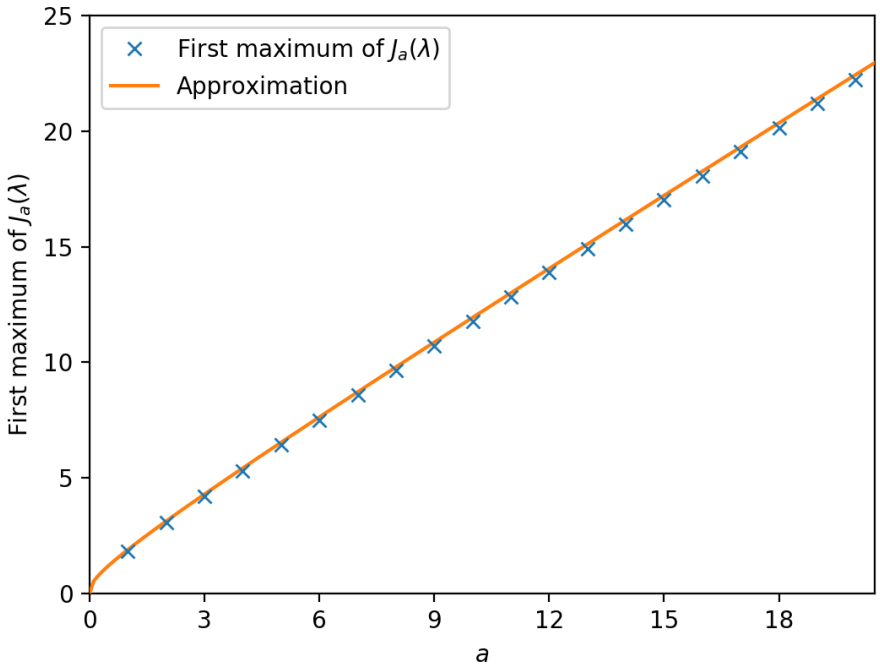


Figure C.2: First maximum $j'_{a,1}$ of the Bessel functions $J_a(\lambda)$ as function of $a$. We also give the approximate expression $j'_{a,1} \approx a + 0.8086165a^{1/3}$.

The position of the first maximum $j'_{a,1}$ of a Bessel function $J_a(\lambda)$ is important for us. We will explicitly exclude $J_0(\lambda)$ from this discussion because it behaves differently for small $\lambda$. From [25] §10.21.40 we know that the first maximum is distributed as

$$j'_{a,1} \sim a + 0.8086165a^{1/3}. \tag{C.7}$$

We give a plot of them as well as the approximation in figure C.2. In fact if $a$ is not too large (as in our case) we find that the maximum is only a bit above $a$. For our relevant range of $a$, say $a < 20$, the maximum is somewhere between $a + 1$ and $a + 2$. As we do not need to determine the position of the maximum more precise, we will conclude that the maximum is somewhere around $a + 1.5$.

## C.5 Neumann's addition theorem

Bessel functions satisfy the following relation (see [25] §10.23):

$$\sum_a J_{b-a}(\lambda_1)J_a(\lambda_2) = J_b(\lambda_1 + \lambda_2). \tag{C.8}$$

We only need two special cases, namely $b = 0$ and $\lambda = \lambda_1 = \pm\lambda_2$:

$$\sum_a (-1)^a J_a(\lambda)^2 = \sum_a J_{-a}(\lambda) J_a(\lambda) = J_0(2\lambda) \tag{C.9}$$

$$\sum_a J_a(\lambda)^2 = \sum_a J_{-a}(\lambda) J_a(-\lambda) = J_0(0) = 1. \tag{C.10}$$

## C.6 Taylor expansion of $v_1$

In section 3.3 we find:

$$v_1 = \sum_a \frac{|u| J_a(\lambda)^2}{|u| - a} - 1. \tag{C.11}$$

Let us quickly do a Taylor expansion around $\lambda = 0$ up to second order. Note that $J_a(\lambda)^2$ for $|a| > 1$ will grow too slow to be included (see equation (C.5)). We are left with

$$J_0(\lambda) = 1 - \frac{\lambda^2}{4} + \mathcal{O}\left(\lambda^4\right) \tag{C.12}$$

$$J_1(\lambda) = \frac{\lambda}{2} + \mathcal{O}\left(\lambda^3\right). \tag{C.13}$$

Inserting this into $v_1$ and simplifying gives

$$v_1 = \frac{|u| J_1(\lambda)^2}{|u| + 1} + J_0(\lambda)^2 + \frac{|u| J_1(\lambda)^2}{|u| - 1} - 1 + \mathcal{O}\left(\lambda^4\right) \tag{C.14}$$

$$= \left(1 - \frac{\lambda^2}{4}\right)^2 - 1 + \frac{|u|^2}{|u|^2 - 1} \frac{\lambda^2}{2} + \mathcal{O}\left(\lambda^4\right) \tag{C.15}$$

$$= -\left(1 - \frac{|u|^2}{|u|^2 - 1}\right) \frac{\lambda^2}{2} + \mathcal{O}\left(\lambda^4\right) \tag{C.16}$$

$$= \frac{1}{|u|^2 - 1} \frac{\lambda^2}{2} + \mathcal{O}\left(\lambda^4\right). \tag{C.17}$$

APPENDIX D

# Various calculations

## D.1 Gauge transformation

This section provides more detail on the gauge transformation, in particular on how to calculate $\mathbf{U}_0^\dagger \hat{\mathbf{H}}_\mathrm{H} \mathbf{U}_0$. Recall their definitions:

$$\mathbf{H}_\mathrm{H} = \sum_{n\sigma} \mathbf{c}_{n\sigma}^\dagger \mathbf{c}_{n+1\sigma} + \mathbf{c}_{n+1\sigma}^\dagger \mathbf{c}_{n\sigma} \tag{D.1}$$

$$\mathbf{U}_0 = e^{-i\lambda \mathbf{V} \sin\phi} \tag{D.2}$$

$$\mathbf{V} = \mathbf{n}_{0\uparrow} + \mathbf{n}_{0\downarrow}. \tag{D.3}$$

For convenience we will abbreviate $\mathbf{U}_0 = e^{-ia\mathbf{V}}$ where $a = \lambda \sin\phi$. There are many ways to evaluate $\mathbf{U}_0^\dagger \hat{\mathbf{H}}_\mathrm{H} \mathbf{U}_0$. We will go on as follows. Define the operator

$$\mathbf{c}_{n\sigma}(a) = e^{ia\mathbf{V}} \mathbf{c}_{n\sigma} e^{-ia\mathbf{V}}. \tag{D.4}$$

Now differentiate the expression w.r.t $a$:

$$i\frac{\mathrm{d}}{\mathrm{d}a}\mathbf{c}_{n\sigma}(a) = e^{ia\mathbf{V}} \big[\mathbf{c}_{n\sigma}, \mathbf{V}\big] e^{-ia\mathbf{V}} \tag{D.5}$$

$$= e^{ia\mathbf{V}} \big[\mathbf{c}_{n\sigma}, \mathbf{n}_{0\sigma}\big] e^{-ia\mathbf{V}} \tag{D.6}$$

$$= e^{ia\mathbf{V}} \mathbf{c}_{n\sigma} e^{-ia\mathbf{V}} \delta_{n,0} = \mathbf{c}_{n\sigma}(a)\delta_{n,0}. \tag{D.7}$$

We see that only the annihilation operator at site 0 is influenced by the gauge transformation. For $n = 0$ we can solve the first order differential equation (note that $\mathbf{c}_{n\sigma}(0) = \mathbf{c}_{n\sigma}$):

$$\mathbf{c}_{n\sigma}(a) = e^{ia\mathbf{V}} \mathbf{c}_{n\sigma} e^{-ia\mathbf{V}} = \begin{cases} e^{-ia}\mathbf{c}_{0\sigma} & n = 0 \\ \mathbf{c}_{n\sigma} & \text{else.} \end{cases} \tag{D.8}$$

We can insert these results into the hopping Hamiltonian by replacing the corresponding creation/annihilation operators:

$$e^{+ia\mathbf{V}}\mathbf{H}_{\mathrm{H}}e^{-ia\mathbf{V}} = \sum_{\sigma}\Big[e^{-ia}\mathbf{c}^{\dagger}_{-1\sigma}\mathbf{c}_{0\sigma} + e^{ia}\mathbf{c}^{\dagger}_{0\sigma}\mathbf{c}_{-1\sigma} + e^{ia}\mathbf{c}^{\dagger}_{0\sigma}\mathbf{c}_{1\sigma} + e^{-ia}\mathbf{c}^{\dagger}_{1\sigma}\mathbf{c}_{0\sigma} \tag{D.9}$$

$$+ \sum_{n\neq -1,0}\mathbf{c}^{\dagger}_{n\sigma}\mathbf{c}_{n+1\sigma} + \mathbf{c}^{\dagger}_{n+1\sigma}\mathbf{c}_{n\sigma}\Big]. \tag{D.10}$$

We will conveniently write this as

$$\mathbf{U}_0^{\dagger}\hat{\mathbf{H}}_{\mathrm{H}}\mathbf{U}_0 = \sum_{n\sigma} g_n(\phi)\mathbf{c}^{\dagger}_{n\sigma}\mathbf{c}_{n+1\sigma} + g_n(\phi)^{*}\mathbf{c}^{\dagger}_{n+1\sigma}\mathbf{c}_{n\sigma} \tag{D.11}$$

where

$$g_n(\phi) = \begin{cases} e^{-i\lambda\sin\phi} & n=-1 \\ e^{i\lambda\sin\phi} & n=0 \\ 1 & \text{else} \end{cases}. \tag{D.12}$$

## D.2 Calculation of transmission amplitude

Consider a particle on an infinite chain with abstract Hamiltonian:

$$\mathbf{H}^{\text{abstract}} = -J_{\text{eff}}\Big[\sum_{n\neq -1,0}\Big(|n\rangle\langle n+1| + |n+1\rangle\langle n|\Big) + \gamma\sum_{n=-1,0}\Big(|n\rangle\langle n+1| + |n+1\rangle\langle n|\Big)$$

$$+ v_0|0\rangle\langle 0| + v_1\Big(|-1\rangle\langle -1| + |1\rangle\langle 1|\Big)\Big]. \tag{D.13}$$

The hopping away from the center is given by $J_{\text{eff}}$, while the hopping from and to site 0 is scaled by $\gamma$. Also there is a symmetric scattering potential at sites $-1, 0, 1$. We consider a particle coming from the left with momentum $k$ and energy $\epsilon_k = -2J_{\text{eff}}\cos k$ and we would like to calculate the transmission amplitude. The wavefunction has the general form:

$$\psi_n = \begin{cases} e^{ikn} + r_k e^{-ikn} & n<0 \\ \psi_0 & n=0 \\ t_k e^{ikn} & n>0 \end{cases}. \tag{D.14}$$

We need to satisfy the following three equations for $n = -1, 0, 1$ respectively:

$$\psi_{-2} + \gamma\psi_0 + v_1\psi_{-1} = 2\cos(k)\psi_{-1} \tag{D.15}$$

$$\gamma\psi_{-1} + \gamma\psi_1 + v_0\psi_0 = 2\cos(k)\psi_0 \tag{D.16}$$

$$\gamma\psi_0 + \psi_2 + v_1\psi_1 = 2\cos(k)\psi_1. \tag{D.17}$$

Inserting (D.14) we find

$$e^{-2ik} + r_k e^{2ik} + \gamma\psi_0 = \big(2\cos k - v_1\big)(e^{-ik} + r_k e^{ik}) \tag{D.18}$$

$$\gamma\Big(e^{-ik} + r_k e^{ik} + t_k e^{ik}\Big) = \big(2\cos k - v_0\big)\psi_0 \tag{D.19}$$

$$\gamma\psi_0 + t_k e^{2ik} = \big(2\cos k - v_1\big)e^{ik} t_k . \tag{D.20}$$

Using the last and the first equation we obtain

$$\psi_0 = \frac{1 - v_1 e^{ik}}{\gamma} t_k \tag{D.21}$$

$$t_k = r_k + \frac{1 - v_1 e^{-ik}}{1 - v_1 e^{ik}} . \tag{D.22}$$

The second equation then finally gives

$$t_k = \frac{\gamma^2}{1 - v_1 e^{ik}} \frac{-2i\sin k}{\big(2\cos k - v_0\big)\Big(1 - v_1 e^{ik}\Big) - 2\gamma^2 e^{ik}} . \tag{D.23}$$

In order to obtain the transmission probability we have to square this expression $T_k = |t_k|^2$.

### The case $v_0 = 2v_1$

We only need the case $v_0 = 2v_1$, which is why we will only compute $T_k$ in this case. We have:

$$T_k = |t_k|^2 = \gamma^4 \left| \frac{-i\sin k}{1 - v_1 e^{ik}} \right|^2 \left| \frac{2}{\big(2\cos k - 2v_1\big)\Big(1 - v_1 e^{ik}\Big) - 2\gamma^2 e^{ik}} \right|^2 . \tag{D.24}$$

We will treat both fractions separately:

$$\left| \frac{-i\sin k}{1 - v_1 e^{ik}} \right|^2 = \frac{\sin^2 k}{1 + v_1^2 - 2v_1\cos k} \tag{D.25}$$

$$= \frac{\sin^2 k}{\sin^2 k + \big(\cos k - v_1\big)^2} \tag{D.26}$$

$$= \frac{1}{1 + \left(\frac{\cos k - v_1}{\sin k}\right)^2} \tag{D.27}$$

$$\Big|\big(\cos k - v_1\big)\Big(1 - v_1 e^{ik}\Big) - \gamma^2 e^{ik}\Big|^2 = \Big|\big(\cos k - v_1\big)\Big(e^{-ik} - v_1\Big) - \gamma^2\Big|^2 \tag{D.28}$$

$$= \Big[\big(\cos k - v_1\big)^2 - \gamma^2\Big]^2 + \big(\cos k - v_1\big)^2 \sin^2 k . \tag{D.29}$$

We find:

$$T_k = |t_k|^2 = \frac{\gamma^4}{1 + \left(\frac{\cos k - v_1}{\sin k}\right)^2} \frac{1}{\left[\left(\cos k - v_1\right)^2 - \gamma^2\right]^2 + \left(\cos k - v_1\right)^2 \sin^2 k}. \tag{D.30}$$

### The case $v_0 = v_1 = 0$

Note that in the case $v_0 = v_1 = 0$ the above formula drastically simplifies to

$$T_k = \frac{\gamma^4}{1 + \left(\frac{\cos k}{\sin k}\right)^2} \frac{1}{\left[\cos^2 k - \gamma^2\right]^2 + \cos^2 k \sin^2 k} \tag{D.31}$$

$$= \frac{\gamma^4 \sin^2 k}{\cos^2 k - 2\gamma^2 \cos^2 k + \gamma^4} \tag{D.32}$$

$$= \frac{\gamma^4}{\left(1 - 2\gamma^2 + \gamma^4\right)^2 \cot^2 k + \gamma^4} \tag{D.33}$$

$$= \frac{1}{1 + \left(\frac{1}{\gamma^2} - 1\right)^2 \cot^2 k}. \tag{D.34}$$

## D.3 Transmission in the resonant case

In this section we would like to calculate the transmission in the resonant case. We will use conclusions 2 and 3 of theorem 1 which give the full wavefunction in the $\mathbf{P} = \mathbf{P}_0$ sector (i.e. paired states in layer 0). Note that we can apply them because $\bar{\mathbf{K}}\mathbf{V}_0^{\text{eff}} = 0$ (see equation (5.58)) and therefore all three conclusions of theorem 1 hold.

We first would like to remind the reader of all appearing quantities. Depending on whether $|u_0|$ is an odd or an even number we define:

$$|a\rangle_{\text{odd}} = \frac{1}{\sqrt{2}}\begin{pmatrix}1\\0\\-1\end{pmatrix} \qquad |b\rangle_{\text{odd}} = \frac{1}{\sqrt{6}}\begin{pmatrix}1\\-2\\1\end{pmatrix} \qquad |c\rangle_{\text{odd}} = \frac{1}{\sqrt{3}}\begin{pmatrix}1\\1\\1\end{pmatrix} \tag{D.35}$$

$$|a\rangle_{\text{even}} = \frac{1}{\sqrt{2}}\begin{pmatrix}1\\0\\-1\end{pmatrix} \qquad |b\rangle_{\text{even}} = \frac{1}{\sqrt{6}}\begin{pmatrix}1\\2\\1\end{pmatrix} \qquad |c\rangle_{\text{even}} = \frac{1}{\sqrt{3}}\begin{pmatrix}1\\-1\\1\end{pmatrix}. \tag{D.36}$$

In both cases we have that

$$\mathbf{K} = |a\rangle\langle a| + |b\rangle\langle b| \tag{D.37}$$

$$\bar{\mathbf{K}} = \mathbf{P} - \mathbf{K} \tag{D.38}$$

$$\mathbf{L} = |c\rangle\langle c| \tag{D.39}$$

$$\bar{\mathbf{K}}\mathbf{V}_1^{\text{eff}}\bar{\mathbf{K}} = v\,|c\rangle\langle c| \tag{D.40}$$

where the exact form of $v$ is not relevant here. Conclusion 2 of theorem 1 states:

$$\mathbf{L}\left|\psi^{+}\right\rangle = \frac{1}{\mathbf{L}-\left(\mathbf{L}-\mathbf{L}\mathbf{G}_0^{\mathrm{P}}\mathbf{K}\frac{1}{\mathbf{K}\mathbf{G}_0^{\mathrm{P}}\mathbf{K}}\mathbf{K}\right)\mathbf{K}\mathbf{G}_0^{\mathrm{P}}\bar{\mathbf{K}}\mathbf{V}_1^{\mathrm{eff}}\mathbf{L}}\left(\mathbf{L}-\mathbf{L}\mathbf{G}_0^{\mathrm{P}}\mathbf{K}\frac{1}{\mathbf{K}\mathbf{G}_0^{\mathrm{P}}\mathbf{K}}\mathbf{K}\right)\mathbf{K}\left|\phi\right\rangle. \tag{D.41}$$

We can easily insert (D.38) - (D.40) and find:

$$\left\langle c\middle|\psi^{+}\right\rangle = \frac{1}{1-\left(\langle c|-\langle c|\,\mathbf{G}_0^{\mathrm{P}}\,|b\rangle\,\frac{1}{\langle b|\mathbf{G}_0^{\mathrm{P}}|b\rangle}\,\langle b|\right)\mathbf{G}_0^{\mathrm{P}}\,|c\rangle\cdot v}\left(\langle c|\phi\rangle-\langle c|\,\mathbf{G}_0^{\mathrm{P}}\,|b\rangle\,\frac{1}{\langle b|\,\mathbf{G}_0^{\mathrm{P}}\,|b\rangle}\,\langle b|\phi\rangle\right) \tag{D.42}$$

because $\langle c|\,\mathbf{G}_0^{\mathrm{P}}\,|a\rangle = 0$ due to parity (as we will see soon). We see that we mainly need to calculate $\mathbf{G}_0^{\mathrm{P}}$.

### The Greens function $\mathbf{G}_0^{\mathrm{P}}$

The Greens function for the pair is defined as

$$\mathbf{G}_0^{\mathrm{P}} = \frac{1}{\varepsilon_0 - \mathbf{h}_0^{\mathrm{P}} + i\epsilon}. \tag{D.43}$$

We have seen in section 2.1.4 that the effective Hamiltonian for a pair $\mathbf{h}_0^{\mathrm{P}}$ is a hopping Hamiltonian with pair hopping parameter $\frac{2}{|u|}$. Therefore we can think of $\mathbf{h}_0^{\mathrm{P}}$ as

$$\mathbf{h}_0^{\mathrm{P}} = -\frac{2}{|u_0|}\left(\mathbf{H}_{\mathrm{H}}-2\right) \tag{D.44}$$

and so the energy is

$$\varepsilon_0 = -\frac{4}{|u_0|}(\cos(k)-1). \tag{D.45}$$

By inserting a complete set of momentum states we can calculate the Greens function in position space (denote $|n,m\rangle = \mathbf{c}^{\dagger}_{n\uparrow;0}\mathbf{c}^{\dagger}_{m\downarrow;0}\,|\Omega\rangle$):

$$\begin{aligned}
\langle n,n|\,\mathbf{G}_0^{\mathrm{P}}\,|m,m\rangle &= \frac{|u_0|}{2}\int_{-\pi}^{\pi}\frac{\mathrm{d}q}{2\pi}\frac{e^{iq(n-m)}}{-2\cos(k)+2\cos(q)+i\epsilon} && \text{(D.46)}\\
&= \frac{|u_0|}{2}\int_{-\pi}^{\pi}\frac{\mathrm{d}q}{2\pi}\frac{e^{iq|n-m|}}{-2\cos(k)+2\cos(q)+i\epsilon} && \text{(D.47)}\\
&= \frac{|u_0|}{2}\int_{C}\frac{\mathrm{d}z}{2\pi i}\frac{1}{z}\frac{z^{|n-m|}}{-2\cos(k)+z+\frac{1}{z}+i\epsilon} && \text{(D.48)}\\
&= \frac{|u_0|}{2}\int_{C}\frac{\mathrm{d}z}{2\pi i}\frac{z^{|n-m|}}{z^2+z(-2\cos(k)+i\epsilon)+1} && \text{(D.49)}
\end{aligned}$$

where $z = e^{iq}$ and $C$ is the unit circle. The denominator has two roots:

$$z_0 = \frac{2\cos(k) - i\epsilon}{2} + \pm\sqrt{\left(\frac{2\cos(k) + i\epsilon}{2}\right) - 1} \tag{D.50}$$

$$= \cos(k) - i\epsilon + \pm i\sin(|k|) \tag{D.51}$$

$$= e^{\pm i|k|} - i\epsilon. \tag{D.52}$$

Due to the infinitesimal $i\epsilon$ the root $e^{i|k|}$ is inside the unit circle, while the other root is outside. The residual theorem then gives:

$$\langle n,n|\,\mathbf{G}_0^{\mathrm{P}}\,|m,m\rangle = \frac{|u_0|}{2}\frac{e^{i|k||n-m|}}{e^{i|k|} - e^{-i|k|}} \tag{D.53}$$

$$= |u_0|\frac{e^{i|k||n-m|}}{4i\sin|k|}. \tag{D.54}$$

For simplicity consider a pair coming from the left s.t. $k > 0$. In the same basis as $|a\rangle, |b\rangle$ and $|c\rangle$ we can write $\mathbf{G}_0^{\mathrm{P}}$ as the following matrix:

$$\mathbf{G}_0^{\mathrm{P}} = \frac{|u_0|}{4i\sin(k)}\begin{pmatrix} 1 & e^{ik} & e^{2ik} \\ e^{ik} & 1 & e^{ik} \\ e^{2ik} & e^{ik} & 1 \end{pmatrix}. \tag{D.55}$$

Using this matrix one can easily calculate (upper sign for 'odd', lower sign for 'even'):

$$\langle a|\,\mathbf{G}_0^{\mathrm{P}}\,|a\rangle = -|u_0|\frac{e^{ik}}{2} \tag{D.56}$$

$$\langle b|\,\mathbf{G}_0^{\mathrm{P}}\,|b\rangle = |u_0|\frac{1}{12i\sin(k)}\left[(e^{ik} \mp 2)^2 - 1\right] \tag{D.57}$$

$$\langle c|\,\mathbf{G}_0^{\mathrm{P}}\,|b\rangle = \langle b|\,\mathbf{G}_0^{\mathrm{P}}\,|c\rangle = |u_0|\frac{\sqrt{2}e^{ik}}{12i\sin(k)}(e^{ik} \mp 1) \tag{D.58}$$

$$\langle c|\,\mathbf{G}_0^{\mathrm{P}}\,|c\rangle = |u_0|\frac{1}{6i\sin(k)}\left[(e^{ik} \pm 1)^2 + \frac{1}{2}\right]. \tag{D.59}$$

We will also need the scalar products with the incoming wave $\sim e^{ikn}$:

$$|\phi\rangle = \begin{pmatrix} e^{-ik} \\ 1 \\ e^{ik} \end{pmatrix} \tag{D.60}$$

$$\langle a|\phi\rangle = -\sqrt{2}i\sin(k) \tag{D.61}$$

$$\langle b|\phi\rangle = \frac{2}{\sqrt{6}}(\cos(k) \mp 1) \tag{D.62}$$

$$\langle c|\phi\rangle = \frac{2\cos(k) \pm 1}{\sqrt{3}}. \tag{D.63}$$

### Calculating the transmission

We are now ready to plug all these expressions into (D.42):

$$\left\langle c\middle|\psi^+\right\rangle = \frac{1}{1-\left(\langle c|\,\mathbf{G}_0^{\mathrm{P}}\,|c\rangle - \langle c|\,\mathbf{G}_0^{\mathrm{P}}\,|b\rangle \frac{1}{\langle b|\mathbf{G}_0^{\mathrm{P}}|b\rangle}\langle b|\,\mathbf{G}_0^{\mathrm{P}}\,|c\rangle\right)\cdot v}\left(\langle c|\phi\rangle - \langle c|\,\mathbf{G}_0^{\mathrm{P}}\,|b\rangle \frac{1}{\langle b|\,\mathbf{G}_0^{\mathrm{P}}\,|b\rangle}\langle b|\phi\rangle\right). \tag{D.64}$$

We can make use of the following identity (which can be shown by explicit calculation)

$$\langle b|\,\mathbf{G}_0^{\mathrm{P}}\,|b\rangle\langle c|\,\mathbf{G}_0^{\mathrm{P}}\,|c\rangle - \langle c|\,\mathbf{G}_0^{\mathrm{P}}\,|b\rangle^2 = \frac{i|u_0|^2}{8\sin k}e^{ik} \tag{D.65}$$

to simplify:

$$\left\langle c\middle|\psi^+\right\rangle = \frac{1}{\langle b|\,\mathbf{G}_0^{\mathrm{P}}\,|b\rangle - \frac{i|u_0|^2}{8\sin k}e^{ik}v}\left(\langle b|\,\mathbf{G}_0^{\mathrm{P}}\,|b\rangle\langle c|\phi\rangle - \langle c|\,\mathbf{G}_0^{\mathrm{P}}\,|b\rangle\langle b|\phi\rangle\right) \tag{D.66}$$

$$= -\frac{4\sqrt{3}i\sin k}{6+\left(3|u_0|v\mp 8\right)e^{ik}+2e^{2ik}}. \tag{D.67}$$

We could now use conclusion three of theorem 1 to obtain the full wavefunction. However there is a more clever way. We know that for $n \geq 1$ the wavefunction looks as follows:

$$\left\langle n,n\middle|\psi^+\right\rangle = t_k e^{ikn}. \tag{D.68}$$

Using this we easily find the transmission amplitude $t_k$:

$$t_k = e^{-ik}\left\langle 1,1\middle|\psi^+\right\rangle \tag{D.69}$$

$$= e^{-ik}\left[\langle 1,1|a\rangle\left\langle a\middle|\psi^+\right\rangle + \langle 1,1|b\rangle\left\langle b\middle|\psi^+\right\rangle + \langle 1,1|c\rangle\left\langle c\middle|\psi^+\right\rangle\right] \tag{D.70}$$

$$= e^{-ik}\langle 1,1|c\rangle\left\langle c\middle|\psi^+\right\rangle \tag{D.71}$$

$$= \frac{e^{-ik}}{\sqrt{3}}\left\langle c\middle|\psi^+\right\rangle \tag{D.72}$$

$$= -\frac{4i\sin k}{6+\left(3|u_0|v\mp 8\right)e^{ik}+2e^{2ik}}e^{-ik} \tag{D.73}$$

where we used $\left\langle a\middle|\psi^+\right\rangle = \left\langle b\middle|\psi^+\right\rangle = 0$. The transmission probability is given by the modulus squared of $t_k$ and computes to:

$$T_k = |t_k|^2 = \frac{1}{1+\left(\frac{3|u_0|v\mp 8+8\cos k}{4\sin k}\right)^2}. \tag{D.74}$$

APPENDIX E

# Error discussion of the numerical method

In this chapter we would like to further discuss the numerical method introduced in section 2.3 and in particular try to estimate its errors.

Let us start with the obvious one: Due to the restriction of the system to finite length $L$ we can only observe $L$ momentum states. These states will be either even or odd states, so that we have about $L/2$ of each kind. The momentum precision of the method is going to be $\Delta k = \frac{\pi}{L/2} = \frac{2\pi}{L}$. For a length $L = 31$, as we use throughout the thesis, this gives about $\Delta k = 0.2$. We would not be able to observe any structures in the transmission which are smaller than $\Delta k$. Also note that we cannot predict the transmission below $k \lesssim \Delta k$ and $k \gtrsim \pi - \Delta k$ because they are outside of the range of sampling points.

Furthermore there are two more sources of error. First there is always an error when fitting the cosine/sine functions to the eigenstates of the system. As described in section 3.4 we discard eigenstates where the fit surpasses an error above 0.001. The other source of error comes from the linear interpolation procedure. The linear interpolation will fail if the parameters $A_k, B_k, C_k, D_k$ change too quickly with $k$ (on length scales smaller than $\Delta k$). But even if the parameters change more slowly of course there will still be an error determined by the second derivative:

Consider a general function $f(x)$ between points $a$ and $b$. Assume that we know the value of $f(x)$ at $a$ and $b$. Then the linear interpolation of $f(x)$ between $a$ and $b$ has an error [29]:

$$|\Delta f| = \frac{1}{2} f''(a)(x-a)(x-b) + O\Big(|b-a|^3\Big). \tag{E.1}$$

We can apply this to $A_k, B_k, C_k$ and $D_k$ with $x = k$ and do some crude approximations: First $(x-a)$ and $(b-x)$ are smaller than $\Delta k$. Second assume that $A_k, B_k, C_k$ and $D_k$ have roughly the same magnitude $A_0$ and change slowly over the Brillouin zone. Then we can approximate the second derivative very roughly by $\left|\frac{\partial^2 A_k}{\partial k^2}\right| \approx \frac{A_0}{\pi^2}$. Combining this we find

$$\Delta A_k \approx \frac{2A_0}{L^2} \tag{E.2}$$

and the same result for $B_k, C_k, D_k$. The error scales as $\Delta A_k \sim 1/L^2$. Since $T_k$ is given by some

combination of $A_k, B_k, C_k, D_k$, we conclude that the error on $T_k$ must scale similarly:

$$\Delta T_k \sim 1/L^2. \tag{E.3}$$

Note that this result is only a very crude estimate based on guessing orders of magnitude of the ingredients and their errors. We should not expect at all that this gives a precise estimate of the error (but only its order of magnitude). For a size of $L = 31$ we can therefore expect that the error of the transmission $T_k$ is of order $\Delta T_k \sim \frac{1}{31^2} = 0.001$.

To summarize we found three sources of error: The precision in momentum space is determined by $\Delta k = \frac{2\pi}{L}$. Apart from that there is an error from the fit and also one from the interpolation, which scales as $1/L^2$.